POTENTIAL EARTHQUAKE, LANDSLIDE, TSUNAMI AND GEO-HAZARDS FOR THE U.S. OFFSHORE PACIFIC WIND FARMS

19-P-202745

BOEM/BSEE E17PS00128

Final Report

May, 2020

Approval for issue

18 May 2020

This final report has been reviewed by the BSEE and approved for publication. Approval does not signify that the contents necessarily reflect the views and policies of the BSEE, nor does mention of the trade names or commercial products constitute endorsement or recommendation for use.

This study was funded by the Bureau of Safety and Environmental Enforcement (BSEE), U.S. Department of the Interior, Washington, D.C., under Contract 140M0119C0004.

This report was prepared by RPS within the terms of engagement with BSEE and in direct response to a scope of services. This report is supplied for the sole and specific purpose for use by BSEE. The report does not account for any changes relating the subject matter of the report, or any legislative or regulatory changes that have occurred since the report was produced and that may affect the report. RPS does not accept any responsibility or liability for loss whatsoever to any third party caused by, related to or arising out of any use or reliance on the report.

Prepared by:

RPS

List of Authors:

Dr. Tayebeh Tajalli Bakhsh: Project Manager

Mahmud Monim

Kent Simpson

Tony Lapierre

Dr. Jason Dahl

Jill Rowe

Dr. Malcolm Spaulding

55 Village Square Drive

South Kingstown RI 02879

T +1 401 789 6224

E Tayebeh.tajallibakhsh@rpsgroup.com

Prepared for:

BOEM

Project Manager:

Jennifer Miller: Geophysicist

Office of Renewable Energy Programs

Camarillo, California

T + 1 805 384-6306

E jennifer.miller@boem.gov

EXECUTIVE SUMMARY

The Bureau of Ocean Energy Management (BOEM) is responsible for issuing leases for potential renewable energy projects, including those for floating offshore wind energy. Five areas were published by BOEM in a Call for Information and Nominations, referred to as a Call Area, in 2016 and 2018 for Hawaii (Oahu North and Oahu South) and California (Humboldt, Morro Bay and Diablo Canyon), respectively. BOEM has not published a Call Area offshore Oregon. Earthquakes, landslides, liquefaction, tsunamis, slope instability, and biogenic gas are some of the hazards that can impact the floating offshore wind farms located off the coasts of California, Oregon, and Hawaii, as they are located in geologically hazardous and active regions. The risks are mainly to the mooring and anchorage systems, as well as buried cables that transmit the power to shore.

The BOEM funded Solicitation No. E17PS00128 to assess the potential threats to wind energy development off the U.S. Pacific coast, including catastrophic geohazards (e.g., seismic activities, landslides, and tsunamigenic earthquakes), gas plumes, liquefaction, and turbidity currents, and the effect on the mooring and anchorage system and buried cable due to geohazards. This evaluation of geohazards is designed to aid in selecting suitable sites for Floating Offshore Wind Farms (FOWF) with the focus on areas already designated as potential lease sites using the best available science, so that potential impacts are understood to the greatest extent possible. The main goal of the study is to provide an understanding of geohazards risks in areas under analysis for the development of FOWF using a geospatial planning approach by providing a guideline on most important geohazards and how they might affect the performance of FOWF.

This report will provide guidance by identifying the best current practices regarding the geologic hazards posing risks to components of FOWF. The report presents a literature review on approaches and standards applicable to the siting and engineering processes associated with floating offshore structures. It should be noted this report does not recommend any specific standards to follow; and BOEM approves technical standards proposed by lessee on a project case basis. The geohazards off the U.S. West Coast and Hawaii that may directly or indirectly affect the FOWF are assessed to determine which potential geologic hazards could impact the siting of potential FOWF locations and pose risks to the mooring and anchorage systems and buried cables. Publicly available datasets of geological and geophysical seabed and soil conditions, ground acceleration and bathymetry slope in the region are analyzed in form of geospatial raster maps. These spatially varying datasets are then weighted and overlaid to determine suitability of the area and define exclusive area that might have more risk for installation of FOWF.

The maps and geospatial data analyzed for the project and the suitability outputs are also available online through an interactive web map interface[1] for the end user.

[1] http://boem-oceansmap.s3-website-us-east-1.amazonaws.com/

Table of Contents

LIST OF TABLES

LIST OF FIGURES

LIST OF ABBREVIATIONS AND ACRYONYMS

AASZ	Alaska- Aleutian Subduction Zone
ALE	Abnormal Level Earthquakes
ALS	Accidental Limit State
AOI	Areas of Interest
BOEM	Bureau of Ocean Energy Management
BSEE	Bureau of Safety and Environmental Enforcement
CPT	Cone Penetrometer Test
Cr	Capacity factor
CSZ	Cascadia subduction zone
DEM	Data Elevation Models
DLE	Ductility Level Event
EEZ	Exclusive Economic Zone
ELE	Extreme Level Earthquake
FOWF	Floating Offshore Wind Farms
FOWT	Floating Offshore Wind Turbines
GOM	Gulf of Mexico
HMRG	Hawaii Mapping Research Group
MCE	Maximum Considered Earthquake
NCEI	National Centers for Environmental Information
NREL	National Renewable Energy Lab
NSHM	National Seismic Hazard Model
OSU	Oregon State University
PGA	peak ground acceleration
SAFZ	San Andreas Fault Zone
SLE	Strength Level Event
SPF	Steel Pipe Crossing Faults
TLP	Tension leg platform
TMD	Tuned Mass Dampers
ULS	Ultimate Limit States
VIM	Vortex-induced motions
VIV	Vortex-induced vibrations

1 INTRODUCTION

Floating Offshore Wind Farms (FOWF) construction and operation of the U.S. Pacific Coast (Figure 1) may face the risk of potential geohazards, as they are relatively new applications of older technologies (land-based wind and mobile offshore drilling units) in tectonically-active regions. Seismic activities, landslides, and tsunamigenic earthquakes are threats to the U.S. West Coast and Hawaii, and uncertainty exists over how FOWF development and siting will be impacted by these threats in proposed areas of development. Events such as the 2011 Tōhoku earthquake and tsunami highlighted the need for a focused effort to minimize loss and damages by developing design considerations and criteria for structures to cope with extreme events. The design of Floating Offshore Wind Turbines (FOWT) installed in any of the earthquake-prone regions must consider:

- the fault conditions relevant to the electrical system;
- the soil condition at the sites and its liquefaction or mud failure;
- the consequent scour on the mooring; and
- the loads imposed on the mooring and anchorage system and buried cables due to seismic activity and hydrodynamic added mass.

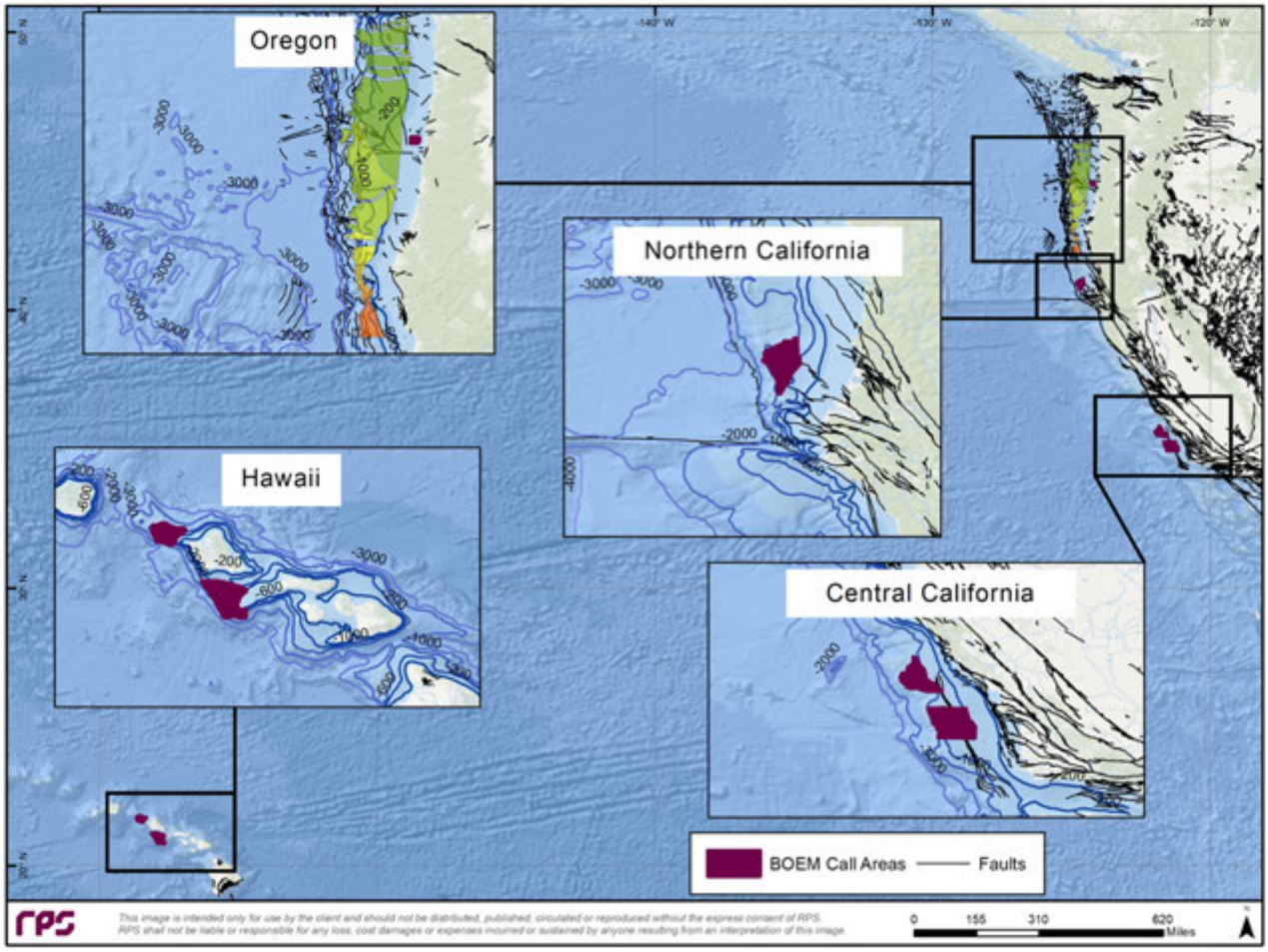

Figure 1. The location of the faults, and FOWF Call Areas in California and Hawaii, and the Oregon FOWF study area.

Also, the effects of earthquake or landslide generated tsunamis on the floating structures should be considered as environmental loads beyond normal condition. The tsunami wavelength, amplitude, and velocity would have effects on the floating wind offshore structural design, mooring and anchorage systems, and power transport cables laid on the ocean basin.

Also, in order to identify the best possible sites and best practices for developing FOWF in the U.S. Pacific region, the current guidelines, standards and regulations relevant to renewable energy development should be reviewed to incorporate their information regarding site selection and the importance of natural geohazards. To aid in selection of the best possible sites, the natural geohazards in the region should be assessed, and the soil type by the offshore engineers and contractors should be identified. Site-specific characterizations need to be conducted and data on seafloor characteristics need to be collected to identify site-specific hazards for project components such as mooring and under water transmission, based on the ground type reaction to an earthquakes and potential bathymetric changes due to landslide.

Based on the DNV-OS-J103 (2013) floating offshore standards, "*Environmental conditions cover virtually all natural phenomena on a particular site, including but not limited to meteorological conditions, oceanographic conditions, water depth, soil conditions, seismicity, biology, and various human activities*", and these conditions need to be further studied. Earthquakes and their associated effects cause great economic and loss of life, and tremendous damage to structures and national infrastructures due to direct seismic effects (shifting, tremors), liquefaction, landslides, and/or tsunamis.

This study identifies 1) the challenges and critical needs for design and installation of FOWT in regions with geohazards; 2) how the existing standards can be applied; 3) where the regulations and standards need to be improved; and 4) what site-specific analyses would be needed. This report undertakes a comprehensive review of different hazards from geologic conditions, seismic activities, earthquakes, landslides, and tsunamis in the Pacific Ocean near the FOWF Call Areas. It begins with a review of FOWT technologies and review of different standards in the area of offshore development, continues with looking at geohazards including seismic and co-seismic data sources, and tsunamis for the U.S. Pacific waters, and presents maps encompassing all relevant available examples of historic earthquake and tsunami hazard sources. To incorporate all the variable inputs of soil type, bathymetry slope and earthquakes, and apply them to the suitable site location selection problem, the data are classified to common scales and overlaid using assigned weights. The weighted overlaid maps show the suitability of the region by using total value of all weighted layers and allows for an understanding of the importance of each variable in finding the best site location. The goals of this study are to provide a comprehensive overview of *in situ* geologic condition and potential threats to the renewable energy development area; a data exploration analysis of relative risk; and a guideline to identify and prioritize the risk to the FOWF. The major objectives of this study are to:

- Review FOWF technologies and the impacts of geohazards on FOWT;
- Review the current and needed site selection process for FOWF;
- Review the potential earthquake sources and seismic activities in the regions;
- Review the potential sources of landslide and underwater slope instabilities in the regions;
- Produce maps of combined soil type, slope gradient and peak ground acceleration (as a representation of earthquake activity in the region); and
- Present suitable areas for FOWF installation.

The results presented in this report reflect the initial implementation of FOWFs in the vicinity of the proposed wind farm Call Areas near California, Hawaii, and Oregon. Before installation of mooring and undersea transmission are undertaken, site-specific characterizations need to be conducted and data need to be collected on seafloor characteristics and unidentified hazards, such as ground type reaction to earthquakes, bathymetry changes due to landslides, and wave-imposed forces on the mooring and anchoring of the FOWF. Desktop characterizations of the site are conducted in this report and integrated to assess and characterize existing seafloor conditions to select appropriate design, construction, and installation techniques.

1.1 Study Area

The Bureau of Safety and Environmental Enforcement (BSEE), in collaboration with the Bureau of Ocean Energy Management (BOEM), provided RPS with six areas for study investigation. Five of the six areas were published by BOEM in a Call for Information and Nominations, referred to as a Call Area, in 2016 and 2018 for Hawaii (Oahu North and Oahu South) and California (Humboldt, Morro Bay and Diablo Canyon), respectively. BOEM has not published a Call Area offshore Oregon. Instead, BOEM provided the area offshore Oregon where FOWF is technically viable (i.e., where wind speeds are greater than 7 m/s and water depths are less than 1,100 m). The study areas for FOWF off the coasts of California, Oregon, and Hawaii (referred to as study areas throughout this report) are presented as Figure 1.

California study area

The California (CA) study areas (Figure 2) include a northern site which encompasses Humboldt Call Area. This Call Area is located offshore Eureka in water depths between 600 m and 1,000 m.

In addition to the northern Call Area, there are two central Call Areas located 22 miles offshore between Monterey Bay and Morro Bay: Morro Bay and Diablo Canyon. The Morro Bay Call Area is approximately 26 nautical miles (48 km) from Point Estero, California in waters between 800 m and 1,000 m deep, and the Diablo Canyon Call Area is in water depths between 600 m and 1,000 m.

Oregon study area

The proposed FOWF site offshore Oregon (OR) is situated on the upper slope in water depths of 200 m to 1,100 m (Figure 3). As the site location has not been finalized by BOEM at the time of this study, this study will cover the regional aspect of geohazards to offshore OR, over an area where a wind speed analysis has been provided by BOEM.

Hawaii study area

The Hawaii study area consists of two Call Areas: Oahu North and Oahu South. The Oahu North Call Area is located 9 miles off the northwest corner of Oahu, at which Kaena Point State Park is located. The study area is over a plateau in waters depths ranging from 600 m to more than 1,000 m.

On the other hand, Oahu South Call Area is located 9 miles offshore of Oahu, south of Honolulu, in a depth range of approximately 500 m to 1000 m (Figure 4).

The study covers the call areas and nearby mainland as potential cable landing regions and a 5 nautical mile radius extending seaward of the areas provided by BOEM. Throughout this report, these

study areas will be referred to as the Areas of Interest (AOIs) with the AOI polygons presented in bold red on Figure 2 to Figure 4.

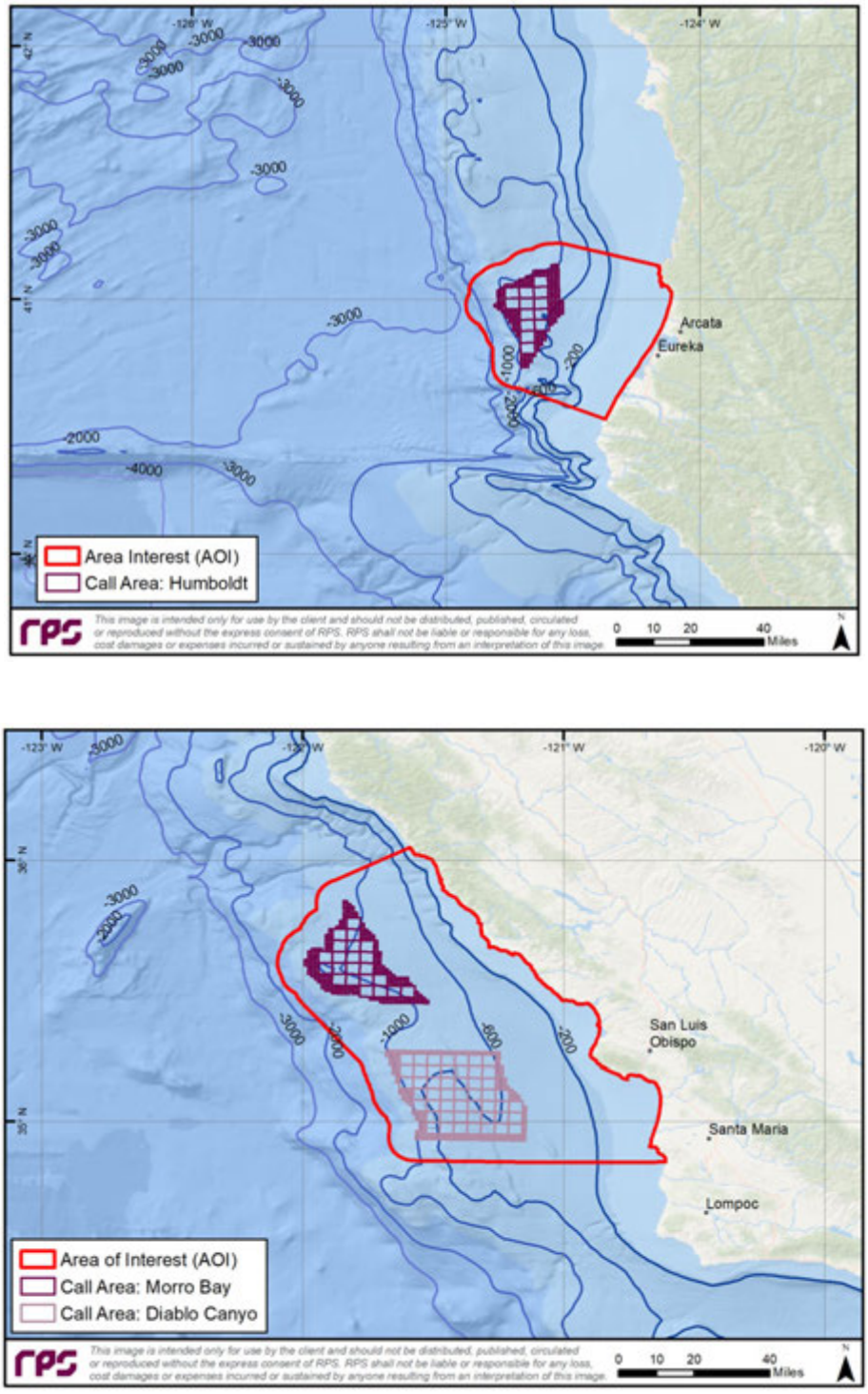

Figure 2. Northern (Upper Panel) and Central (Lower Panel) California FOWF Study area.

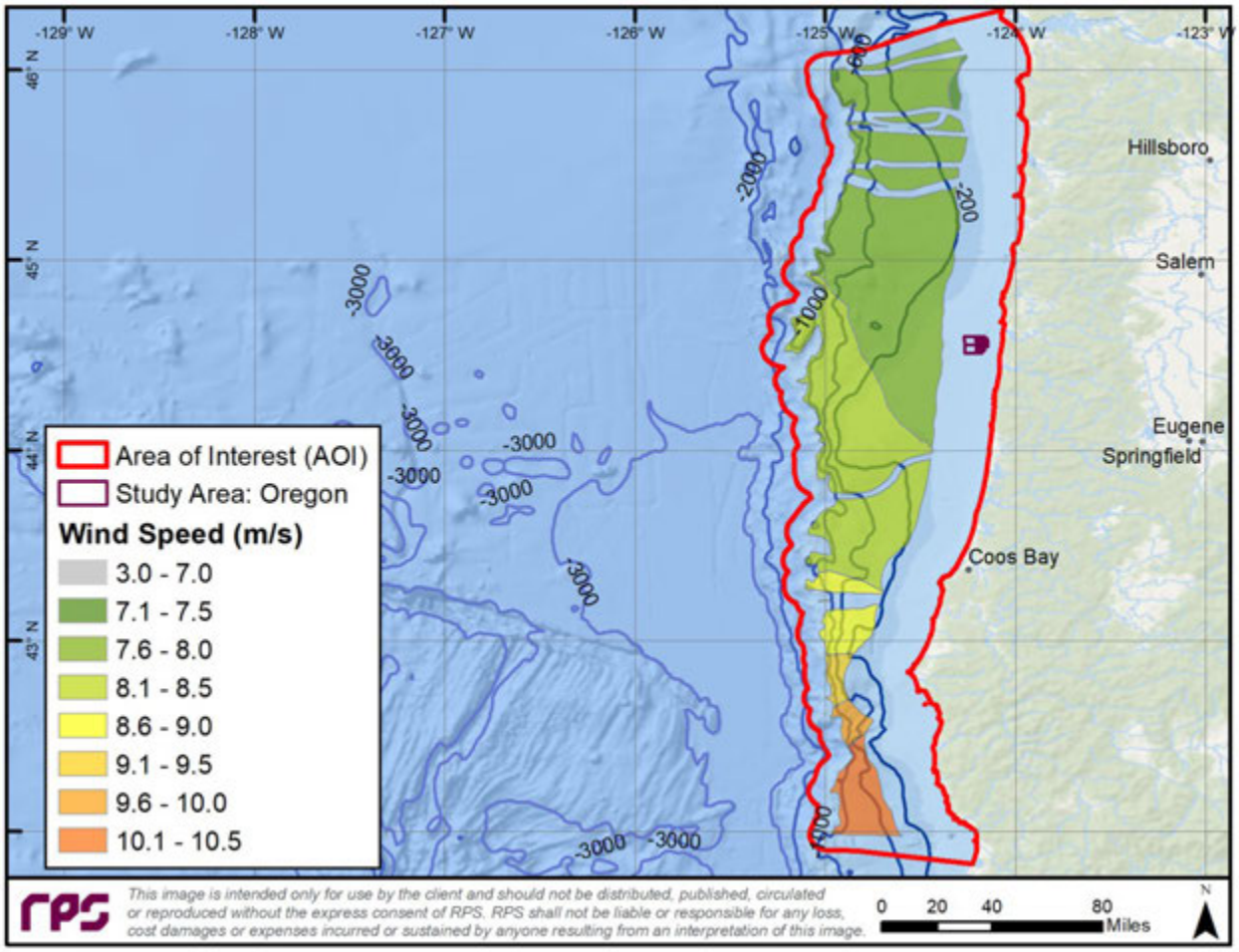

Figure 3. Oregon State FOWF Study area and Processed Wind Speed Map for Potential Sites.

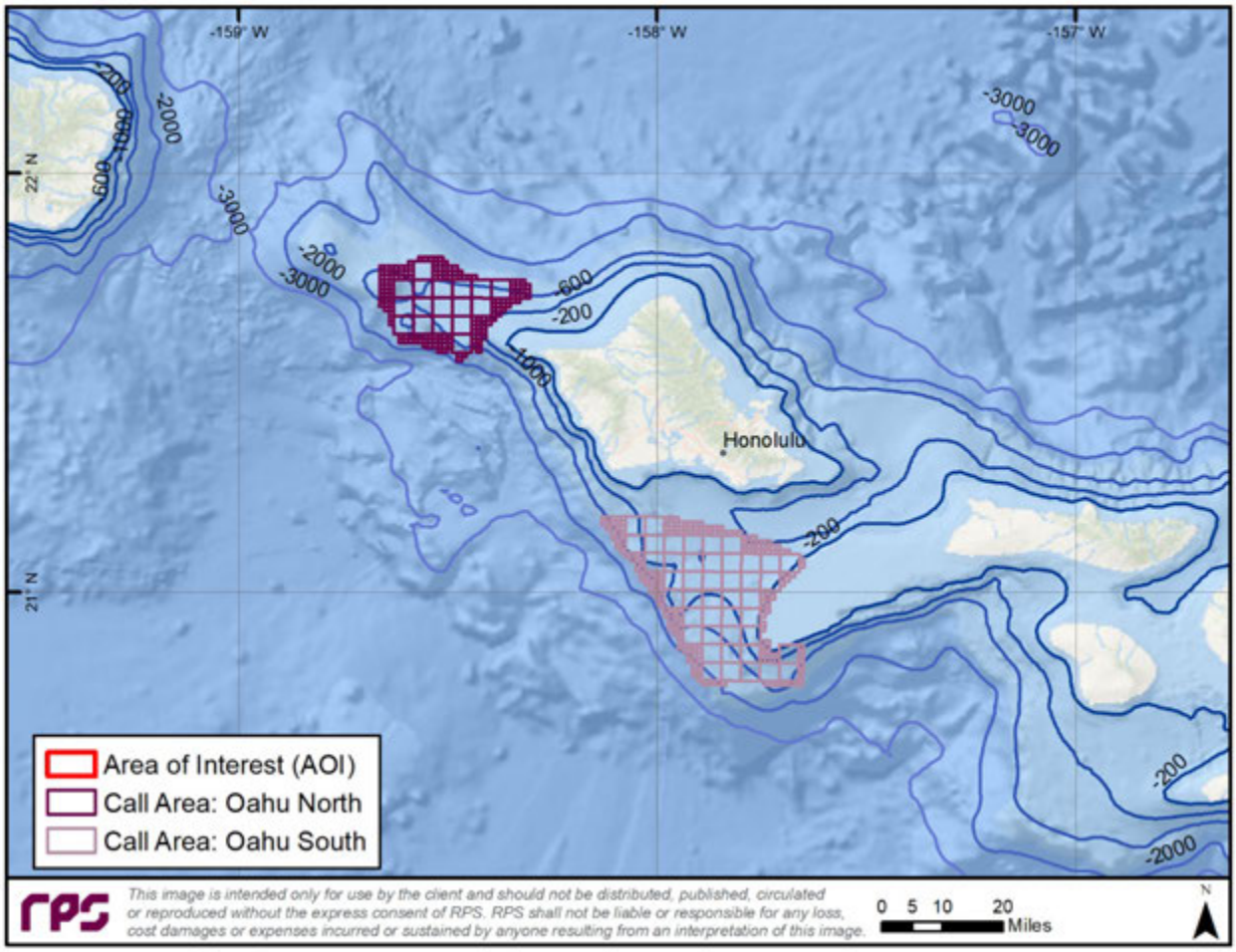

Figure 4. Hawaii FOWF Study areas North and South of Oahu.

1.2 Report Format

This report is presented in the following format:

- Section 2 contains a review on the major types of FOWT, along with their advantages and disadvantages;
- Section 3 describes impacts of geohazards on FOWF developments;
- Section 4 presents the site selection process for FOWT;
- Section 5 contains review of potential geohazards in Pacific;
- Section 6 discusses the methodology of the weighted overlay modeling conducted;
- Section 7 contains the suitability analysis models outputs;
- Section 8 discusses the finding and results of the suitability analysis;
- Section 9 presents conclusions, data gap analysis, and recommended follow-on-work;
- Section 10 contains the references;
- Appendix A presents the metadata table of publicly available datasets used in this study; and
- Appendix B discuss the analytical approach for calculating the effects of tsunamis on FOWT.

2 FLOATING WIND FARMS TECHNOLOGIES

The idea of large-scale FOWT was proposed by Professor William E. Heronemus at the University of Massachusetts (Heronemus, 1972), due to the practical limitations of building bottom mounted structure (e.g., monopiles) tall enough to reach depths greater than 30 meters. At greater depths, the monopile method of turbine installation (foundation) becomes impractical and expensive. Although the concept of FOWT was introduced in 1972, the mainstream research community did not begin investigating larger installations of FOWT in the continental shelf area until the mid-1990's, when the commercial wind industry was well established. FOWT has the potential to be established in relatively deeper water than a fixed foundation offshore wind turbine, which allows it to have access to higher wind resources. The major advantage of using FOWT over other types is that it significantly reduces construction costs and the use of heavy offshore equipment at sea. In addition, if a major repair of the turbine is needed, the entire unit can be disconnected from its mooring and electrical umbilical and towed back to shore which reduces operation and maintenance costs.

To undertake a review on the standards and regulation, understanding of the status of the technology and the challenges associated with different kinds of its components are needed. This section includes a discussion of FOWF technology and its components.

2.1 Key Components

FOWF consist of multiple turbines buoyed on a floating platform, with several mooring cables connecting the floating platform to anchors implanted on the ocean floor. There are different types of platforms and station-keeping systems, including anchors and cables for different situations and costs (Table 1), some of which are still under review and development. The major mainstream components of FOWF are discussed in this section.

Table 1. Various parts of FOWT (modified from Devin, 2019)

Platform	Anchor	Mooring Material	Mooring Orientation
• Spar buoy • Semi-submersible • Tension leg platform (TLP)	• Drag embedment anchor • Driven pile • Suction pile • Gravity anchor	• Chain • Cable • Fiber	• Catenary • Taut • Semi-taut

2.1.1 Floating Wind Turbines Platform

Although the configuration of FOWT may vary depending upon the architecture, size, and topology of the platform, a classification system was developed by ABS (2013) to divide all FOWT platforms into three major categories: 1) spar buoy (Figure 5); 2) semi-submersible (Figure 6); and 3) Tension Leg Platforms (TLP; Figure 7; Butterfield et al., 2007; IRENA, 2016). This classification system is based on the physical principle used to attain static stability. These designs are adapted from the oil and gas industry, and each has different strengths and weaknesses influenced by site conditions. There are some variations of these technologies (e.g., multi-turbine floating platform) which are not discussed in this report.

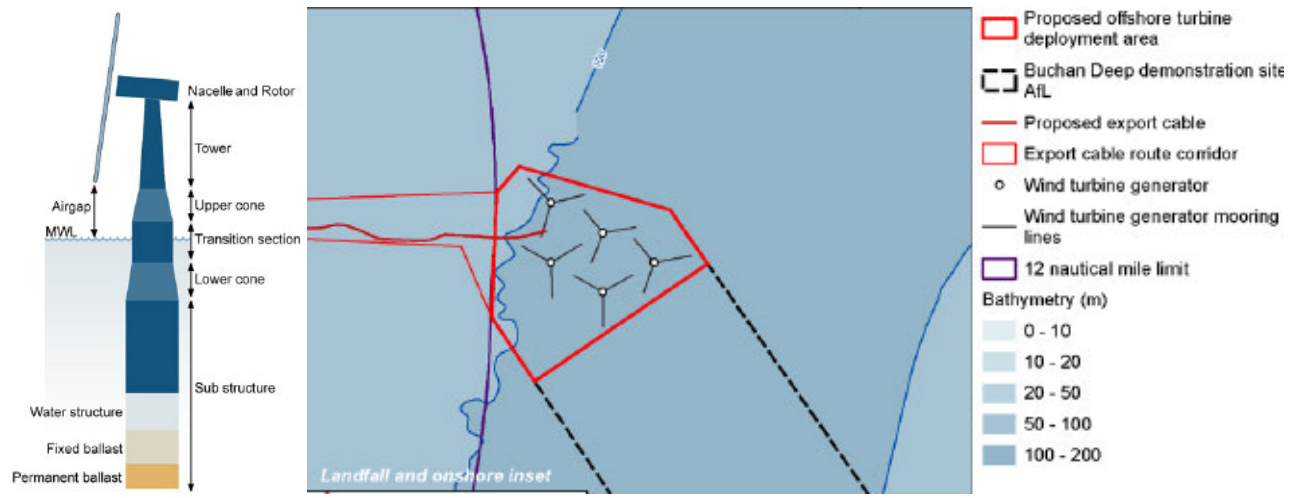

Figure 5. Spar-type FOWT (Figure from: Statoil, 2015).

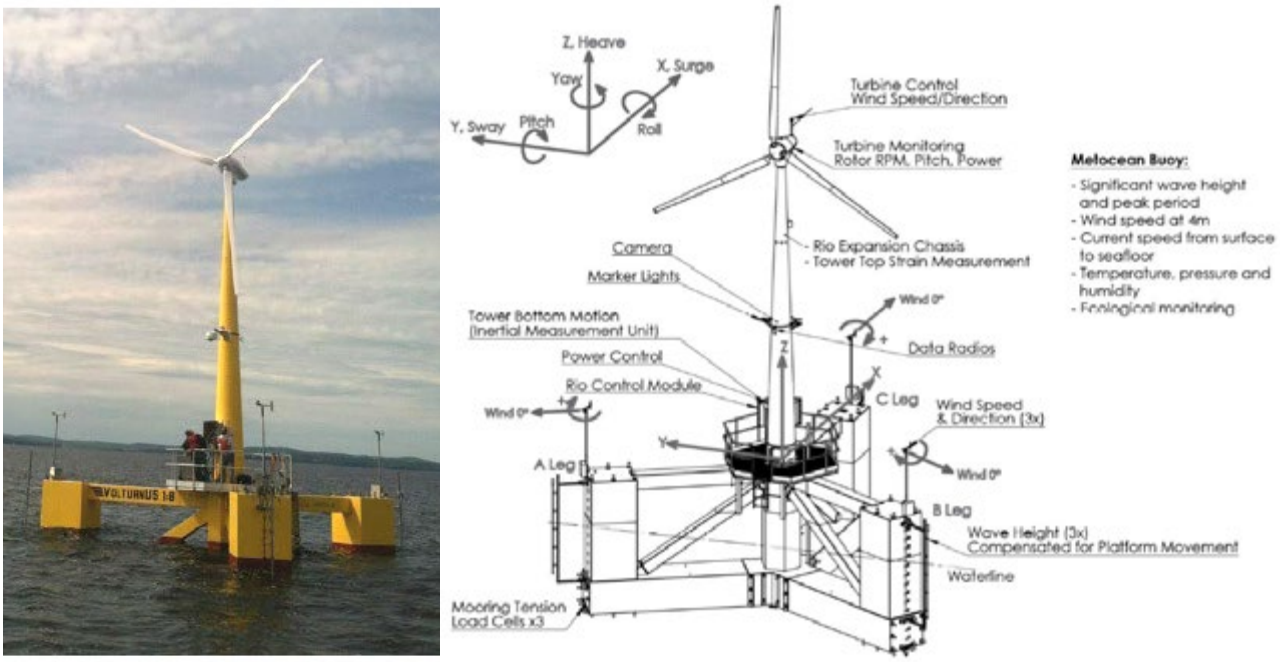

Figure 6. Semi-submersible FOWT (VolturnUS 1:8-scale) (left panel) and its structural components (right panel) (figure from Viselli, 2015).

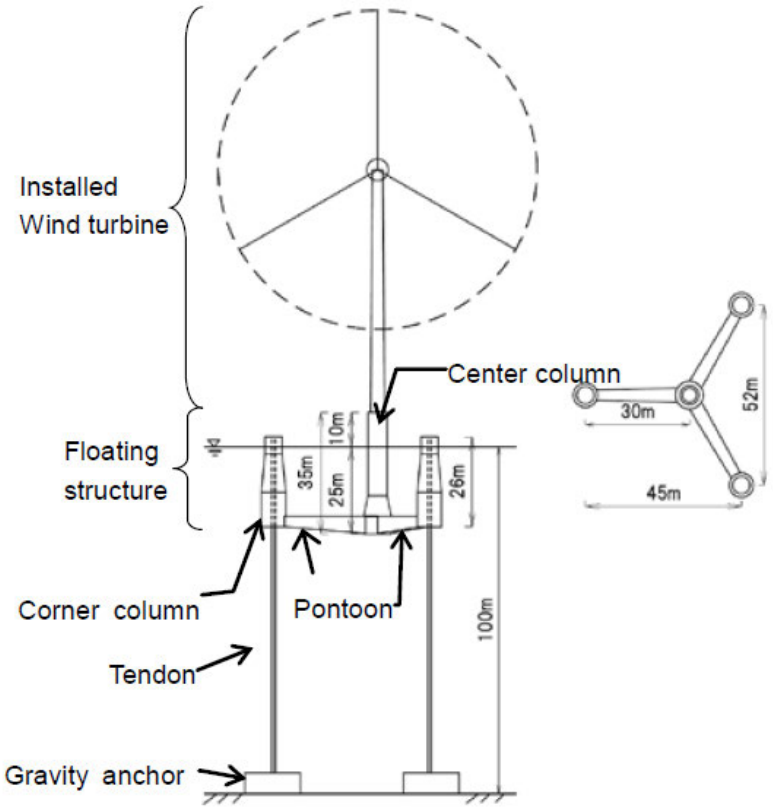

Figure 7. General arrangement of the TLP (figure from Suzuki et al., 2010).

2.1.1.1 Spar buoy

The spar buoy platform consists of a cylinder with low water plane area, which is ballasted to keep the center of gravity below the center of buoyancy (Figure 5). This mechanism creates a righting lever (distance between the center of gravity and the vertical line of action of the buoyancy force) that provides inertial resistance to pitch motion (rotations about y/transverse axis) and roll motion (rotations about x/longitudinal axis). This system also achieves stability by generating sufficient draft to offset heave motion (vertical/up-down motion) (Figure 8; Musial et al., 2004).

An example of a spar buoy wind turbine is the Hywind floating spar FOWT developed by Statoil. It is the world's first full-scale FOWT initially deployed 10-km west of the island of Karmøy off the Norwegian west coast at a water depth of 220 m. This FOWT consists of a spar platform that supports a 2.3-MW wind turbine with a rotor diameter of 82.4 m. The spar extends 100 m below the water surface with a diameter of about 8.3 m (Hanson et al., 2011; Skaare et al., 2015). The spar minimizes wave-induced movements and loading to the structure by reducing the cross-sectional area in the splash zone. The structure is attached to the seabed by three separate catenary mooring lines which are attached to anchors. Near the surface, the mooring line divides into a bridle attachment that is connected to the hull, increasing the yaw (rotation about z axis; Figure 8) stiffness (Driscoll et al., 2016). Mooring systems for FOWT are further discussed in the next section.

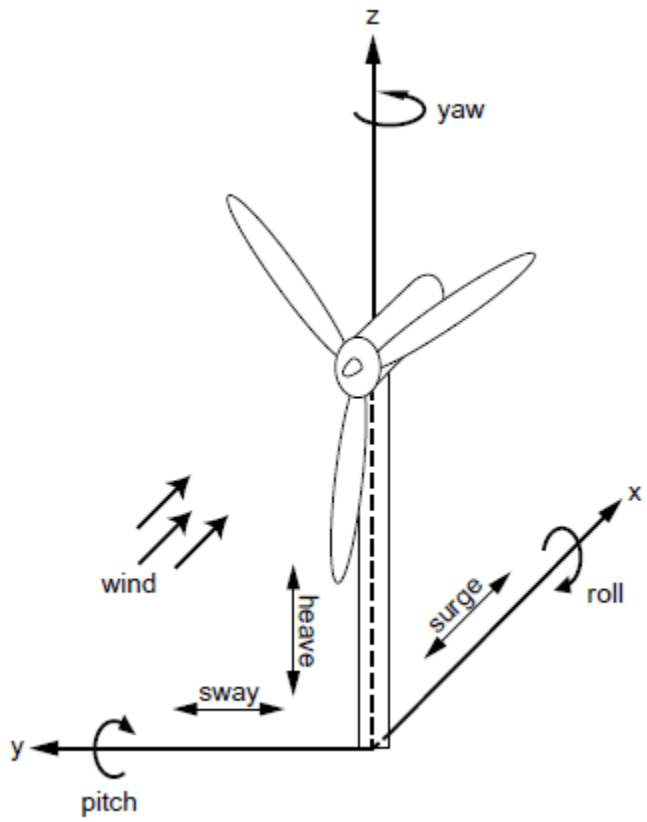

Figure 8. Schematic presentation of six degrees of freedom of motion for a floating structure (BV, 2019).

2.1.1.2 Semi-Submersible

This type of buoyancy stabilized platform contains a number of large columns linked by connecting bracings/submerged pontoons. The columns provide the hydrostatic stability, and pontoons provide distributed buoyancy taking advantage of the weighted water plane area to attain stability (Figure 6; Newman, 1977). This type of platform is also kept in position by catenary or taut spread mooring lines and drag anchors (Butterfield et al., 2007).

2.1.1.3 Tension Leg Platform (TLP)

The TLP platform attains stability through mooring line tension (Figure 7). This type of platform is highly buoyant, which offsets the weight of the platform and allows for a smaller and lighter structure. Since TLP uses clusters of stiff tendons which do not allow vertical movement and relies on mooring line tension for righting stability (Musial et al., 2004), the stress on the tendon and anchor increases (James and Ross, 2015).

Each type of FOWT platform has advantages and disadvantages depending on the design of foundation, logistics associated with manufacturing and site of installation. The strengths and weaknesses associated with the three main types of FOWT platform are summarized in Table 2.

Table 2. Advantages and disadvantages related to different types of FOWT platforms (based on IRENA, 2016).

Type of FOWT	Advantages	Disadvantages
Spar buoy	• Lower critical wave-induced motions • Relatively lower cost for mooring installation	• Installation of the system requires heavy-lift vessels and currently can be done only in relatively sheltered, deep water • Needs deeper water (>100 meters) than other types of platforms
Semi-submersible	• Construction is done onshore or in a dry dock • The complete platform (including turbines) can float with drafts below 10 meters during transport • Transportation to site can be done using conventional tugboats • Deployable in water depths with a minimum of about 40 meters • Relatively lower cost for mooring installation	• Prone to higher critical wave-induced motions • Likely to use more material and larger structures in comparison to other platforms • Manufacturing process is more complex compared with other concepts, especially spar buoys
TLP	• Lower critical wave-induced motions • Relatively lower mass • Manufacturing process can be carried out onshore or in a dry dock • Deployable in minimum water depths of 50-60 meters, depending on metocean conditions	• Can be difficult to keep stable during transportation and installation process • Special purpose vessel may be required contingent on the design of the platform. • Relatively higher cost for mooring installation

To passively control vibration of different components of a spar-type FOWT, Dinh and Basu (2015) discussed the role of Tuned Mass Dampers (TMDs). TMD is a device installed in FOWT structures to mitigate mechanical vibrations and various environmental impacts such as wind, wave, and hydrodynamic loads. In this numerical study, 5 MW NREL spar-type FOWT with several sets of TMD configurations has been examined to assess the control effectiveness and feasibility of using the TMD. It was found that if a single TMD is tuned at the wave peak frequency, the control is more effective in comparison with other tuning frequencies, especially for the nacelle sway and spar roll. It was also demonstrated that control by spar TMD at the mean water level is feasible and optimal while control is less effective when the TMD position is lower. The study concluded larger initial cable tension between seabed and fairlead creates higher sway natural frequency and less resonance with wave loading components which allows more effective control of the FOWT. Another interesting finding of this investigation is that to reduce the nacelle sway, spar-mounted TMD plays a more important role than a nacelle-mounted TMD. For the use of multiple TMDs, it is suggested that motion control is more effective when the TMDs are tuned around the wave frequency especially when TMDs are mounted on both nacelle and spar. However, the control effectively does not increase significantly when more than two TMDs are used.

2.1.2 Mooring Systems

Catenary or taut spread mooring lines (Figure 9) are the most common mooring configurations that keep the foundation of FOWT in position with drag or suction anchors. However, some FOWT concepts leverage the idea of using a Semi-taut mooring system, which is not as common as the first two types of systems.

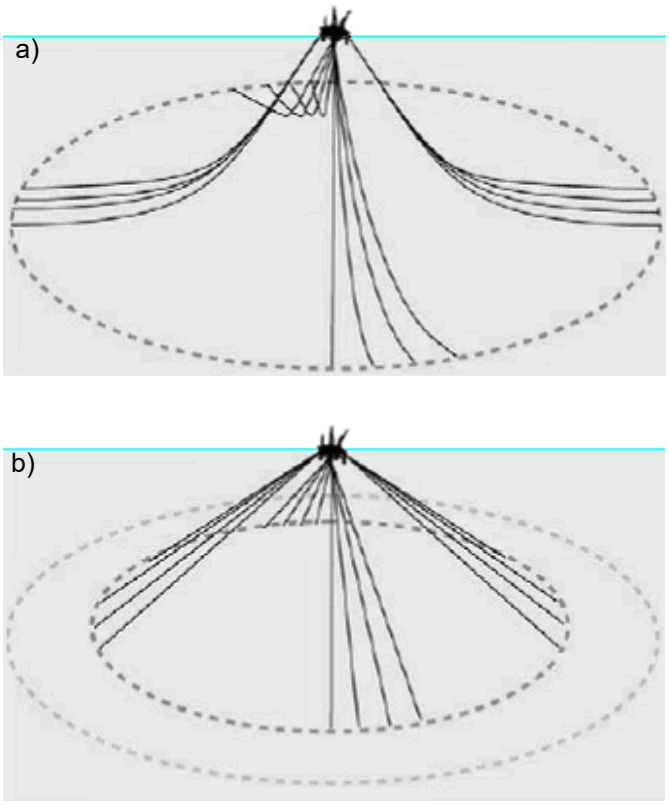

Figure 9. Different types of mooring system: a) Catenary[2], b) taut leg[2] and c) Semi-taut[3]

[2] http://dredgingengineering.com/moorings/lines/Offshore%20mooring%20lines%20mooring%20system.htm

[3] https://www.windpowermonthly.com/article/1318520/windtech-aerodyn-two-blade-floating-8mw-scd

Catenary mooring systems, which are used with spar-buoy and semi-submersible platforms, consist of free hanging lines. These systems provide restoring forces through the suspended weight of the mooring lines, which terminate at the seabed horizontally. The anchor point is only subjected to horizontal forces at the seabed. Taut leg systems are used with TLPs and have mooring lines that are pre-tensioned until they are stretched. These mooring lines terminate at a 30°- 45° angle at the seabed. As a result, the anchor points are loaded by both horizontal and vertical forces.

Table 3 summarizes the differences between taut leg and catenary mooring systems and the advantages and disadvantages associated with each system.

Based on stability test preparations standards (46 C.F.R. § 170.185, 2012), each of the mooring lines must be arranged in a way that does not restrict the inclination of the FOWT unit during its stability test. After the installation of a mooring system, information related to the system should be documented and transmitted to all relevant parties (API RP 2SK, 2005). This information includes, but is not limited to, the following:

- heading and global position of the structure;
- individual line headings;
- initial and final anchor locations;
- general conditions, composition, length and location of all mooring like sections;
- location, number, general conditions and type of connectors (e.g., shackle, connecting links, subsea connectors, etc.);
- type, size, general condition, serial number and fluke angle of anchor;
- test load at fairlead and anchor shackle as well as estimated anchor drag distance; and estimation of accuracy of mooring pretension and mooring line angle at fairlead.

Table 3. Comparisons of Catenary and taut leg mooring systems (James and Ros, 2015).

	Catenary	Taut Leg	Semi-taut
Material	Steel chains/wires whose weight and curved shape keeps the floating platform in place	Fibers/wires made of synthetic materials to maintain high tension between the floater and anchor, and keep the floater stable	Fibers/wire made of synthetic materials are integrated to the turret system
Footprint	Part of the chain rests on the seabed which makes a large footprint	Minimal disruption to the seabed which leaves a small footprint	It creates relatively lower disruption to the seabed than catenary system, thus leaving a medium footprint
Type of loading	Experiences horizontal loading at the point of anchoring	Encounters vertical loading at the point of anchoring	Action of loading happens at 45° to the point of anchoring
Movement	Allows more horizontal movement than taut leg	Allowance for horizontal movement is very small	Although the allowance for horizontal movement is limited, the floating structure can rotate around the turret system
Installation Process	Relatively uncomplicated	Relatively complicated	Relatively uncomplicated

2.1.3 Anchoring Systems

Based on the mooring system and seabed condition and the holding capacity, different anchor systems are available for use. The catenary mooring system is usually used with drag-embedded anchors, and taut leg mooring systems use drive piles, anchor piles, or gravity anchors. James and Ros (2015) discussed several anchoring systems for mooring configurations. The attributes of the different kind of anchoring systems is summarized in Table 4. These systems have been used extensively in the oil and gas industries.

Table 4. Characteristics of different anchoring systems for FOWT mooring (James and Ros, 2015).

	Drag-embedded	Driven pile	Suction pile	Gravity anchor
Seabed suitability	Mostly applicable to cohesive sediments	Suitable for a wide range of soil condition	Limited application due to right soil conditions; not suited in loose sandy soils or stiff soils	Needs medium to hard seabed condition
Type of load handling	Horizontal	Vertical or horizontal	Vertical or horizontal	Usually vertical , but also horizontal
Difficulty of installation	Simple installation process	Because of hammer piling, creates noise during installation	Relatively simple installation process	Can have higher installation cost
Recovery	Recoverable during decommissioning process	Difficult to remove during decommissioning	Easy to remove during decommissioning	Difficult to remove during de-commissioning
Mooring system suitability	Mostly used by catenary mooring system	Applicable to taut leg mooring system because of its capability to handle vertical loading		

The embedment depth of the anchor depends on the various factors such as the unit weight of the soil, ultimate pullout capacity and the area of the anchor. Dietrich (2014) presented the following equation that can be used to determine the embedment depth of an anchor:

$$H = \frac{Q_u}{\gamma * A * N_\gamma}$$

Where *H* is the embedment depth of the anchor, Q_u is the ultimate pullout capacity, γ is the unit weight of the soil, A is the area of the anchor, and N_γ is a dimensionless number that represents the ultimate anchor capacity.

The properties and configuration of the station-keeping system of FOWT depends on various features of its mooring system (ABS, 2013). These characteristics are:

- Type of mooring/tendon system;
- Arrangement and number of mooring lines;
- Type of material used for constructing mooring/tendon line components, especially elasticity of the mooring line;
- Length of mooring line;
- Pretension;
- Anchor type along with its size and holding capacity;
- Linking between the hull and the station-keeping system; and

- Types, properties, and fatigue resistance of other components of mooring system such as windlass, winches, fairleads, inline buoys, clamp weights, chain stoppers, etc.

For example, to hold the FOWT, DTL (2016) proposed drag embedded anchors to be installed in gravelly sand. To increase the holding capacity, it is suggested that more than one anchor be connected to each mooring line. Stevpris Mk 5 (30 ton) anchors, which are approximately 9 m wide and 9 m long, are suggested to be used and capable of penetrating approximately 10-15m into the seabed. However, penetration length in a specific location is dependent upon seabed conditions.

2.1.4 Cables

The power transmission systems for FOWT are another critical part of the technology which need to be carefully analyzed. When particularly considering the size of substations and the severe impact of power outages, a conservative methodology is needed to select appropriate cable materials. Different methodology and concepts have been proposed for power transmission of FOWT due to their frequent motion, and also subjectivity to crossing faults.

For power transmission from turbine to shore, export cables are used that will have copper or aluminum conductors insulated by Cross-Linked Polyethylene or Ethylene Propylene Rubber (Sharples, 2011). The insulation is covered with a lead allow sheath, which works as an insulation screen and makes the insulation watertight. The suggested export cable for FOWT is 33 kV cable, which is consistent with the industry standard specification to prevent the direct emission of electric fields. DTL (2016) suggested that 80% of the export cable length should be buried to water depths between 1m and 2m using ploughing and/or jetting installation techniques. The rest of the export cable length may require protection through concrete mattresses or rock dump. The maximum width and depth of cable protection will be 8m and 0.5m, respectively. Sharples (2011) noted power cables for FOWT might need to be different than the cables used with fixed foundation turbines, as FOWTs are subjected to frequent motion. This researcher suggested copper might be the preferred material for sheathing of FOWF electrical cable design since it is resistant to fatigue; very malleable; and more tolerant to large bending deflection than lead.

Taninoki et al. (2017) also developed a dynamic cable system that can transmit power to the shore from FOWT facilities subject to significant movement. While traditional submarine cables are installed on the seabed, the cables for FOWT have floating components which allow the cable to move with the floater (Figure 10). The study used a 6.6 kilovolt (kV) cable with waterproof layers provided around its cross-linked polyethylene insulation. The cable was continuously subject to bending and twisting forces caused by the tidal current and floater behavior; as a result, the cable was likely to suffer mechanical damage in various sections. However, the study showed that the dynamic cable system performed well during the demonstration period without any safety issues.

Sharples (2011) also discussed the potential use of umbilical power cables as submarine cables for FOWT. Umbilical cables have been used for electric dredgers. Although the average lifetime for this cable in protected waters is presently about 6 years, it can be extended to 10-15 years by using advanced technology. Based on the advice of the operators of electric dredgers, it is important to have a subsea connecting point underneath the FOWT unit to allow for a changeout of any cable when it is necessary. The electric cables used in these dredgers mostly have double armor with a polyurethane protection on the outside.

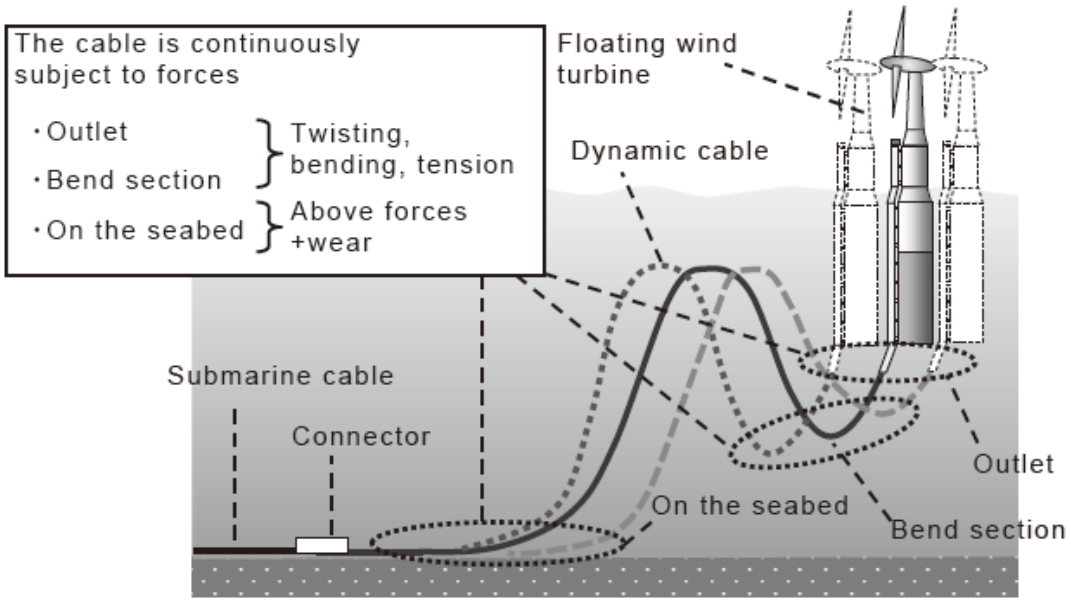

Figure 10. Schematic of cable connection to a FOWT facility (Taninoki et al., 2017).

Wham et al. (2016) conducted a study to assess how Steel Pipe Crossing Faults (SPF) can handle axial and bending deformation and evaluate the capability of SPF and its "wave feature" (Figure 11) to accommodate fault rupture and other ground movements that are in the area of the pipeline.

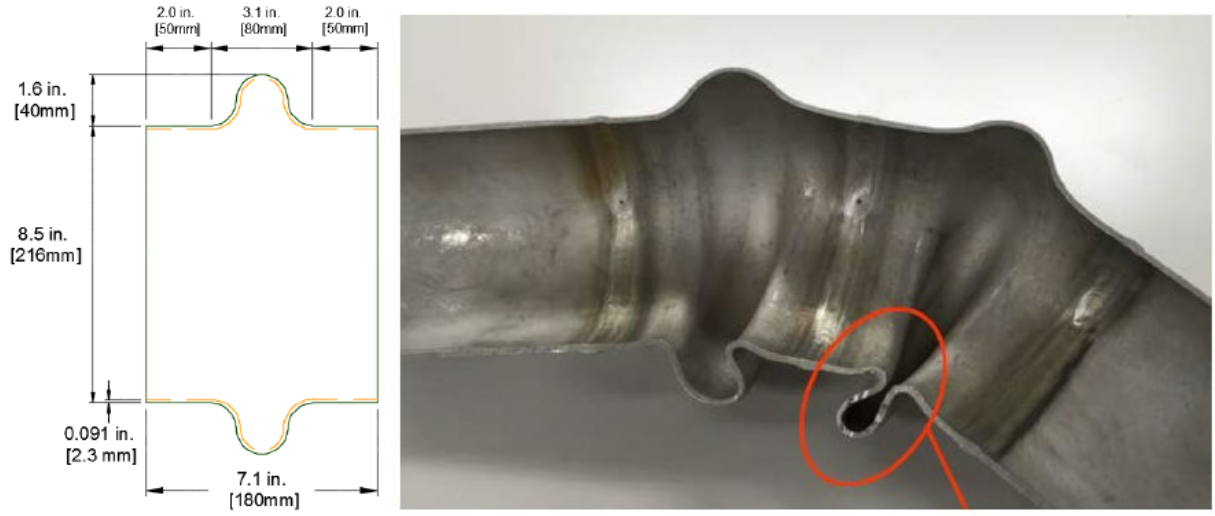

Figure 11. Geometry of SPF Wave Feature (left panel) and cross-section of deformed Wave Feature (right panel) (Source: Wham et al., 2016).

The experiment demonstrated that the pipeline has the capability to handle significant fault movement with the help of axial movement and the deformation of the wave feature (Figure 11) without any pipe rupture. The measurements recorded also explain how the fault movement was handled by the wave absorbing stresses enforced on the rest (i.e., straight part) of the pipeline. Therefore, steel pipelines can be used as a shield of power transmission cable of FOWT in an area with earthquake and fault rupture hazards.

For protecting the power transmission system of FOWT from various geohazards, the concept of using iPVC pipe was investigated by Price et al. (2018). The study focused on the performance of pipelines made of iPVC pipe in response to ground movement, and suggested using a 15cm-diameter DR 18 AWWA C900 iPVC pipe with restrained joints to handle ground deformation. The primary focus of the study was to evaluate the performance of iPVC pipe during fault movement; however, the results can also be used to assess pipeline performance under other geohazards such as landslides and liquefaction. The test successfully handled significant ground deformation during the simulation of fault rupture through axial deformation and flexure, as well as rotation of the joint and pipe barrel. The study researchers also found the amount of fault movement that can be handled by the iPVC pipeline is a function of the burial depth of the pipe, as well as the spacing of linkages relative to the ground site.

2.2 Case Studies: Configurations of Support Structure for FOWT

As there are not many operational FOWF, two case studies by ABS (2013) and Dagher et al. (2015) were reviewed to illustrate different configuration of FOWF.

The case study conducted by ABS (2013) adapted three conceptual designs of the floating support structures from OC3-Hywind Spar, the MIT/NREL mono-column TLP, and the generic WindFloat semi-submersible concepts for installation in the U.S. outer continental shelf. Among the designs of FOWT foundations, the spar type was tested only in Oregon, while TLP was analyzed in Oregon and Gulf of Mexico. The semi-submersible type was tested in all three case study sites, including the northeast and west coasts of U.S. and Gulf of Mexico (GoM). The goals of each case study included:

- studying dynamic interactions among the turbine rotor and control system, floating support structure, and station-keeping system; and
- gaining further insights into the study critical design parameters and modeling strategies for station-keeping systems.

Adjustments to the original designs were made to fulfil the case study requirements for the 100-year return storm conditions in the GoM Central Region. The main aspects of the adapted conceptual designs of the floating support structure are summarized in Table 5.

Table 5. Main parameters of the support structures for FOWT (Source: ABS, 2013).

	Spar (for West and Northeast Coasts)	Spar (for GoM Central Region)	Semi-Submersible (for all sites)	TLP (for all sites)
Draft	120 m	120 m	17 m	47.89 m
Displacement	8230 ton	10279 ton	4640 ton	12485 ton
Column Diameter	6.5m – 9.4m (tapered)	6.5 m – 10.6 m (tapered)	10 m	18 m
Center of Gravity below Still Water Level	89.474 m	89.56 m	8.098 m	38.154 m
Mooring System	3 lines	3 lines	4 lines	8 lines
	902.2 m length each line	1000 m length each line	80 m 4-inch top chain; 718 m 5-inch polyester rope; 80 m 4-inch bottom chain	163 mm spiral wire rope
	77.7 kg/m dry weight per unit length	68.7 kg/m dry weight per unit length	-	-
	970 kN pretensions	3000 kN pretensions	975 kN – 1000 kN Pretension	6000 kN Pretension
	-	45 ton clump weight on each line	30 ton clump weight	-
	-	-	-	35 m tendon fairlead radius

ABS (2013) analyzed both mean and dynamic loads generated by wind, wave and current for all three types of FOWTs. One of the key findings for the Spar FOWT located in Oregon was that wind loads were larger than the combination of viscous drag and the wave drift loads in average. However, the dynamic loads from waves were higher than the ones from wind. For this reason, it is crucial to determine the wave load (e.g., the load caused by hazards such as tsunamis) in study areas.

The other case study was described by Dagher et al. (2015). The study discusses the design, construction, deployment, testing, retrieval, and inspection of a semi-submersible FOWT, Volturn US in Maine, which is the first grid-connected FOWF demonstration in the U.S. The Volturn US 1:8 scale model was designed and constructed using full-scale structural materials, arrangements, and methods while preserving desired hydrostatic and dynamic characteristics established by dockside testing.

The general properties of these Volturn model and full-scale system are summarized in Table 6. The assembly of the hull, tower, and turbine all took place on land at the Cianbro Modular Manufacturing Facility in Brewer, Maine. The test of the Volturn US prototype showed the catenary mooring system can be successfully used as part of the station-keeping system of the semi-submersible FOWT.

Table 6. General properties of the 1:8 scale and full-scale systems for Volturn US.

Parameter	Volturn US (1:8 Scale)	Volturn US (Full-Scale)
Draft	2.9 m	20 m
Hub Height	12.2 m	100 m
Rotor Diameter	9.6 m	152 m

Parameter	Volturn US (1:8 Scale)	Volturn US (Full-Scale)
Rated Power	12 kW	6 MW
Peak Thrust Load	1.37kN	700kN
Hull Material	Concrete	Concrete
Tower Material	Composite	Composite
Water Depth	15-27 m	100 m
Number of Mooring Lines	3 x catenary chain	3 x catenary chain
Anchors	Drag Anchor	Drag Anchor

While the aforementioned case studies have been useful in terms of understanding features of FOWT concepts, similar studies should be done focusing on geological hazards to understand their impacts on FOWT supporting structure.

3 EXISTING STANDARDS ON GEOHAZARD CONSIDERATIONS FOR FOWF

Environmental conditions affect the installation, commissioning, performance, and decommissioning of FOWF developments. In order to ensure the safe operation of a FOWF, it is important to understand the effects of geohazards on the floating structure that supports the turbine along with its mooring system and power transmission system to the grid. Seismic activities can impact FOWT in the form of ground motions as well as by associated sudden wave loading. These loads can cause failure of mooring line, scouring of the foundation and damages to the power transmission cable. As FOWT may be deployed in areas susceptible to earthquakes, the design of FOWT must consider the fault conditions relevant to the power transmission system, the seabed condition at the site, and the liquefaction or mud failure and consequent scour effects on the mooring. In addition, the loads generated by seismic activity on the mooring system and buried cables should be investigated. The impacts of earthquake triggered tsunamis on the FOWT should be considered as environmental loads beyond normal conditions. The range of expected variations of environmental conditions should be calculated by statistical models and probabilistic methods.

In addition to earthquake and tsunami loads, there are other environmental loads that are variable in magnitude and direction over time. Landslide and slope stability require investigations based on the conditions of a specific site. While finalizing the siting and design of FOWF developments, wind loads; hydrodynamic loads induced by waves and current, including drag and inertia forces; tidal effects; marine growth; and snow and ice loads should also be taken into account (ABS, 2013).

There are several standards and studies that have addressed different aspects of external forces caused by tsunami waves on FOWT components. While analyzing tsunami wave loading for a FOWT, ISO 19901-1 (ISO, 2015) suggested emphasis should be given to the exposure of the FOWT site to the potential directions of tsunami wave approach and related earthquake-induced currents. Although for most offshore structures, the environmental loads are dictated by extreme wind-generated waves, the very long periods of tsunami waves can make significant impact on moored floating structures. As tsunami wave heights can drastically increase due to shoaling and refraction, special attention should be paid to sites located in shallow water near complicated bathymetry. If the FOWT is installed in deep water, the environmental loading on the structure caused by tsunamis can be characterized by variation of sea surface elevation and horizontal currents. If the natural period of a station-keeping system is close to the wave period of tsunami, resonant responses of the station-keeping system should be examined. A usual wave period of tsunami is in the range from 5 minutes to 60 minutes in the area close to the epicenter (Goto, 1993) and in the range from several hours to 30 hours in the area far from the epicenter (IEC, 2019). BV (2019) also recommended that while designing FOWT, hydrodynamic loads from tsunami waves resulting from sub-sea earthquakes need to be considered for units of the gravity-based anchor type. More detailed examples of needed analyses in regard to tsunami waves are presented in Appendix B.

It should be noted that this report does not recommend any specific standards to follow, and is an overview of relevant existing standards. Additionally, BOEM approves technical standards proposed by the lessee on a project-case basis.

3.1 FOWT Platform

To assess the impact of earthquakes and tsunamis on a FOWT platform for a particular site, the expected seismicity of an area should be established based on regional and site-specific data. Examples of such data include magnitudes and recurrence intervals of seismic events; proximity to active faults; type of faulting; attenuation of ground motion between the faults and the site; subsurface soil conditions; and records from past seismic events at the site (ABS, 2012). The FOWT system can also be impacted by an earthquake-triggered shock wave. This shock wave can travel upward through the water column causing an abrupt impulsive action on buoyant or semi-buoyant structures, thus resulting in an increase in hull pressures and tendon/mooring line forces. However, this situation is only possible for the Abnormal Level Earthquakes (ALE) (ISO, 2004). ALE represents severe earthquakes under the action of which the structure should not suffer complete loss of integrity. In addition to ground motion, other earthquake-related phenomena such as liquefaction of subsurface soils, submarine slides, and tsunamis should be considered. Several standards and publications have focused on these natural hazards from various perspectives and using different methodologies, and they are reviewed in this report section.

Yoshida et al. (1996) investigated the effects of tsunamis and seaquakes on large floating structures, indicating the necessity of considering the effects of tsunamis on the design of a large floating structure. The findings of the study are:

- the effects of tsunamis are minimized when a floating structure is set at a depth of at least 40 m to 50 m;
- chain length should be determined by equalizing the breaking weight with the load at which the structure starts to move; and
- a structure should be set at a position in which it is not attacked by a transverse wave (a moving wave that oscillates in perpendicular direction to the direction of the wave).

DNV-OS-J101 (2004) also discussed how the load effect of tsunamis on the wind turbine structure can vary based on the site-specific depth. It also suggested that an acceptable approach to account for load impacts generated by tsunamis on wind turbines is to compute the loads for maximum sea wave that can occur on the site for a specified water depth. In deep waters, tsunami wave crests are usually too small to be noticeable by ships. However, as it travels from deep waters to shallower waters, the wave crest becomes amplified. As a consequence, the effect of tsunamis is related to water depth. The impact of tsunamis is also related to the motions that are restrained by mooring lines. If the area of wind turbine installation is seismically active and the structure can be impacted by earthquakes, an assessment should be made of the local and regional geology to determine:

- the site and alignment of faults as well as focal and epicentral distances;
- the source mechanism for releasing energy; and
- attenuation characteristics from the source to site.

This is especially applicable for areas where the record of seismicity is available. However, if detailed information regarding seismic activity is not available, the seismicity should be determined from comprehensive investigations including a study of the seismic events as well as the geological history of the region.

Chock (2015) also investigated tsunami impacts on structures; however, unlike other research this study analyzed the impacts from a structural design perspective. Based on the findings of Chock (2015), the following loads should be considered for the structural design:

- buoyant force, hydrostatic and additional fluid gravity loads from retained water;
- hydrodynamic uplift forces;
- forces from debris impact; and
- pore pressure softening impacts on soil and foundation scour.

ASCE (2010) also examined various design loads on structures including wave and seismic loads. It should be noted that ASCE (2010) is not focused on floating structures; however, in order to provide an overview of recommendations through different standards the main objective of that study is applicable to this discussion. Wave loads are generated by waves at the sea surface. If a structure has the potential to experience wave loads in its lifetime, there are several things that should be taken into account while designing and in the manufacturing process. These loads include:

- uplift forces under the structure caused by change of wave height while entering shallow water;
- waves breaking or wave runup encountering any part of the structure; and
- drag, inertia forces and scour caused by wave at the base of the foundation.

ASCE (2010) also states that in case of a seismic event, the structure should have a force-resisting system (both lateral and vertical) to help it withstand the design ground motions, which can occur along any horizontal direction of a structure. The adequacy of strength of the structural systems should be evaluated with the assistance of a mathematical model. During the process of foundation design, several factors need to be considered such as the expected ground motion and the dynamic nature of seismic force, energy dissipation and strength of the structure, and the soil properties. Application of these factors in design procedures will make the structure foundation capable of handling the seismic forces, as well as the movements transferred to the structure by the design ground motions.

Among all three major types of FOWT, spar type structure has been the first commercially successful in the building a FOWF (Driscoll, 2016). Therefore, it is imperative to understand the impact of seismicity on this type of FOWT. Kokubun et al. (2013) discussed the effects of earthquake and tsunami on spar type FOWT using a numerical simulation. The model results are based on the assumption that the installation site has a water depth of 150 m. The study found that the minimum breaking load of the mooring chain, which is designed for storm condition, is sufficiently (8 times) bigger than the maximum tension of the chain under a strong earthquake condition. The external condition for FOWT caused by a tsunami was represented by variation of water surface elevation and horizontal current, which is based on the Tohoku earthquake and tsunami (Mori et al., 2011). The variation of water surface elevation (5.22 m) is equivalent or less than wave height in a typhoon around Japan, while the current velocity (1.3 m/s) caused by tsunami is equivalent to the ocean current or tidal current around Japan. However, a separate analysis is needed to examine the potential for vortex-induced motions of FOWT system caused by tsunami currents. An example of this analysis is presented in Appendix B.

As with Spar type, TLP type FOWT can also be an applicable solution in FOWF developments in regions with geohazards. Shaji and Retnamma (2016) carried out an analysis on the impact of earthquake-generated random waves on Mini-TLP. The study found that the maximum response due

to earthquakes decreases as the depth of the mini TLP site increases. This decreased rate of response is more in heave motion than in surge and pitch motion.

The magnitudes of the parameters characterizing the earthquakes with return periods relevant to the design life of the structure should also be determined for the structural analysis of a FOWT (ABS, 2013). The return period of earthquakes should be considered based on the probability of occurrence during the wind turbine's lifetime. GL guidelines (GL, 2003) and IEC guidelines (IEC, 2005) discussed attributes of the design level earthquake which has a 475-year return period event. A 475-year return period is equivalent to a 10% probability of occurrence for a wind turbine with 50 years lifetime. If the lifetime is shortened to 20 years, the return period of the same earthquake will have a 4% probability of occurrence (Powell and Veers, 2009). The resulting loads must be combined with the greater of the lifetime-averaged operating loads or the emergency shutdown loads (Powell and Veers, 2009).

API RP 2T (2010) stated floating offshore oil and gas production installations are generally considered to have a Level 1 exposure level, which requires 100-year return environmental conditions for design assumptions. The report required the following two levels of earthquake conditions be evaluated to address the risk of damage and failure of tendon foundation, respectively:

- Strength Level Event (SLE): Ground motion which has a reasonable prospect of not being exceeded at the site during the design life of a FOWT; and
- Ductility Level Event (DLE): Ground motion for a rare, intense earthquake to be applied to examine the risk of failure of tendon foundation of TLP-type floating structure (ABS, 2012).

As TLP is widely used in the offshore production of oil and gas, there are available regulations that address strength analysis of this type of structure along with its tendon tension. For TLP type FOWT, consideration of earthquake can significantly impact the design process as the sensibility to earthquake is related to the motions restrained by tendons (DNVGL-ST-0119, 2018). Based on API RP 2T (2010), for a TLP site in an earthquake-prone location, appropriate time histories of ground acceleration should be collected. For tendon tension responses in a TLP, vertical ground motion is more important than horizontal ground motion. However, for foundations, both vertical and horizontal motion are crucial. During the calculation of maximum tension, both tension variation from wave forces and wave-induced vessel motion should be considered. Although this regulation discussed the importance of wave forces in TLP design, there is a lack of regulations that mandate the analysis of hydrodynamic loading from extreme events (e.g., tsunamis) which can be of great importance in a seismically-active area.

ABS (2013) and DNVGL-ST-0119 (2018) also discussed tendon tension from a seismic impact perspective. ABS (2013) states for the TLP-type floating support structures, the robustness assessment under survival load cases should consider the determination of minimum tendon tension. When assessing the load with one-tendon removed, the robustness check for the tendon system should be subjected to a 50-year return extreme environmental event. Moreover, fatigue damage caused by a single extreme environmental event in the tendon system with a return period of 50 years should be investigated. DNVGL-ST-0119 (2018) proposed an alternative tendon design in TLPs based on the Accidental Limit State (ALS) rather than using Ultimate Limit State (ULS). ALS encompasses survival conditions in a damaged condition or in the presence of abnormal environmental conditions, while ULS corresponds to the maximum load-carrying resistance. While using ALS, the characteristic environmental dynamic compressive force in the tendon should be assumed as the dynamic compressive force with a return period 500 years.

However, ISO 19901-2 (ISO, 2004) suggested a two-level seismic design approach should be followed for FOWT design. The structure should be able to meet ULS for strength and stiffness. The seismic ULS design event is the Extreme Level Earthquake (ELE), which is similar to, but not exactly the same as the SLE (API RP 2T, 2010). Once the structure meets the ULS strength, the structure should be checked to make sure it meets the ALS. The ALS design event is the ALE which is similar to, but not exactly the same as the DLE (API RP 2T, 2010). Checking the structure to ALS confirms that it meets the necessary requirements for reserve strength and energy dissipation. Also, according to the requirement of ISO 19901-2 (ISO, 2004), addressing the ALE requirements would comprise consideration of riser stroke, mooring line rotation angle, and similar geometric allowances. For TLP-type FOWT, a design process is recommended to avoid catastrophic system failure in the ALE, especially considering extreme displacements and shock waves in the mooring system. This process is necessary due to the absence of well-defined seismic reserve capacity factor (Cr) for TLP-type FOWT. Cr is a function of static reserve strength and represents the ability to sustain large non-linear deformations of each structure type.

DNVGL-ST-0437 (2016) suggested during the application of seismic response spectrum, it must be ensured that the recurrence period is consistent with the chosen method of analysis and a three-dimensional model of the structure should be used. For various design load case scenarios, different combinations of earthquake loads with other loads should be considered, assuming:

- the scenario of an earthquake while normal operation of the turbine;
- a combination of the earthquake and a shut-down procedure possibly activated by the earthquake;
- a grid failure and activation of the safety system triggered by earthquake detecting vibration sensor; and
- a combination of the earthquake and a previously occurred grid loss.

DNVGL-ST-0437 (2016) also states a dynamic response analysis (due to seismic loading) should be performed using accepted procedures such as response spectrum analysis and time history analysis. Seismic activity can cause dynamic loading on the wind turbine, where structural dynamics and coupling of vibration could occur. It should be noted that DNVGL-ST-0437 (2016) is not designated for floating structures; however, the recommendations are helpful in understanding similar concerns and considerations.

Although existing standards (ABS, 2013) suggest considering the return period of extreme environmental (e.g., hurricane) conditions for designing offshore structures, for the design of FOWT structures Yu et al. (2011a; 2011b) suggested the return period of environmental conditions should be determined by the total design approach and not just the return period of metocean conditions. However, specific guidance on the return period of geological hazards that need to be considered for safe deployment of FOWT application are yet to be developed.

3.2 Anchorage and Mooring

Geotechnical conditions and soil type are important factors in choosing the right anchoring system with the goal of being able to maximize the holding capacity while having flexibility over the choice of anchor type. For a site-specific FOWF development, the appropriate type of mooring and anchoring should be determined based on the characteristics of the seabed. BV (2019) also recommended that while designing FOWT, earthquake loads, as well as hydrodynamic loads from tsunami waves resulting from sub-sea earthquakes, need to be considered for units with the gravity-based anchors.

DNV-OS-J103 (2013) discussed properties of soil in regard to the structural design and anchoring system of FOWT. The soil conditions should be determined in the positions where the FOWT station-keeping systems are anchored. These anchor positions are known as foundation positions, as they can be different from the position of floating structure, which can be located some distance away from the foundation positions. The optimal conditions depend on the selected anchoring system, but typically involve cohesive soils, which are not too stiff to allow for penetration into the seabed and not too loose to limit the resistance of the soils (James and Ros, 2015). Based on DNV-OS-J103 (2013), a typical range of soil properties are summarized in Table 7.

Table 7. Soil parameters for both cohesionless and cohesive soils (DNV-OS-J103, 2013).

Class	Soil Type	Friction angle φ	Undrained shear strength S_u (kN/m^2)	Submerged unit weight γ' (kN/m^3)	Poisson's ratio ν	Void ratio e
Cohesionless	Loose	28 – 30º	-	8.5 – 11.0	0.35	0.7 – 0.9
	Medium	30 – 36º	-	9.0 – 12.5	0.35	0.5 – 0.8
	Dense	36 – 41º	-	10.0 – 13.5	0.35	0.4 – 0.6
Cohesive	Very soft	-	< 12.5	4 – 7	0.45	1.0 – 3.0
	Soft	-	12.5 – 25	5 – 8	0.45	0.8 – 2.5
	Firm	-	25 – 50	6 – 11	0.45	0.5 – 2.0
	Stiff	-	50 – 100	7 – 12	0.45	0.4 – 1.7
	Very stiff	-	100 – 200	10 – 13	0.45	0.3 – 0.9
	Hard	-	> 200	10 – 13	0.45	0.3 – 0.9

API RT 2SK (2005) suggested that if site-specific soil data is unavailable, upper and lower bound soil conditions for the operations area of the floating structures should be assessed. But in case the soil conditions are unusual (e.g., under-consolidated/over-consolidated soil, shallow cementation, sand layers), seabed characteristics should be detected by the help of 3-D seismic data, usually analyzed in support of exploration plan submission for drilling (30 C.F.R. § 250.201, 2017). The 3-D seismic data interpreted characteristics that present signs of unusual soil conditions include but are not limited to shallow gas and mass transport deposits, erosion features (e.g., canyons, furrows, etc.), and seafloor faults and expulsion features. If the selected continental shelf area has very limited seismic data available for identifying shallow geological features, a dedicated site survey and soil sampling may be required.

The foundation of FOWT is vulnerable to scouring if the anchoring system is not protected. To prevent the FOWT from being susceptible to seabed erosion, the seabed around the base of the anchors can be secured in several ways such as sandbags, grout-filled bags, stone bags, artificial seaweeds, etc. (DTL, 2016). These methods can be used to minimize the impact of scours on FOWT foundation and the export cables. The most common scour protection system is placing crushed rocks around the cable and anchors. However, the footprint of the scour protection should not exceed a height of 2 m from seabed and should not go beyond 20 m radius from the center of the anchor. The diameter of the crushed rocks should be between 0.06 m and 0.65 m. If a drag anchor reaches the target burial depth of 10-15 m, no scour protection is required.

There are several studies that examined the impact of earthquake on the foundation and anchoring system of TLP type FOWT. Kawanishi et al. (1987a) analyzed the response of a TLP pile foundation when it is subjected to an earthquake. Based on the study, it was suggested that increased spring constant of the pile reduces the maximum relative displacement. Also, the uplift capacity of the pile

foundation must be more than twice the amount of net buoyancy. Kawanishi et al. (1987b) suggested that the horizontal component of seismic force can be ignored as the bending rigidity of the mooring line is almost non-existent. However, the vertical component of the earthquake generated force must be considered as a crucial aspect for FOWT design as it is directly added to the tether pretension directly. The study also found that to cope with the earthquake load, the weight of the gravity anchor in water must be more than two and half times the amount of mooring line pretension. Kawanishi (1991) suggested the vertical component of the seismic factor should be considered an important factor in a TLP design because it directly affects the pretension of the tendon. Rijken and Leverette (2007) also analyzed response measurements of a deepwater TLP to a significant earthquake which occurred about 9.4 miles away from this platform in the GoM. The study found the dynamic tension levels caused by the earthquake were significantly smaller than the extreme tensions under storm and hurricane conditions. The accelerations occurred mainly along the vertical axis with maximum amplitude of 0.005 G.

The FOWT system can also be impacted by an earthquake triggered shock wave. This shock wave can travel upward through the water column causing an abrupt impulsive action on buoyant or semi-buoyant structures; thus, resulting in an increase in hull pressures and tendon/mooring line forces. However, this situation is only possible for the most severe earthquakes (ISO, 2004). In order to provide failure of mooring lines, it is important to make sure that maximum tendon tension calculated in extreme conditions is well under the tendon breaking strength with a sufficient safety factor. Suzuki et al. (2010) also carried out numerical analyses on the dynamic response of a TLP when subjected to seismic force. One of the main objectives of this study was to evaluate the safety factor considered for the model to seismic force (Figure 7). The conceptual design of the TLP had 241 wires in total with each of the wires having a 7 mm diameter. The breaking stress of the wire was assumed to be 1570 N/mm^2. For the dynamic response analysis, maximum amplitude of velocity was considered to be 25 cm/s from a rare seismic load. The study found that tendon tension is well within the design value when subjected to a rare earthquake. Also, the safety factor (3.0) was shown to be sufficient to keep the TLP safe during earthquake.

Unlike TLP or taut-line mooring systems, a catenary mooring system is not impacted by earthquakes because of the small stiffness (IEC TS 61400-3-2; IEC, 2019). The dynamic tension caused by the earthquake causes all three translational motions (surge, sway and heave) for taut-line mooring, but only heave motions for the station-keeping of TLP-type FOWT. However, for the design analysis of substructures of a FOWT system with multiple mooring lines, it is crucial to consider different phases of forcing for different anchor points to cause rolling and pitching motions (IEC, 2019).

3.3 Power Transmission Cables

Earthquakes, landslides, and turbidity currents generated by earthquakes are well-documented geohazards. Several studies demonstrated the vulnerability of submarine cables to landslides and turbidity currents, especially in earthquake-prone regions. As the cables are spread out over the shelf to the coastline, they are the most vulnerable part of the FOWF development. For them to function throughout the lifetime of the FOWF development, it is necessary to avoid direct fault areas and have monitoring and emergency response plans for earthquakes and tsunamis, and apply standards and regulatory recommendations.

Krause et al. (1970) showed turbidity currents can cover long distances and great depths and consequently damaging the cables. For instance, turbidity currents generated by an earthquake near the Markham River delta off Papua New Guinea, disrupted cables at least 280 km away in water

depths of over 6,600 m (Carter, 2010). In the aftermath of the 2003 Boumerdes earthquake (magnitude 6.8), landslides and turbidity currents damaged six cables off Algeria to disrupt all submarine networks in the Mediterranean region (Joseph and Hussong, 2003). In 2006, nine submarine cables broke under an earthquake-triggered flow in southern Taiwan (Hsu et al., 2009).

Sharples (2011) proposed several ways to mitigate impacts of seismic activity on submarine cables, including:

- circumventing direct fault areas when selecting the route of submarine cable;
- providing sufficient length to the submarine cable if areas of strong seismicity cannot be circumvented, and laying it in the direction of the fault line;
- enhancing the deformation capability of the submarine cable;
- building a secondary cable with a backup route for important submarine cables; and
- developing a submarine earthquake monitoring and emergency repair plan.

Sharples (2011) stated design provisions in the codes for the submarine cables should consider the maximum displacement from an earthquake with a 1,000-year return period when the structure is designed for a 100-year return period. This researcher suggested laying spare cable parallel to the fault line direction to minimize the probability of damage for smaller quakes.

In addition to earthquakes, tsunamis may also cause damage to submarine cables, especially along coasts vulnerable to wave attack. When the wave propagates towards the shore in shallow water, the height of the wave increases due to bottom friction. The action of bottom friction on the soil caused by wave approaching shore in shallow water and receding water from the shore creates the possibility for scour. If cables are buried in sandy sediments, liquefaction can also cause cables to become exposed and thus vulnerable. These instances should be considered when selecting the burial depth of submarine cable near the shore. Submarine cables can also be damaged by tsunami debris washed offshore (Strand and Masek, 2005). Therefore, in addition to the mitigation and technology discussed in Section 2.1.4 for the hazardous regions, a more comprehensive site-specific feasibility study is needed for the regions where crossing the major active faults is unavoidable.

4 SITE SELECTION PROCESS FOR FOWF DEVELOPMENT

For selecting suitable sites for FOWT, several factors should be considered to evaluate potential effects in the environment and possible socio-economic impacts. Malhotra (2011) discussed the role of various environmental and economic factors in the site selection process of the offshore wind turbine foundation. Diaz et al. (2019) developed and implemented a methodology to comprehensively evaluate the feasibility of areas for FOWT siting near Madeira Island (Portugal). The methodology for site selection of FOWT can be divided into four major process steps: data collection, exclusion criteria, evaluation criteria, and finalizing locations. This report section provides a review of the steps to select a suitable site location in relation to geohazards.

4.1 Data Collection

The methodology starts with collecting data that can affect the site selection process and the development and deployment of FOWT. The necessary datasets must encompass not only the oceanographic and atmospheric parameters such as ocean currents, temperatures, wind statistics, and wave spectra, but also geotechnical investigation to detect subsurface conditions. The presence of an unexpected geological feature (e.g., paleochannel) or foreign object (e.g., shipwreck, abandoned pipeline, anchor) can negatively impact the installation cost of the wind turbine foundation and cable pathways. To analyze the subsurface conditions, Malhotra (2011) suggested a three-step geological analysis in the following order:

- Desktop study of the geology of the potential installation area;
- Survey of bathymetry and geophysics; and
- Cone Penetrometer Test (CPT) along with geotechnical boring.

CPT is an *in situ* method of determining geotechnical properties of soil. The apparatus used for CPT consists of a cone with its tip facing down and at a usual apex angle of 60°. The cone is connected to an internal rod which runs through an outer hollow rod. The outer rod is attached to a sleeve. While the cone is pushed into the soil, the resistance at the tip of the cone and the skin friction of the sleeve is measured which determines the strength of soil. Geotechnical boring involves making vertical holes in the ground, which allows engineers to get soil samples and assess their geotechnical properties. This study by Malhotra (2011) can assist with the first step of this recommended multi-step site selection process. There is a need for more site-specific data collection to analyze the suitability of different region for various purposes including locating the FOWT and mooring and cables.

4.2 Exclusion Criteria

In order to determine unsuitable areas for the siting of FOWT, a set of exclusion criteria should be developed. It is assumed that some of the exclusion criteria (e.g., military areas; maritime traffic; exploration and exploitation of hydrocarbons or minerals; environmental protected areas; and heritage areas) were already considered during the selection of the BOEM Call Areas for FOWT. However, there are other factors that can disqualify an area from being a potential site for FOWT. For example, areas with significant water depth can cause issues related to technical design and cost of FOWT (Diaz et al., 2019). Increased depth of FOWT deployment site adds difficulty in terms of

designing efficient mooring lines and anchors, and also increases the installation, operation and maintenance cost.

Malhotra (2011) discussed multiple geohazards that can make an area unsuitable for FOWT foundation. Examples of these geohazards include a fracture zone that involves seismic activity; a submarine slope failure; and rough seafloor in the path of the transmission cable. Also, a small slope in the site can make it vulnerable to submarine landslides, and can ultimately cause damage to the foundation and cables. The suitability maps presented in the upcoming report sections, provide an overview of some exclusive areas and more suitable regions based on the analysis of available datasets at the time of this study. However, more comprehensive data collection and analysis are needed to define exclusion areas for locating moorings, anchorages and burying cables based on soil type.

4.3 Evaluation Criteria

After the elimination of certain areas based on exclusion criteria (Section 4.2), some additional criteria need to be analyzed before siting of FOWT can be finalized. The evaluation criteria based on Diaz et al. (2019) and Malhotra (2011) are summarized and modified in Table 8.

Table 8. Evaluation criteria for site selection of FOWT (modified from Diaz et al., 2019).

Category	Evaluation Criteria	Objective
Metocean data	Wind velocity	**Maximize**
	Water depth	Minimize
	Wave conditions	Minimize
	Marine currents	Minimize
	Temperature	Minimize
Viability	Technical feasibility	**Maximize**
	Sufficient study times	**Maximize**
Proximity to facilities	Distance from shore	Minimize
	Distance to local electrical grid	Minimize
	Distance from coastal facilities	Minimize
	Distance from residential areas	**Maximize**
	Distance from the maritime routes	**Maximize**
	Distance from underwater lines	**Maximize**
	Distance to marine recreational activities	**Maximize**
	Distance from airport	**Maximize**
Marine environment	Distance from protected areas	**Maximize**
	Proximity to migratory birds' paths	**Maximize**

Category	Evaluation Criteria	Objective
	Proximity to migratory marine life paths	**Maximize**
Techno-economic data	Area of the territory	**Maximize**
	Proximity to the area of electric demand	**Maximize**
	Population served	**Maximize**
	Multiple competing resources	Minimize
Local geology	Submarine slope failure	Minimize
	Sea floor rupture	Minimize
	Rough sea floor	Minimize
	Seabed scouring	Minimize
	Seismic activity	Minimize
	Liquefaction potential	Minimize
	Lateral spread potential	Minimize
	Slope of seabed	Minimize
	Coral reefs	Minimize

4.4 Finalizing Locations

The eligible areas for the siting of FOWT in a lease block correspond to the regions that remain after the omission of certain areas based on exclusion criteria (Diaz et al., 2019). After evaluating the collected data for the eligible areas, the selection process of FOWT site can be finalized by maximizing and/or minimizing the relevant evaluation criteria. The maps generated in this report, which look at the geohazards in the region, can be used in parallel with the data collected from site surveys to finalize the site location and land use based on the soil type and type of structural components.

5 REVIEW OF POTENTIAL GEOHAZARDS

5.1 Seismic Sources in the Pacific Ocean

There are only a few detailed real case studies on seismic activity impacts on FOWT and its mooring and anchoring systems, due to scarcity of the seismic event and the fact FOWT is a new technology. As mentioned in previous report sections, it is highly recommended that the effect of earthquakes on different designs of FOWF be studied further after collection of site-specific data. Investigations provided in this report involve thorough research, review, and evaluation of all historically reported earthquakes that have affected, or that could reasonably be expected to have affected the site. In general, the horizontal motion of the sea bottom is transmitted through the mooring to the floating structure. The floating structure is practically isolated from the effects of an earthquake and the impact of the earthquake will be generally limited to the mooring system, or the effects could be due to direct seismic effects (i.e., shifting, tremors), or due to landslides and/or tsunamis. However, if the seismic center is close to the site and the vibration gets transmitted vertically through the water column, the impact to the structure may not be negligible (Suzuki, 2005). Recent studies have shown that communications cables can be utilized to monitor seismic events (Williams et. al., 2019); thus, cables for offshore windfarms may provide valuable information on seismic activity in the future.

Regarding the design life of the FOWF, the appropriate return period of every event should be considered. Earthquake conditions, risk of damage, and survivability should also be evaluated. The potential of earthquake activity in the vicinity of the proposed site is determined by investigating the seismic history of the region (i.e., in defined radius, depending upon magnitude of the event) surrounding the site, and relating it to the geological and tectonic conditions based on the soil databases. Also considering that earthquakes can potentially initiate chains of surface processes, such as triggering landslides and slope failures; flushing of excess debris (Fan et al., 2018); and inducing tsunamis directly or indirectly through landslides (which can travel across the ocean and affect far distance coasts), there is a need for a more complete understanding of seismic effects and activities in the region, and of site-specific soil type. Figure 12 schematically presents consequences of an earthquake that can affect siting of FOWF directly or indirectly.

Figure 12. Primary and secondary geological effects of earthquakes (selected from Rodriguez-Pascua, et al., 2009)

Oceanic trenches and volcanic arcs encircling the Pacific Basin form the so-called Ring of Fire, a zone of frequent earthquakes and volcanic eruptions (Figure 13). More comprehensive database of seismic information should be evaluated to assess hazards in the Pacific Basin by specific state at: https://earthquake.usgs.gov/earthquakes/byregion/.

Earthquakes are reported on the Richter scale, within which each increase in magnitude indicates in increase in amplitude of ten times; that corresponds to the release of about 31 times more energy (USGS, 2019a). Potential damage is generally described as follows:

- **Less than 3.5**: generally, not felt, but recorded;
- **3.5-5.4**: often felt, but rarely causes damage;
- **5.5 to 6.0:** at most slight damage to well-designed buildings, can cause major damage to poorly constructed buildings over small regions;
- **6.1-6.9:** can be destructive in areas up to about 100 kilometers across where people live;
- **7.0-7.9:** major earthquake, can cause serious damage over larger areas; and
- **8 or greater:** great earthquake, can cause serious damage in areas several hundred kilometers across.

While there are no specific data to categorize earthquake damage to FOWF facility structures, it has been assumed that there would be damage causing partial structural failure to the FOWF above Richter 5.0 and major structural damage at Richter 7.0. For this study, the most recent earthquakes with magnitude of Richter +7 in the Pacific region have been compiled from the USGS database (USGS, 2019c) and presented in Table 9. A more comprehensive list and exact locations of Richter +3.5 magnitude earthquakes can be obtained and visualized in the following figures provided in this report, and through the OceansMap[4] webpage developed as part of this project.

[4] http://boem-oceansmap.s3-website-us-east-1.amazonaws.com/

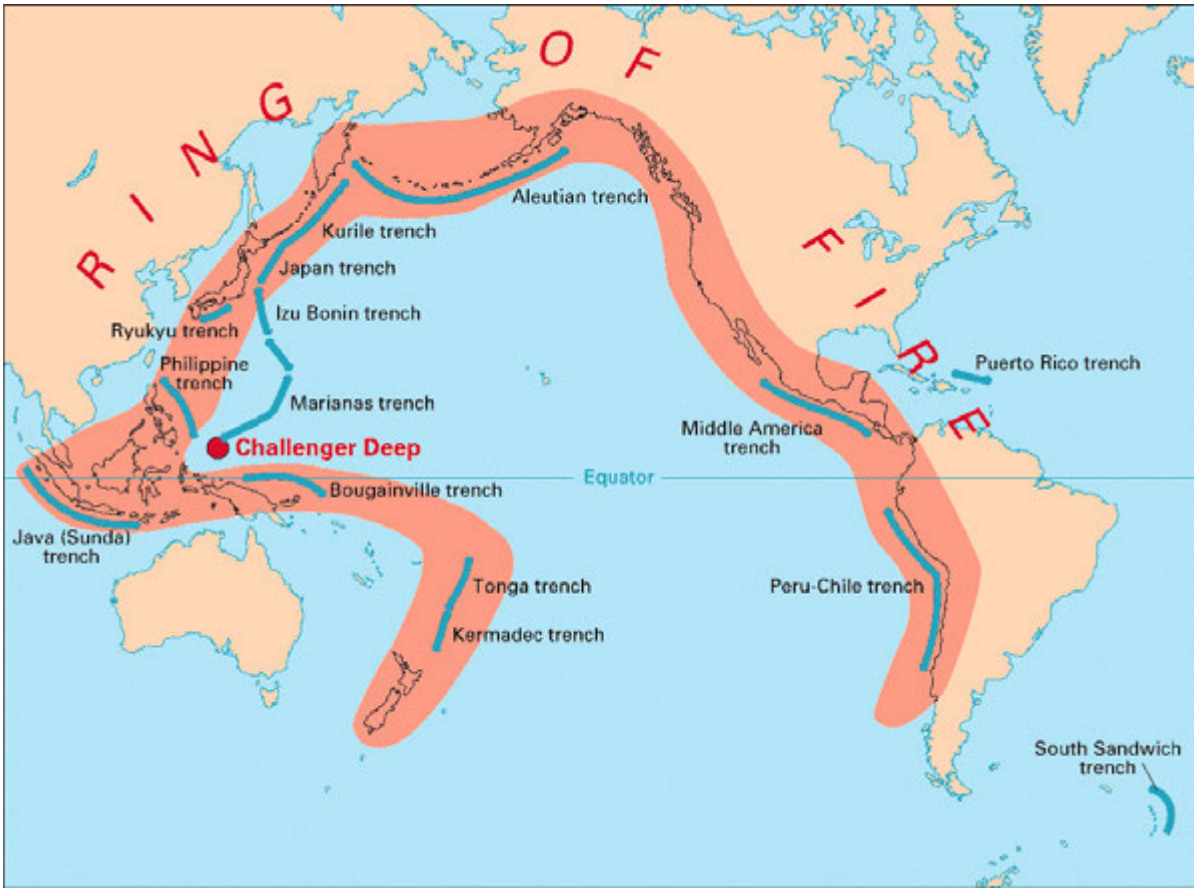

Figure 13. Ring of Fire: zone of frequent earthquakes and volcanic eruptions (Source: USGS,2019b)

Table 9. Recorded earthquakes greater than 7.0 magnitude since 1900 within 500 km of Pacific study areas.

Location	Earthquake Time	Magnitude	Depth (km)	Latitude	Longitude
California - Humboldt	2005-06-15 02:50:54.190Z	7.2	16	41.292	-125.953
California - Humboldt	1994-09-01 15:15:48.310Z	7	4.972	40.4055	-126.303
California - Humboldt	1992-04-25 18:06:05.180Z	7.2	9.856	40.33533	-124.229
California - Humboldt	1980-11-08 10:27:34.000Z	7.2	19	41.117	-124.253
California - Humboldt	1922-01-31 13:17:31.000Z	7.3	15	41.115	-125.54
California - Morro Bay, Diablo Canyon	1952-07-21 11:52:15.460Z	7.5	6	34.95817	-118.998
California - Morro Bay, Diablo Canyon, Humboldt	1906-04-18 13:12:27.700Z	7.9	11.7	37.75	-122.55
Hawaii	1975-11-29 14:47:40.100Z	7.7	8.95	19.333	-155.002

Location	Earthquake Time	Magnitude	Depth (km)	Latitude	Longitude
Oregon	1946-06-23 17:13:19.000Z	7.3	30	49.76	-125.34
Oregon, California - Humboldt	1991-08-17 22:17:09.970Z	7	1.303	41.679	-125.856

To obtain more general and comprehensive information on earthquake-prone regions, this report section provides a review of the existing information representative of major faults in the Pacific which historically have endangered the U.S. coasts. Additionally, the review focuses on the Alaska- Aleutian Subduction Zone (AASZ), which can affect all the study areas through secondary effects but does not directly run through any of them (Figure 12).

5.1.1 Alaska- Aleutian Subduction Zone (AASZ)

The Aleutian subduction zone is a 3,800 km (~2,500 mile) convergence boundary between the Pacific Plate, which is subducting underneath the North American plate and extends from the Gulf of Alaska to the Kamchatka Peninsula. This zone does not directly run through any of the study areas; however, it can affect these regions by generating far-field tsunamis that may travel across the ocean and affect the sites. The rate of subduction changes from 7.5 cm/yr to 5.1 cm/yr from west to east. It is one of the most active plate boundaries in the world, comprised of multiple zones that have been the source of many historic earthquakes (Figure 14). In the last 80 years, four massive (>8M) earthquakes have occurred in this zone. The region is active with slow earthquakes that occur continuously (Li and Gosh, 2017).

The 1964 Prince William Sound earthquake generated the largest distant tsunami on the Oregon coast (Lander et al., 1993). The earthquake, which is the largest one in written North American history, lasted approximately 4.5 minutes. The earthquake rupture started approximately 25 km beneath the water surface, and its epicenter was about 6 miles (10 km) east of the mouth of College Fiord, 56 miles (90 km) west of Valdez, and 75 miles (120 km) east of Anchorage. The return period of this large earthquake near the source is 600-800 years.

In 1946, another earthquake was generated off Unimak Island at the western end of the Alaskan Peninsula, occurring along the plate margin off Unimak Island in a region that transitions from Alaska to the Aleutian convergent margin system. Unimak Island is part of the Alaskan continent, and is geographically part of the Alaska Peninsula landmass but is separated by a narrow marine passage. The resulting earthquake-generated tsunami damaged Pacific coastal areas from Alaska to Antarctica and had a 42-m runup at Scotch Cap, Unimak Island. The tsunami took 159 lives in the Hawaiian Islands and caused 26 million dollars of property damage (Fryer and Tryon, 2005). The far-field tsunami was generated by tectonic seafloor displacement of the earthquake with the epicenter in the shallow reaches of the Aleutian subduction zone (Lopéz and Okal, 2006); however, the near-field tsunami was inferred to be caused by a large landslide (Okal and Herbert, 2007; Miller et al., 2014).

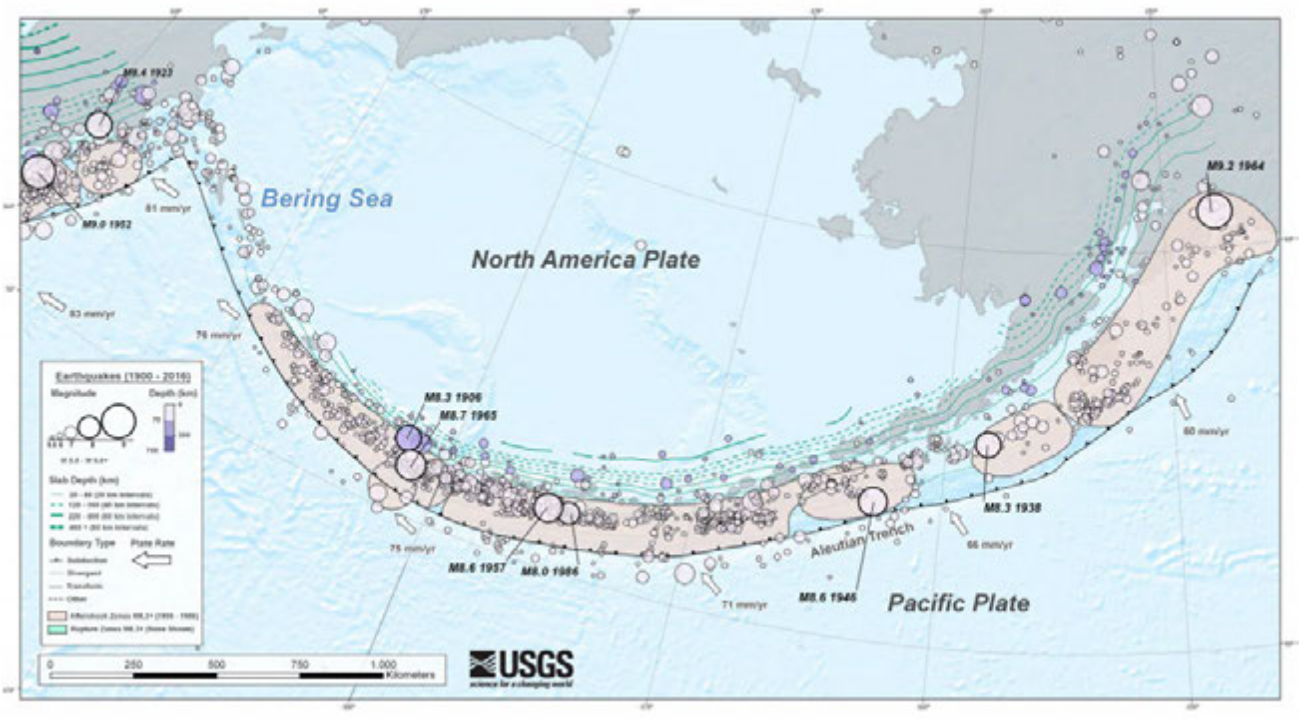

Figure 14. Alaska- Aleutian Subduction Zone Seismic Activities.

5.1.2 Seismic Activities: California and Oregon

As part of the Ring of Fire, California and Oregon are subject to earthquakes, landslides and tsunamis (Figure 13). Both states have many recorded earthquakes due to several faults running through them (Figure 15). The subduction of the Gorda and Juan de Fuca Plates at the Cascadia subduction zone, which is a 680-mi-long fault running 50 mi (80 km) off the coast of the Pacific Northwest from northern California to Vancouver Island, British Columbia, forms the major part of this active region. The largest fault passing through continental California is the San Andreas Fault, with its activity also correlated with the behavior of the Cascadia subduction zone.

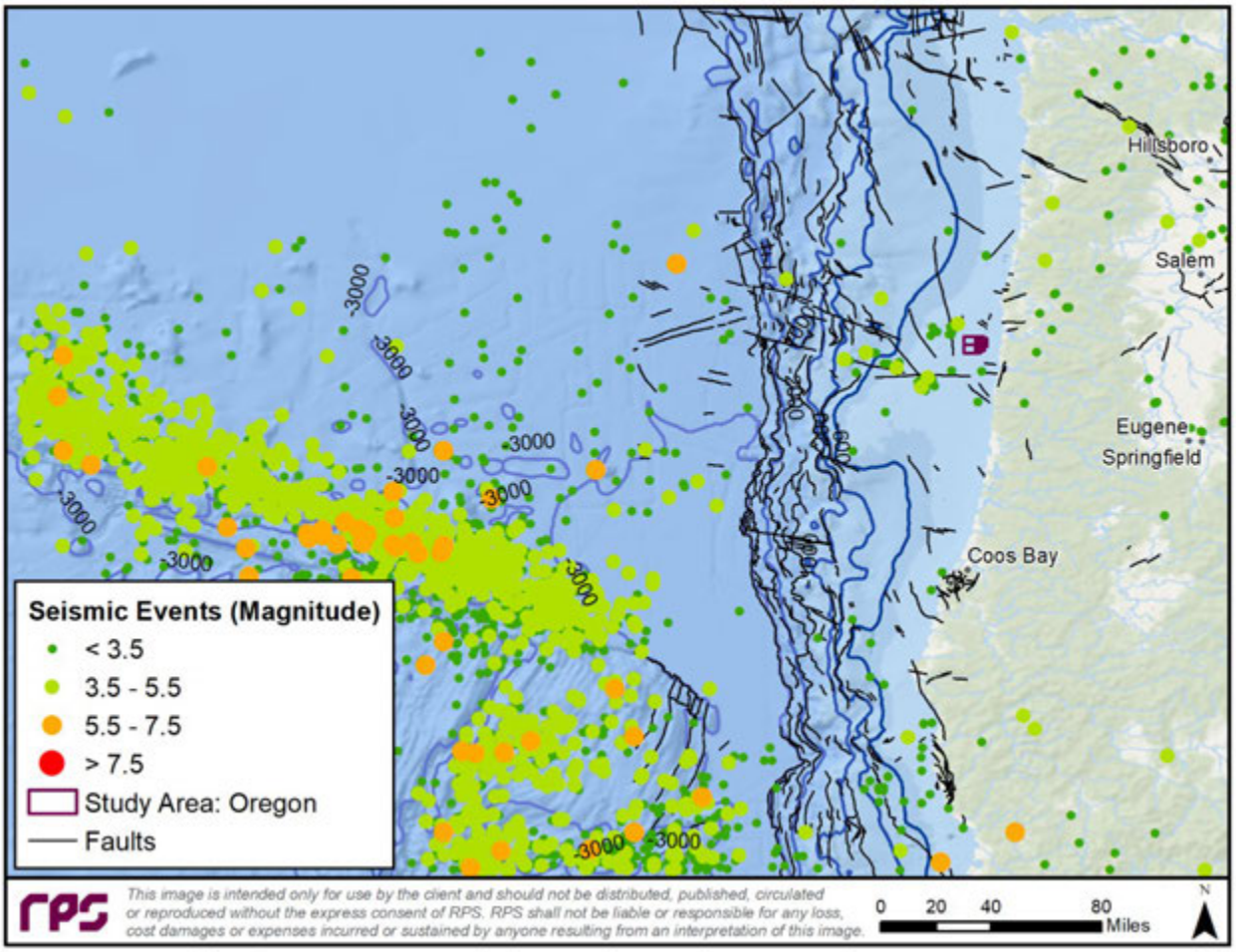

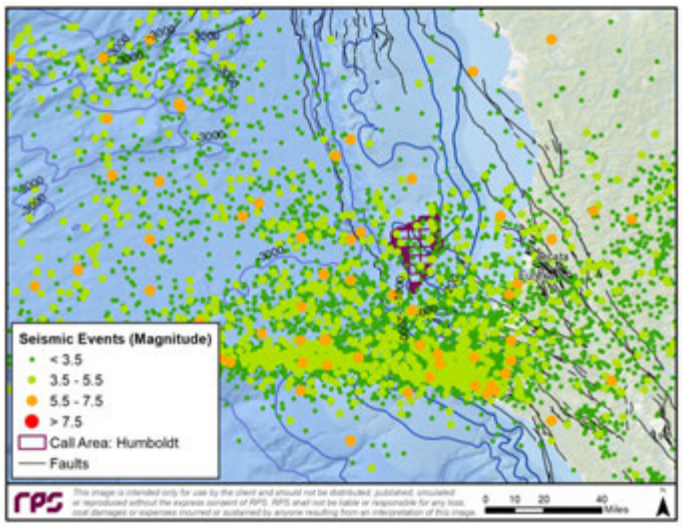

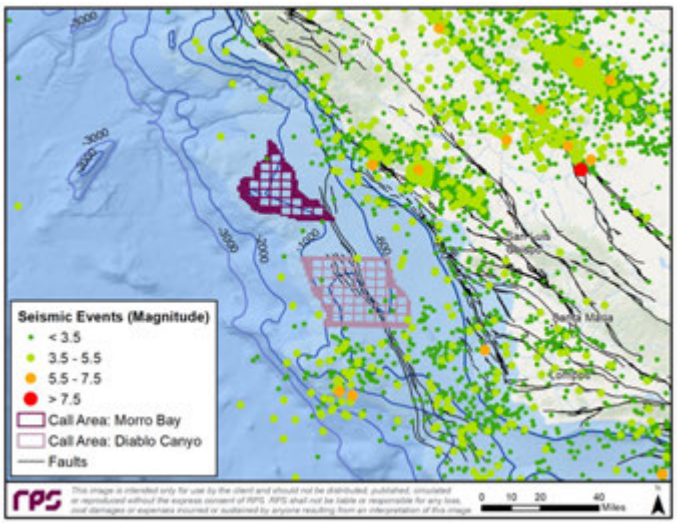

Figure 15. Historic Earthquakes Close to the Study Areas of Oregon and Northern and Central California Based on USGS (USGS, 2019c) Datasets.

5.1.2.1 Cascadia Subduction Zone

The Cascadia subduction zone (CSZ) is a convergent plate boundary of sloping subduction, in which the Explorer, Juan de Fuca, and Gorda plates move to the east and slide below the much larger, and mostly continental, North American Plate off the Pacific Coast. The 1,300 km-long fault extends from Northern California to Vancouver Island (Figure 16). The Juan de Fuca Plate is a remnant part of the once-vast Farallon Plate, which is now largely subducted underneath the North American Plate. In general, the slope in the study area and off the Oregon coast is part of a forearc basin formed by oblique subduction of the Faralon Plate beneath North America. Based on tidal marsh records of subsidence, there have been 12 great subduction earthquakes in the last 6,700 years, most of which were ruptures of the entire subduction zone (Witter et al., 2003). Deformation of the slope initiates with reverse faulting and anticlinal folding at the base of the slope above the subducting oceanic plate. As accretion continues, the bathymetric basins between folds fill with sediment from the continent, the faults steepen, and the folds shorten (Kulm and Fowler, 1974). The upper slope and shelf consist of modern sediment unconformably overlying an extensively folded and faulted accretionary complex. The CSZ has produced multiple earthquakes, including a major magnitude 9.1 event on 26 January 1700 (CREW, 2005; CREW, 2013) and two additional earthquakes around British Columbia with magnitudes >7.5, i.e., 8.1M in 1949 and 7.7M in 2012. On 15 June 2005, a 7.2M earthquake occurred off the coast of northern California at 41.284°N 125.983°W and depth of 16 km. This earthquake was the result of shallow strike-slip faulting within a deformed section of the southernmost oceanic crust of the Juan de Fuca plate, with a left-lateral northeast-southwest-striking fault or on a right-lateral southeast-northwest-striking fault. However, this earthquake did not produce a tsunami. Earthquakes with strike-slip mechanisms are less likely to produce tsunamis because they cause relatively little vertical ground displacement (Hayes et al., 2017).

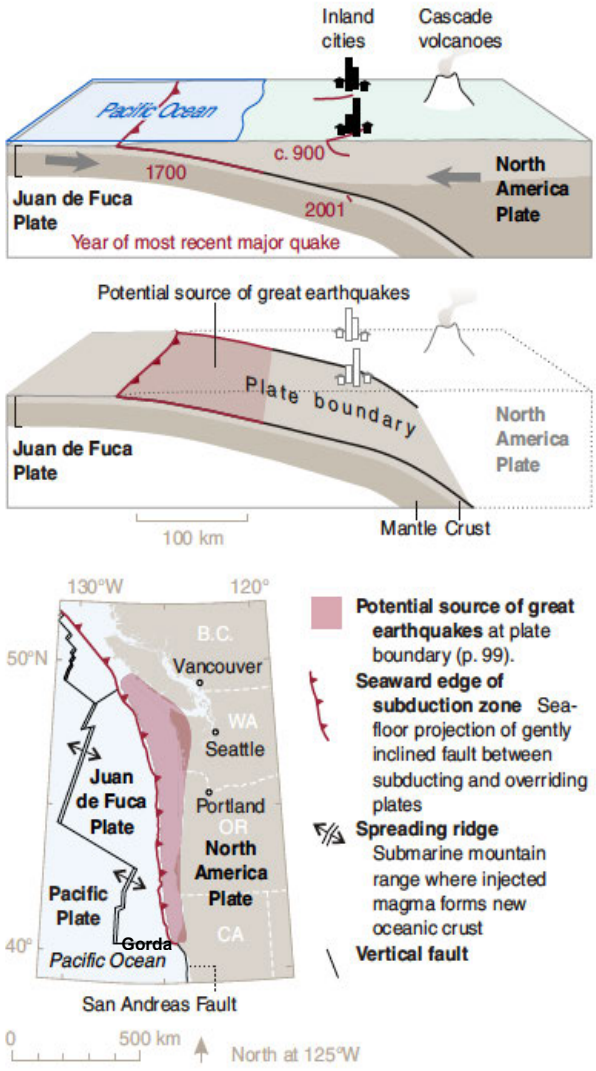

Figure 16. Earthquake sources at Cascadia (figure modified from Atwater et al., 2015).

The CSZ is one of the greatest sources of uncertainty in probabilistic modeling due to its “large epistemic uncertainty and high-dimensional stochastic space”. Studies by Goldfinger et al. (2012) show that earthquakes have an average recurrence interval of approximately 500 years for the northern and central side; about 240 years (a minimum of 20-50 years) in the southern segment; and about 300 years for the great earthquakes in full rupture.

The northern California continental shelf is both active tectonically and has relatively high rates of sedimentation. The high levels of seismic activity in this region are due to over-thrusting of the Gorda lithospheric plate by the North American plate and a right lateral slip along the Gorda Escarpment. Deposits were made several hundred thousand years ago off the Klamath River and form a shelf of a complex sequence of folded and faulted rocks. These formations can cause a landslide by earthquake-induced liquefaction of sediment lands on the continental shelf. This is similar to the event that occurred off northern California in 1980, which followed a large (7.0M) earthquake (Field, 2002).

5.1.2.2 San Andreas Fault Zone (SAFZ)

California is known for its seismic activity, particularly along the San Andreas Fault Zone (SAFZ) (Figure 17). The SAFZ is the main part of the boundary between the Pacific tectonic plate on the west side and the North American plate on the east side. While the emphasis for hazard protection is on land-based locations, the seismic activity would also be felt in offshore areas, including the study areas offshore of California. In northern California, the zone includes the Hayward, Calaveras, as well as the Northern San Andreas and other faults and in southern California, the zone encompasses the Southern San Andreas, the San Jacinto, and other faults in the Los Angeles area.

The Hayward fault in the San Francisco Bay area was the source of an approximately 6.9M earthquake in 1868. The fault has been moving about 4.6 mm/yr (0.2 inches/yr) for the last several decades, but stress is building on this fault as this rate is only half of the long-term slip rate. A paleo-seismic study in 2007 found evidence for 12 paleo-earthquakes with an average time between earthquakes of about 160 years, while the average time interval between the 5 most recent earthquakes was shorter (about 140 years). This constitutes a 33% likelihood of a surface-rupturing earthquake within the next 30 years. Studies of the Maacama fault, the northward continuation of the Hayward-Rodgers Creek fault system in northern California, suggest infrequent large earthquakes, however, a large one is expected to occur in the near future.

The Hazel Dell site near Corralitos, CA characterizes the Santa Cruz Mountains section of the San Andreas Fault. The Santa Cruz section stretches 62 km (39 mi) from Los Gatos (near San Jose) to San Juan Bautista, CA and last ruptured in the famous 1906 San Francisco earthquake. The average time between earthquakes includes some short and long intervals. Studies of the North Coast section of the San Andreas Fault north of San Francisco suggest an average recurrence interval of 200-300 years (Figure 17).

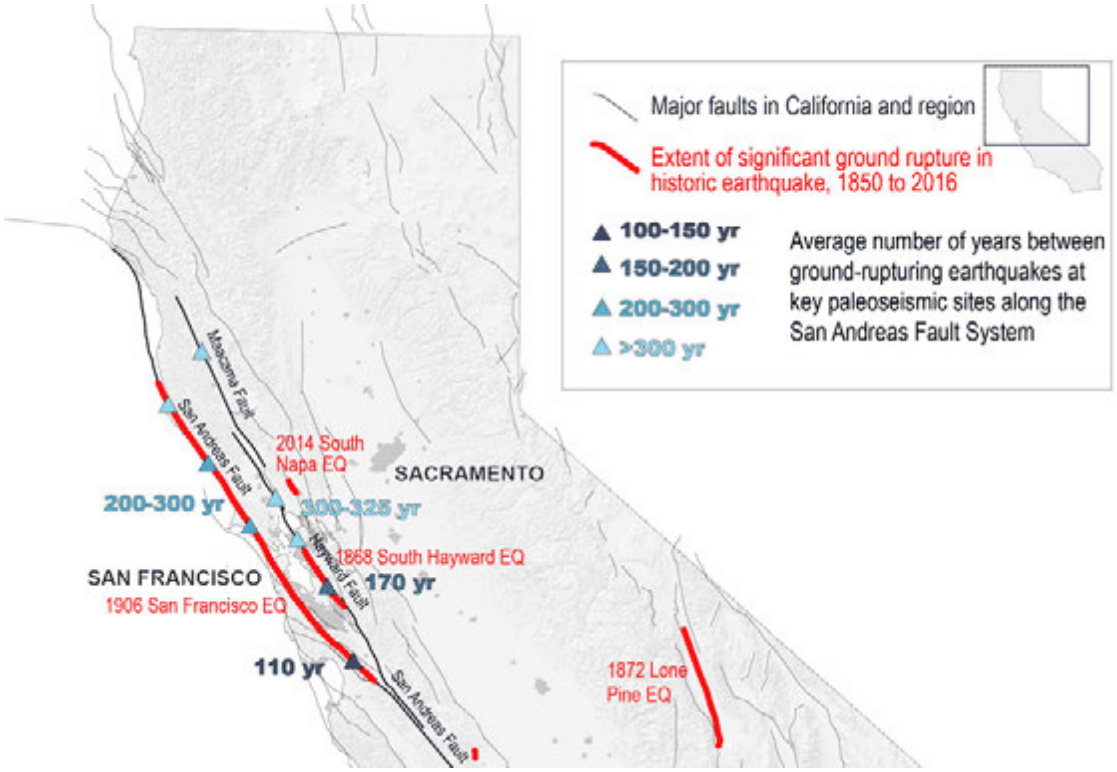

Figure 17. Major Faults and Earthquakes in California (source: USGS,2019d)

5.1.3 Seismic Activities: Hawaii

The Hawaiian Islands are known to have a high degree of seismic activity, particularly near the island of Hawaii (Klein et al., 2001). There have been 53 earthquakes over M5.0 (and under M7.0) in the last 100 years, or 0.53 per year, and one earthquake over M7.0, or 0.01 per year. The only earthquake of M7.1 was in November 1975 centered on the southeastern side of the island of Hawaii near Kalapana. There have also been earthquakes near Oahu (e.g., M4.0 earthquakes in 1978, 1980, 1988, and 1990; and M5.0 earthquakes in 1973 and 2012). A 6.7 magnitude earthquake in Kiholo Bay, Hawaii, in October 2006 was felt and caused moderate damage in Oahu (Figure 18).

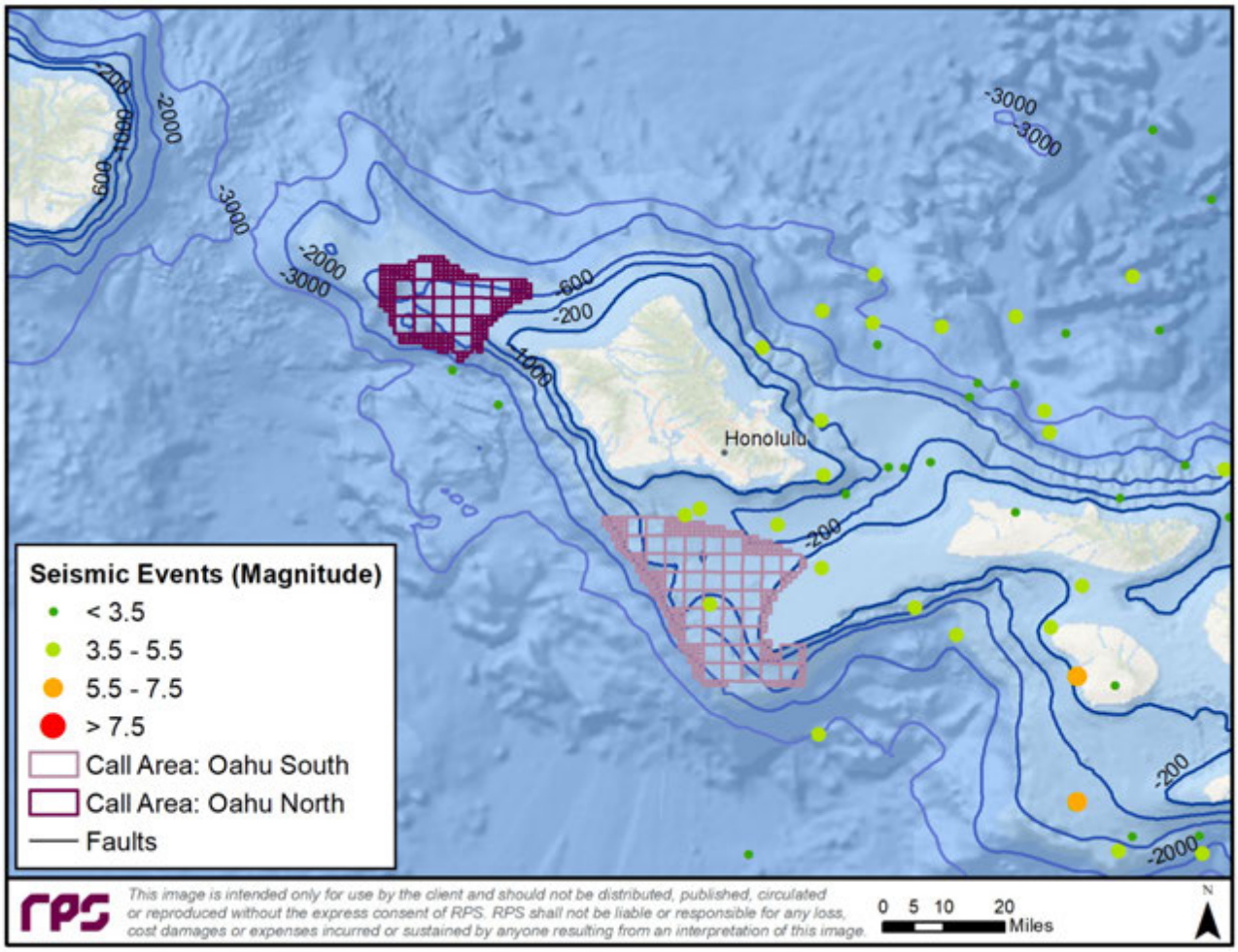

Figure 18. Seismic Activity around Hawaii Oahu Study areas

5.2 Landslides

Field investigations of landslide occurrence caused by earthquake have facilitated the analysis of hazards and risks associated with earthquake-induced landslides. One of the first comprehensive post-earthquake inventories of landslides was made for the 1957 (*ML* = 5.3) earthquake in Daly City, California (Keefer, 2002; Bonilla, 1960). Based on an historic review of earthquake-induced landslides, Keefer (1984) found that approximate magnitude of the smallest earthquakes causing underwater landslides types was ~5.0. However, because earthquake-caused landslides can also be triggered by non-seismic agents, underwater landslides can randomly occur in earthquakes with magnitudes smaller than 5.0. Although submarine landslides are known to be caused by local earthquakes, recent research by Johnson et al. (2017) showed submarine landslide can also be induced by remote earthquakes. This study used 3 years of ocean bottom seismometer deployments on the Cascadia margin in the Pacific Northwest to demonstrate that submarine landslides can also triggered by remote earthquakes, including a distant large magnitude earthquake on the Sumatra margin, over 13,000 km distant from the eastern Pacific Ocean.

Submarine landslides can be far larger than those on land and are one of the most important processes for moving sediment across the continental shelf and into the deep ocean. Landslides that are fast enough to disintegrate can generate potentially very hazardous tsunamis and produce long run-out turbidity currents that break strategically important cable networks (Clare et al., 2014). These landslides occur at locations where the downslope component of stress exceeds the resisting stress, which causes movement along one or several concave to planar rupture surfaces (Hampton et al., 1996).

Underwater landslides are common on inclined areas of the seafloor, particularly in environments where weak geologic materials (e.g., rapidly deposited, fine-grained sediment, fractured rock) are subjected to strong environmental stresses like earthquakes, large storm waves, and high internal pore pressures. However, submarine slope failure can occur on remarkably low (< 2°) gradients, which are almost always stable on land, perhaps due to high excess pore pressures. Earthquakes can cause large submarine landslides, but not all major earthquakes trigger widespread slope failure. Recurrence intervals of major (>M7.3) earthquakes could be implicated as triggers. However, not all major earthquakes appear to generate widespread turbidites, and yet some other unknown triggers or sequential combinations of processes could produce the same effect (Clare et al., 2014).

Submarine landslides can involve huge amounts of material, with slide volumes as large as 20,000 km³, and can move great distances with runout distances potentially exceeding 140 km (Hampton et al., 1996). Although earthquakes generate most tsunamis, local "surprise tsunamis" are mainly created by submarine landslides. Landslide-generated tsunamis are mainly destructive locally, in contrast with earthquake generated tsunamis, that commonly cause damage at great distances (Lee et al., 2003). The “surprise tsunamis” can initiate far outside of the epicentral area of an associated earthquake, or larger than expected from the earthquake size (Ward, 2001). For example, Tappin et al. (2014) proposed that the additional forces to generate the Tōhoku tsunami of 11 March 2011 came from a submarine landslide, while many studies suggested that they occurred entirely due to a slip on an earthquake fault. The characteristics of a tsunami created by a submarine landslide are mainly determined by the volume, the initial acceleration, the maximum velocity, and the possible retrogressive behavior of the landslide (Harbitz et al., 2006).

Lee et al. (1993) suggested the environments within the U.S. Exclusive Economic Zone (EEZ) with high sedimentation rates and areas within Puget Sound, Washington are more prone to slope failure. Lee (2005) stated submarine landslides occur in environments including fjords, deltas on the continental shelf, submarine canyons, volcanic islands and the open continental slope. This study report provides a review of these environments within the west coast of the U.S. and Hawaii (HI) using coarse resolution publicly available datasets. Therefore, to have a better understanding of the risk of landslides and decreasing the risk affecting different components of FOWF, for example at the location of cable burial or the anchorage, more site-specific data collection of subsurface soil type is needed to analyze the seabed strength.

5.2.1 Submarine Landslides Off the Coast of California and Oregon

Fjords are glacially-eroded valleys fed by sediment-laden rivers and are more susceptible to failure due to high sedimentation rates and steep slopes extending to 1,000 m or more. Some fjord-delta deposits are so instable that they fail during greater than average tides, and also fail episodically (Lee, 2005). The vulnerability of these areas is high, both in terms of the proportional areal extent of deposits that can become involved in mass movement, and also in terms of the recurrence interval of slope failures at the same location (Lee et al., 1993).

Active river deltas are the next most likely sites for slope instability in the U.S. EEZ as many rivers contribute large quantities of sediment to relatively localized areas on the continental margins. For instance, slope failures exist on active deltas on the continental shelf off southern Alaska due to glacially-fed rivers adjacent to sounds and inlets which contribute 450 million tons of sediment per year (Milliman and Meade, 1983). On the west coast of the U.S., there are indications of slope instability on some deltas due to their thick, gas charged deposits that can fail even on very gentle slopes (<1°); such as the Klamath River delta which failed during a M7 earthquake in 1980 (Field et al., 1982).

Field and Barber (1993) also studies the submarine landslide related to shallow sea floor gas and gas hydrates off Northern California. The study analyzed the role of gas in reducing sediment strength and increasing the possibility of slope instability in the continental slope off Eureka, Northern California. The continental slope off Eureka in northern California is situated within the Eel River Basin, which is an active forearc basin consisting of over 4,000 meters of Pliocene- and Quaternary-age sediment deposited during the past 5 million years. Another consequence of the regional tectonic activity in this region has been uplift of onshore regions, which caused substantial erosion and sediment transport to the continental shelf and slope. In addition, local rivers supply more than 20 million metric tons of organic-rich sediment to the coast per year (Field et al., 1980). Biogenic gas provided by these deposits, joined with the upward migration of thermogenic gas from sources deeper in the basin deposits, brings an abundance of gas in the near-surface deposits.

Lee et al. (1993) suggested liquefaction as another source of submarine landslide, which happens if loosely packed sediment crumble under a force. In this case, the grains temporarily lose contact with one another, and the particle weight is temporarily transferred to the pore fluid. The liquefied sediment may spread laterally or flow downslope. Subsurface liquefaction can occur at shallow depths as a result of extra pore-fluid pressures created in sand by the earthquake. This process can also be enhanced by the presence of gas. During and after the liquefaction process, subsurface sand is reorganized into a denser packing arrangement, which causes expulsion of pore fluids and gases, leading to collapse and flow of surface sediment. However, none of these factors (sediment thickness, earthquake magnitude, and sediment type) were involved in the extraordinary event of liquefaction of sediment off the Klamath River in 1980 (Field et al., 1993). The mass movement occurred off the Klamath River was on a nearly flat (0.25° slope) area of the sea floor. Considering most of the continental margin has greater slopes ranging from 1.0° to 4.0°, they may be more vulnerable to liquefaction by earthquake. An important aspect of the 1980 earthquake-induced landslide is that the earthquake had a magnitude of about 7.0, 60 km from the submarine landslide. Earthquakes exceeding 30 times that amount of energy and much closer to the California shelf have occurred in the past and have the possibility of happening in the future; thus, the likelihood of similar or bigger landslides due to liquefaction is high. At this landslide site, the thickness of the Upper Quaternary sediment, which deposited during the past 20,000 years, is only 20 to 30 m. This likely means thick accumulations of modern sediment are not required for slope failure. As the thickness of upper Quaternary sediment in many areas of the California shelf and slope is similar or even higher than this, many areas of this region have the potential of landslides (Figure 19).

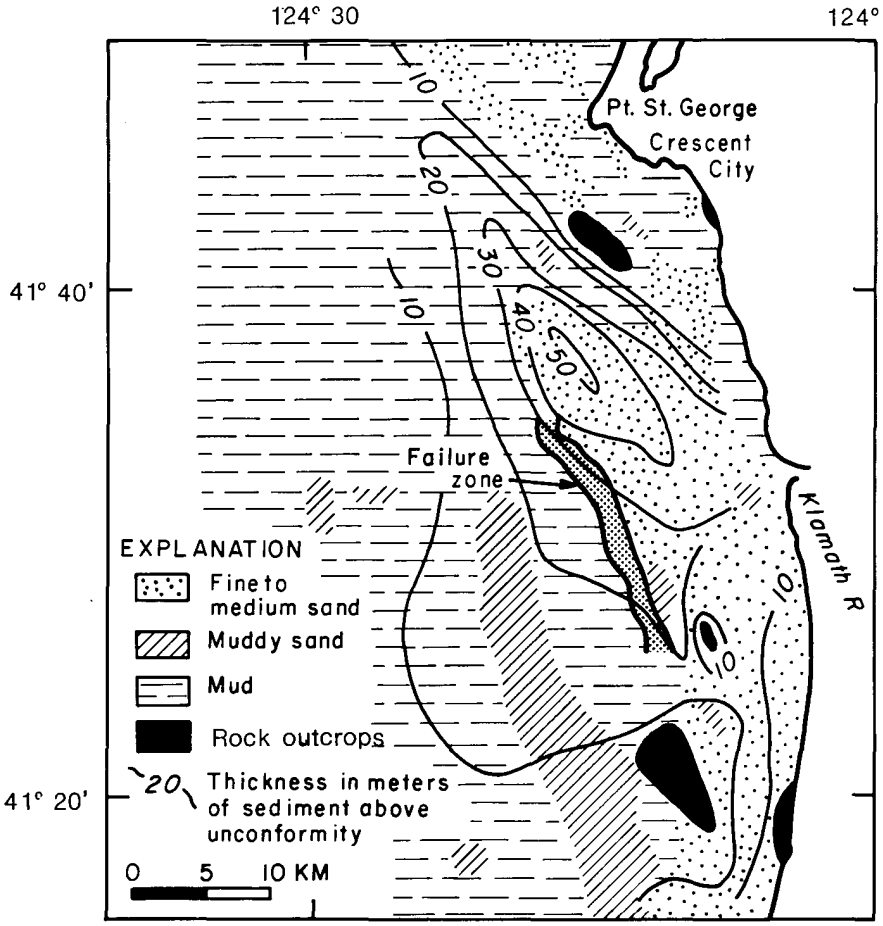

Figure 19. The general location of the landslide zone based on the nature and thickness of surface sediment in Northern California continental shelf (figure from Field et al., 1993).

Another typical environment for underwater landslides along the California slope is the area between submarine canyons on the continental slope. These canyon-fan systems serve as channels for sediment passing from the continental shelf to the deep sea, where landslides can be initiated by earthquakes or storms that can result in a dilute turbulent cloud flowing for hundreds of kilometers from the canyon head (Hampton, 1972; Lee, 2005). Furthermore, landslides in the inter-canyon area of the continental slope area (i.e., removed from canyon-fan systems) usually occur both near and far from river mouths. These landslides are likely to be triggered by seismic activity because these regions were on otherwise stable slopes of 5° or less. It is important to mention that the continental margin off California north of Cape Mendocino contains more landslides than any other comparable region along the west coast of the U.S. Humboldt Slide Zone, which is on a 4° slope at water depths of 250 to 500 m west of Eureka, is one of the major areas of slope instability (Figure 20; Field and Barber, 1993).

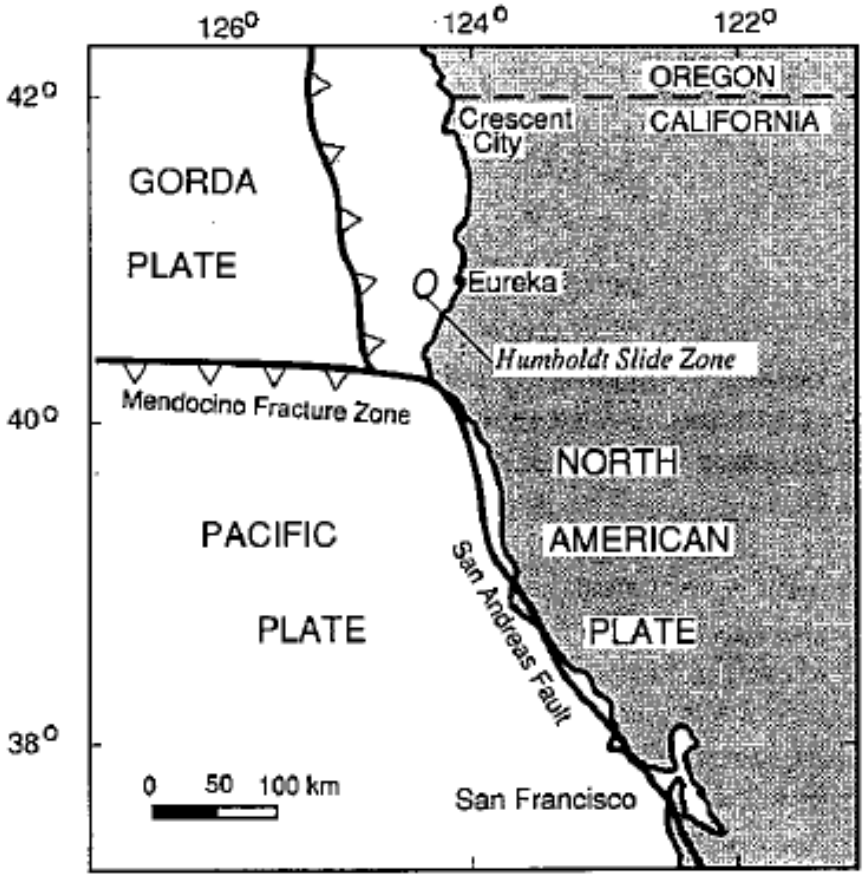

Figure 20. Northern California continental margin (Field and Barber, 1993).

Gutmacher and Normark (1992) discussed a deep-water sediment slope failure that originated on the continental slope west of Point Sur, central California (Figure 21). The failed material moved downslope onto the surface of the adjacent Monterey Fan (Hess et al., 1979) and settled between 3,200 m and 3,750 m water depth. The resulting mass movement deposit is 70 km long, 5 to 25 km wide, and covers almost 1,000 square km. The thickness of the deposit ranges from few centimeters to approximately 75 m and has an estimated volume of 35 cubic km.

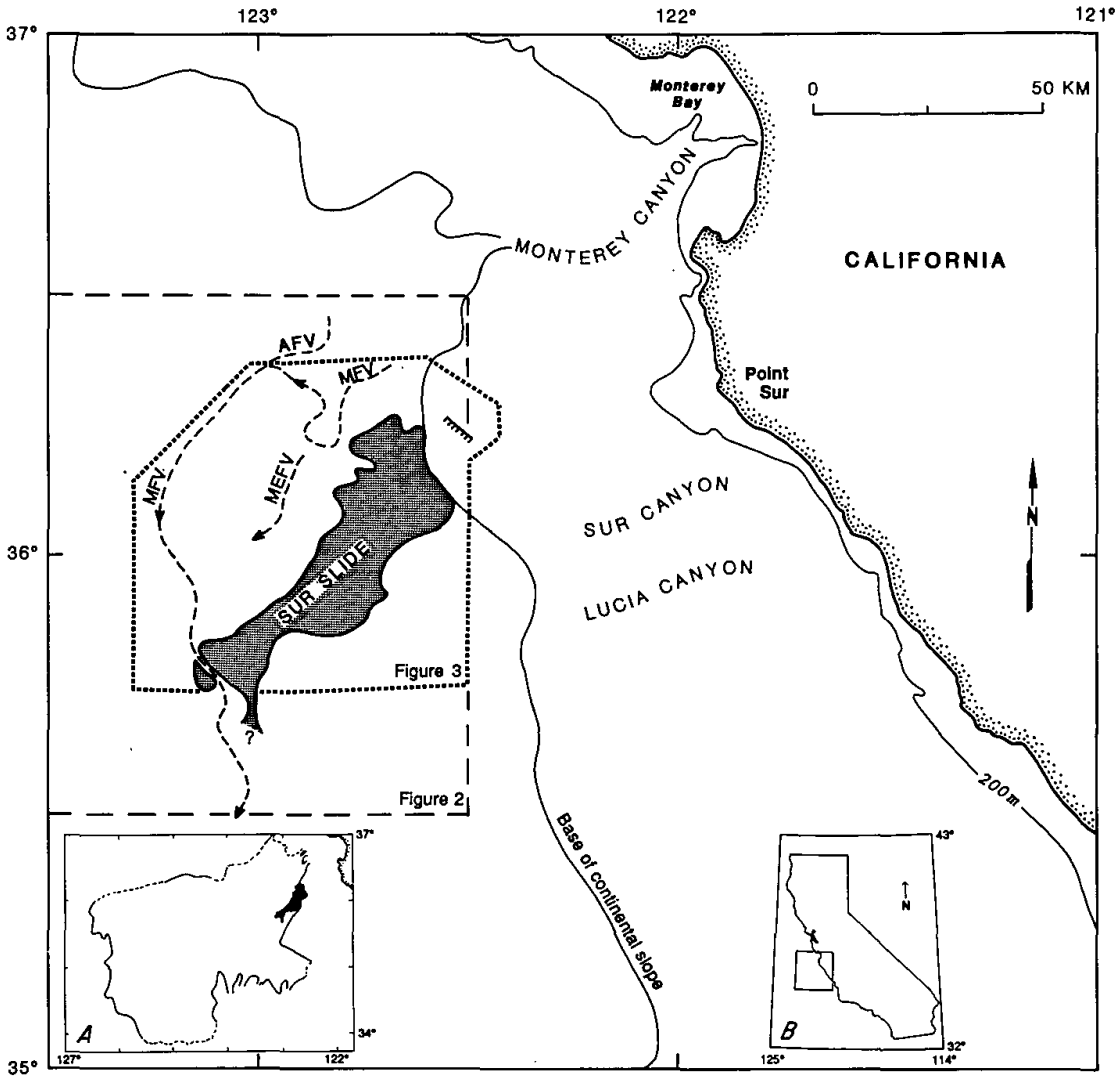

Figure 21. Location of Sur landslide deposit in relation to the outline of Monterey Fan (A); B shows location of the figure on California. The heavy dashed lines indicate major fan valleys including Monterey fan valley (MFV), conduit of sediment from Monterey Canyon and, thus, from the rivers that empty into Monterey Bay; Ascension fan valley (AFV), a hanging tributary to Monterey fan valley that receives sediment that moves along the outer continental shelf; Monterey East fan valley (MEFV) (from Gutmacher and Normark, 1992).

5.2.2 Submarine Landslides Off the Coast of Hawaii

Normark et al. (1993) discussed giant volcano-related landslides and their role in the development of Hawaiian Islands. Their study defined 37 major landslides (Figure 22) where the associated area is covered by massive submarine mass-movement deposits. These landslides can be divided into two types: slumps and debris avalanches. Most of the landslides moved into, and locally across, the axis

of the Hawaiian Trough, which flanks the Hawaiian Ridge. Hence, mass movement is a primary mechanism for filling the trough and widening the base of the ridge.

The eruptive behavior of volcanoes can also be balanced by landsliding. Most of the larger, older landslides near Hawaii seem to have occurred late in the shield-building phase of the host volcano (Moore et al., 1989). Thus, the age of lavas of this phase of volcano development provide a rough estimate of age of the youngest landslide (Clague and Dalrymple, 1987). The most active volcanoes, Mauna Loa and Kilauea, which have not yet completed their shield-building phase, exhibit enough evidence of major landslides. This event indicates that slope failure is a continuing process through much of the history of volcano growth and is not confined to the end of shield building (Figure 22).

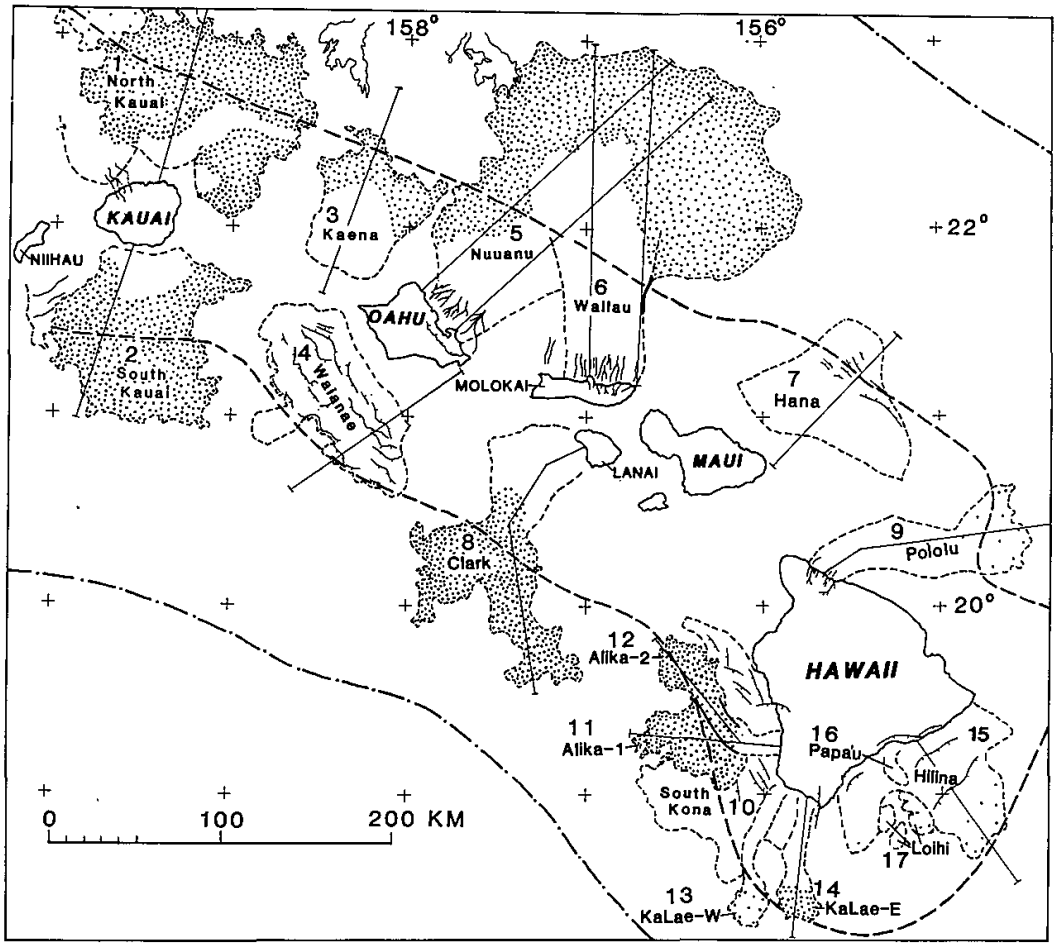

Figure 22. Hawaiian Ridge showing major landslides. The main islands are depicted in black and the landslides around them are shown with dotted lines. (Figure from Normark et al., 1993).

5.3 Tsunamis

Tsunamis are long waves generated by sudden changes and quick motions of the ground under water, often due to undersea earthquakes or landslides. They are potential social and economic hazards, especially when approaching shorelines (Fuhrman et al., 2015). Tsunamis in deep water

are rapidly moving, low wave height, long wavelength features. When tsunamis approach shore, they behave like a very fast-moving tide which extends far inland, without breaking. Because of the large volume of moving water, the energy transfer is substantial, and the wave can create scour due to action on the sediment while the wave is approaching the shore. The run-up, inundation, and destructive potential of tsunami events and their associated interaction with the seabed (i.e., induced sediment transport) are important issues and processes which can affect coastal regions and contribute to the failure of coastal structures and systems (Fuhrman et al., 2015). Hence, it is very important to have disaster resilience infrastructure and facilities in place, especially in the states of OR, CA, and HI where the warning time is short due to the proximity of the local sources of tsunamis. A detailed understanding of the threat, underlying processes, and general structure vulnerability are needed; especially as the historical records alone do not provide a sufficient measure of the potential for future tsunamis, and the future event could be greater than the historical records as a function of seismicity of the region (Chock, 2015).

Tsunamis generated by submarine landslides often have very large runup heights close to the source area but have more limited far field effects than earthquake tsunamis. It is further shown that the combination of landslides and earthquakes may be necessary to explain observed tsunami behavior (Herbitz et al., 2006). The characteristics of a tsunami generated by a submarine landslide are mainly determined by the volume, the initial acceleration, and the maximum velocity of the landslide. The influence of these features, as well as water depth and distance from shore, are important factors on the strength of the tsunami. Submarine landslides are often clearly sub-critical (Froude number <<1), and the maximum tsunami elevation generally correlates with the product of the landslide volume and acceleration divided by the wave speed squared. Only a limited part of the potential energy released by the landslide is transferred to wave energy.

Based on engineering guidelines, floating structures are supposed to be designed and installed to not collapse or drift at the time of an earthquake or tsunami (Kyoki, 2012). However, since there are no records of the behavior of FOWF in significant tsunamis (or earthquakes), it is assumed that if there were an earthquake of M8.0 or higher, there would be a major failure of FOWF (Etkin, 2017). Earthquake data are available from the U.S. Geological Survey (USGS, 2019a) or from the NGDC/WDS (NOAA, 2019d), as described above. In addition, the history of tsunamis in the region can be analyzed to determine the relative frequency of events of this magnitude (USGS, 2019b). The relative frequency of tsunamis can be compared between different sites to develop a measure of relative risk.

There are some historic events that affected all three regions of interest, such as the tsunami of 27 March 1964 caused by a M9.2 earthquake off Prince William Sound, Alaska. The generated tsunami caused over 100 known deaths in Alaska, Oregon, and California (with 5 deaths in Oregon and waves as high as 12 ft.) and an estimated $20 million in coastal damage, as well as property loss all along the Pacific coast of North America from Alaska to southern California and in Hawaii (Lander, 1996).

The most recent tsunami affecting all three regions was caused by an earthquake (9.0 – 9.1 Mw) in Tōhoku, Japan on 11 March 2011, which struck near the coastline of Honshu, Japan. It was the fourth most powerful earthquake in the world since modern record-keeping began in 1900. As reported by 2011 Tohoku Earthquake Tsunami Joint Survey Group (MORI et al., 2011), the highest wave from the tsunami was 38.9 m in the Iwate Prefecture. Up to 2-m waves were observed at tide gauges in South America, Hawaii, and the U.S. West Coast. The highest wave that has ever been recorded by an ocean-bottom sensor was a 1.78 m wave recorded by DART® station 21418 located 450 nautical miles northeast of Tokyo. The maximum wave amplitude in California was measured at 2.47 m in

Crescent City Harbor with over $50 million in damage to two dozen harbors. Those most significantly affected were Crescent City, Noyo River, Santa Cruz, Moss Landing, and southern Shelter Island (Wilson et al., 2012).

FOWT should be constructed to withstand location-specific waves and sea states that occur during storms that are not associated with hurricanes or cyclones. FOWT can withstand waves of 45 feet (13.7 m); (Butterfield et al., 2007; Diamond, 2012). FOWT should be constructed for the maximum tsunami that has occurred in the past in the location where the structures are to be installed; and this needs to be further investigated by the design engineers. If the water is deep enough, the effect of a tsunami would be expected to be similar to that of tides, but with higher speed currents.

5.3.1 Tsunami Hazards in California and Oregon

The historical tsunami events from 2000 B.C. recorded or observed in OR and CA are extracted from the NGDC database (NOAA, 2019c) and presented in Figure 23 and Figure 24**.** According to the NGDC data, there have been several recorded tsunamis affecting Central CA, about one every 12.5 years (NOAA, 2019b). For the study area, there is an annual probability of 0.08 for partial failures. The most recent tsunami in Central CA was in November 2000 with waves of up to 15 feet (4.6 m) high near Point Arguello. The average magnitude of the tsunamis (based on earthquake magnitude) for the 200-year time frame in Central CA was 6.4 (for events for which magnitude of the precipitating earthquake was recorded; Etkin, 2017). There is no recorded tsunami event of magnitude over 8.0 for Central CA.

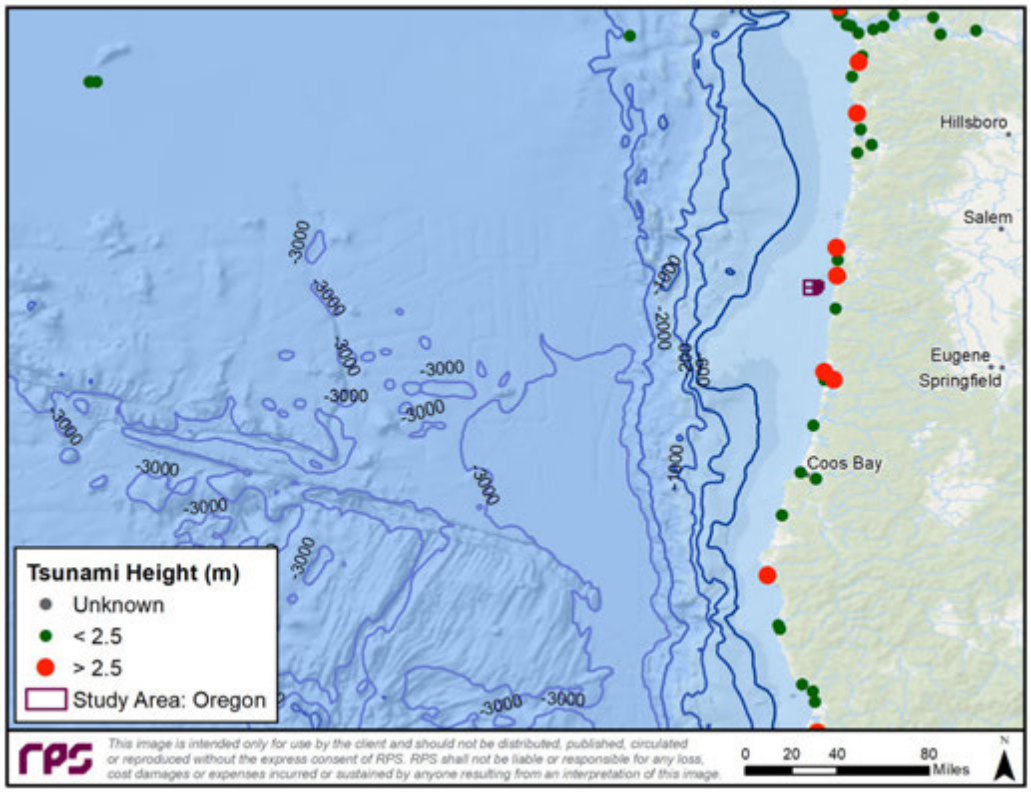

Figure 23. Historic Tsunami Measured or Observed on Coast of Oregon (Data Extracted from NOAA, 2019c).

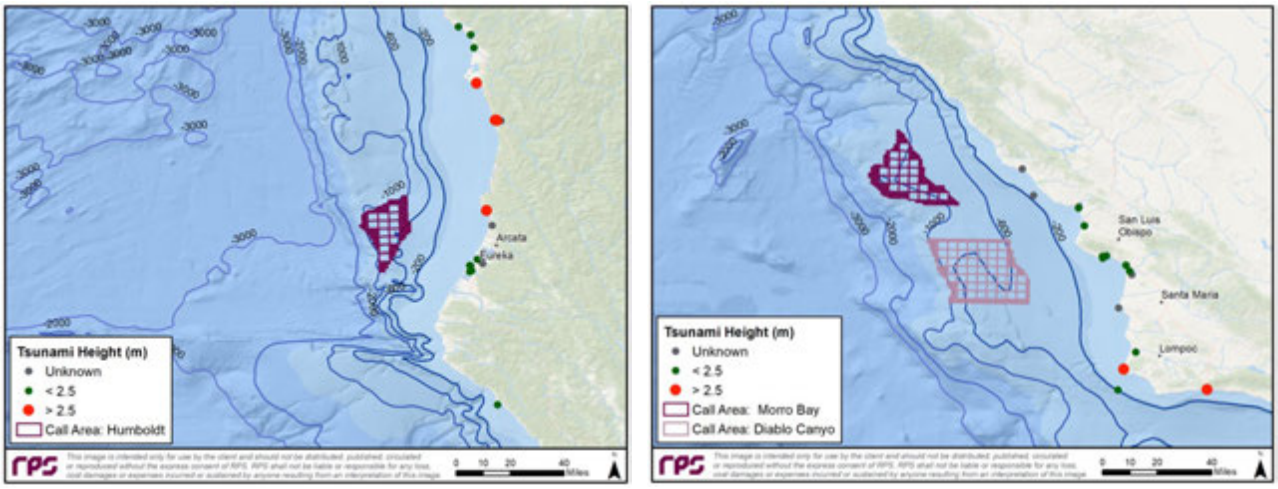

Figure 24. Historic Tsunami Measured or Observed on Coast of CA (Data Extracted from NOAA, 2019c).

The 9.2 magnitude earthquake of 28 March 1964 in Prince William Sound, Alaska generated about 20 landslide tsunamis in addition to a tectonic tsunami that was detectable in all of the study areas in the Pacific. The 1964 earthquake was responsible for the largest observed tsunamis proximate to both the Humboldt Call Area and Morro Bay Call Area. Wave height was reported to be 2.7 m on the shore of Trinidad, California, located east of the Humboldt Call Area (Lander et al., 1993). In Pebble Beach, California, north of the Morro Bay Call Area, runup was reported to reach a maximum wave height of 2.25 m (Lander et al., 1993).

5.3.2 Tsunami Hazards in Hawaii

The historical tsunami events from 2000 B.C. recorded or observed around Oahu are extracted from the NGDC database (NOAA, 2019c) and presented in Figure 25. One of the most recent tsunamis occurred in the region in October 2006, when a magnitude 6.7 earthquake caused small waves near Kiholo Bay, on the island of Hawaii. This sort of event would be unlikely to cause partial failure in an offshore wind farm, but this event illustrates the fact that wave height can be extremely variable in an earthquake-caused tsunami. The average magnitude of the tsunamis (based on earthquake magnitude) for the 200-year time frame in Hawaii was 6.75 (for events for which magnitude of the precipitating earthquake was recorded). According to the NGDC (NOAA, 2019 b,c) data, there have been 40 recorded tsunamis affecting Hawaii since 1800, and 15 in the last century (or about one every 6.7 years; NOAA, 2019b), or an annual probability of 0.15. There was one recorded tsunami event of over 7.9 (in the year 1868), which makes a return rate of one in 150 years (0.007 per year).

The tsunami generated from the earthquake of 1946, which struck off the coast of Unimak Island in Alaska's Aleutian Islands, caused the greatest damage and number of deaths in Hawaii's history. This event then led to the creation of the United States' first tsunami warning system. In Hawaii, the waves from the M7.5 Alaskan earthquake reached about 55 ft (16.8 m) high and killed 158 people, mostly in the town of Hilo (L´opez and Okal, 2006), 3,000 km away from the source. This was one of the largest tsunami runups affecting the region near the Oahu Call Areas (Soloviev and Go, 1975). Along Kaena Point, Hawaii, located between the Oahu North and Oahu South Call areas, the tsunami was reported to have maximum runup of 10.9 meters (Lander et al., 1989; Figure 25).

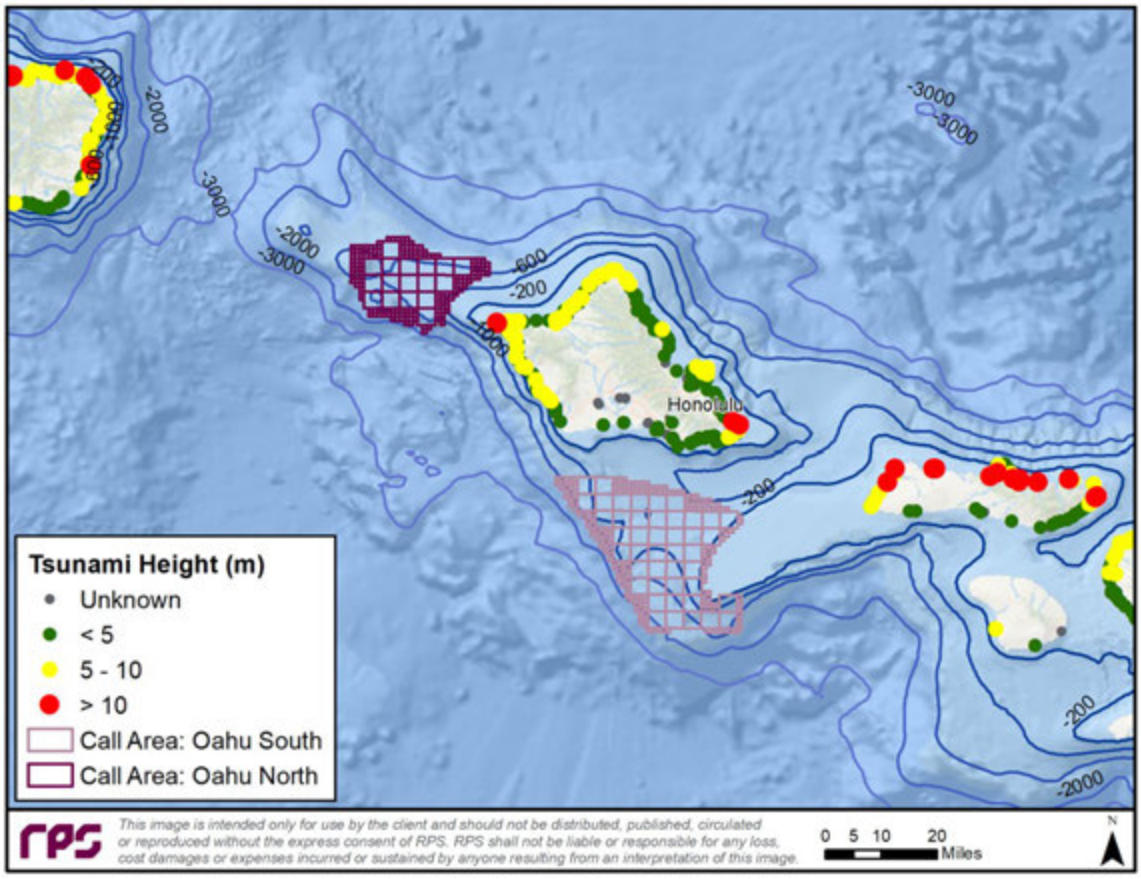

Figure 25. Historic Tsunami Measured or Observed on Oahu Coasts (data extracted from NOAA, 2019c).

6 SUITABILITY ANALYSIS METHODOLOGY

Given the vast areas covered in this study, and the fact this is a regional assessment based on coarse and sparse data, RPS data-mined and gathered publicly available geological and geophysical datasets to perform a GIS-based suitability analysis. This analysis was performed by considering three key factors to geohazards, including information on bathymetry and its gradient (slope); seafloor geology from regional mapping and near-surface seabed soils; and regional seismicity and probabilistic seismic hazard maps as defined by Peak Ground Acceleration (PGA), to evaluate the potential surface and near-surface geohazards in relation to seismic hazards.

These data were processed into raster format and coalesced into a single combined raster for each representative geological and geophysical layer of Soil Type, Slope Gradient, and PGA. To determine the suitable locations for FOWF from potential study areas, suitability analysis in GIS is applied and performed with five different weighting models and totaling using these three input raster maps. Suitability modeling through weighted overlay analysis allows for the assignment of a relative influence value to each layer, and by viewing different optional outputs, a ranking of the geospatial domain from least suitable to most suitable. In this study, five weighted overlay suitability analysis models are created for each study area to present the effect of variable weights on each input layer to the overall suitability of the study areas. The GIS suitability approach allows both suitable or unsuitable characteristics to be assessed, and the results of this analysis presented as maps are used to highlight areas from high to low suitability.

The weighted percent criteria and the methodology used for the models are presented and discussed in Section 7. This report section provides a discussion of the model inputs, and the methodology of suitability analysis.

6.1 Geological Data Inputs and Their Utility

Publicly available geological and geophysical datasets including bathymetry and slope (calculated from bathymetry), faults, near-surface seabed soil type, and PGA data were utilized for this study. This report section provides an explanation of the different type of inputs, where they were obtained, and the methodology and processes used to format each into a raster form, with standard classifications and common evaluation scales for the weighted suitability analysis.

6.1.1 Bathymetry (Slope Gradient)

Erosion and transportation processes cause the deposition of thick layers of unconsolidated sediments on slopes in the ocean. The probability of failure of rapidly deposited and unconsolidated sediments increases with bathymetry gradient and further increases under conditions (i.e., wave loading or ground-shaking) related to seismic events and related tsunamis. Since probability of slope failure is related to the bathymetry gradient, the bathymetry, or more directly its spatial derivative (i.e., slope), was determined and used as input in this study.

For this study, regional bathymetric Data Elevation Models (DEM) were used to compute slope gradients, which were subsequently used as a weighted data input for site suitability analysis. The polygon extents and the color hill shades of bathymetric and topographic DEMs for the U.S. Pacific West Coast and Hawaii, hosted at National Centers for Environmental Information (NCEI) and Hawaii Mapping Research Group (HMRG), are shown in Figure 26 and

Figure 27 and described in Table 10 and Table 11. The high-resolution DEMs are built for tsunami or hurricane storm-surge inundation modelling and sea-level rise, and the regional DEMs can be used for visualizing the coastal zone or to model ocean dynamics (NOAA, 2019e; https://maps.ngdc.noaa.gov/viewers/bathymetry/).

For the U.S. Pacific West Coast AOIs (Oregon Regional, Northern California Humboldt and Southern California Morro Bay and Diablo Canyon), Coast Relief Digital Elevation Models were used for bathymetric data analysis (https://ngdc.noaa.gov/mgg/coastal/crm.html; NOAA 2019d).

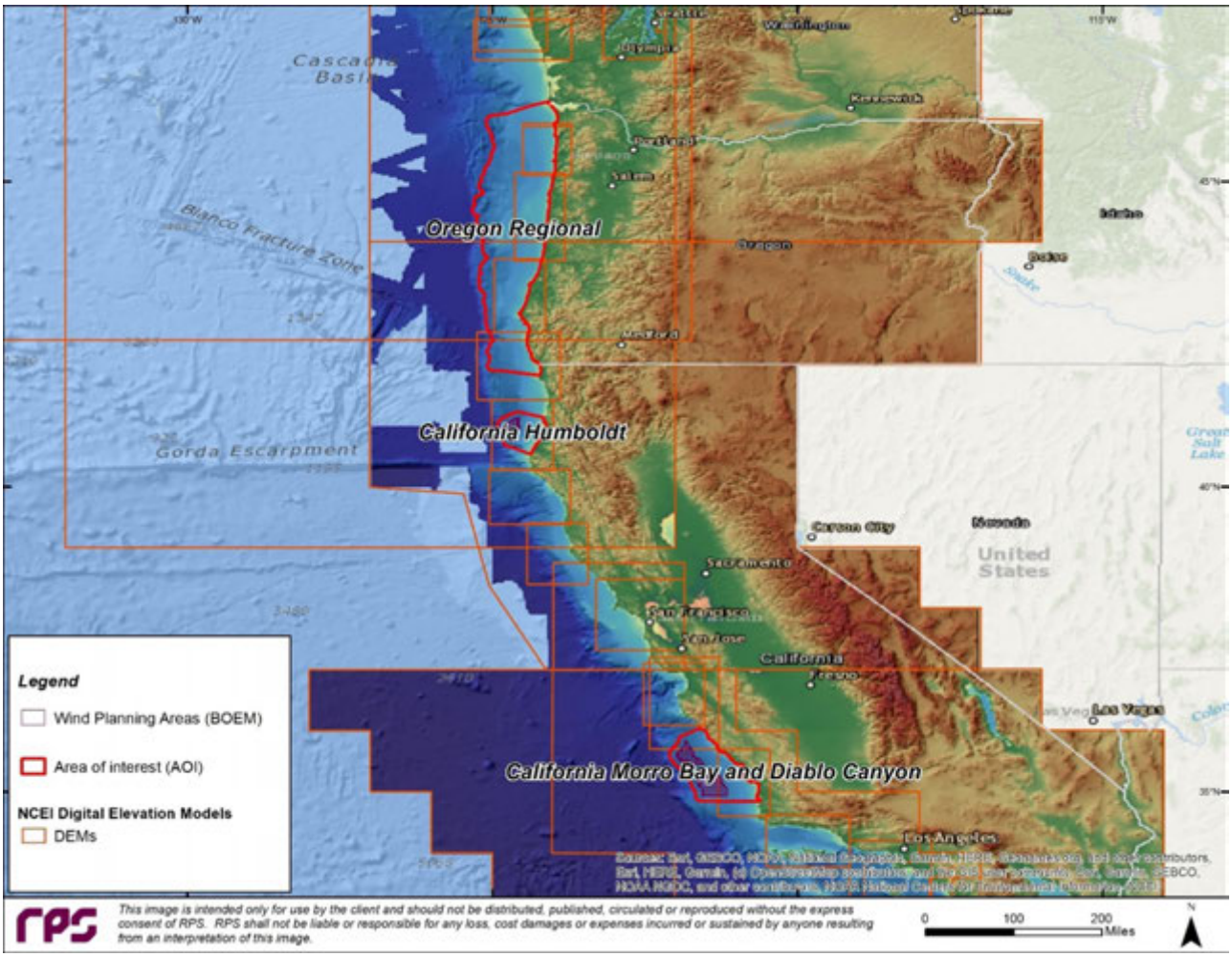

Figure 26. Extents for National Centers for Environmental Information (NCEI), and Digital Elevation Models. Study AOI Polygons are shown in red.

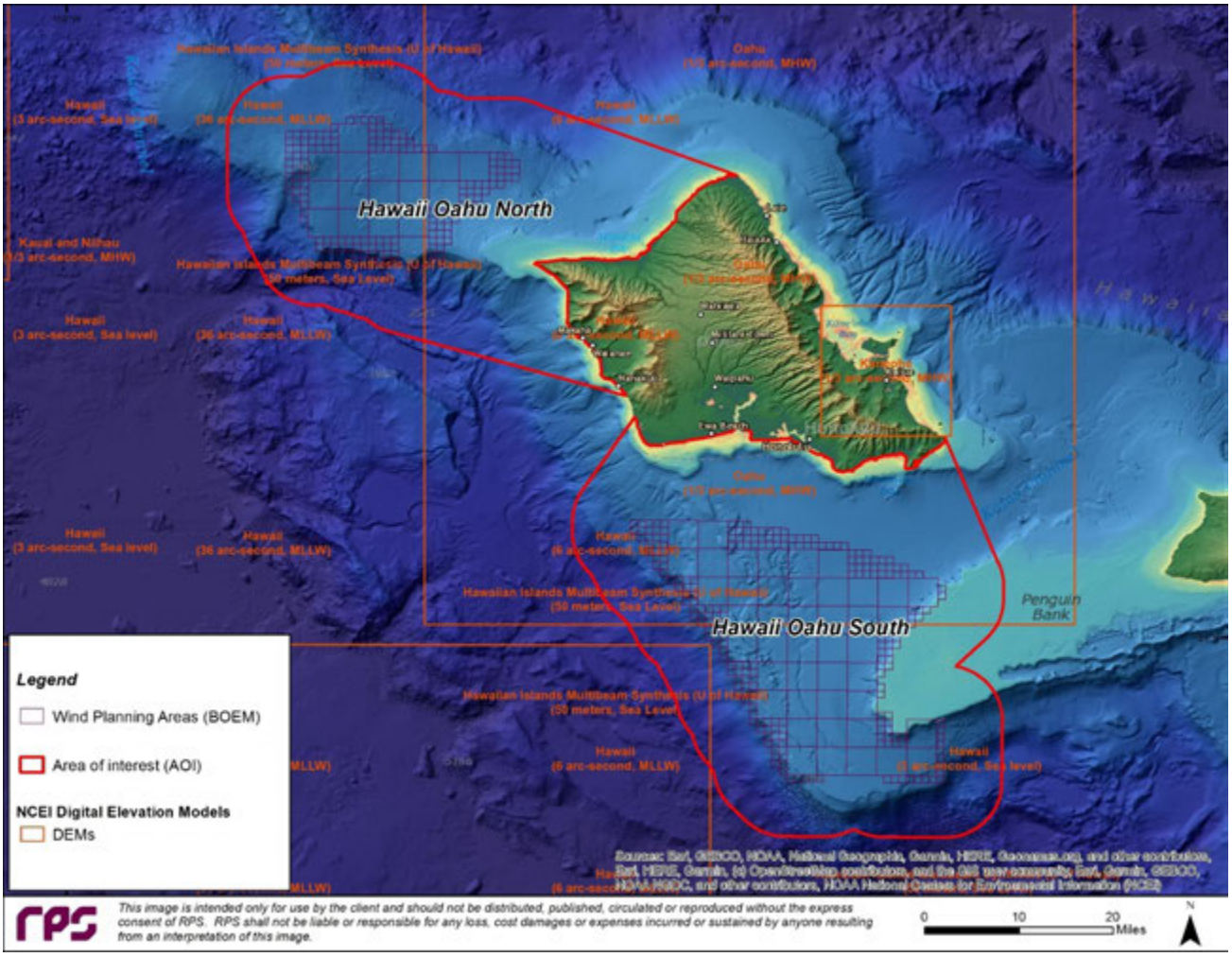

Figure 27. Extents for Hawaii Mapping Research Group (HMRG) Digital Elevation Models, and Study AOI Polygons are shown in red.

Table 10. NCEI Coastal Relief DEMs for U.S. West Coast

Name and Details	Year	Spatial Resolution	Filename	Area of Interest (AOI)
Vol. 8 – Northwest Pacific	2003	3 arc-seconds (~90m)	crm_vol8.nc	Oregon Regional
Vol. 7 – Central Pacific	2003	3 arc-seconds (~90m)	crm_vol7.nc	Oregon Regional, California Humboldt
Vol.6– Southern California	2003	3 arc-seconds (~90m)	crm_vol6.nc	California Morro Bay and Diablo Canyon

For the U.S. Hawaiian Islands AOIs (Hawaii Oahu North and Hawaii Oahu South), Bathymetry Synthesis Digital Elevation Models, prepared by the Hawaii Mapping Research Group (HMRG) at the School of Ocean and Earth Science and Technology, University of Hawaii at Manoa, were used for bathymetric data analysis (https://www.soest.hawaii.edu/HMRG/multibeam/bathymetry.php).

Table 11. Hawaii Mapping Research Group DEMs for U.S. Hawaiian Islands

Name & Details	Year	Spatial Resolution	Filename	Area of interest (AOI)
Bathymetry Synthesis	2016	~50 meters	mhi_mbsyn_bathyonly_50m_v21.nc	Oahu North and South

6.1.2 Geology (Soil Type)

Liquefaction is a phenomenon in which the strength and stiffness of a soil is reduced by earthquake shaking. Liquefaction occurs in water-saturated soils and the phenomenon is most often observed in loose (low density or uncompacted), sandy soils. When liquefaction occurs, the strength of the soil decreases and the ability of a soil deposit to support foundations (e.g., seabed anchors) is reduced or eliminated. Thus, the presence of saturated unconsolidated sediments on the seabed have the potential for liquefaction and clean sands or gravels should be avoided by potential FOWF.

Revised surficial geologic habitat mapping (version 4) of the Outer Continental Shelf off Washington, Oregon and northern California was conducted by the Active Tectonics and Seafloor Mapping Lab at Oregon State University (OSU). This research was designed to provide baseline information of seafloor geology at a regional scale through an integrated approach of new mapping, synthesis of existing data, conducting biological assessments, and developing new predictive models (Goldfinger et al., 2014). The interpreted regional geology relevant to Oregon Regional and California Humboldt AOIs was integrated from a combination of new local scale surveys and existing regional surveys using a combination of seafloor, shallow sub-seabed sampling and dense grid of seismic reflection profiles. Water depths were mapped using high-resolution multibeam bathymetry (accuracy of a few centimeters), and seabed grab samples were acquired from soft seabed areas. Geological interpretation was aided by the combination of USGS usSEABED database of sediment texture (Reid et al.,2006) and 104 grab samples and 152 box cores within the six study sites illustrated in Figure 28 (Goldfinger et al., 2014).

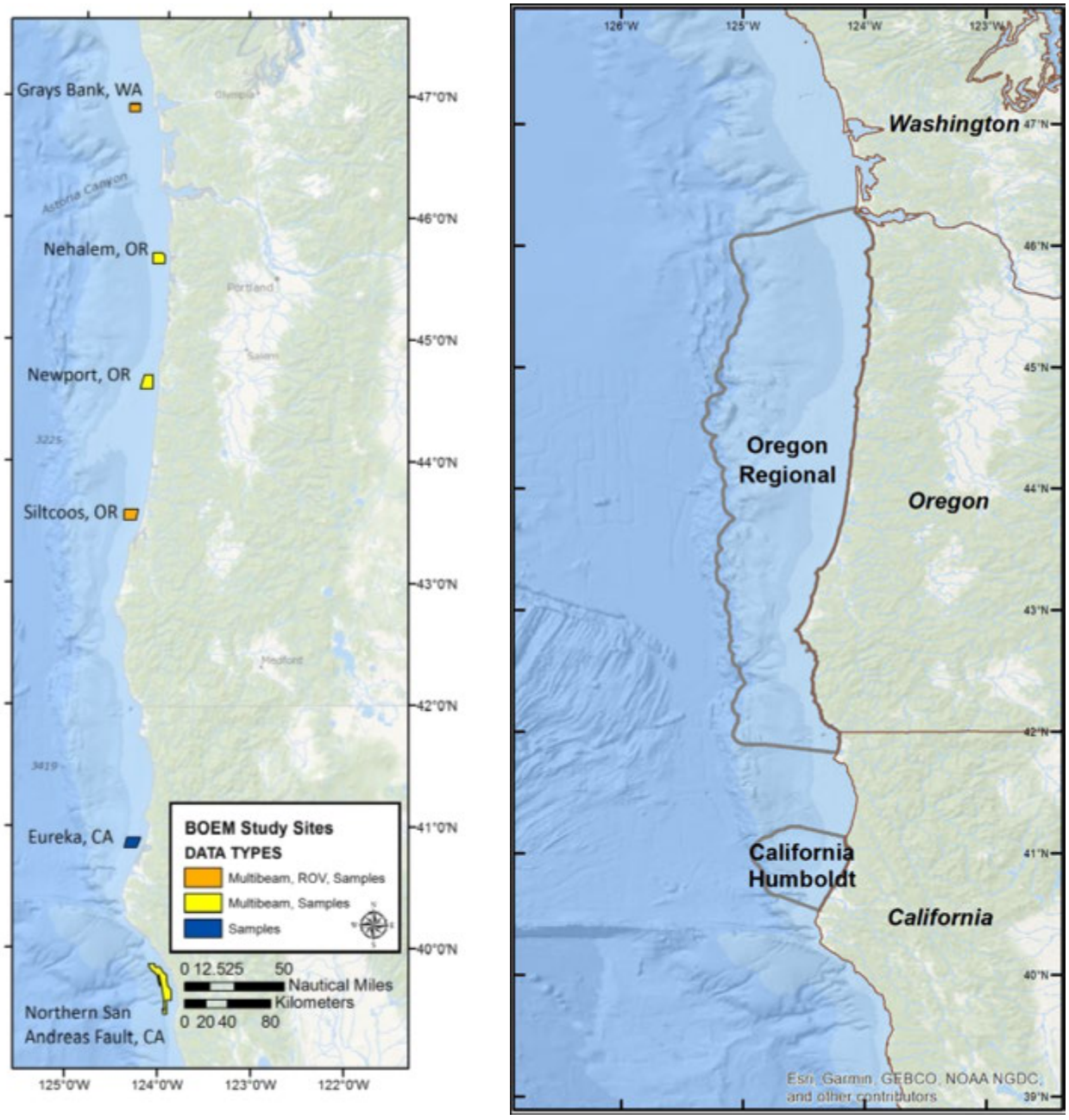

Figure 28. Locations of BOEM study sites and samples and core data collections (from Goldfinger et al., 2014) on the left, and AOIs of this report for comparison on the right.

A revised surficial geologic habitat mapping (version 4) of the Outer Continental Shelf off Washington, Oregon and northern California supported by BOEM and other agencies (Goldfinger et al., 2014) contributed to the higher spatial resolution of geological and benthic habitat mapping. This research was designed to provide baseline information of seafloor geology at a regional scale through an integrated approach of new mapping, synthesis of existing data, conducting biological assessments, and developing new predictive models. This data coverage for the AOI in Oregon Regional and California Humboldt is represented in Figure 29.

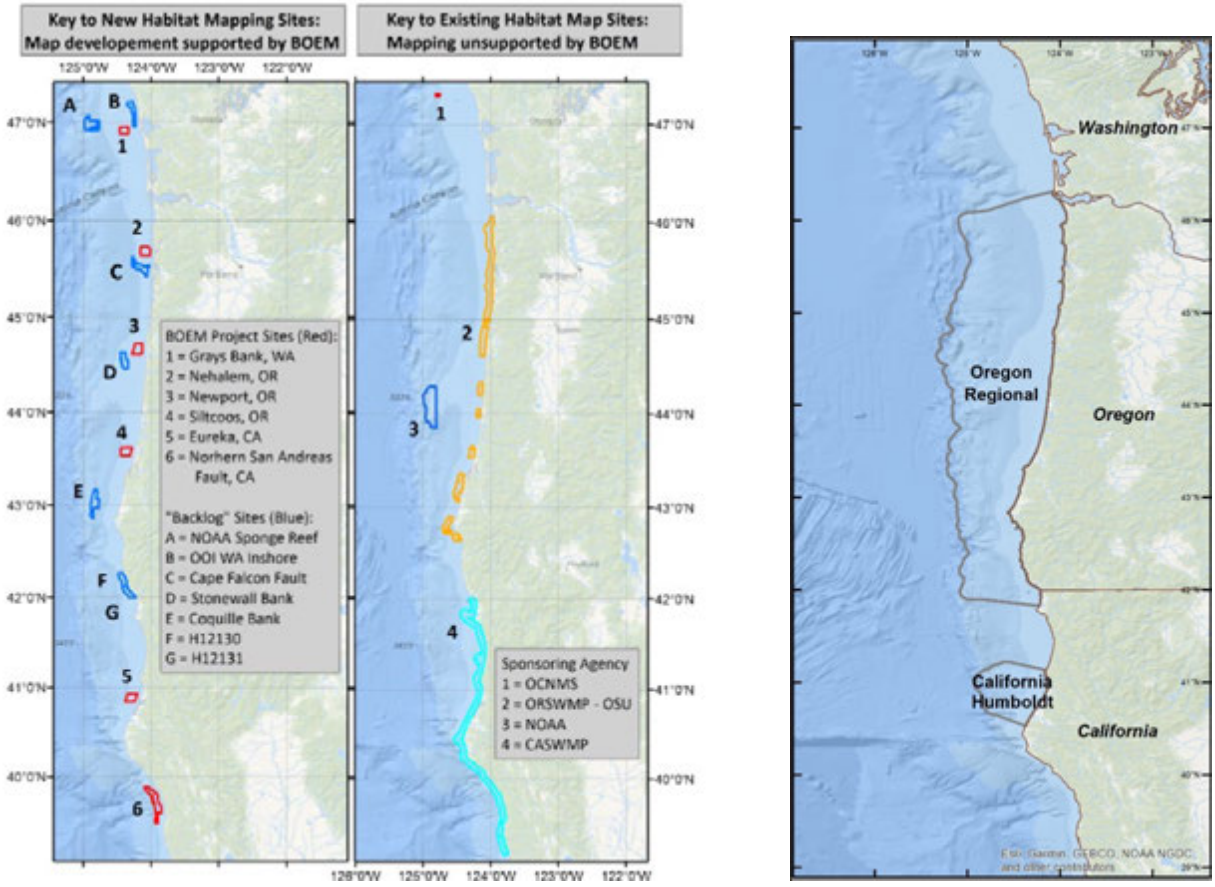

Figure 29: New and existing data for habitat maps (from Goldfinger et al., 2014) on left, and the AOI of this study on right for comparison.

Figure 30 presents data sources for the surficial geology mapping of the California Morro Bay and Diablo Canyon AOIs, as modified after McCulloch et al. (1982). That study summarized the regional geologic framework offshore California. For the Santa Maria Basin, geohazards potentially include gas-charged sediments, shallow soil failures, deep-seated lateral displacement landslides, and potential fault offsets at the seafloor. This interpretation was supported by regional 2D seismic data acquired in 1979 (cross-sections a, b, c, d on Figure 30).

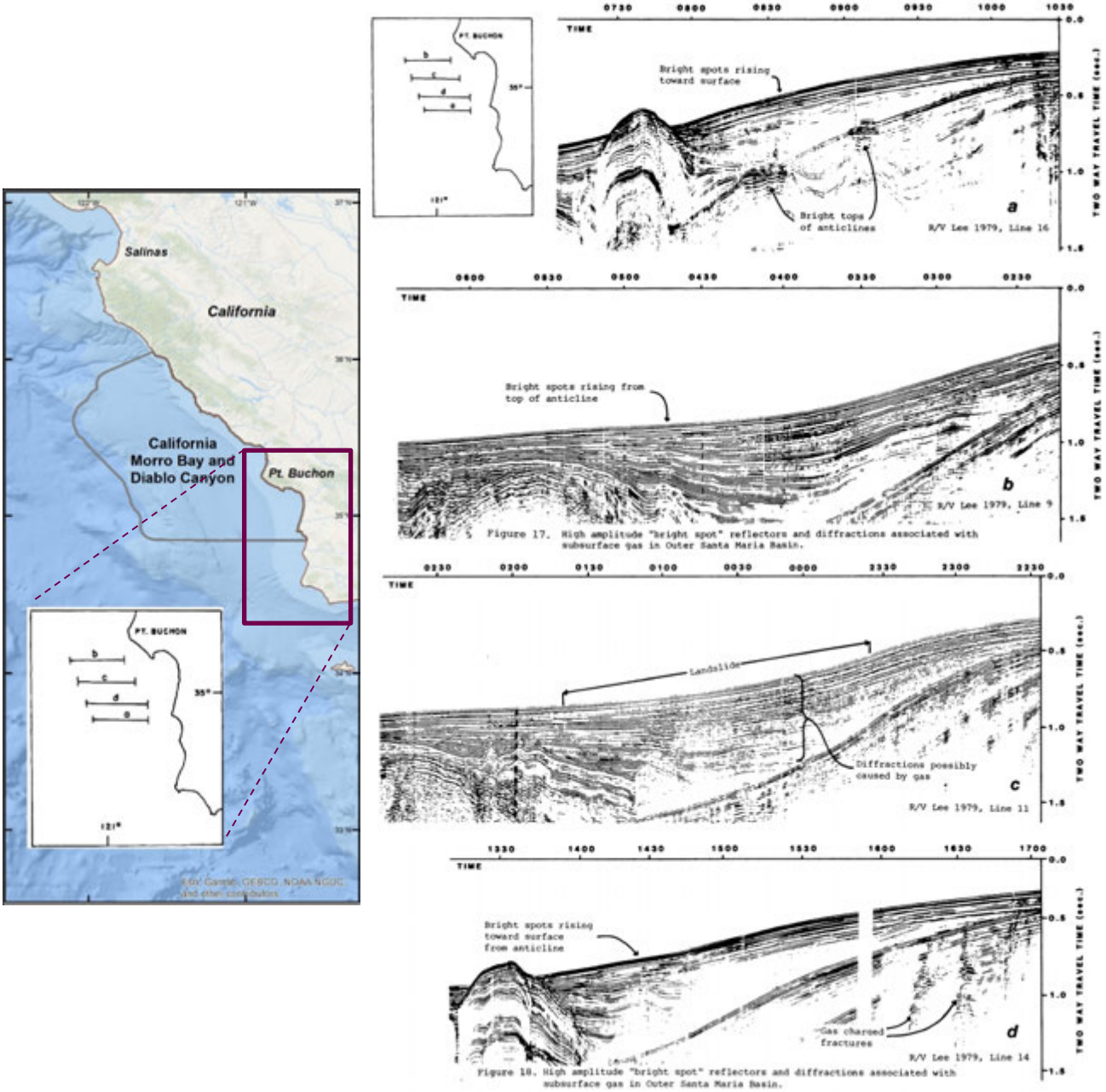

Figure 30. Seismic profiles Offshore Diablo Canyon AOI (from McCulloch et al., 1982) on the right, and their location relative to AIOs of this study on the left.

Figure 31 presents data sources for the seafloor geology of the US Pacific West Coast AOIs (Oregon Regional, California Humboldt, Morro Bay and Diablo Canyon) used in this study. For the Oregon and California Humboldt study areas, seabed hardness and texture were interpreted from the multibeam backscatter data acquired coincident to the bathymetry data. The seabed grab samples and box cores were used to establish relationships between sediment grain size, multibeam bathymetry, and coincident backscatter data. Additionally, through interpretation of a dense grid seismic reflection

profiles, interpreted iso-core, and slope stability contours, a predictive rock substrate model for the continental shelf was generated (Goldfinger et al., 2014).

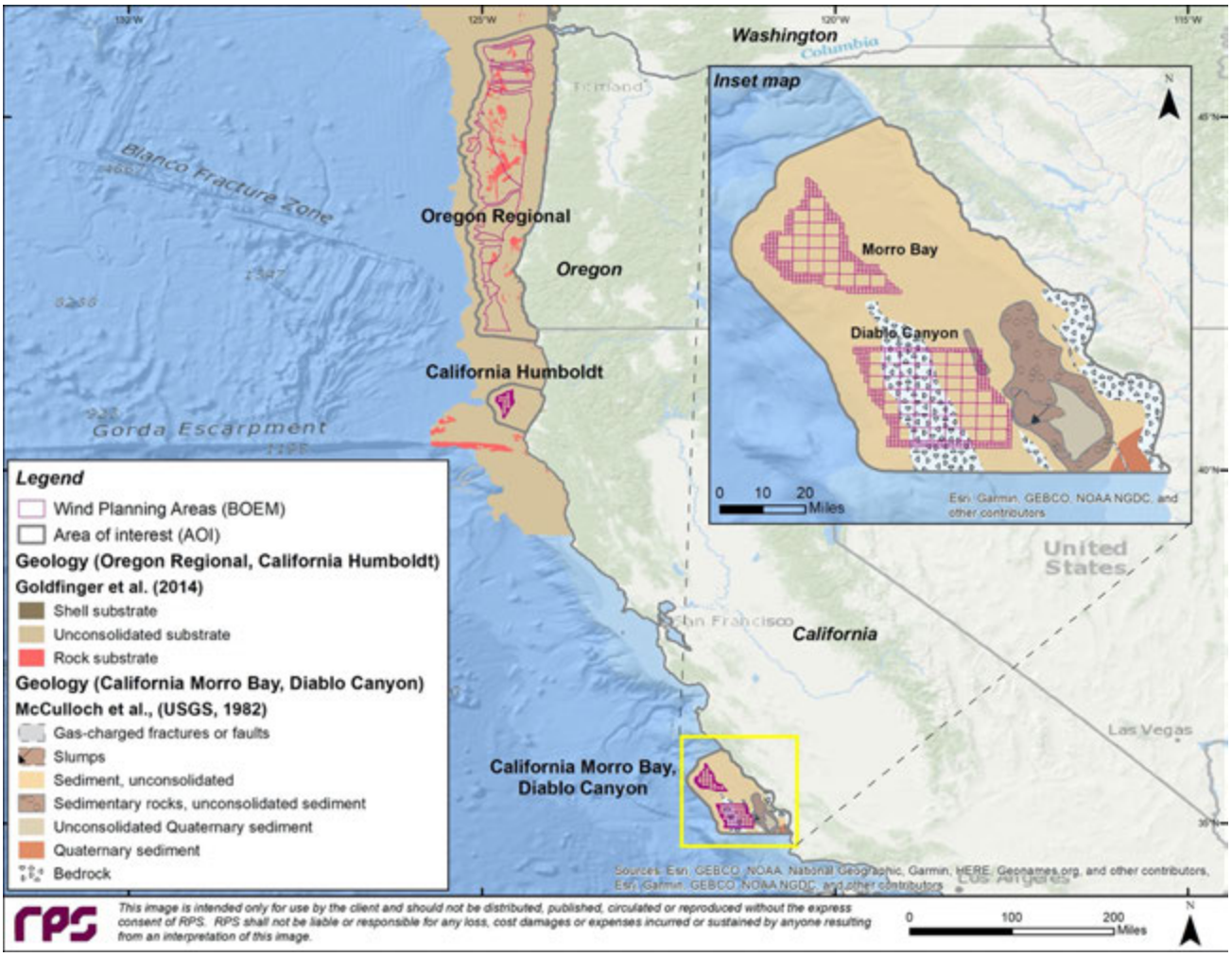

Figure 31. Compilation of Geology Offshore Oregon and California (Sources: Goldfinger et al., 2014 and McCulloch et al., 1982).

Figure 32 provides the geologic map relative to the study AOIs (modified from Holcomb and Robinson, 2004) around the Hawaiian Islands. The geology of the seabed was derived from GLORIA (Geological Long-Range Inclined Asdic) side-scan sonar survey data collected in 1986-1989 from the southeastern Hawaiian Ridge Exclusive Economic Zone (EEZ), which covers more than 1,000,000 km2 of sea floor. The seafloor is characterized by a variety of volcanic and sedimentary processes. Cretaceous age seafloor underlies both subaerial and subaqueous erupted lava forming the Hawaiian Ridge and various Cretaceous seamounts. Subaerial lava quenches and brecciates (i.e., breakdown of rock) as it enters the ocean forming smooth slopes. The mobile flanks of the islands have given way to slumps and debris avalanches.

While using these datasets, differences in the methodologies used to acquire the data (e.g., seismic, grab samples, cores) through different studies, differences in time the data were acquired and the

variable spatial resolution (accuracy) of those studies should be considered as important factors in determining certainty of data and consequently the analysis output.

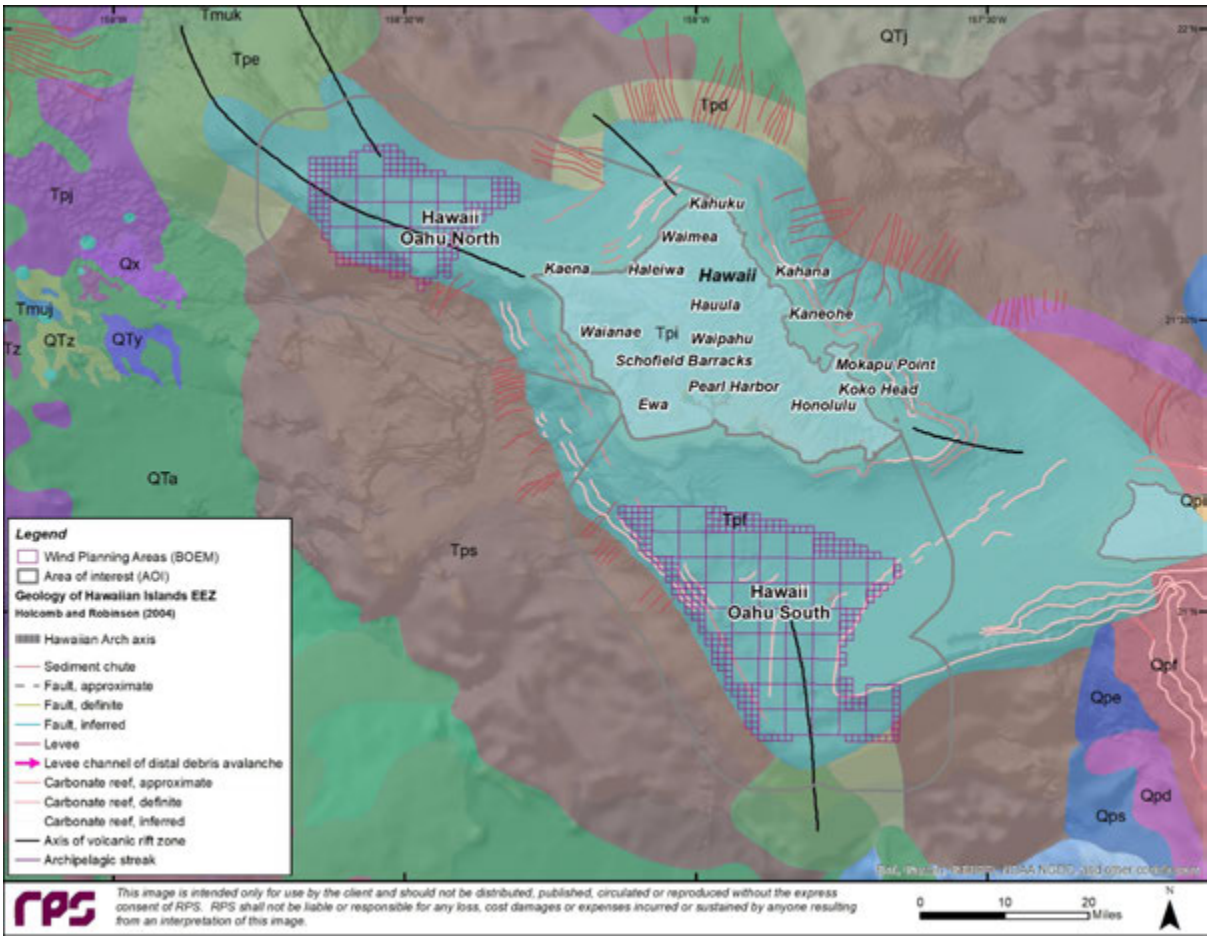

Figure 32. Geology of Hawaiian Islands Exclusive Economic Zone (modified from Holcomb and Robinson, 2004).

6.1.3 Seismic Hazard (Peak Ground Acceleration)

Seismic activity in the study areas was comprehensively discussed in the literature review for this study (Section 5.1, Figure 15 to Figure 18).

To determine the seismic hazard in the study areas, it is appropriate to draw from relevant earthquake engineering codes and standards as opposed to adopting historic datasets directly. These standards, based on the U.S. National Seismic Hazard Model (NSHM) provide a unified measure of intensity of earthquakes for all study areas and are the basis for structural design in the U.S. (ASCE/SEI 7-16). For this project, the NSHM and acceleration value data were extracted from USGS Scientific Investigations Map 3325 for the Conterminous United States (2014) and USGS Geologic Investigation Series I-2724 for Hawaii (2000). Between the USGS Conterminous U.S. and Hawaii seismic hazard data available, relevant hazard levels include:

- 2% probability of exceedance in 50 years (2500-year event, Extreme Events)

  - Peak ground acceleration (Figure 33)
  - Horizontal spectral acceleration for 0.2s period (5% of critical damping)
  - Horizontal spectral acceleration for 1.0s period (5% of critical damping)
- 10% probability of exceedance in 50 years (500-year event, Serviceability Events)
  - Peak ground acceleration (Figure 34)
  - Horizontal spectral acceleration for 0.2s period (5% of critical damping)
  - Horizontal spectral acceleration for 1.0s period (5% of critical damping)

Based on ASCE/SEI 7-16, which is the current standard that many state building codes in the U.S. adopt as a basis for determining structural loads on buildings, probabilistic ground motions with a 2% chance of exceedance in 50 years are used to determine the spectral accelerations levels for collapse prevention design of buildings and other structures. The 2% in 50-year event is commonly known as the 2500-year earthquake. This event reflects the nation-wide adoption of “uniform” hazard criterion across the United States to on an equal hazard footing in the late 1990s. Prior to the adoption of this “uniform hazard” approach focusing on the 2500-year event, it was more common to talk about the so-called 500-year earthquake in California, which approximately represented the maximum deterministic values for earthquake ground accelerations. In probabilistic terms, the 500-year earthquake can be understood approximately as having a 10% chance of exceedance in 50 years. The 2500-year earthquake, or Maximum Considered Earthquake (MCE), became important on a national level because it was able to account for rare extreme events in moderate seismic regions that were not captured within the 500-year earthquake frame of reference.

This study focuses on Peak Ground Acceleration (PGA), for a 10% probability of exceedance in 50 years (500-year event), as appropriate for long-term design performance considerations (Figure 34). PGA is equal to the maximum ground acceleration that occurred during an earthquake at a location in horizontal and vertical directions and is equal to the largest absolute acceleration recorded during the earthquake. ASCE/SEI 7, Section 11.8 identifies PGA as the appropriate measure for assessment of geologic hazards. Use of PGA instead of historic earthquake magnitude was suggested by Dr. Eric Hines, PE. through the direct communication and contact by RPS. RPS would like to acknowledge and thank Dr Hines for his inputs here; and clarify that use of PGA is not needed, requested, or recommended by BOEM.

It should be noted that PGA layer (Figure 34) obtained from the USGS does not cover the western side of the Oregon AOI, and consequently affects the final analysis as it does not produce any results in that area.

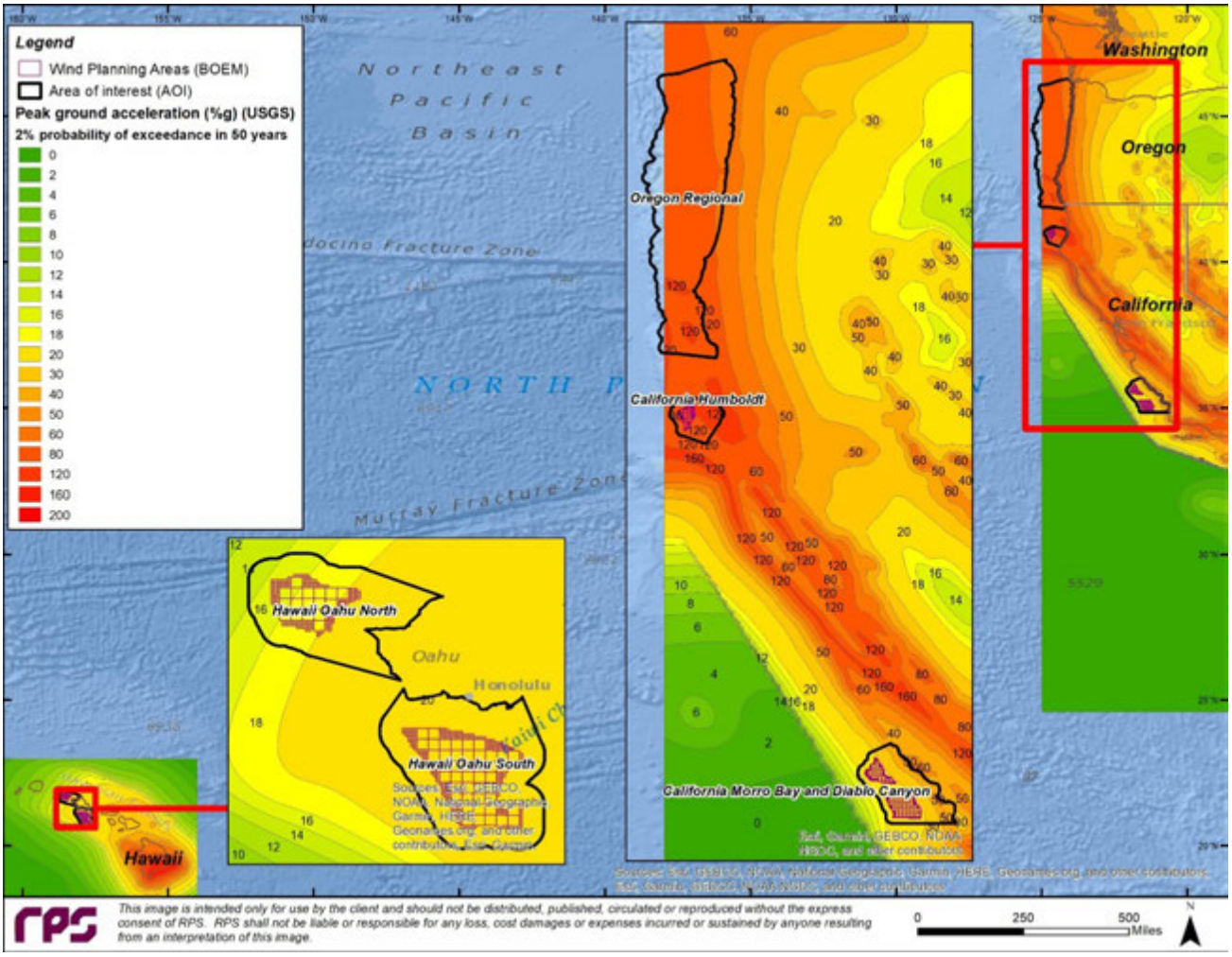

Figure 33. Probabilistic seismic hazard peak ground acceleration, 2500-year event (modified from USGS, 2000 and 2015).

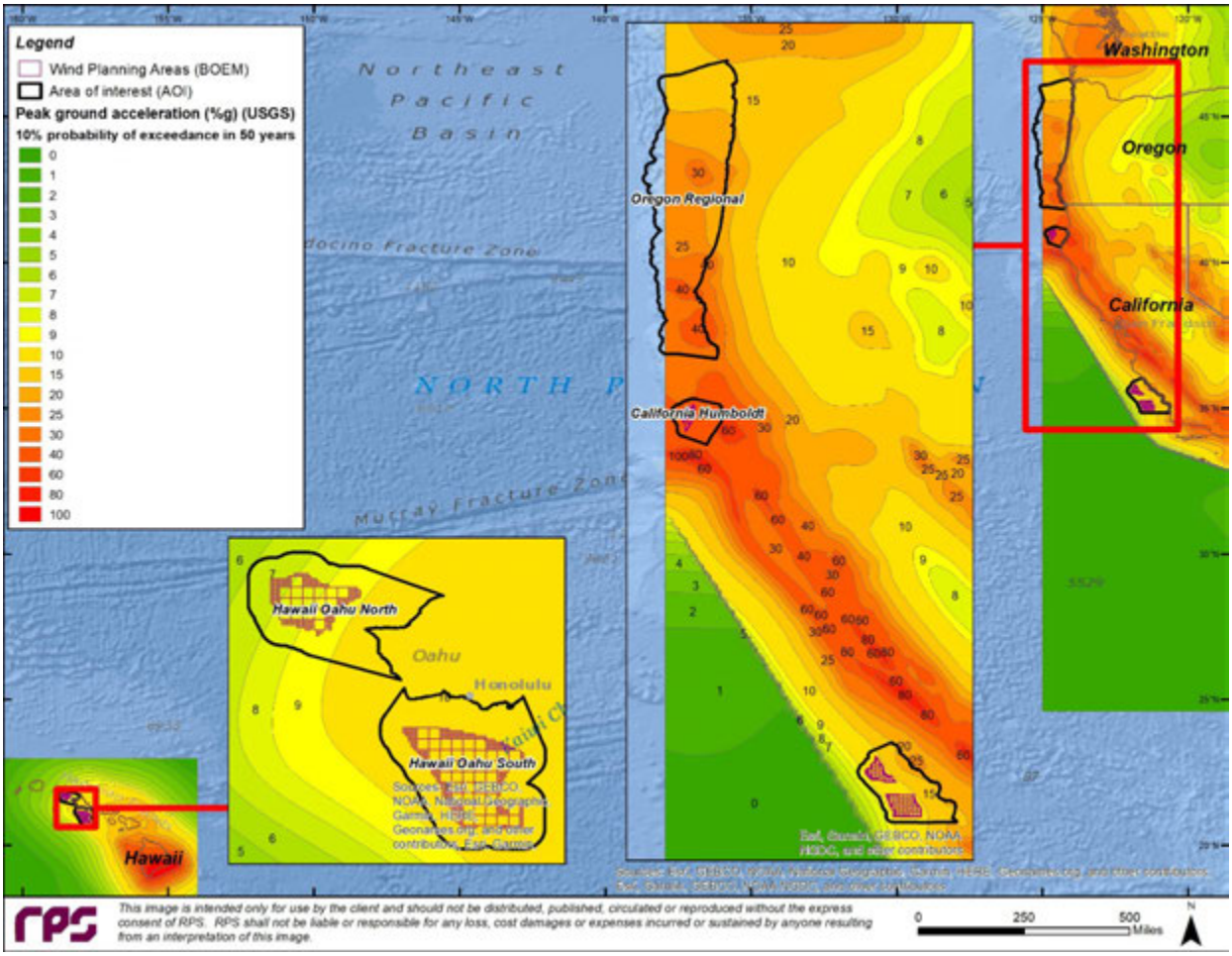

Figure 34. Probabilistic seismic hazard PGA, 500-year event (modified from USGS, 2000 and 2014).

6.2 Data Pre-Processing

To use the soil and seismic hazards data in a suitability analysis, they should be mapped into raster format. The soil type data (Section 6.1.2) was based on the type of geospatial datasets of soil type, and seismic hazards (Section 6.1.3) was based on geospatial data of PGA.

6.2.1 Bathymetry (Slope Gradient)

Global Mapper[5], developed by Blue Marble Geographic, was used to compute slope gradient for the DEMs within the entire AOIs. The polygons for all AOI's were loaded into Global Mapper as an overlay to the regional DEMs. Each AOI was sequentially selected, and the slope gradient was calculated and extracted by clipping the output data to the extents of the AOI, using the export option to "Export

[5] https://www.bluemarblegeo.com/products/global-mapper.php

slope values instead of elevations". Slope gradients for all AOIs were exported to Float/Grid format, directly compatible with Esri ArcGIS Desktop[6] .

6.3 Weighted Overlay Modeling (Suitability Analysis)

To perform site suitability analysis for all AOIs, the Weighted Overlay7 functions of Esri™ ArcGIS Desktop's Spatial Analyst tools were used. The Weighted Overlay tool applies one of the most widely used approaches for overlay analysis to solve multicriteria problems, such as site selection and suitability models, as is desired in this study. In order to perform weighted overlay analysis, the resultant output models are initially broken into sub models to identify the input layers. The input layers utilized for this study are seabed slope, seabed soil type, and PGA. The function overlays multiple input rasters, previously reclassified to a common measurement scale, and computes multiple output models based on assignment of variable weighting (influence) to the input layers, according to the prescribed models. Each input layer is composed of different quantification schemes and ranges. In order to combine input layers for weighted overlay analysis, all input data layers were reclassified (See Section 6.3.1 Reclassification) into a common evaluation scale (i.e., 1 to 9, with 9 being the most suitable). The final step of the weighted overlay analysis process was to validate the model to ensure the model presented a reasonable result, considering the variability of the input data layers. In summary, the Esri™ Weighted Overlay tool combines several of the typical steps in an overlay analysis process into a single tool. These steps are outlined by Esri™ below:

1. "Reclassifies values in the input rasters into a standardized evaluation scale of suitability or preference, risk, or some similarly unifying scale
2. Multiplies the cell values of each input raster by the raster's (user directed) weight of importance
3. Adds the resulting cell values together to produce the output raster"[5].

6.3.1 Reclassification (common evaluation scale)[8]

The Weighted Overlay function of Esri™ ArcGIS Desktop's Spatial Analyst tool only accepts integer rasters as input. Thus, the continuous (floating point) rasters need to be reclassified into a classified format which assigns each of the polygonal areas that make up a raster with a user-specified integer values. Examples of the slope reclassification schemes used for slope, soils, and PGA are provided in Sections 6.3.1.1 – 6.3.1.4.

6.3.1.1 Slope Gradients

Since probability of failure increases with gradient, lower bound slope values have been classified as most suitable and higher bound slope values (above 10°) have been classified as least suitable. The upper bound number is based on a recent BOEM study (Goldfinger et al., 2014) which suggests high slope areas >10° effective maximum angle of repose were likely areas of exposed rock. The ranges

[6] http://desktop.arcgis.com/en/
[7] http://desktop.arcgis.com/en/arcmap/latest/tools/spatial-analyst-toolbox/how-weighted-overlay-works.htm
[8] http://desktop.arcgis.com/en/arcmap/latest/tools/spatial-analyst-toolbox/an-overview-of-the-reclass-tools.htm

of slope gradients were reclassified for suitability based on the following lower and upper bounds (Table 12).

Table 12. Reclassification Suitability of Bathymetry Slope Gradient Following Criteria from Goldfinger et al. (2014): Slopes > 10 Degrees

Reclassification Suitability of Bathymetry (slope gradient)			
Lower bound (degrees)	**Upper bound (degrees)**	**Reclass value**	**Suitability**
0	1	9	Most suitable
1	2	8	
2	3	7	
3	4	6	
4	5	5	
5	6	4	
6	7	3	
7	10	2	
10	100	1	Least suitable

6.3.1.2 Peak Ground Acceleration

Since probability of seismic hazard increases with acceleration value, the lowest acceleration value (0 %g) within the study area as most suitable (9) and the highest acceleration value (60 %g) within the study area as least suitable (1). Acceleration values between the lowest and highest were assigned appropriate suitability based on a linear scaling (Table 13).

Table 13. Reclassification Suitability of Peak Ground Acceleration, 10% probability of exceedance in 50 years (500-year event).

Reclassification Suitability of Peak Ground Acceleration			
Lower bound (PGA)	**Upper bound (PGA)**	**Reclass value**	**Suitability**
0	5	9	Most suitable
5	12	8	
12	19	7	
19	26	6	
26	33	5	
33	40	4	
40	47	3	
47	54	2	
54	60	1	Least suitable

6.3.1.3 Geology (U.S. West Coast)

Geology (soil type) data available as polygon shapefiles (Figure 31) were converted from polygons to rasters using Esri™ ArcGIS “Polygon to Raster” tool and by assigning suitability to the soil types by way of a value field directly in the polygon shapefiles. The value field contained the reclassification values presented in Table 14 and Table 15. The areas mapped as sand (sand mud, sandy gravel, sandy mud) were assigned the least suitability (1 and 2) due to higher risk of liquefaction. Areas mapped as hard (including rock, rock mix, boulder) were also assigned lower suitability (3 and 4) due

to potential engineering constraints related to suction piles and anchoring. Suitability values generally increased (5 to 9) by decreasing grain size from cobble to mud.

Table 14. Geology Soil Type: Offshore Oregon and Northern California (Humboldt)

Geology (soil type): offshore Oregon and Northern California (Humboldt)		
Description	**Reclass value**	**Suitability**
Mud, muddy sand	9	Most suitable
Gravelly mud, gravelly sand	8	
Gravel, gravel mix	7	
Shell	6	
Cobble, cobble mix	5	
Boulder	4	
Hard, rock, rock mix	3	
Sandy mud, sandy gravel, sand mud	2	
Sand	1	Least suitable

The detailed maps of the geology offshore AOI Diablo Canyon (Santa Lucia Bank) by McCulloch et al. (1982) provided the basis for assigning lowest suitability (1 and 2) to areas mapped as bedrock (or bedrock close to the surface), and to areas mapped as gas-charged fractures or faults. A mid-range suitability (5) was assigned to all Morro Bay AOI (east of Davidson Seamount) due to the dearth of detailed geological mapping (i.e., from a geological perspective, AOI Morro Bay could neither be assigned completely suitable or completely unsuitable). Based on geological descriptions, there was a lack of justification for assigning high suitability (6 to 9) to any mapped areas (see Table 15 and Figure 31 and Figure 41).

Table 15. Geology (Soil Type): Offshore Southern California (Morro Bay and Diablo Canyon)

Geology (soil type): offshore Southern California (Morro Bay and Diablo Canyon)		
Description	**Reclass value**	**Suitability**
Input data does not meet the level of suitability*	9	Most suitable
Input data does not meet the level of suitability*	8	
Input data does not meet the level of suitability*	7	
Input data does not meet the level of suitability*	6	
Unconsolidated sediment of Quaternary age and NODATA areas	5	
Base of unconsolidated Quaternary sediment	4	
Wave-cut erosion surface across deformed pre-Quaternary rocks	3	
Gas-charged fractures or faults	2	
Bedrock, slumps	1	Least suitable

*The weighted overlay suitability analysis requires a common measurement scale for all data inputs, so the full range of values, 1 (least suitable) to 9 (most suitable), are applied to all available data inputs. Therefore, the rows with descriptions of “Input data does not meet the level of suitability” are not indicative of NO DATA. They instead portray that for the data available, reclass values 6 to 9 (mid-suitable to most suitable) were not applicable to the input data.

6.3.1.4 Geology (Hawaii)

The geology offshore Hawaii is described by Holcomb and Robinson (2014), and is presented in Figure 32 as:

- **Present island (Tpi):** "Presently subaerial terrain" which includes a basaltic core surrounded by reefs and other sedimentary structures.
- **Intact flank (Tpe):** Submarine flanks which are composed of undisturbed lava flows on Hawaiian Islands, with slopes less than about 10 degrees, but highly variable with range of 0 – 45 degrees over short distances (less than a few kilometers).
- **Slump (Tps):** "Faulted and warped terrain" which consists of kilometers of blocks or slice, in parallel to the flanks of the Ridge and on Hawaiian volcanic edifices.
- **Debris flank (Tpd):** Debris on steep submarine flanks with > 10 degrees slope. On the Island of Hawaii, young volcanoes typically have slope > 20 degrees.
- **Former island (Tpf):** "Submerged shallow platforms or benches" with < 10 degrees slope over deeper area of >10 slopes.

A narrow band of the Present island (Tpi) unit was incorporated into the AOI for Oahu North and South, due to clipping of the study AOI using a coastline boundary that did not coincide precisely with the coastline used in the geological mapping of the Hawaiian Islands Exclusive Economic Zone (EEZ) (Holcomb and Robinson, 2004). Whereas the Present island (Tpi) unit is subaerial terrain(on or near land surface), it was assigned the least suitability (1). The units of Intact flank (Tpe), Slump (Tps) and Debris flank (Tpd) were assigned low but relative increasing suitability (2 to 4) based on the high slope and slumping geological descriptions documented. The remaining unit, Former island (Tpf), covering nearly 100 per cent of the Oahu North and South AOIs was assigned close to a mid-range, but slightly higher (6) due to the relative certainty of geology mapped but still without justification for assigning a high suitability (Table 16).

Table 16. Suitability Values for Geology (Soil Type): Offshore Hawaii Oahu (North and South)

Suitability Value for Geology (soil type): offshore Hawaii Oahu (North and South)		
Description	**Reclass value**	**Suitability**
Input data does not meet the level of suitability*	9	Most suitable
Input data does not meet the level of suitability*	8	
Input data does not meet the level of suitability*	7	
Former island (Tpf)	6	
Input data does not meet the level of suitability*	5	
Debris flank (Tpd)	4	
Slump (Tps)	3	
Intact flank (Tpe)	2	
Present island (Tpi)	1	Least suitable

*The weighted overlay suitability analysis requires a common measurement scale for all data inputs, so the full range of values, 1 (least suitable) to 9 (most suitable) must be applied to all available data inputs. Therefore, the rows with descriptions of "Input data does not meet the level of suitability" are not indicative of NO DATA, they instead portray that for the data available, this reclass value was not assigned mid to high suitability.

6.4 Integer Raster Maps (Data Inputs)

The following maps show the processed integer rasters for each of the dataset inputs of soil type, slope gradient, and PGA, at each of the AOIs: Oregon Regional, Humboldt, Morro Bay and Diablo Canyon California, and North and South Oahu Hawaii. NOAA depth zone contours, which mark the boundaries between the Shallow Zone (0-30m), Transition Zone (30m - 60m), and Deepwater Zone (60m - 900m), are included on each map for water depth reference purposes. Where appropriate, a short discussion is included on the right panel of the map.

6.4.1 Oregon Regional

Panel display of geology (soil type), slope gradient and earthquake magnitudes:

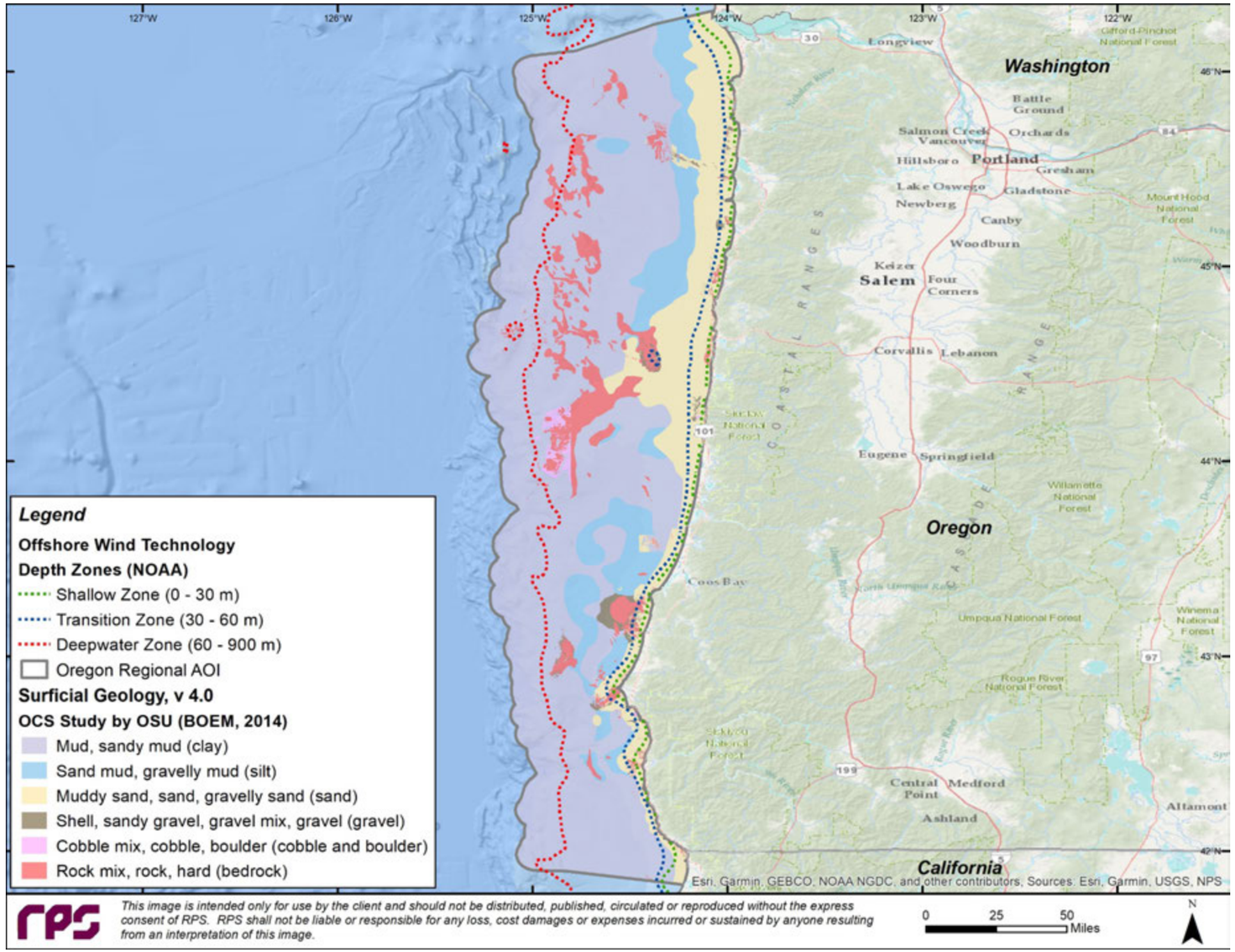

Soil types along the western regional coast of Oregon show primarily coarse gravels in the shallow and transition zones between 0 and 60m water depth. Sands and muds occupy the bulk of the deepwater zone between 60 and 900 m water depth.

Figure 35. Oregon - Geology (Soil Type)

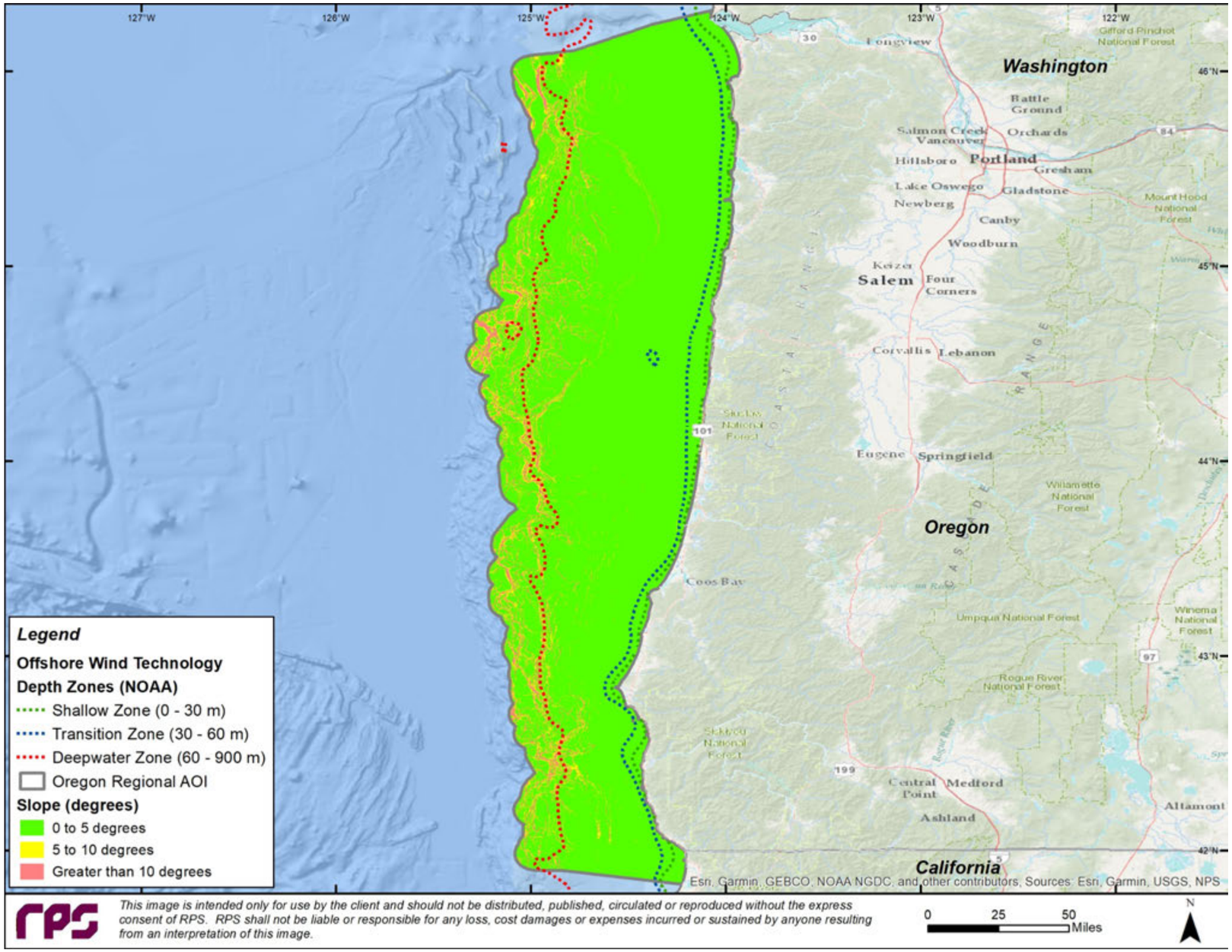

Slope gradients in the shallow and transition zones are less than 5 degrees. Slope gradient appears to only increase along the shelf edge and into deeper water where several terraces are marked by slopes >5° or higher.

Figure 36. Oregon - Slope Gradient

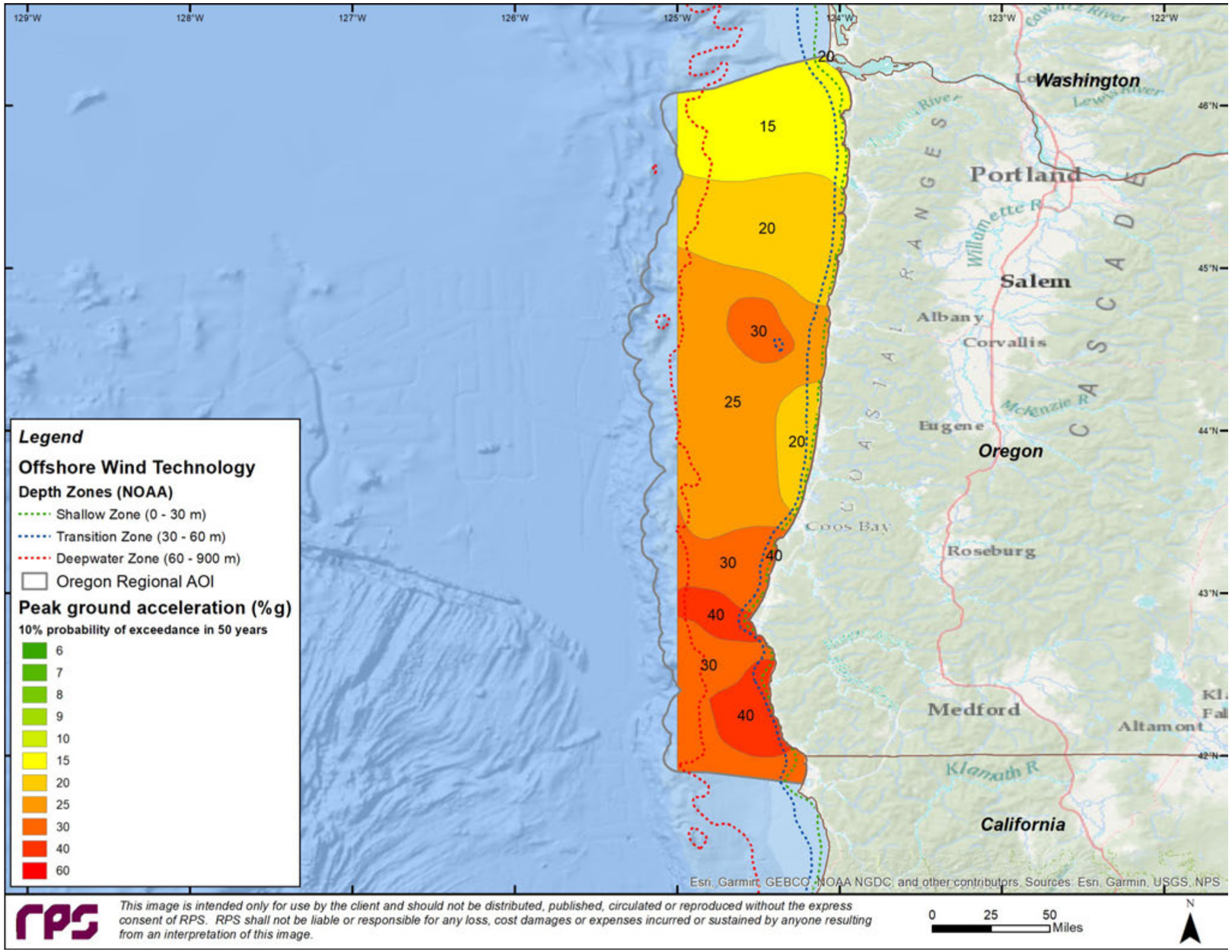

Peak ground acceleration varies from 15%g in the north to 40%g in the south of Oregon Regional AOI.

Note absence of PGA input on western edge of Oregon AOI.

Figure 37. Oregon - PGA

6.4.2 California Humboldt

Panel Display of Geology (Soil Type), Slope Gradient and Earthquake Magnitudes:

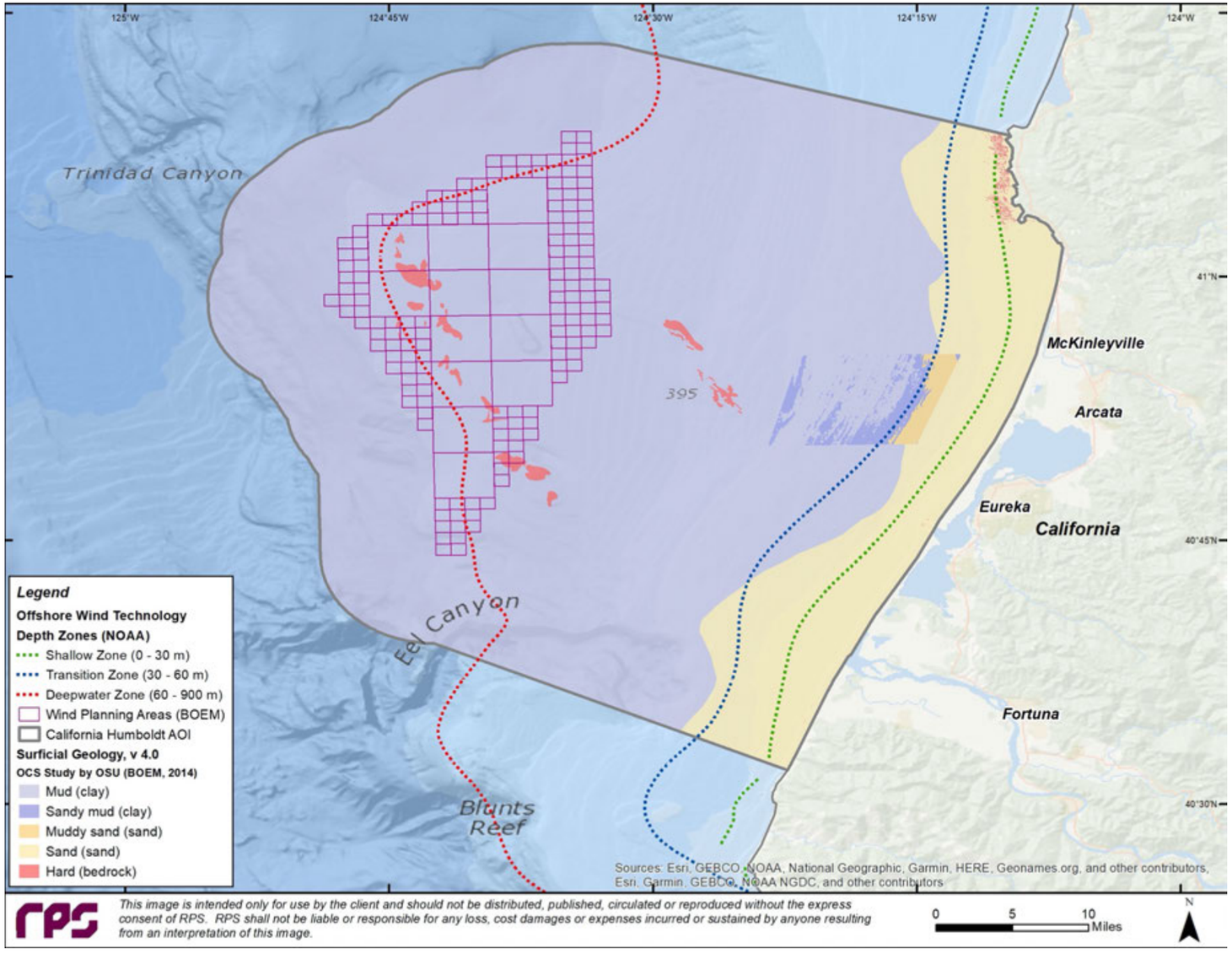

Figure 38. California Humboldt - Geology (Soil Type)

Soil types along the western coast of the Humboldt AOI show primarily coarse sands in the shallow and transition zones between 0 and 60m water depth. Mud and hard rock dominate the bulk of the deepwater zone between 60 and 900 m water depth. There is an obvious difference in reported seabed sediment type(s) in the central eastern portion of the map, where detailed site-specific mapping from high-resolution data was available and used to improve interpretation of regional surficial geological mapping.

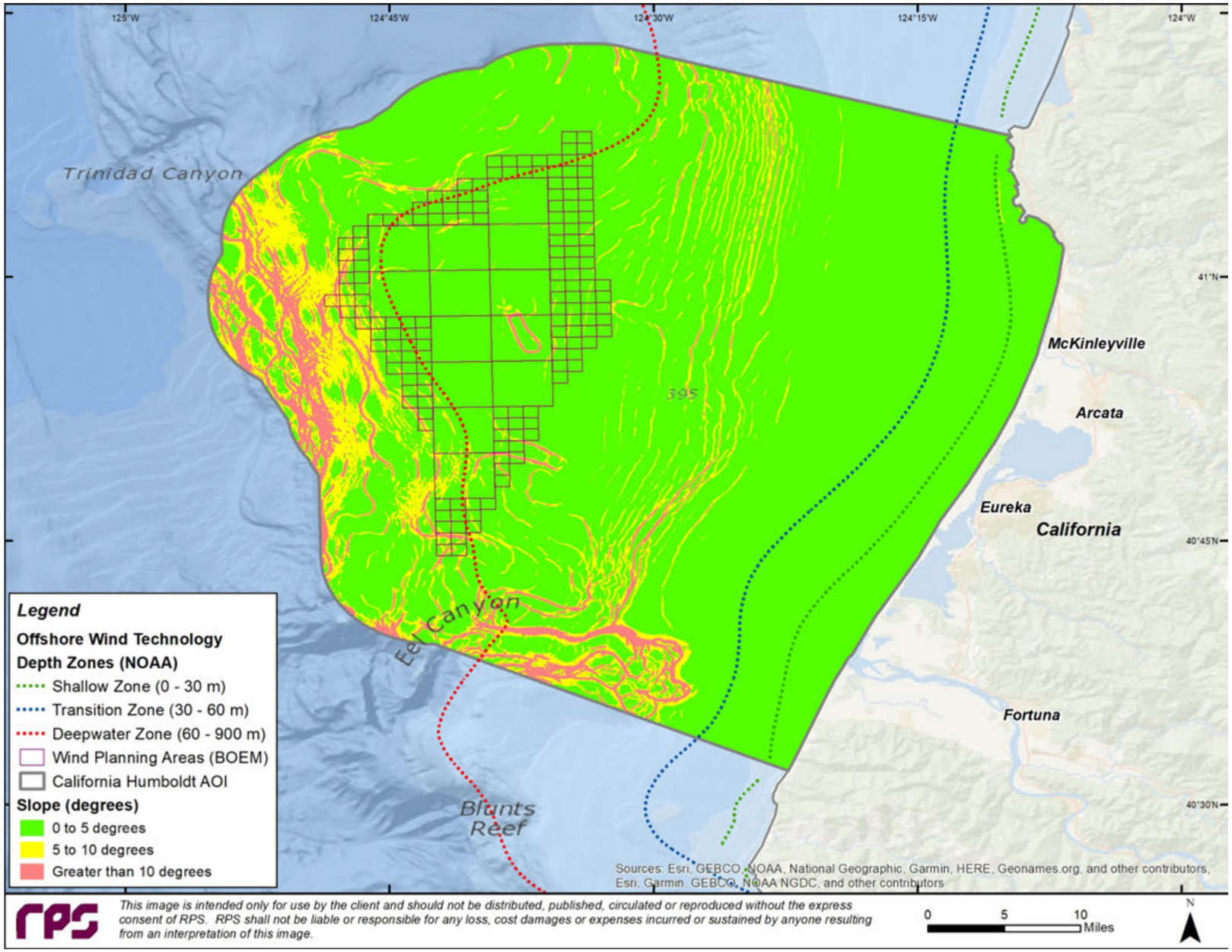

Slope gradients in the shallow and transition zones are less than 5 degrees. The stair-step artifact present in the slope gradient map suggest this map was generated from inadequately spaced data points and the resultant slope gradient displayed here is questionable.

Figure 39. California Humboldt - Slope Gradient

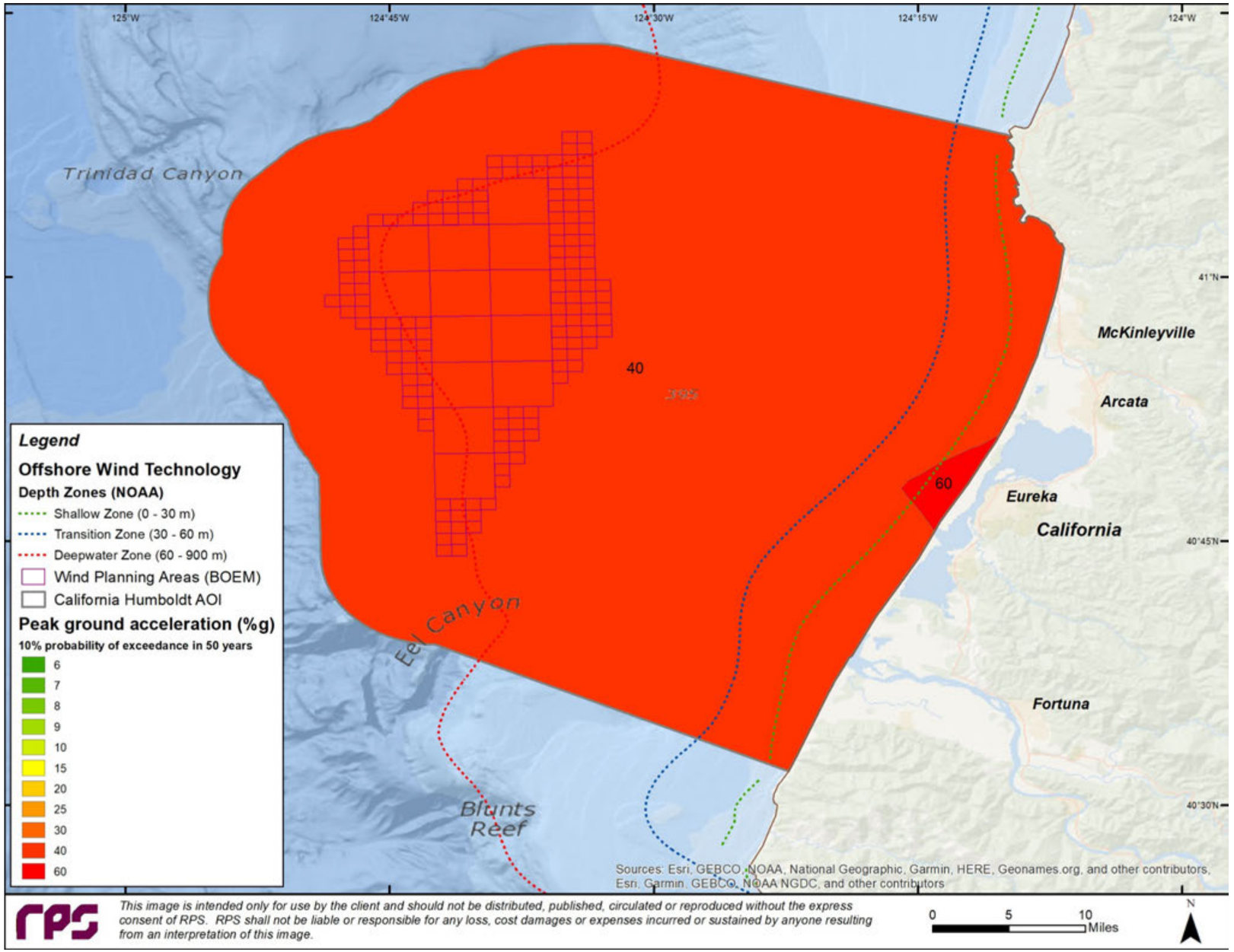

Peak ground acceleration is relatively high across the California Humboldt AOI, varying from 40 to 60%g.

Figure 40. California Humboldt - PGA

6.4.3 California Morro Bay and Diablo Canyon

Panel display of geology (soil type), slope gradient and earthquake magnitudes:

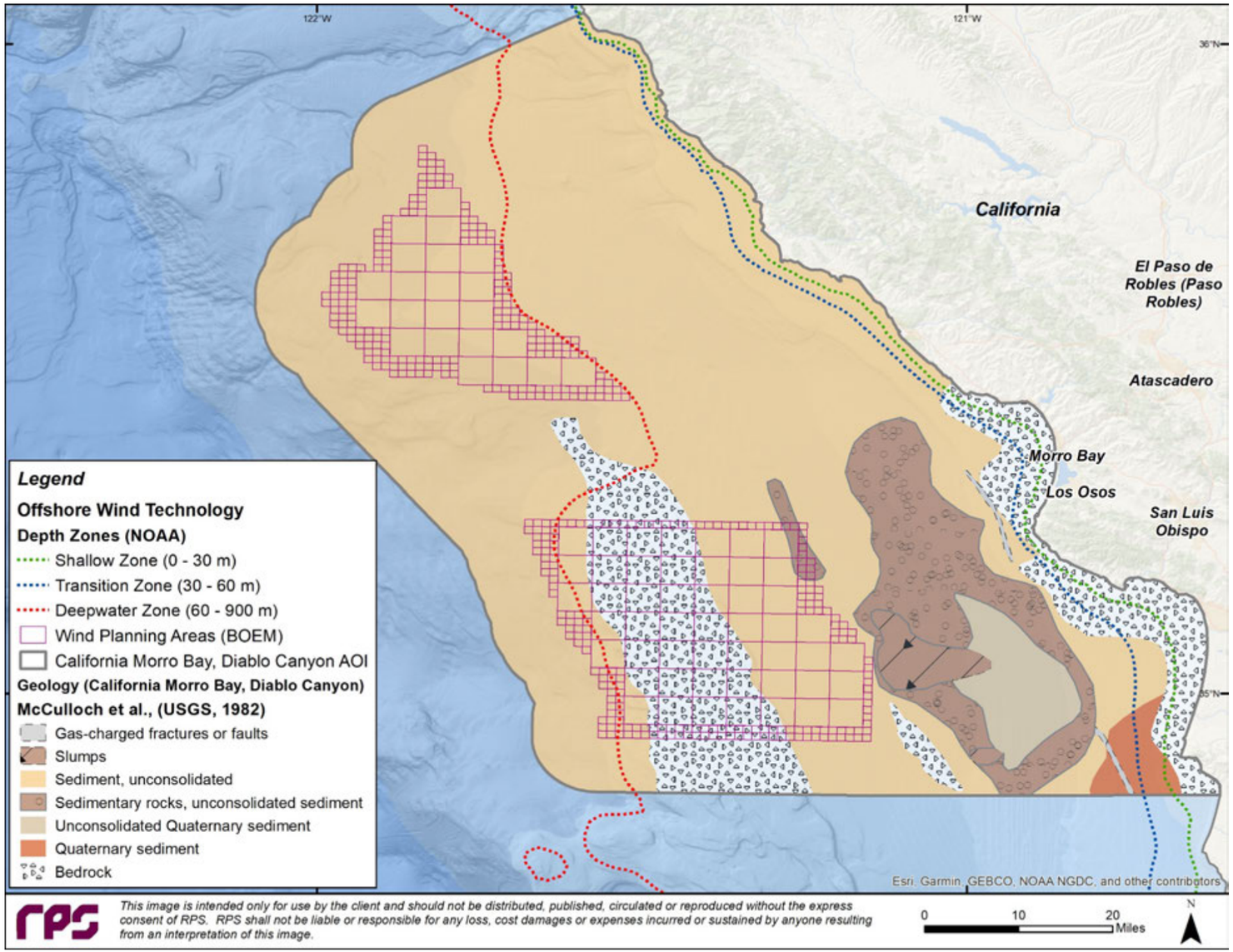

Figure 41. California Morro Bay and Diablo Canyon - Geology (Soil Type)

Soil types along the western coast of Morro Bay and Diablo Canyon AOI are primarily bedrock or coarse sands in the shallow and transition zones between 0 and 60m water depth. Muds likely dominate the Morro Bay proposed study area and bedrock outcrop and muds dominate in the Diablo Canyon study area in the deep water zone between 60 and 900 m water depth. Though the deeper water sediments of this AOI are likely mud, the information on grainsize is clearly lacking.

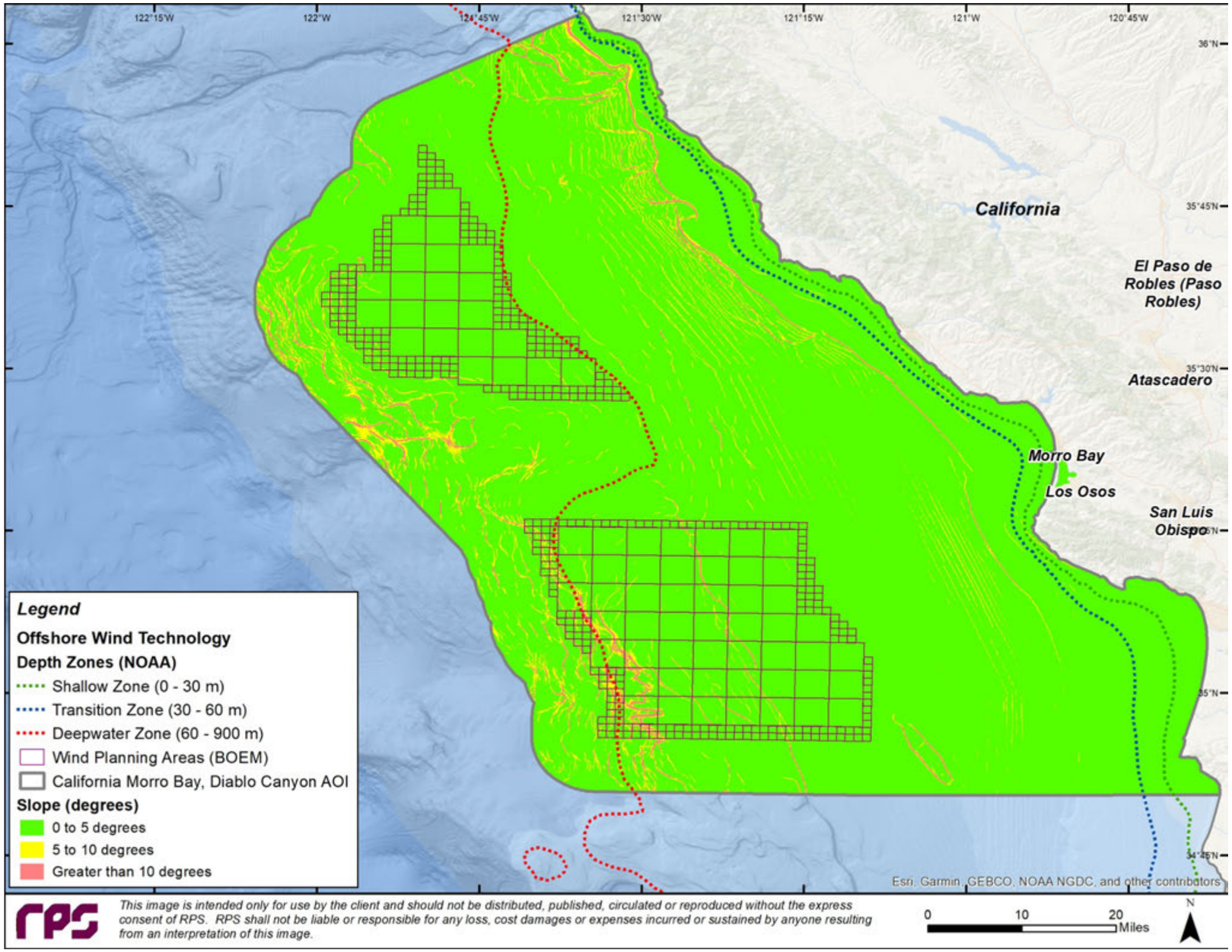

Slope gradients in the shallow and transition zones are less than 5 degrees. The stair-step artifact present in the slope gradient map suggest this map was generated from inadequately spaced data points and the resultant slope gradient displayed here is questionable.

Figure 42. California Morro Bay and Diablo Canyon - Slope Gradient

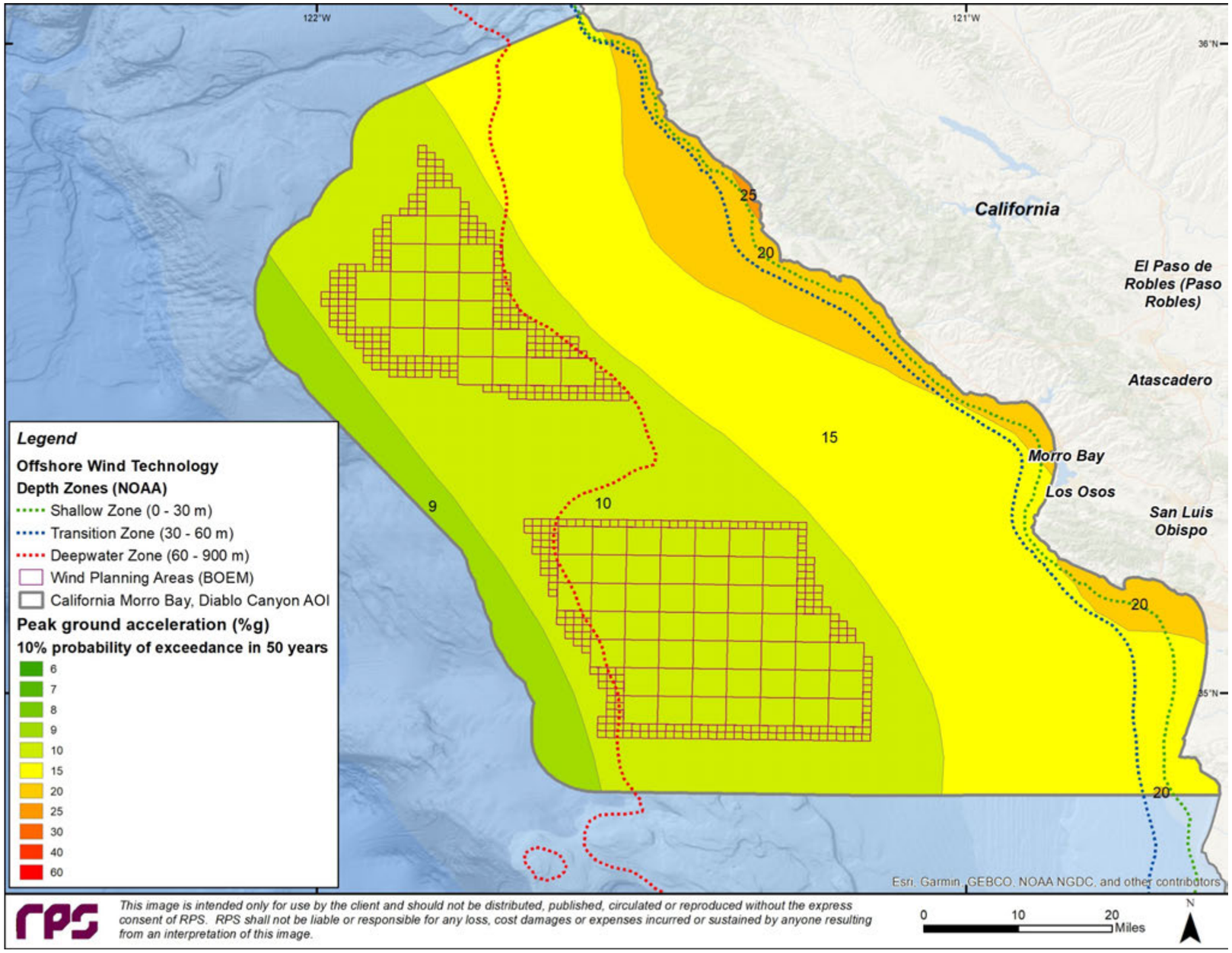

Peak ground acceleration decreases seaward from 25 to 9%g across the California Morro Bay and Diablo Canyon AOI.

Figure 43. California Morro Bay and Diablo Canyon - PGA

6.4.4 Hawaii Oahu North

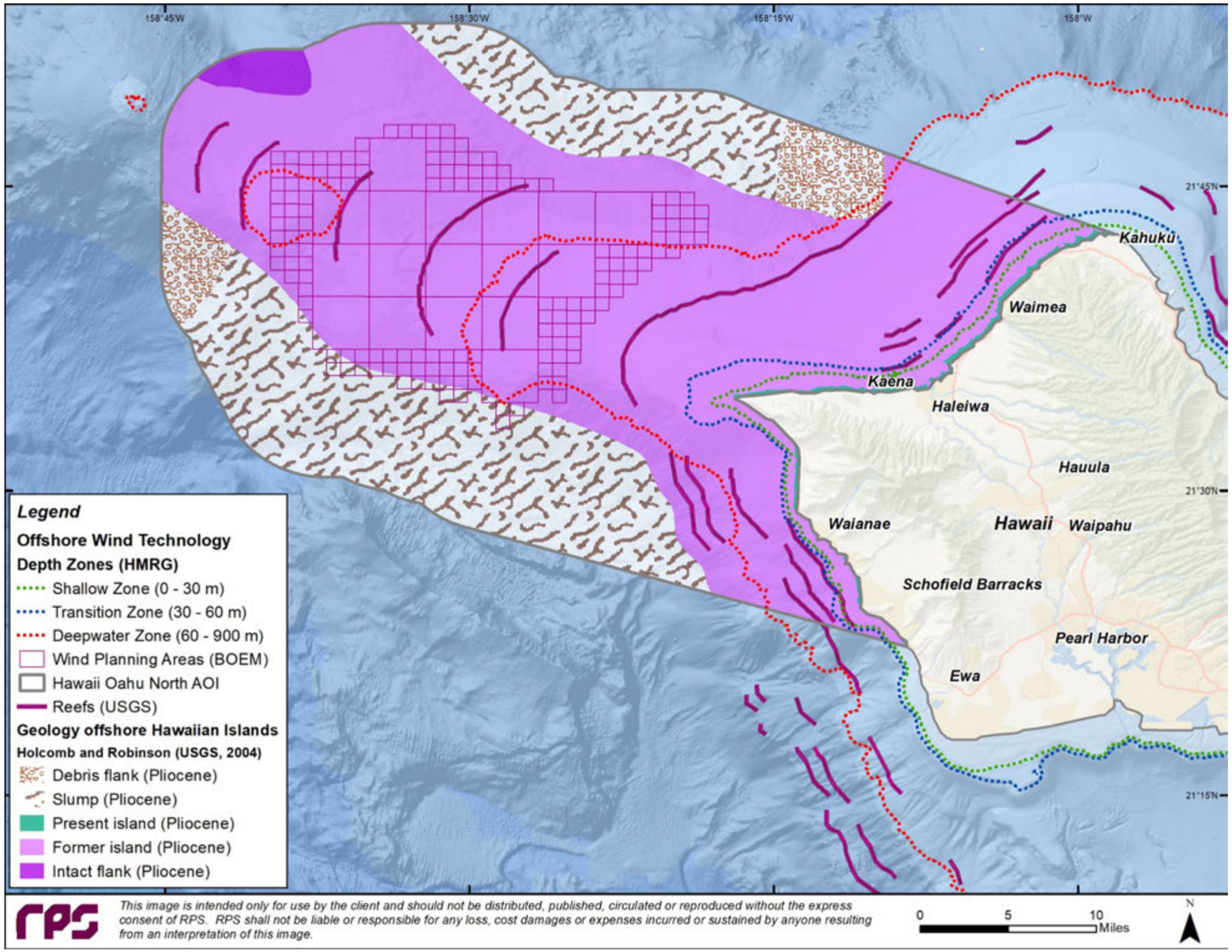

Figure 44. Hawaii Oahu North - Geology (Soil Type)

No near-seabed core data was available for this AOI. The USGS map suggests the bulk of the central northwestern portion of the Oahu North AOI is Pliocene aged sediments. The presence of the now inundated reefs suggest that a shallow water and low sediment input environment prevailed during the Pliocene. Near seabed sediments in this AOI may be composed of limey muds and sands.

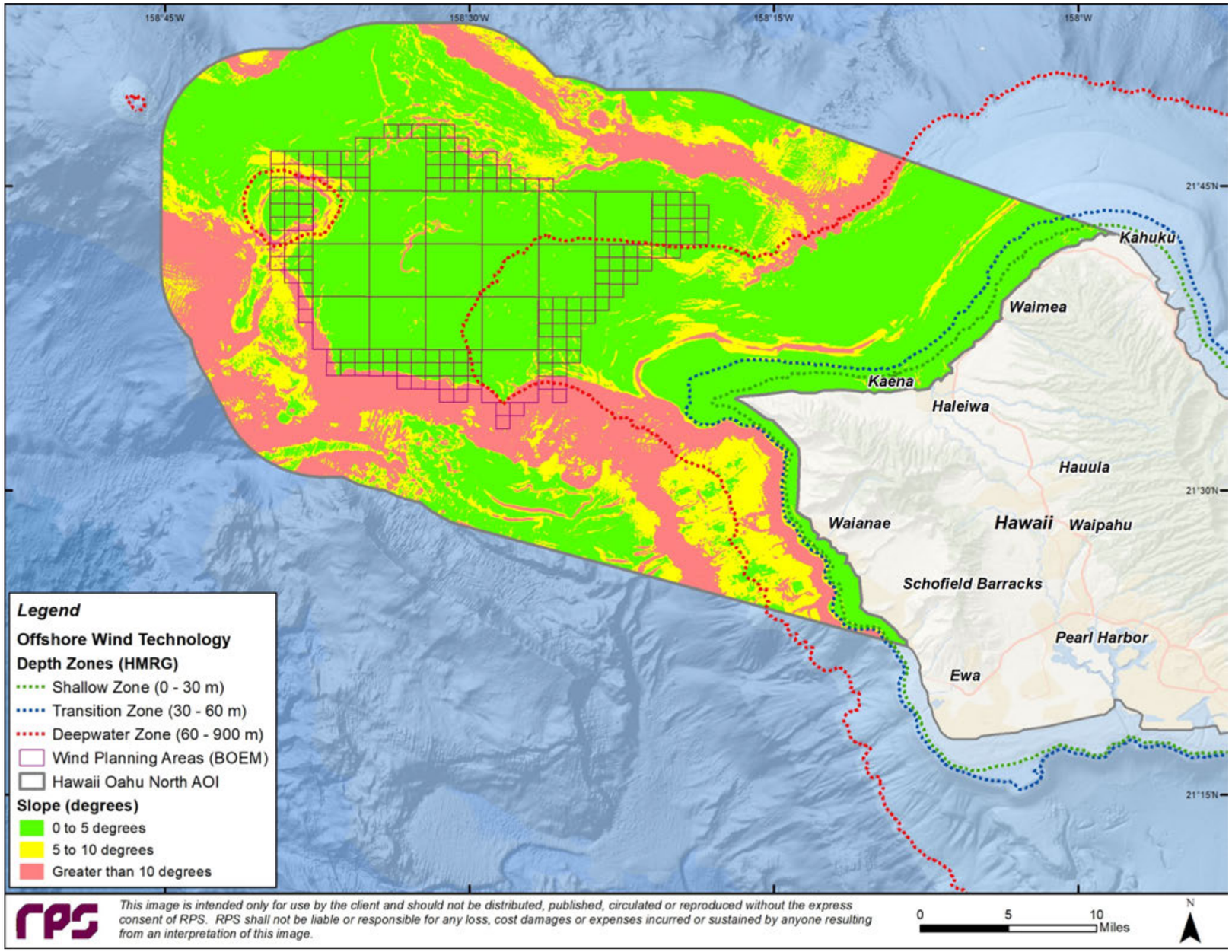

Slope gradients in the northwest central portion of the AOI are in general less than 5 degrees.

Figure 45. Hawaii Oahu North - Slope Gradient

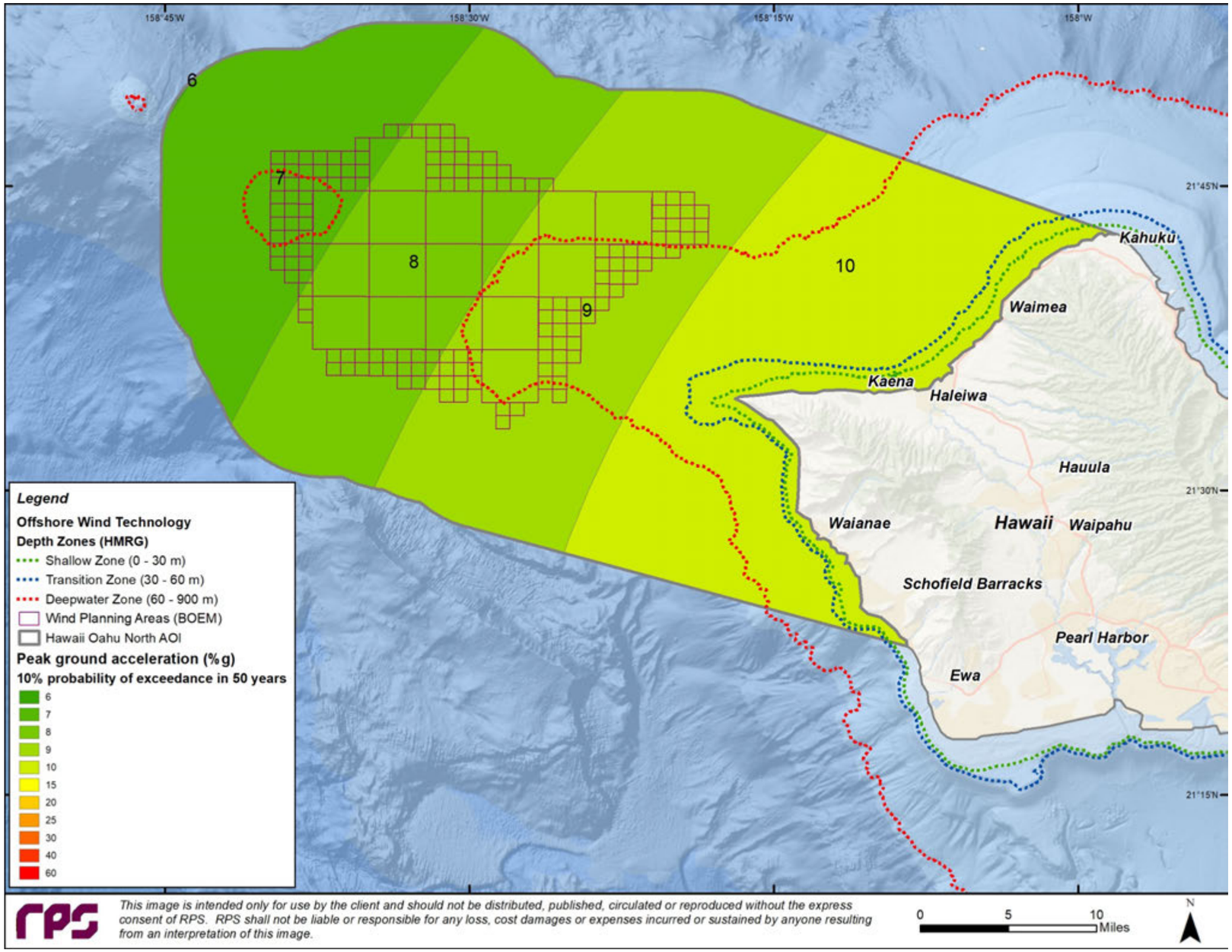

Peak ground acceleration decreases seaward from 10 to 6%g across the Hawaii Oahu North AOI.

Figure 46. Hawaii Oahu North - PGA

6.4.5 Hawaii Oahu South

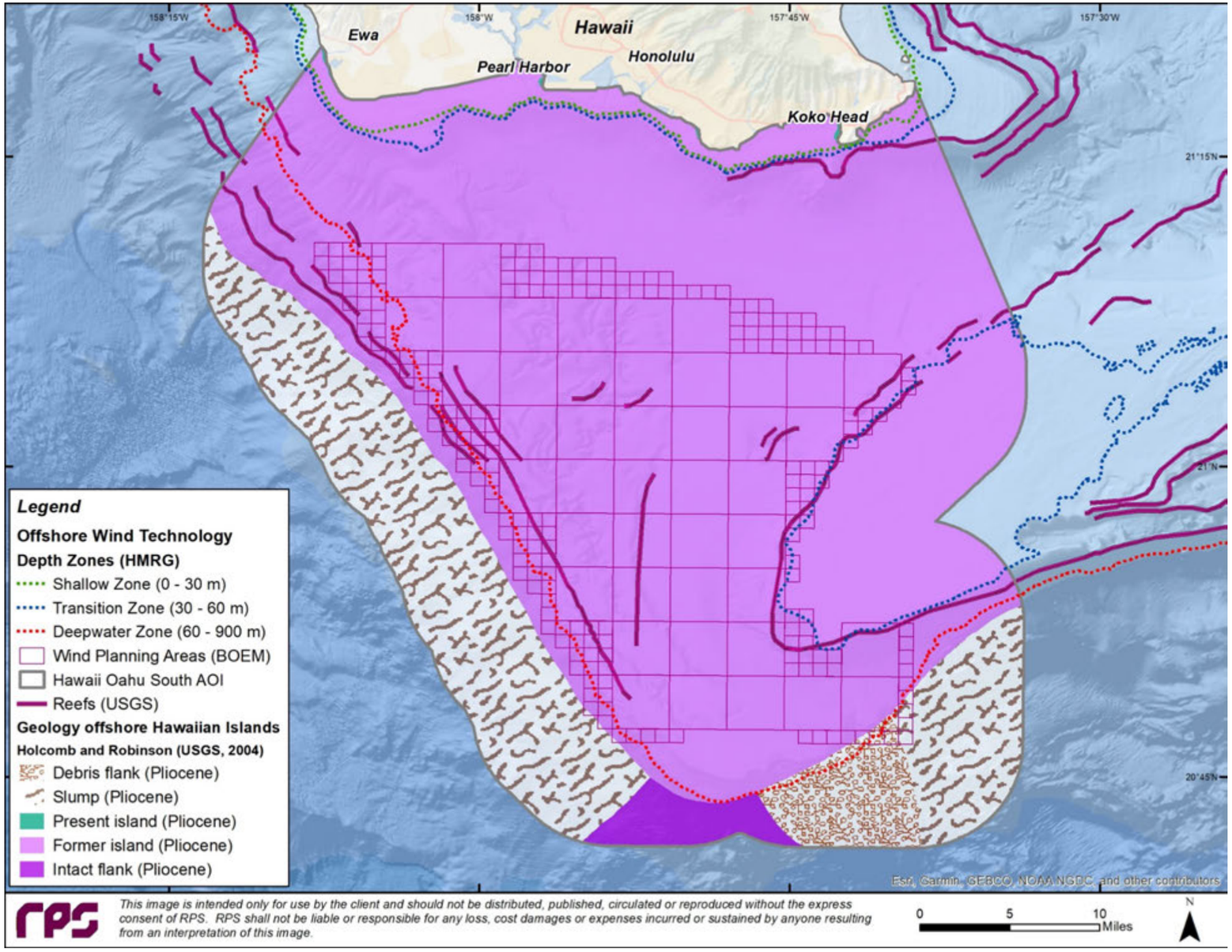

Figure 47. Hawaii Oahu South - Geology (Soil Type)

No near-seabed core data was available for this AOI. The USGS map suggests that all the proposed study areas of the Oahu South AOI is Pliocene-age sediments. The presence of the inundated reefs suggests a shallow water and low sediment input environment prevailed during the Pliocene. Near seabed sediments in this AOI may be composed of limey muds and sands. Slumped materials are evident along the southwestern and southeastern flanks of the proposed study area.

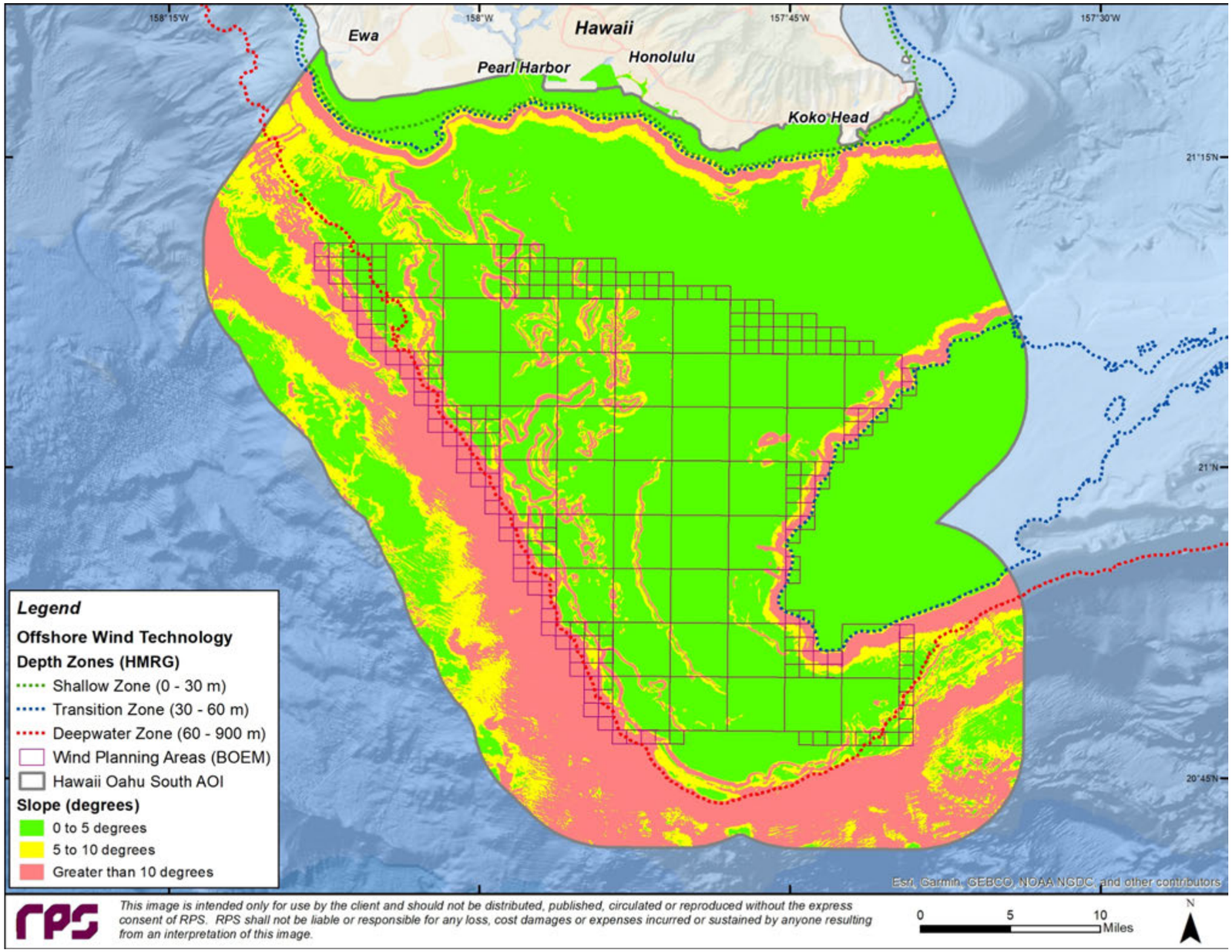

Slope gradients in the northwest central portion of the AOI are in general less than 5 degrees except where circular and elongate high-dip features mark the seabed.

Figure 48. Hawaii Oahu South - Slope Gradient

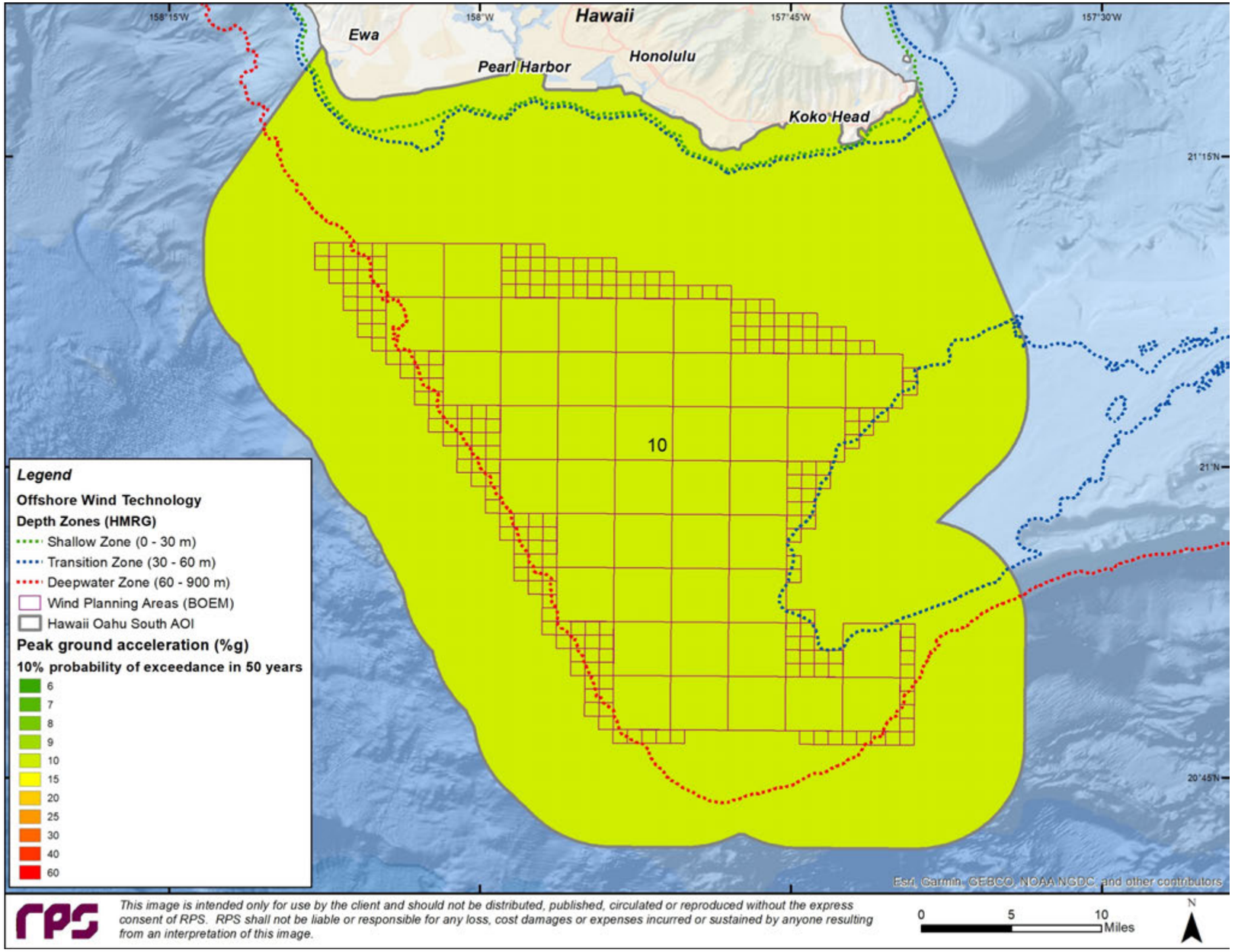

Peak ground acceleration is 10%g across the entire Hawaii Oahu South AOI.

Figure 49. Hawaii Oahu South - PGA

7 SITE SUITABILITY ANALYSIS RESULTS

The following maps show the results from each of the five site suitability analysis models run for each AOI: Oregon Regional, Humboldt, Morro Bay and Diablo Canyon California, and North and South Oahu Hawaii, using inputs from soil type , slope, and peak ground acceleration (presented with “g s, p” respectively, on the figures). Depth zone contours, which mark the boundaries between the Shallow Zone (0-30m), Transition Zone (30m - 60m), and Deepwater Zone (60m - 900 m) are included on each map for water depth reference purposes. Where appropriate, a short discussion is included on the right panel of the map. A discussion of what is deemed the most representative model for each of the AOI’s is included in the conclusions (Section 8).

Five suitability analysis models were created for each AOI. Model 1 is an equally weighted analysis. Model 2 assigns more weight on the effect of Soil Type, while depressing PGA. Model 3 considers Slope Gradient the most important factor, while depressing Soil Type. Model 4 puts emphasis on the PGA, while depressing Slope Gradient. Model 5 removes the effect of Soil Type while distributing the effects of Slope Gradient and Peak Ground Acceleration equally (Table 17). The last model was developed due to variable uncertainty with geology inputs across the Study Area with 0% weight on geology (and 50% slope / 50% seismic hazard). The goal is to account for uncertainty and variable data quality of soil types, and the depth of the core data. A dedicated multibeam, shallow seismic and coring program would be required for a proper assessment of geohazards, slope stability, and any site-specific investigation.

It should be noted that faults were considered as input and tested for weighted overlay. However, as the faults pass through each block, the results follow the centerline of the fault traces as a linear unsuitable feature and do not capture regional hazard associated with seismic events. On the other hand, faults were integrated in the development of the PGA data by USGS. Rates of future earthquakes are modeled on known faults and historic seismicity to account for unknown faults and the incomplete fault inventory (Peterson et al., 2015).Therefore, due to the complexity of selecting active faults and geological uncertainty, and to avoid double counting them while using PGA data, it was concluded that faults should be added as an informative layer (only visualized) on the suitability analysis outputs, without being integrated into the weighted calculations of suitability analysis.

Variable weighting factors were selected to test sensitivity to input data types (slope, geology, seismic hazard PGA) and determine the most critical factors. The output models showed that the input data with the highest weight had the most influence in the output model. Therefore, variable weighting does not distinguish the most significant input data; however, this approach produced various model outputs which indicate low to high suitable regions variably across the AOIs. Subsequently, a composite suitability method was used to sum all five models within each AOI, based on exclusion of suitability values of below 5. The composite suitability models portray the “best of the best” for each AOI in terms of suitability, considering the combination of data inputs with variable certainty and quality.

Table 17. Weighted Suitability Analysis Weighting Assignments

Input Raster (abbreviation)	Model 1	Model 2	Model 3	Model 4	Model 5
Soil Type (g)	33%	50%	20%	30%	0%
Slope Gradient (s)	33%	30%	50%	20%	50 %
Peak Ground Acceleration (p)	34%	20%	30%	50%	50 %

7.1 Oregon Regional

Panel display of variably weighed overlay suitability analysis:

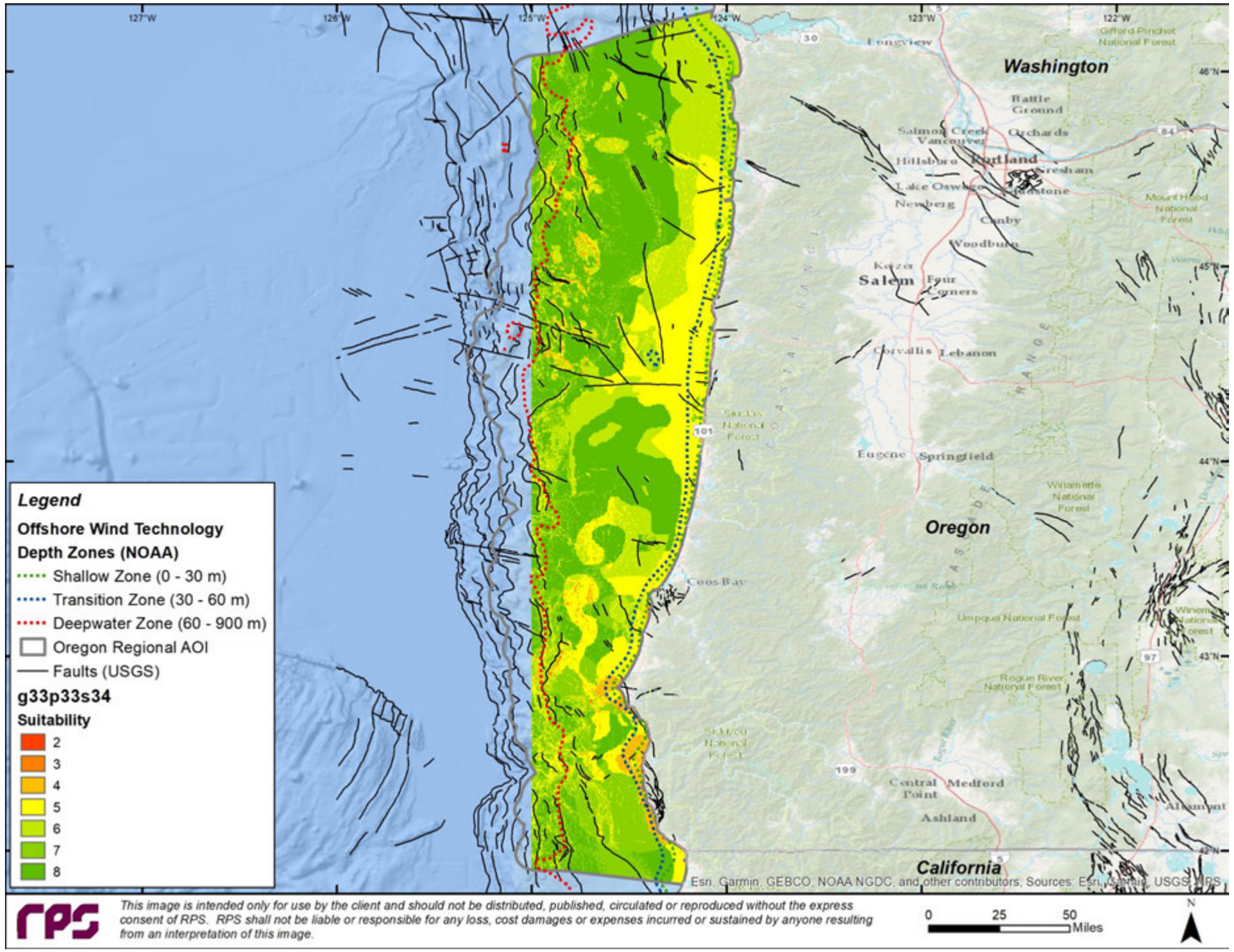

Variable Weighted Overlay

Suitability based on the following weighting:

Geology = 33%

PGA= 33%

Slope = 34%

Location of Faults (USGS)

Note: NO DATA in the PGA input (western edge of Oregon Regional), and consequently NO DATA for weighted overlay and composite suitability outputs (western edge of Oregon Regional AOI)

Figure 50. Oregon Suitability - g33 p33 s34

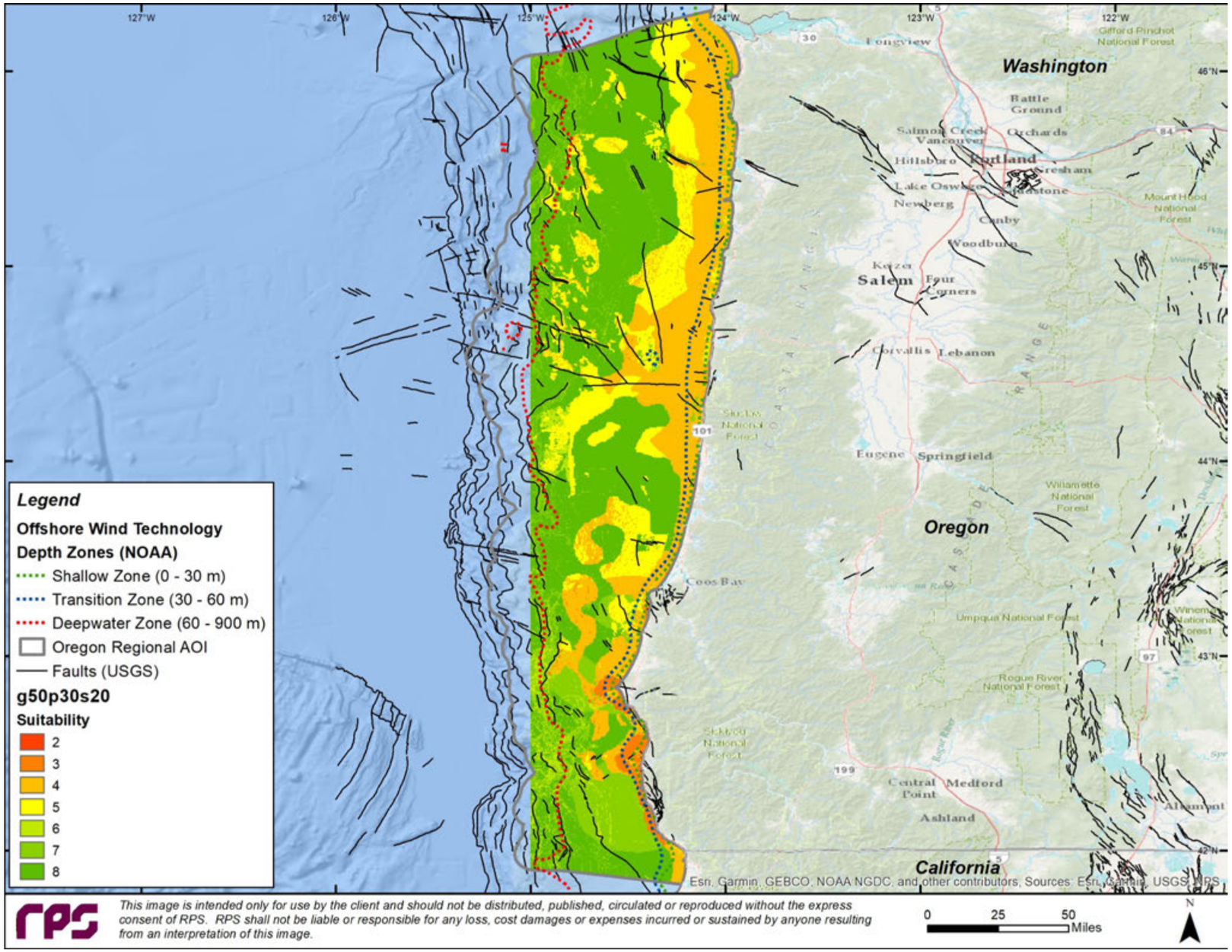

Variable Weighted Overlay

Suitability based on the following weighting:

Geology = 50%

PGA = 30%

Slope = 20%

Location of Faults (USGS)

Note: NO DATA in the PGA input (western edge of Oregon Regional), and consequently NO DATA for weighted overlay and composite suitability outputs (western edge of Oregon Regional AOI)

Figure 51. Oregon Suitability - g50 p30 s20

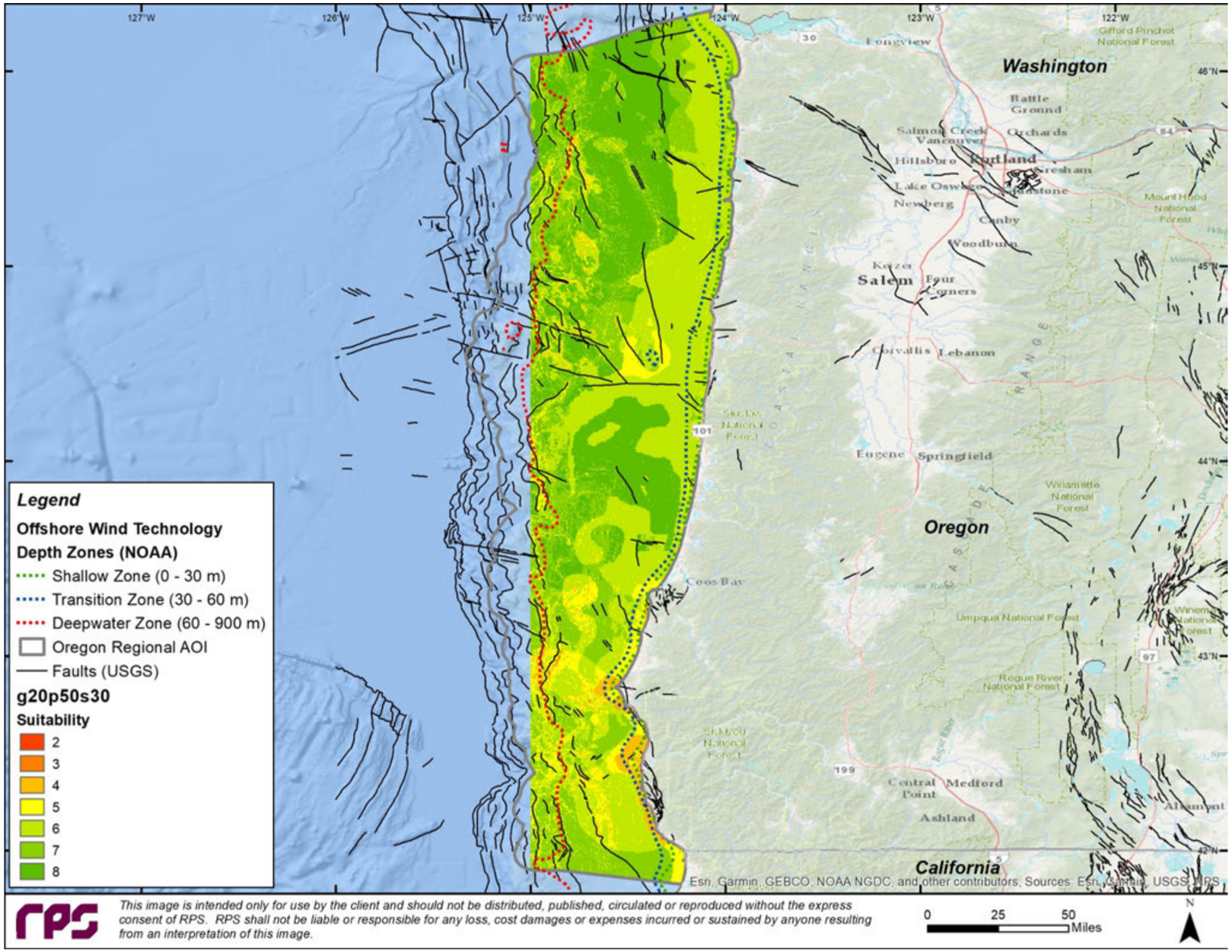

Figure 52. Oregon Suitability - g20 p50 s30

Variable Weighted Overlay

Suitability based on the following weighting:

Geology = 20%

PGA = 50%

Slope = 30%

Location of Faults (USGS)

Note: NO DATA in the PGA input (western edge of Oregon Regional), and consequently NO DATA for weighted overlay and composite suitability outputs (western edge of Oregon Regional AOI)

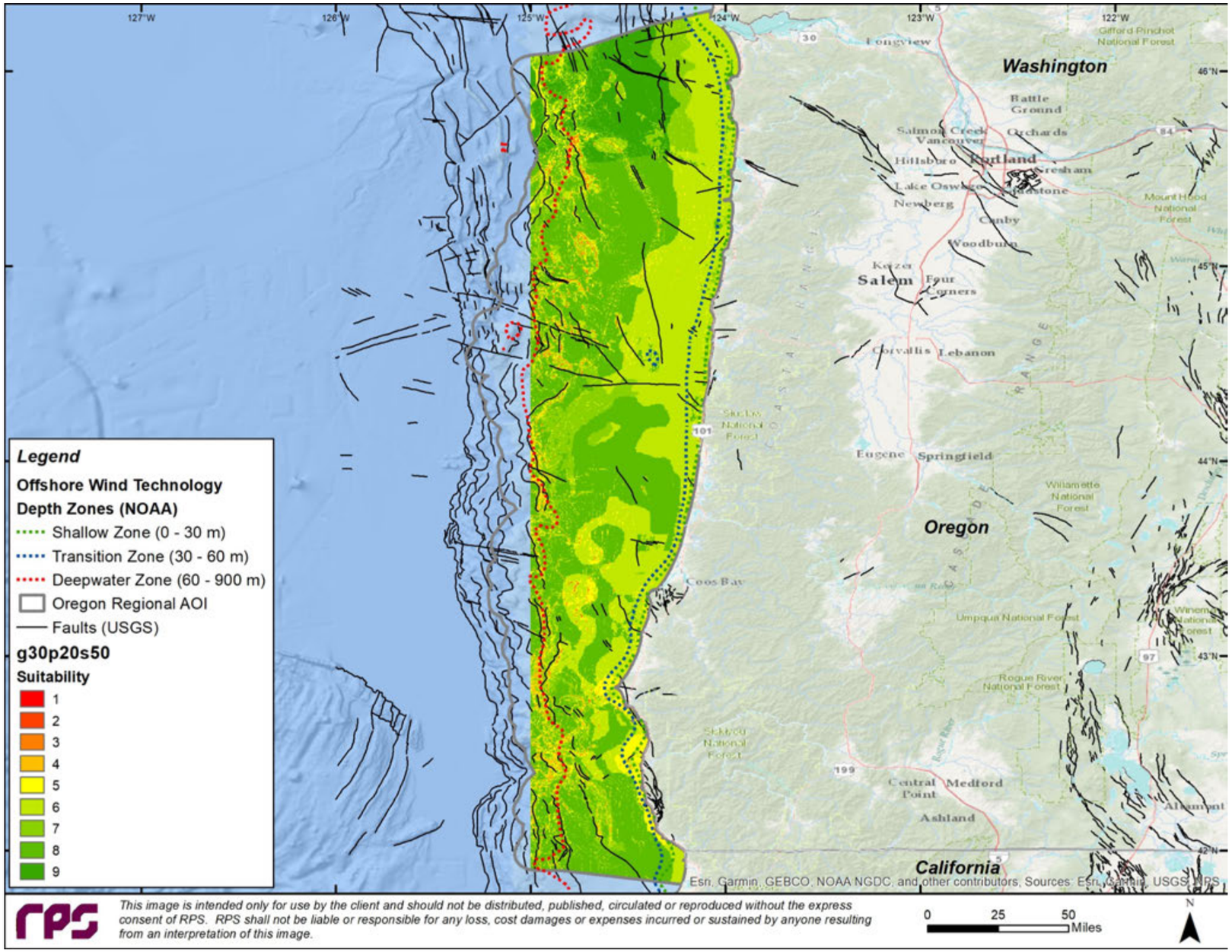

Variable Weighted Overlay

Suitability based on the following weighting:

Geology = 30%

PGA = 20%

Slope = 50%

Location of Faults (USGS)

Note: NO DATA in the PGA input (western edge of Oregon Regional), and consequently NO DATA for weighted overlay and composite suitability outputs (western edge of Oregon Regional AOI)

Figure 53. Oregon Suitability - g30 p20 s50

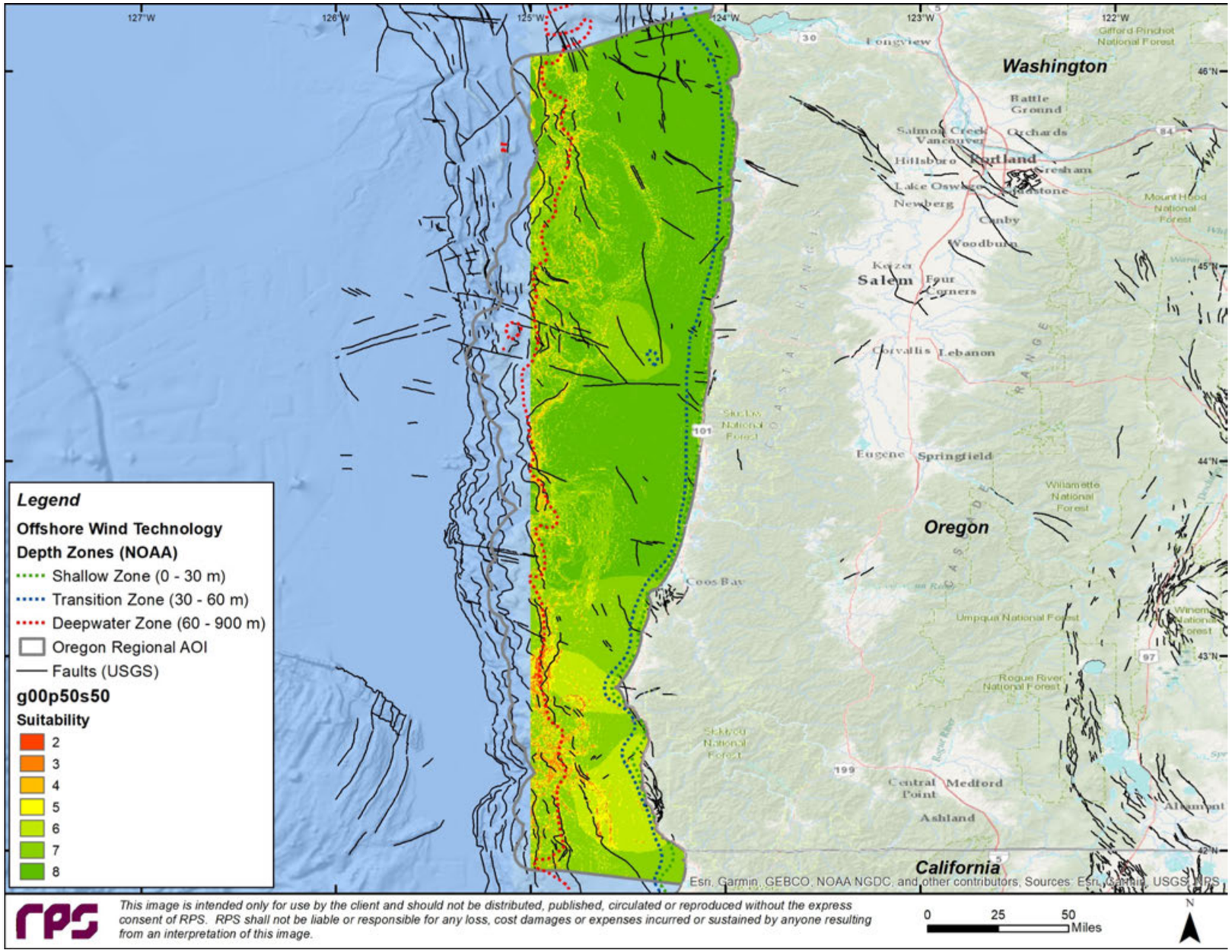

Variable Weighted Overlay

Suitability based on the following weighting:

Geology = 0%

PGA = 50%

Slope = 50%

Location of Faults (USGS)

Note: NO DATA in the PGA input (western edge of Oregon Regional), and consequently NO DATA for weighted overlay and composite suitability outputs (western edge of Oregon Regional AOI)

Figure 54. Oregon Suitability – g00 p50 s50

7.2 California Humboldt

Panel display of variably weighed overlay suitability analysis:

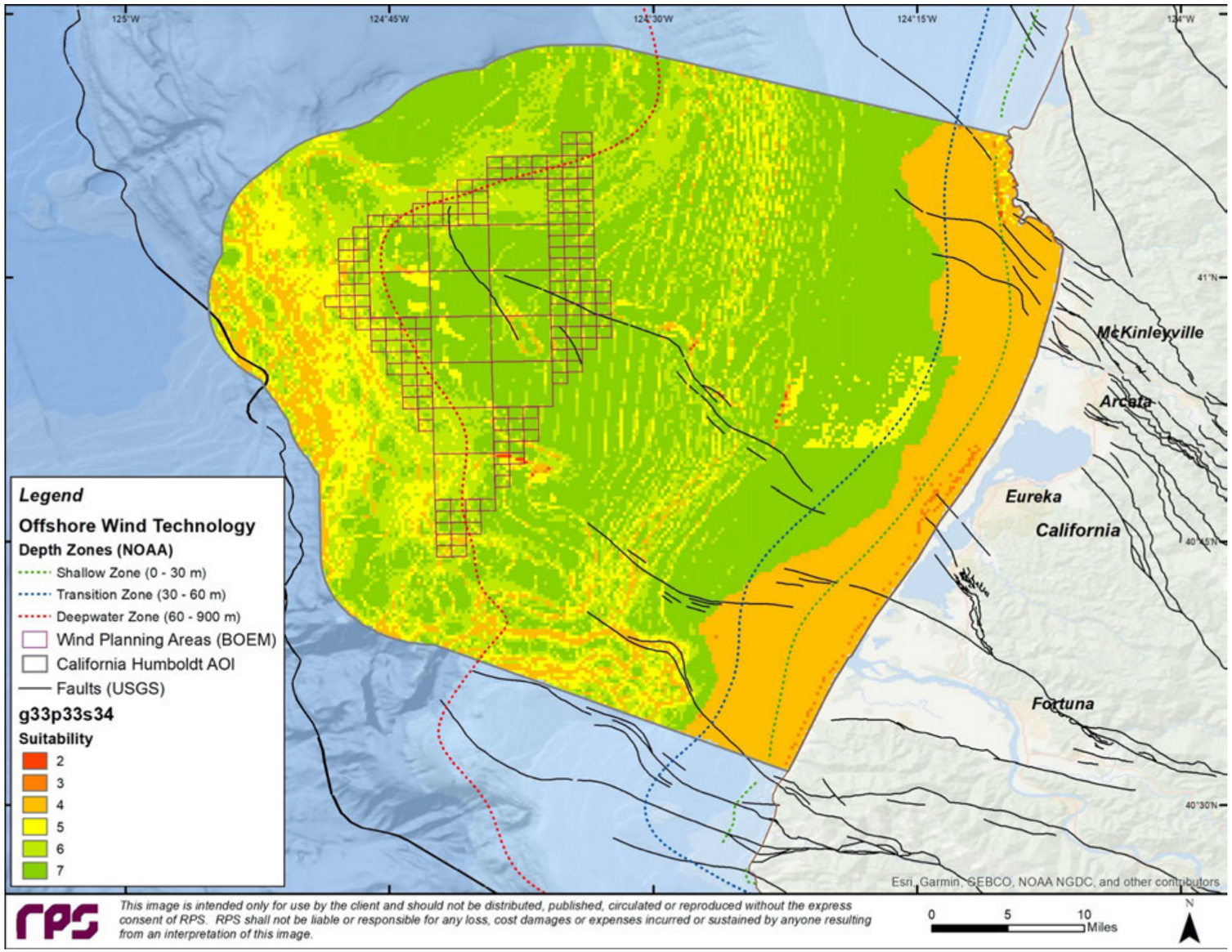

Variable Weighted Overlay

Suitability based on the following weighting:

Geology = 33%

PGA= 33%

Slope = 34%

Location of Faults (USGS)

Figure 55. California Humboldt Suitability - g33 p33 s34

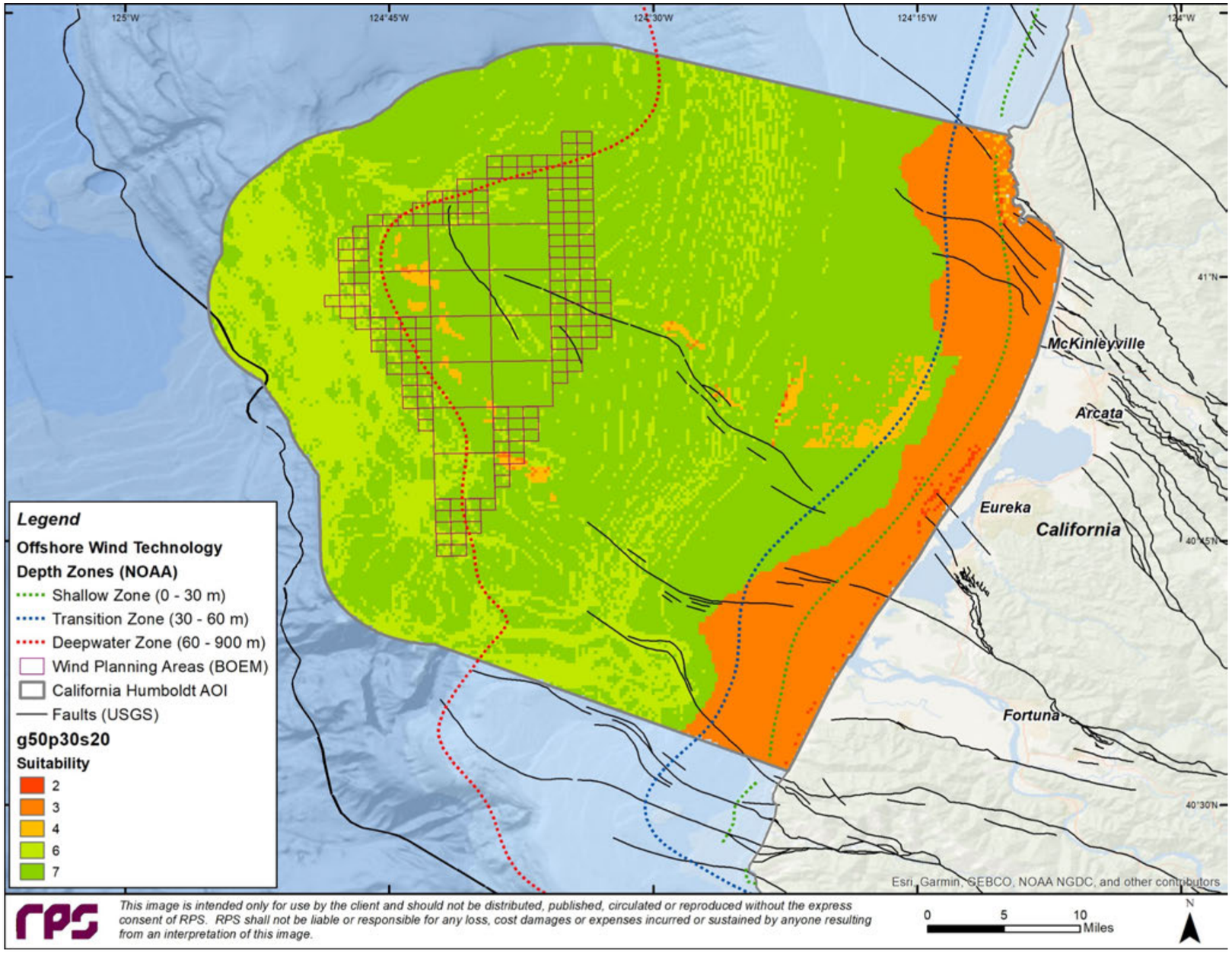

Variable Weighted Overlay

Suitability based on the following weighting:

Geology = 50%

PGA = 30%

Slope = 20%

Location of Faults (USGS)

Figure 56. California Humboldt Suitability - g50 p30 s20

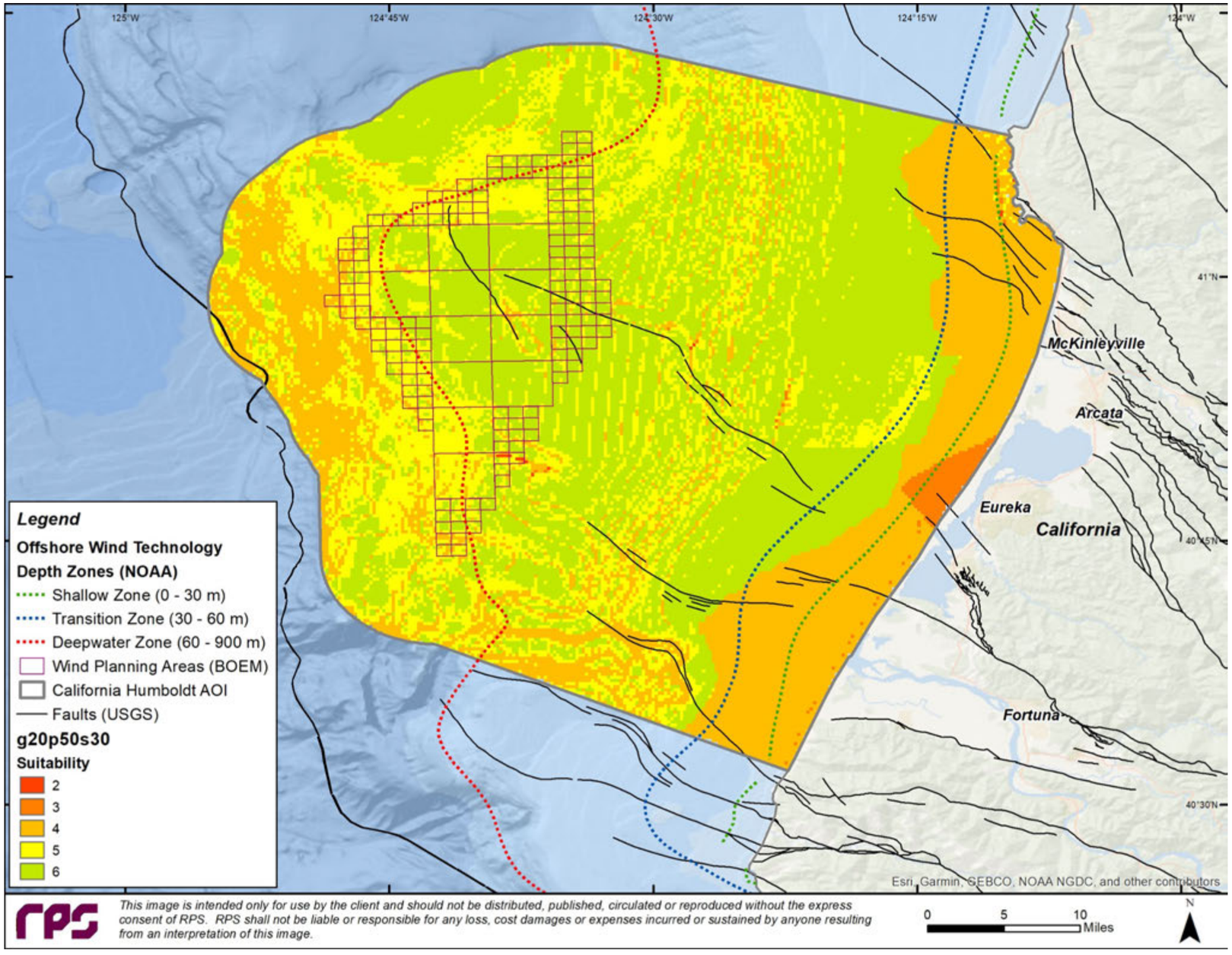

Variable Weighted Overlay

Suitability based on the following weighting:

Geology = 20%

PGA = 50%

Slope = 30%

Location of Faults (USGS)

Figure 57. California Humboldt Suitability - g20 p50 s30

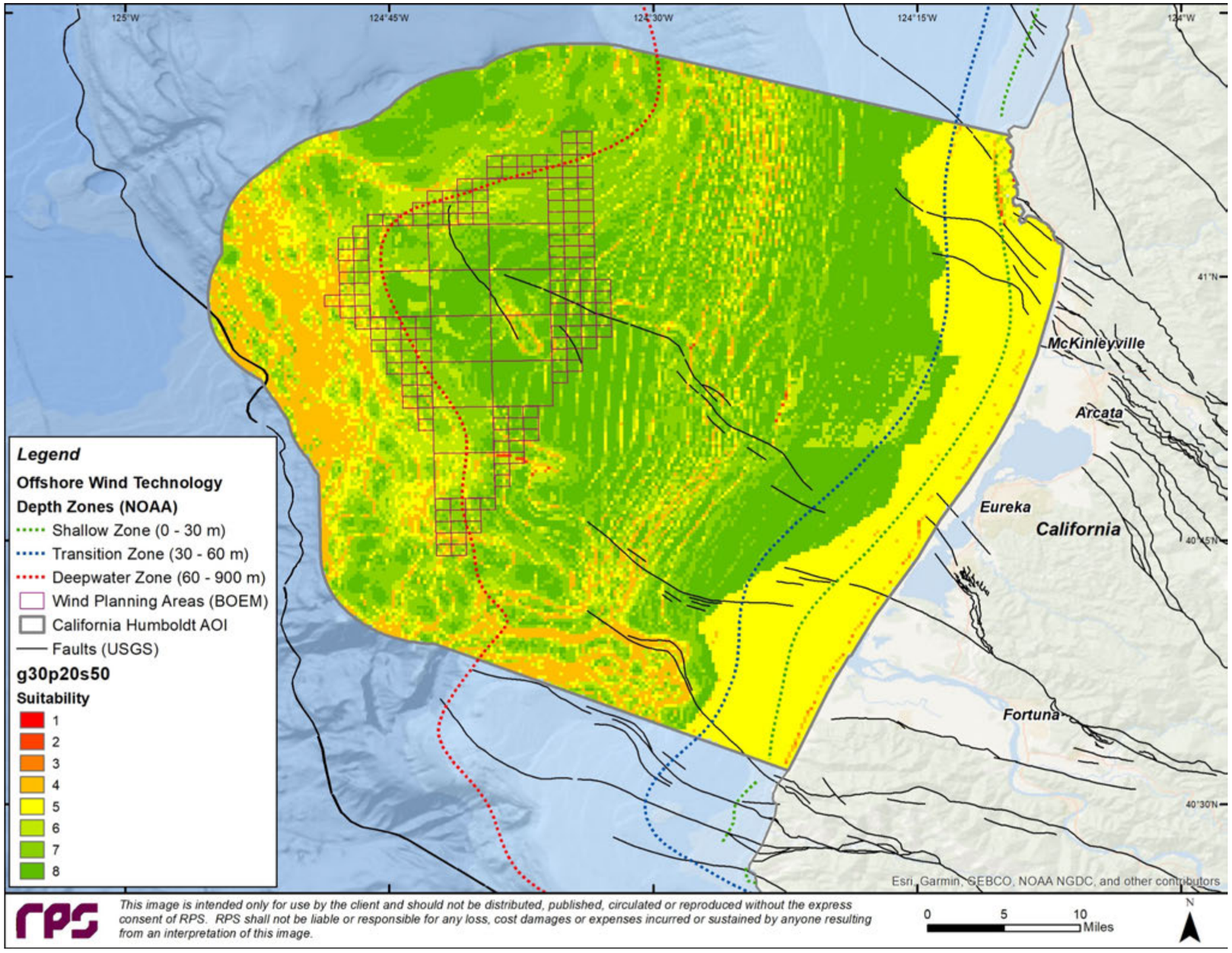

Variable Weighted Overlay

Suitability based on the following weighting:

Geology = 30%

PGA = 20%

Slope = 50%

Location of Faults (USGS)

Figure 58. California Humboldt Suitability - g30 p20 s50

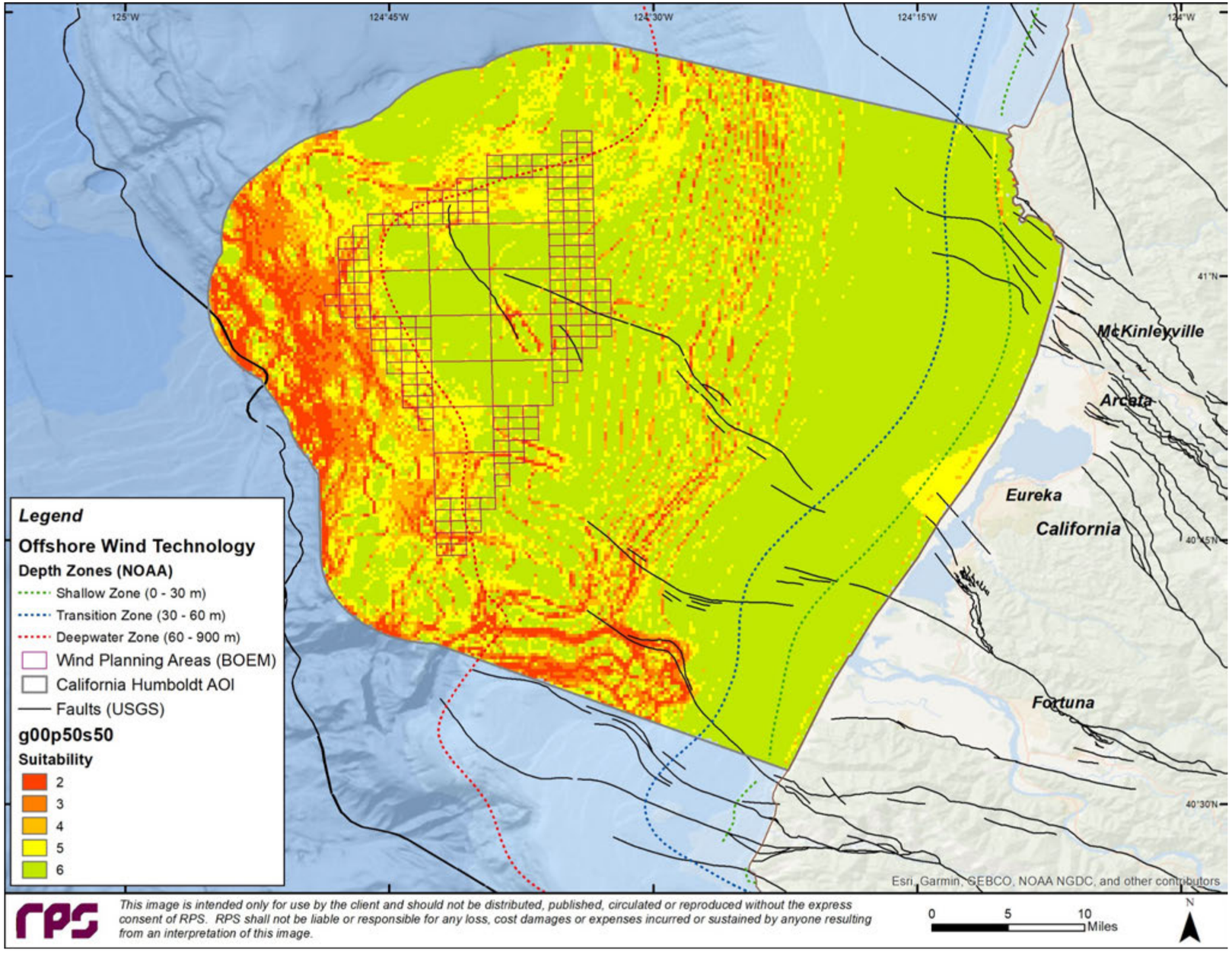

Variable Weighted Overlay

Suitability based on the following weighting:

Geology = 0%

PGA = 50%

Slope = 50%

Location of Faults (USGS)

Figure 59. California Humboldt Suitability – g00 p50 s50

7.3 California Morro Bay and Diablo Canyon

Panel Display of Variably Weighed Overlay Suitability Analysis:

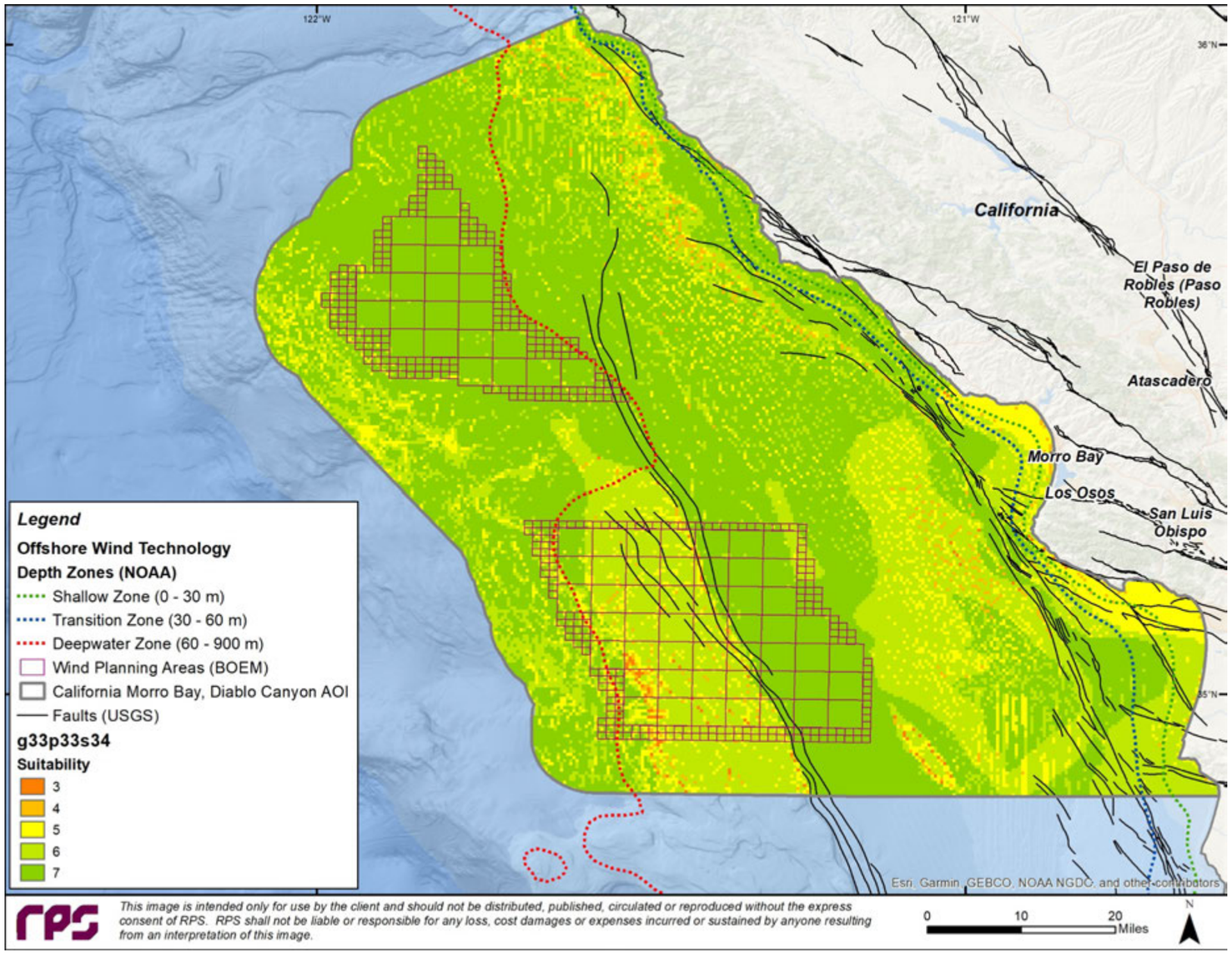

Variable Weighted Overlay

Suitability based on the following weighting:

Geology = 33%

PGA = 33%

Slope = 34%

Location of Faults (USGS)

Figure 60. California Morro Bay and Diablo Canyon Suitability - g33 p33 s34

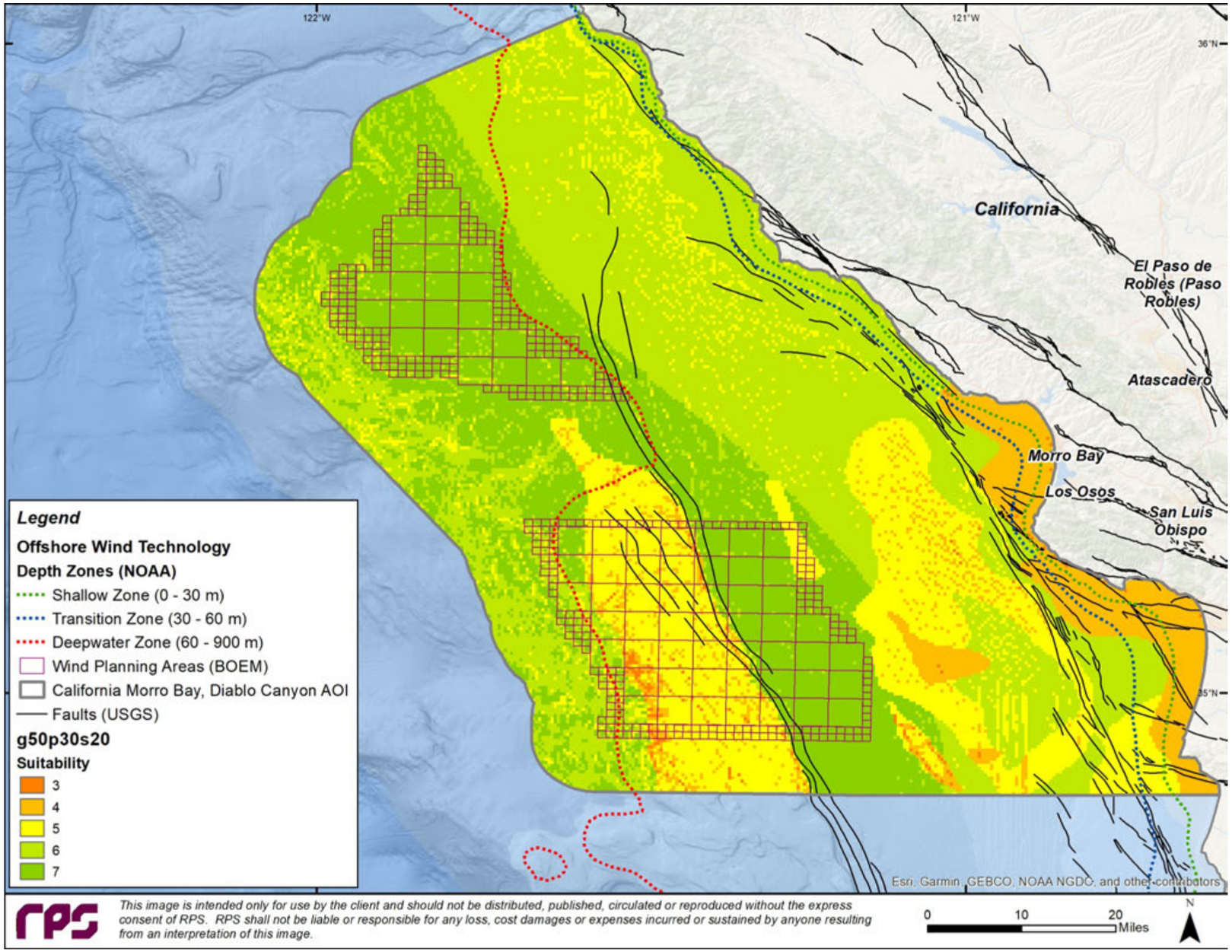

Variable Weighted Overlay

Suitability based on the following weighting:

Geology = 50%

PGA = 30%

Slope = 20%

Location of Faults (USGS)

Figure 61. California Morro Bay and Diablo Canyon Suitability - g50 p30 s20

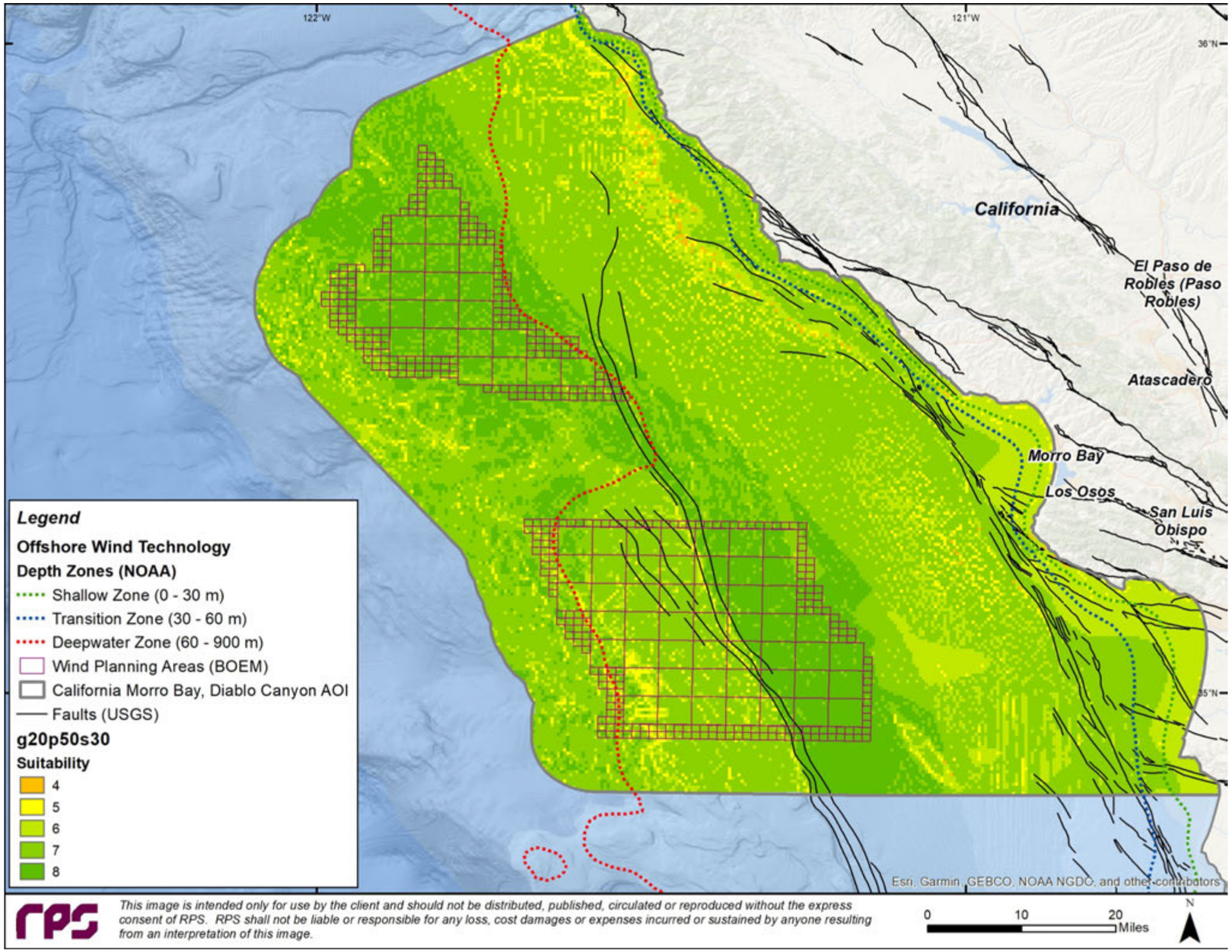

Variable Weighted Overlay

Suitability based on the following weighting:

Geology = 20%

PGA = 50%

Slope = 30%

Location of Faults (USGS)

Figure 62. California Morro Bay and Diablo Canyon Suitability - g20 p50 s30

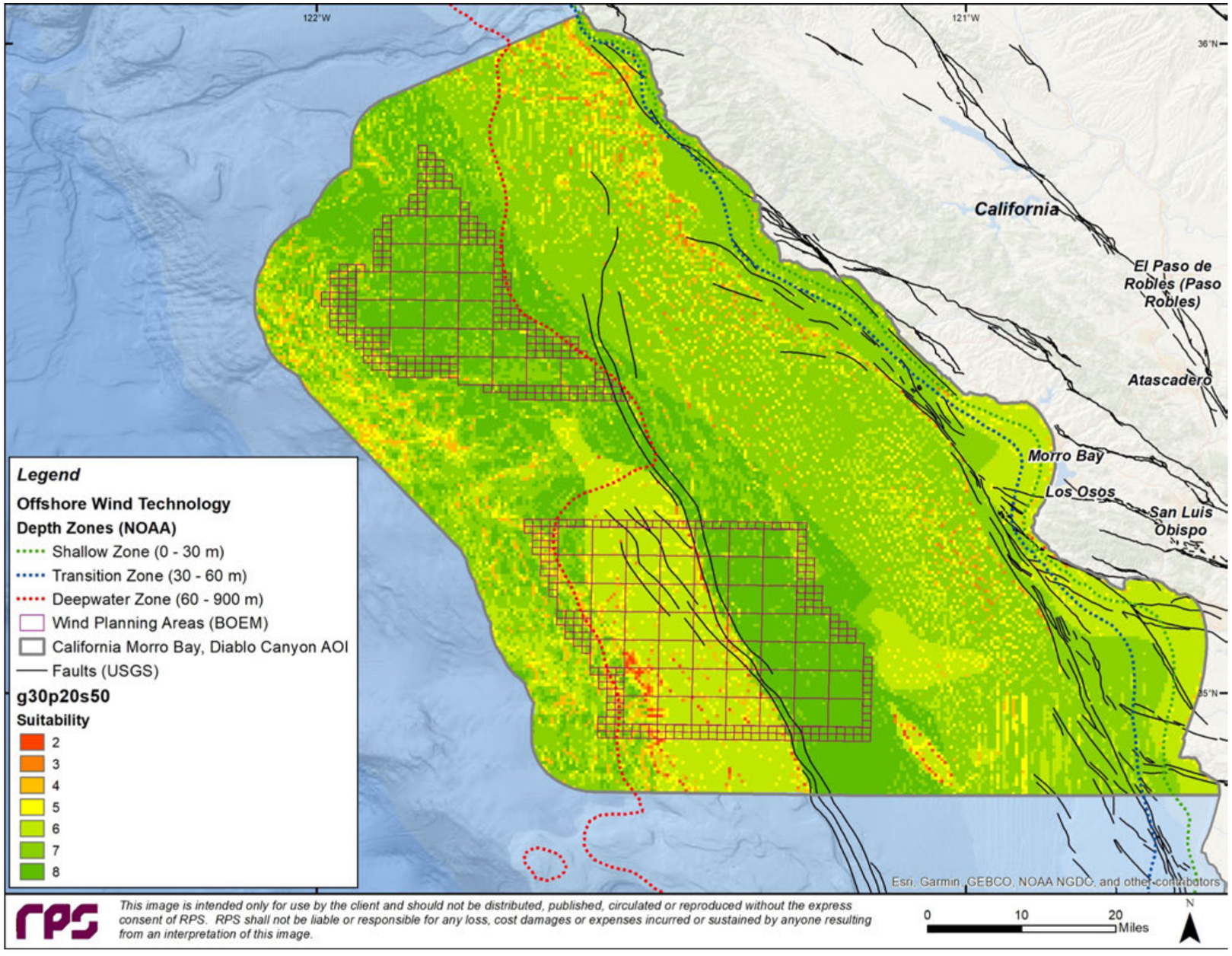

Variable Weighted Overlay

Suitability based on the following weighting:

Geology = 30%

PGA = 20%

Slope = 50%

Location of Faults (USGS)

Figure 63. California Morro Bay and Diablo Canyon Suitability - g30 p20 s50

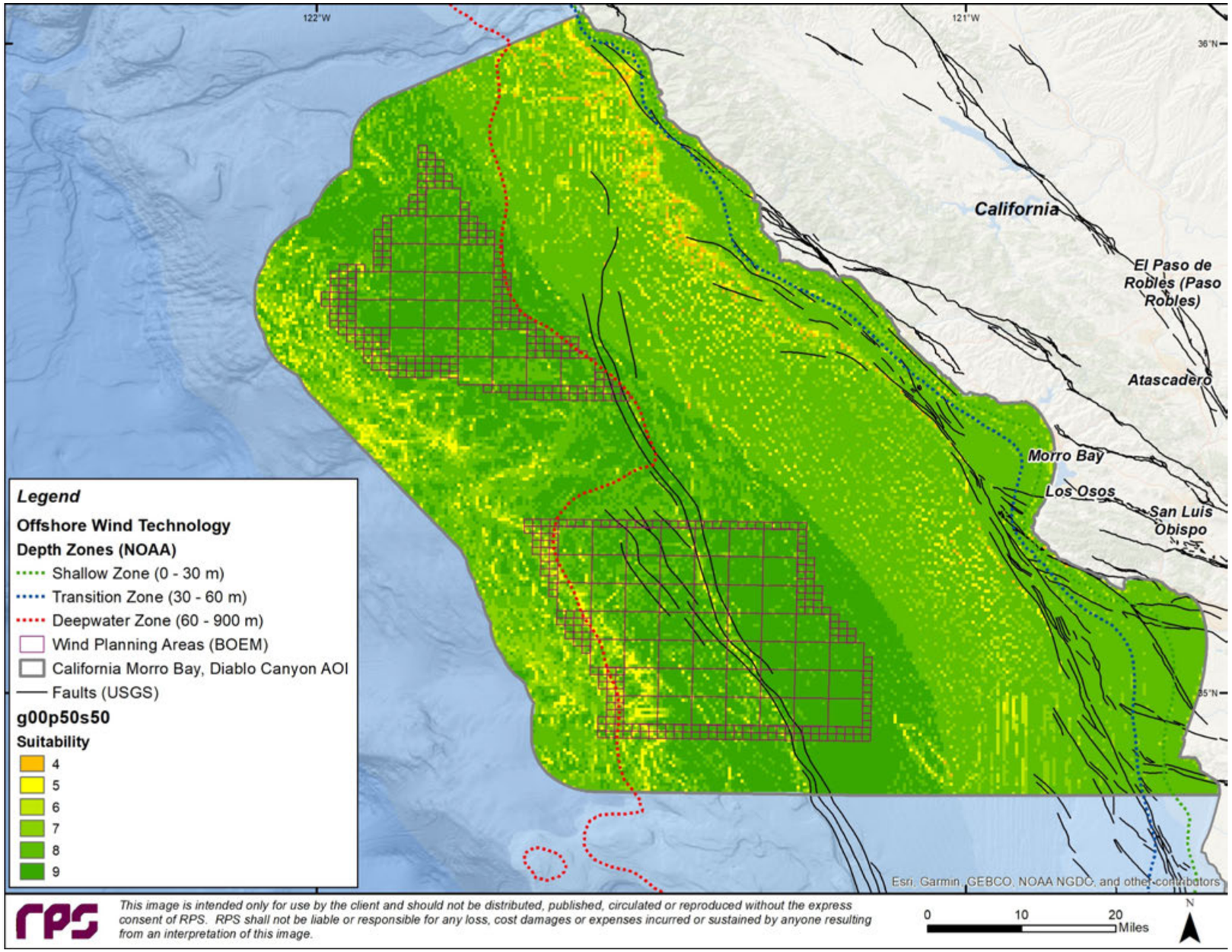

Variable Weighted Overlay

Suitability based on the following weighting:

Geology = 0%

PGA =50%

Slope = 50%

Location of Faults (USGS)

Figure 64. California Morro Bay and Diablo Canyon Suitability – g00 p50 s50

7.4 Hawaii Oahu North

Panel Display of Variably Weighed Overlay Suitability Analysis:

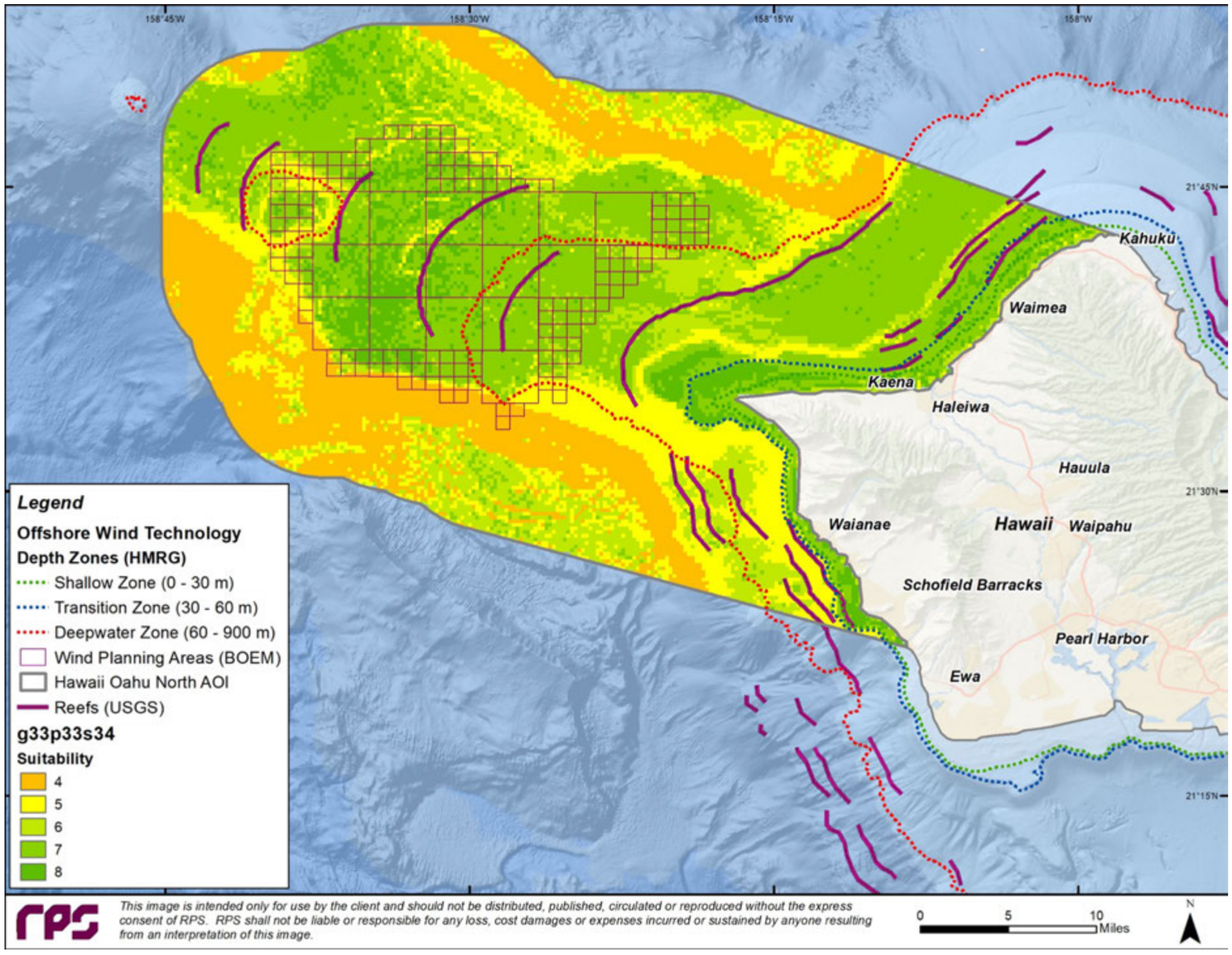

Variable Weighted Overlay

Suitability based on the following weighting:

Geology = 33%

PGA = 33%

Slope = 34%

Location of Faults (USGS)

Figure 65. Hawaii Oahu North Suitability - g33 p33 s34

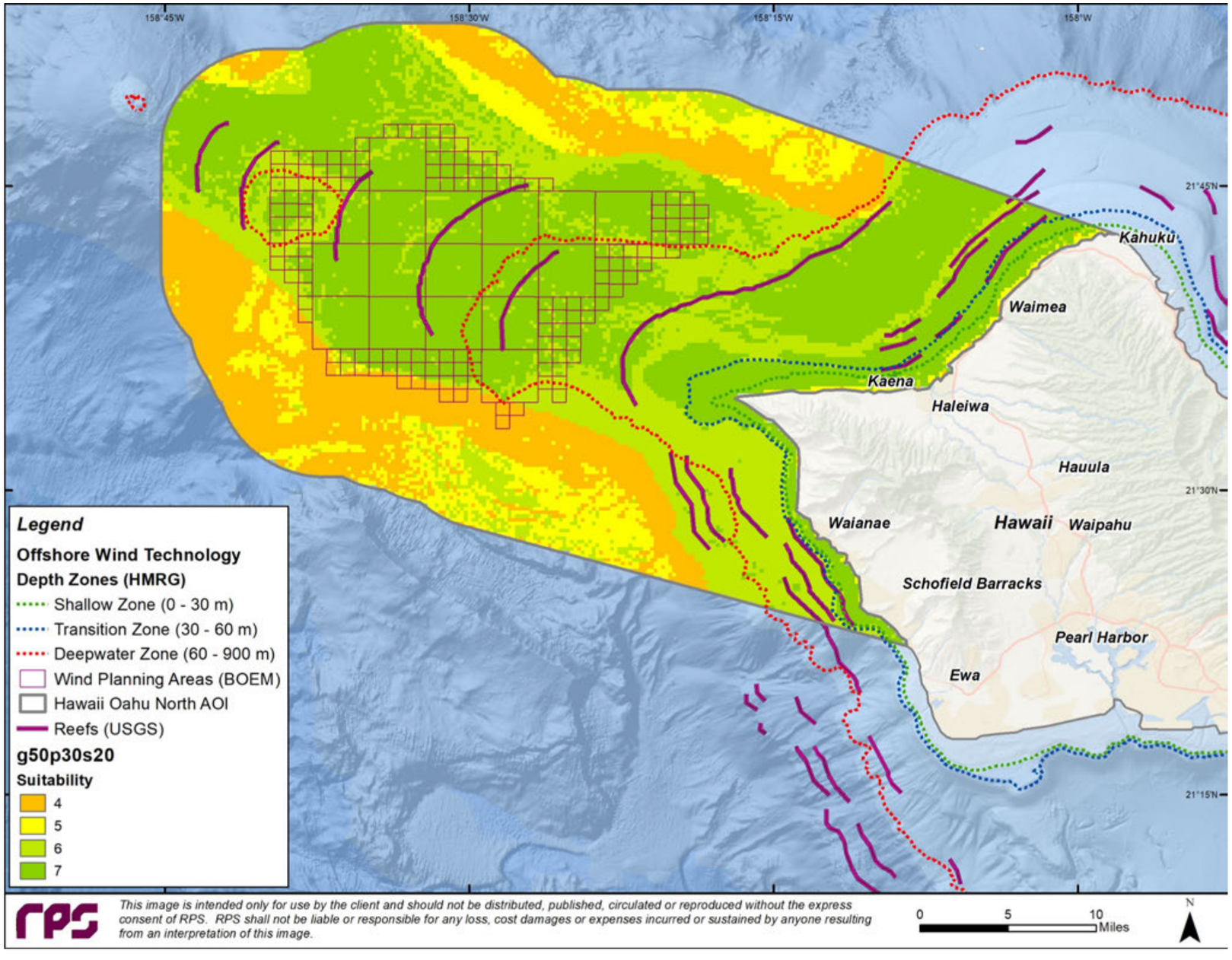

Variable Weighted Overlay

Suitability based on the following weighting:

Geology = 50%

PGA = 30%

Slope = 20%

Location of Reefs (USGS)

Figure 66. Hawaii Oahu North Suitability - g50 p30 s20

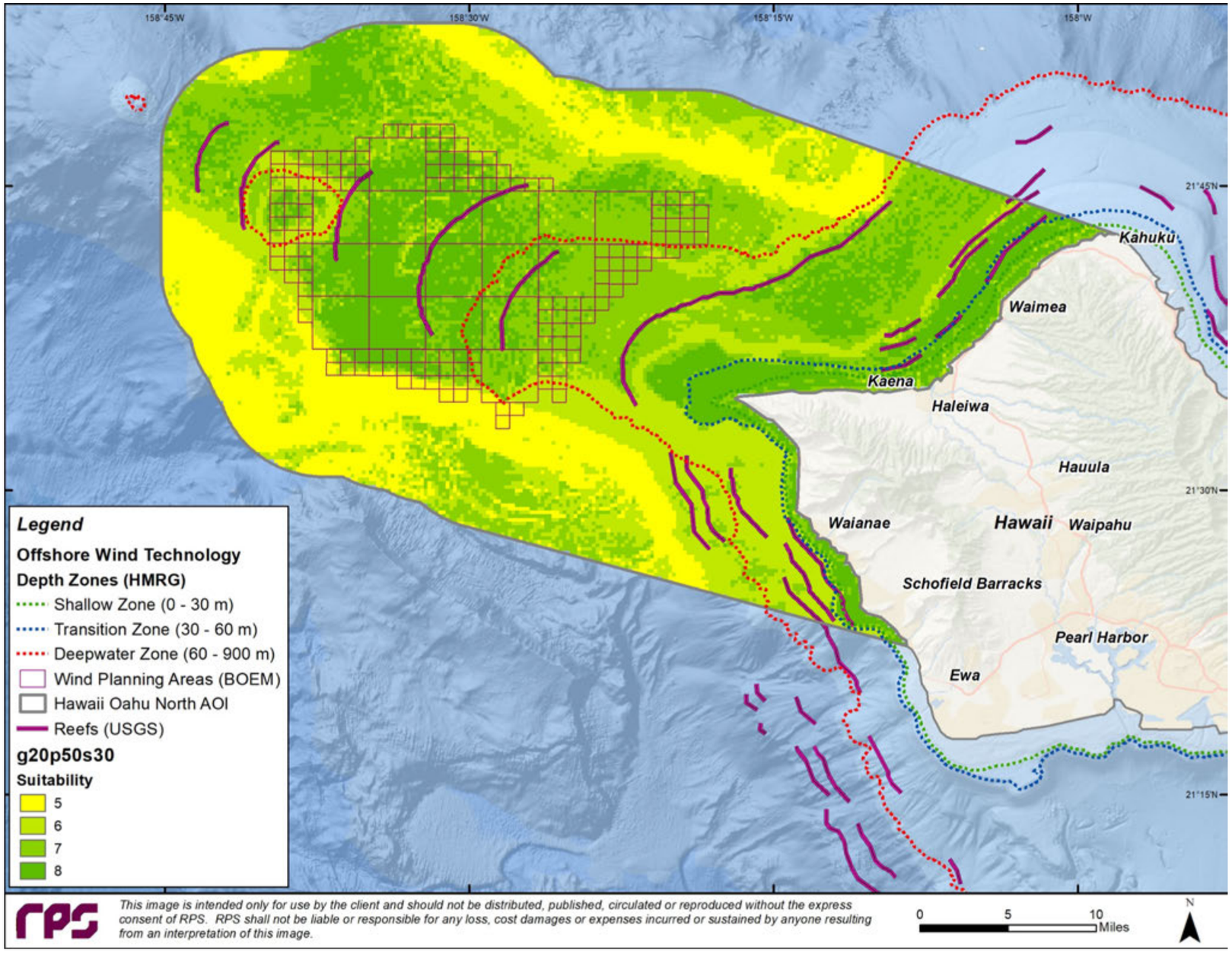

Variable Weighted Overlay

Suitability based on the following weighting:

Geology = 20%

PGA = 50%

Slope = 30%

Location of Reefs (USGS)

Figure 67. Hawaii Oahu North Suitability - g20 p50 s30

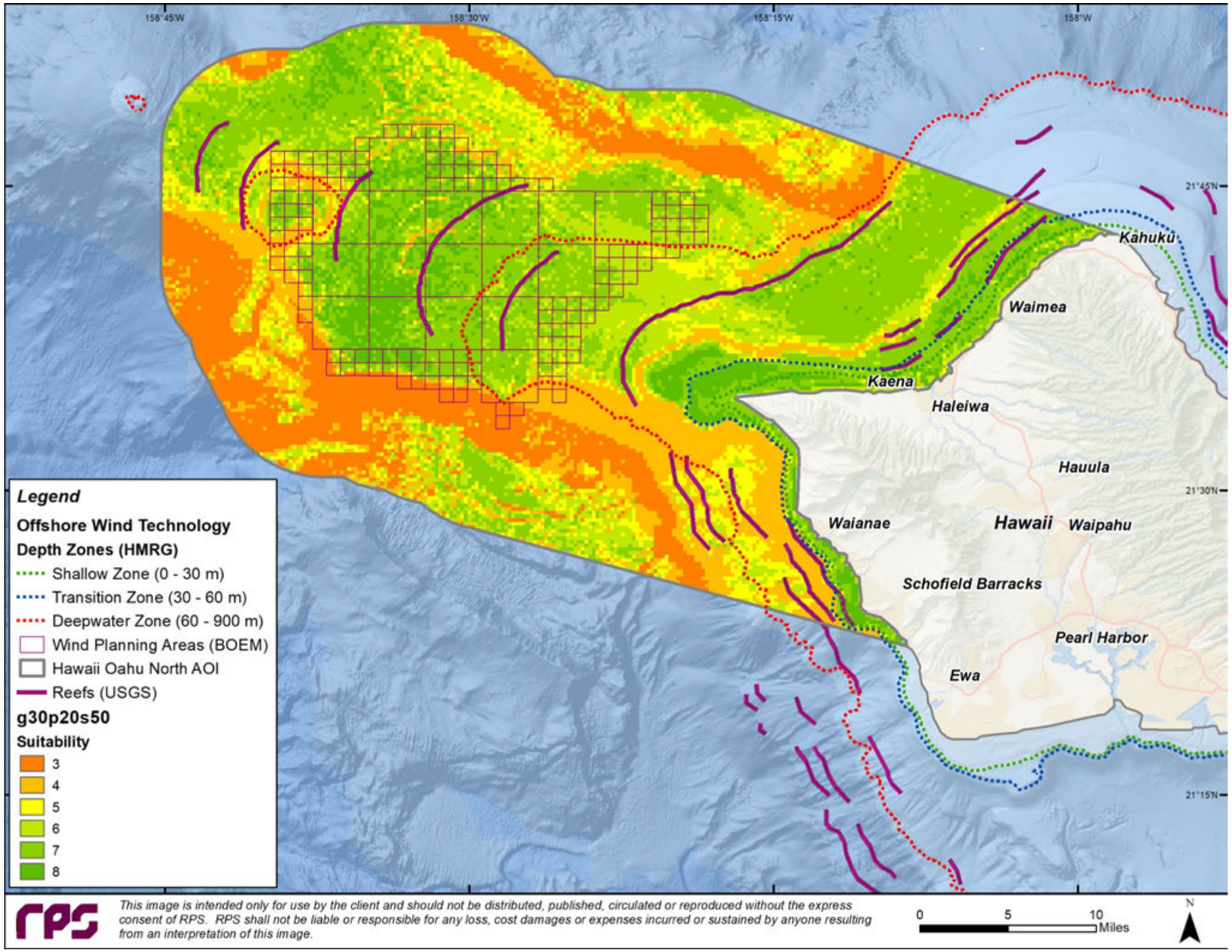

Variable Weighted Overlay

Suitability based on the following weighting:

Geology = 30%

PGA = 20%

Slope = 50%

Location of Reefs (USGS)

Figure 68. Hawaii Oahu North Suitability - g30 p20 s50

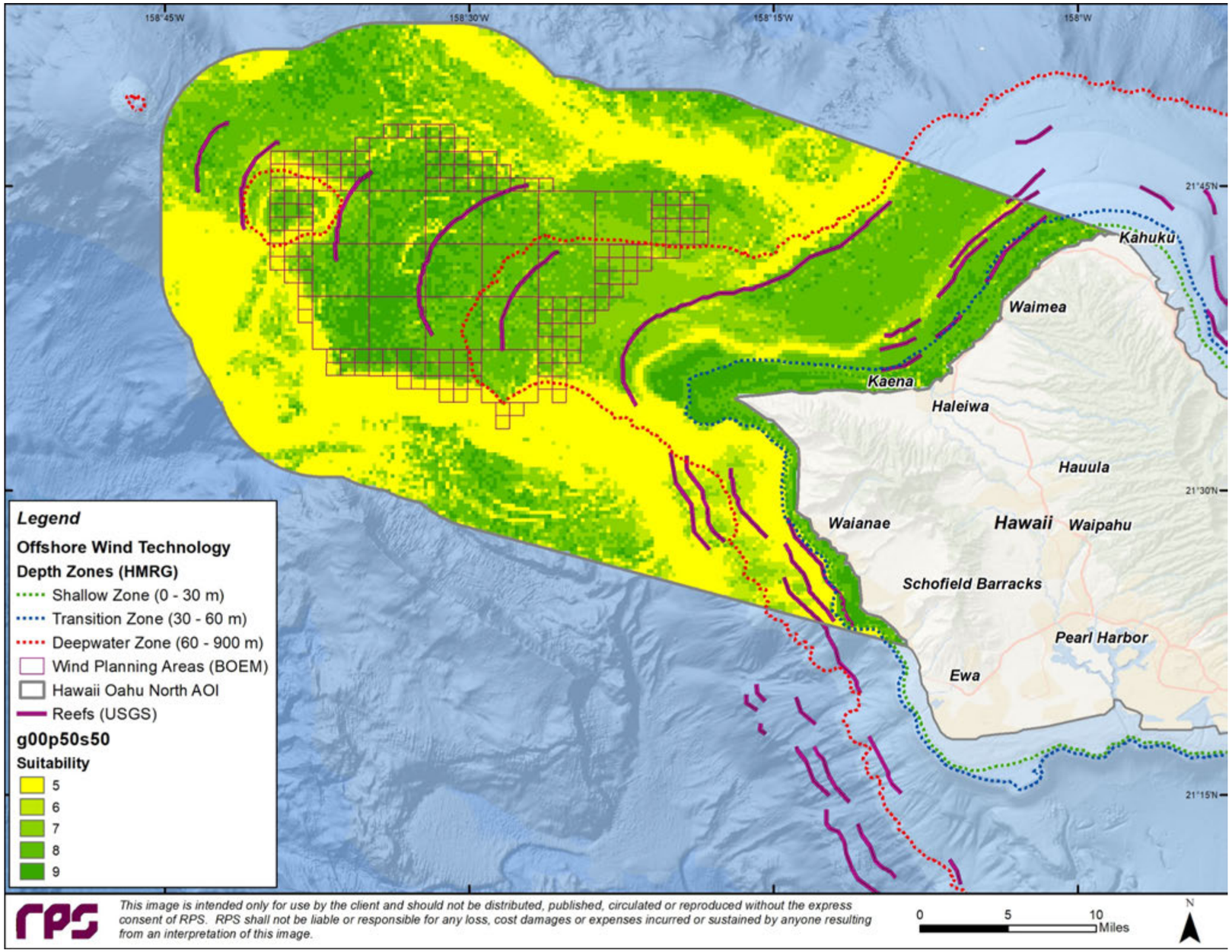

Variable Weighted Overlay

Suitability based on the following weighting:

Geology = 0%

PGA = 50%

Slope = 50%

Location of Reefs (USGS)

Figure 69. Hawaii Oahu North Suitability – g00 p50 s50

7.5 Hawaii Oahu South

Panel Display of Variably Weighed Overlay Suitability Analysis:

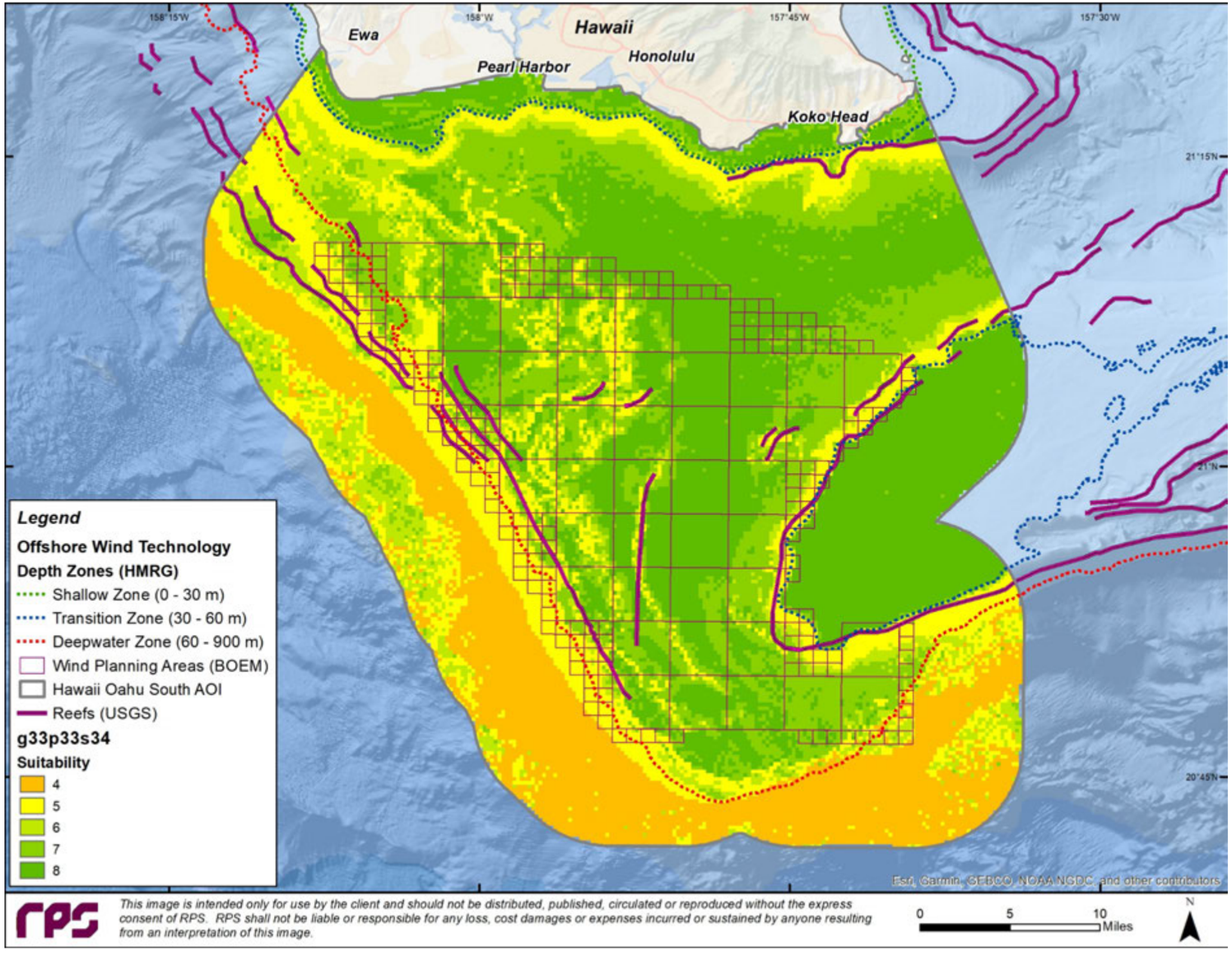

Variable Weighted Overlay

Suitability based on the following weighting:

Geology = 33%

PGA = 33%

Slope = 34%

Location of Reefs (USGS)

Figure 70. Hawaii Oahu South Suitability - g33 p33 s34

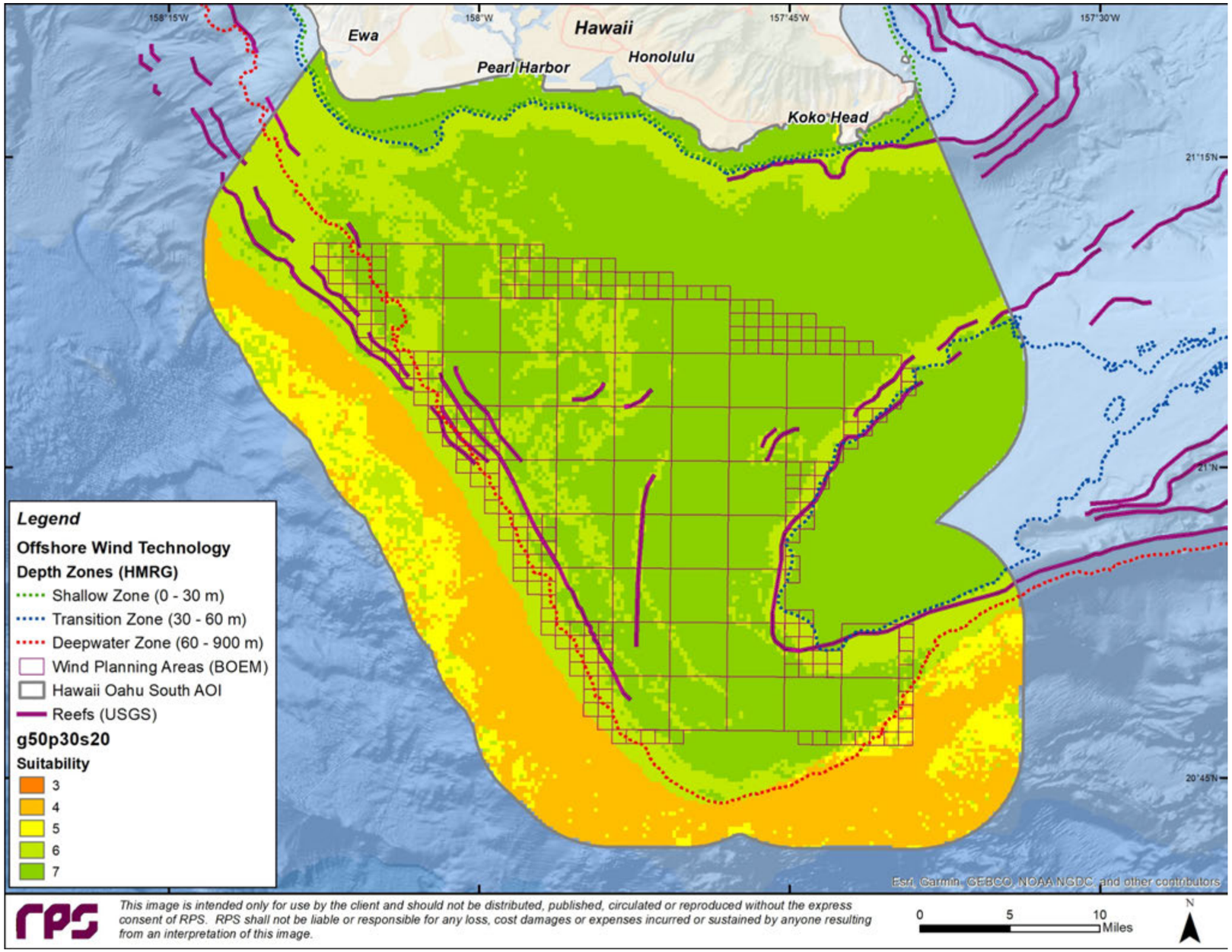

Variable Weighted Overlay

Suitability based on the following weighting:

Geology = 50%

PGA = 30%

Slope = 20%

Location of Reefs (USGS)

Figure 71. Hawaii Oahu South Suitability - g50 p30 s20

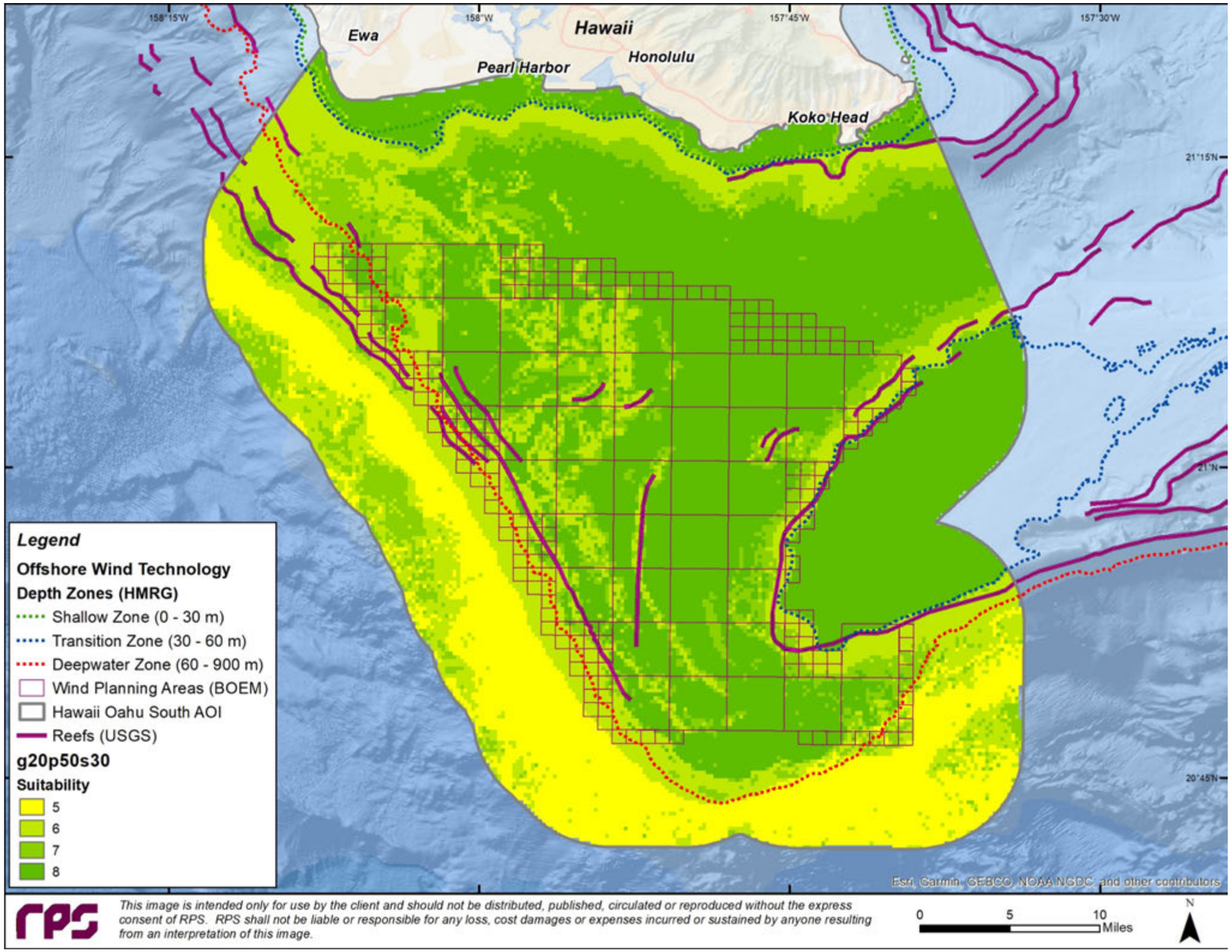

Variable Weighted Overlay

Suitability based on the following weighting:

Geology = 20%

PGA = 50%

Slope = 30%

Location of Reefs (USGS)

Figure 72. Hawaii Oahu South Suitability - g20 p50 s30

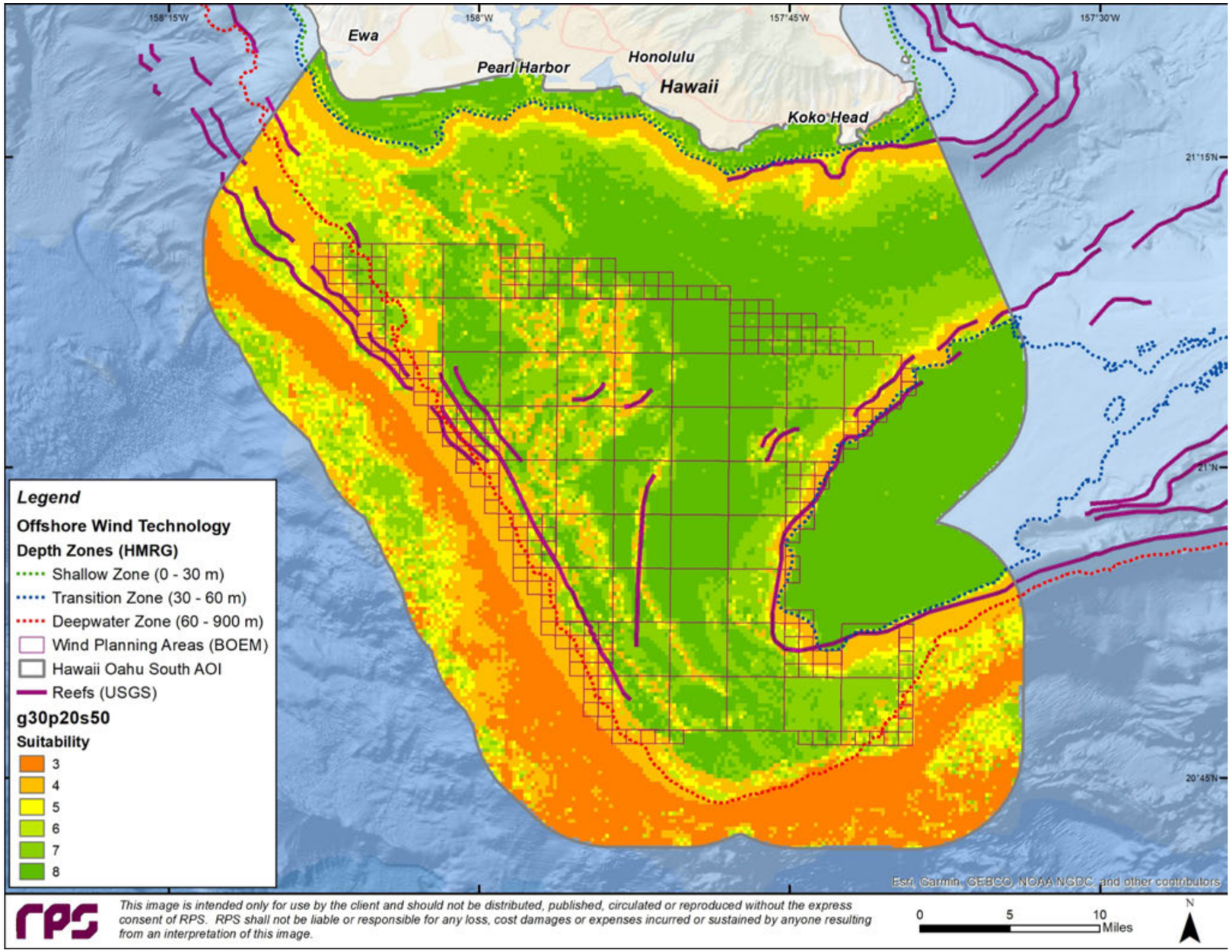

Variable Weighted Overlay

Suitability based on the following weighting:

Geology = 30%

PGA = 20%

Slope = 50%

Location of Reefs (USGS)

Figure 73. Hawaii Oahu South Suitability - g30 p20 s50

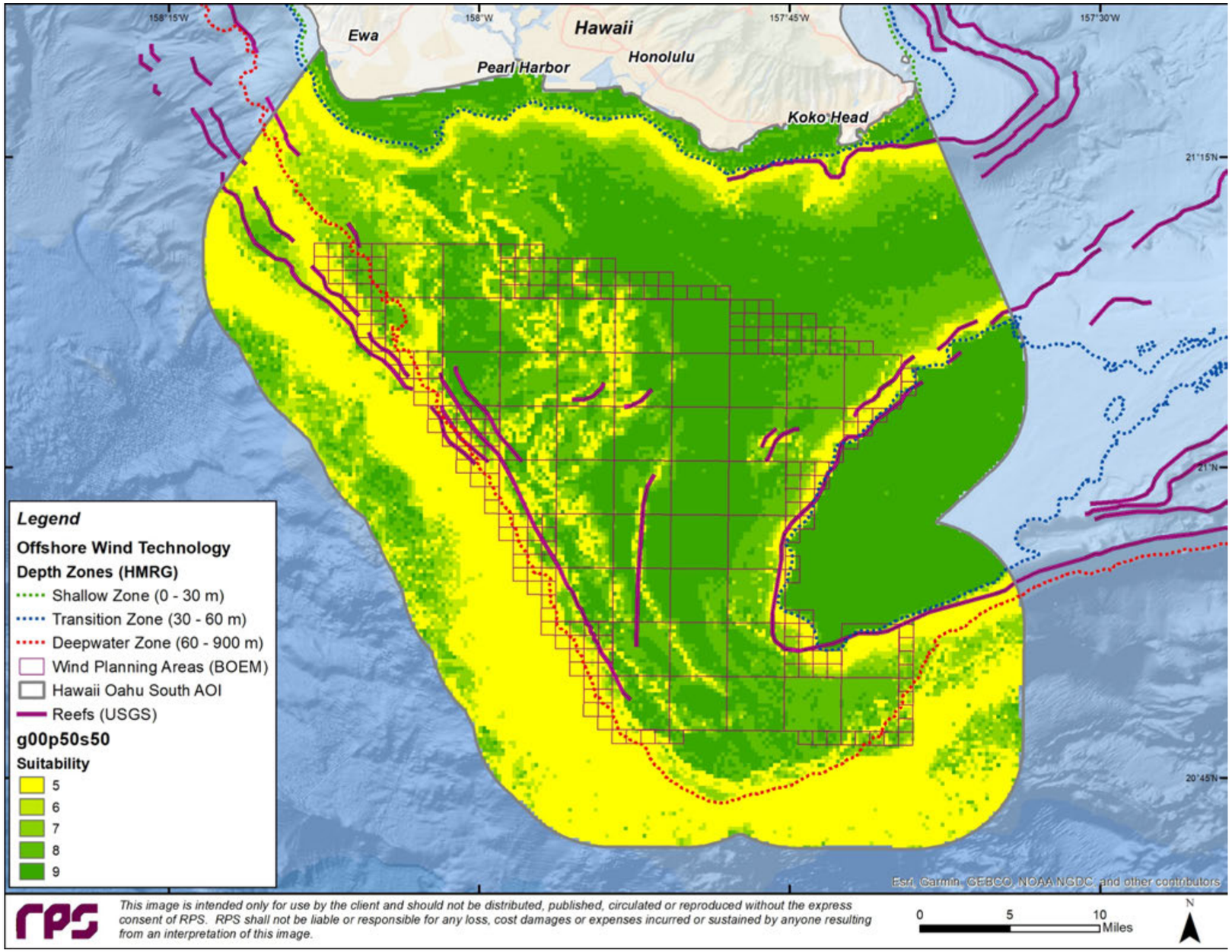

Variable Weighted Overlay

Suitability based on the following weighting:

Geology = 0%

PGA = 50%

Slope = 50%

Location of Reefs (USGS)

Figure 74. Hawaii Oahu South Suitability – g00 p50 s50

8 DISCUSSION

Based on the geospatial analysis of the available data reviewed in the suitability analysis section, and the availability of the BOEM OceansMap data portal, the proposed study areas appear to be good geologic choices for FOWF, in general, and the project team discusses each of them individually in this report section.

8.1 FOWF Developments Based on Depth and Soil Type

Based on the water depth within the study areas, while deployment of a FOWT in a particular area may be possible, there are other factors (e.g., environmental conditions, design of FOWT) that need to be studied to fully investigate the feasibility of deploying the FOWT:

- **Oregon:** The range of depth is very large (approximately 100 to 2,000 m) in Oregon and it allows the draft necessary for any type of FOWT.

  In this study area, soil type is the limiting factor in defining the suitable locations, as the liquefaction of gravely and sandy sediments may be the greatest issue for FOWF seabed-mounted infrastructure in this region. Therefore, further soil data collection is needed to identify soil cohesiveness and geological features to determine anchoring and mooring systems. Thus, 3-D seismic data should be analyzed because of the presence of unconsolidated substrate in the area.

- **Northern California:** The extent of the publicly available bathymetry data is poor and widely-spaced and requires better resolution to derive more precise conclusions. Based on the existing bathymetry data of the Call Areas in Northern California, all types of FOWT will have adequate draft to be deployed. This includes spar type as the depth of study area in Northern California approximately ranges from 500 to 1,000 m, which is deep enough for this type of FOWT.

  For the Humboldt Call Area, use of a driven pile anchoring system might be feasible due to the versatility of different types of soil. The northern part of the study area might be more suitable for installation of FOWT, as faults can be avoided, and a muddy soil type is prevalent. Ultimately, more analysis and data collection are needed to determine accurate soil condition and appropriate anchorage type.

- **Central California:** The bathymetry of the Central California Call Area is adequate for all kinds of FOWT as the depths in Diablo Canyon and Morro Bay study areas approximately range between 500 m to 1,000 m and 900 m to 1,200 m, respectively.

  For the Diablo Canyon and Morro Bay Call Areas, very little detailed soil information is available and targeted site-specific seabed sampling is needed. Based on available datasets at the time of the study and the lack of publicly available 3-D seismic data to identify shallow geological features, a dedicated survey and soil sampling is recommended before installing the FOWT.

- **Hawaii:** The depth in Oahu North Call Area ranges from 500 to 2,000 m, which is sufficient to allow the draft of any FOWT, including spar type. The range of depths in the Oahu South Call Area is relatively large (50 to 2,500 m) and allows the draft necessary for any type of FOWT. However, there are places in the Oahu South Call Area in which the deployment of spar buoy type FOWT is

not possible, as it requires a draft greater than 100 m (i.e., greater than the minimum depth of the study area at 50 m).

For the Oahu North and South study areas, very little soil type information is available except for the region covered by coral reef. A targeted approach to site-specific seabed sampling is recommended. In this area, the bulk of the deep water seabed soil type seems to be limey muds and or sand, except where coral reefs occur (which should be considered as an exclusion area).

Collection of high-resolution site investigation surveys specific to the area using multibeam (bathymetry and backscatter), sub-bottom profiler, and grab sampling, to further determine suitability would increase the accuracy of the suitability analysis and decrease the risk of interpolation from the available datasets where data gaps exist.

8.2 Composite Suitability Analysis

The suitability analysis models are presented using different weighting assignments. The variable weighted site suitability approach used for this effort is infinitely changeable and repeatable and can be updated as new data are collected and integrated. Based on this geospatial analysis of the available data, the Call Areas appear to be good geologic choices for FOWF. In general, the Call Areas selected occur in areas of lower slope gradients, suggesting liquefaction of coarse-grained sediments may be the greater issue in earthquake-prone areas. In general, suitability values of 7-9 are suggested as acceptable for FOWF infrastructure, and this would include areas with muddy sediments that avoid fault prone and reef areas in the shallowest water possible.

In this study, five iterations of suitability analysis resulted in five different resultant maps for each study area, each with a plethora of information that proved challenging to integrate, interpret, and display. The choice of a single result based on professional judgement alone is a qualitative approach that may provide a limiting factor. Therefore, the composite suitability models should portray the “best of the best” for each AOI in terms of suitability considering the variable combination of data inputs (i.e., slope, geology, seismic hazard PGA) of variable certainty and quality.

A composite suitability analysis is also presented as an effort to capture the data in a comprehensive single summary map from all five weighted model outputs. The summary maps quantitatively include all the strengths and weaknesses of all five iterations of the original suitability analysis results for each area.

Composite suitability analysis is accomplished by summing and averaging the results from each iteration of the five suitability analysis maps for each AOI. The lesser values (1 – 4), which are indicative of “unsuitable” areas, are then removed from the AOI map to only display “suitable” results of 5 or greater. Removing the “unsuitable” data simplifies the maps and make them easier to interpret.

The composite suitability analysis is shown in Figure 75 through Figure 79 and discussed for each AOIs.

8.2.1 Oregon Regional

The most representative of the models for the Oregon Regional AOI is deemed to be where the soil type has more weights on the exclusivity of model outputs (Section 7.1), as slope gradient does not appear to be a serious issue on the Oregon shelf and the seismic activity has more effects on the southern side of the AOI, close to CA. However, the liquefaction of gravely and sandy sediments may be the greatest issue for FOWF seabed mounted infrastructure. Thus, a model weighted toward soil type is likely the most representative (g50 s30 e20). The suggested siting area for FOWF infrastructure in this region is the transition to deep water depth in the northern central part of the region, where the suitability values are about 8-9 indicating muddy sediments, lower seismic hazard risk, and possibly avoidance of faults.

In the Oregon Regional Composite Suitability Map (Figure 75), the areas of coarse grained material of gravel and sand (Figure 35) and higher slope areas (Figure 36) are absent, and areas of higher peak ground acceleration (Figure 37) show lesser values of yellow and light green indicating less suitability. This map effectively eliminates the areas of sand and gravel that may be prone to liquefaction during earthquakes and high slope areas with stability issues, and what remains is a simple approximation of the most favorable areas in which to place FOWT.

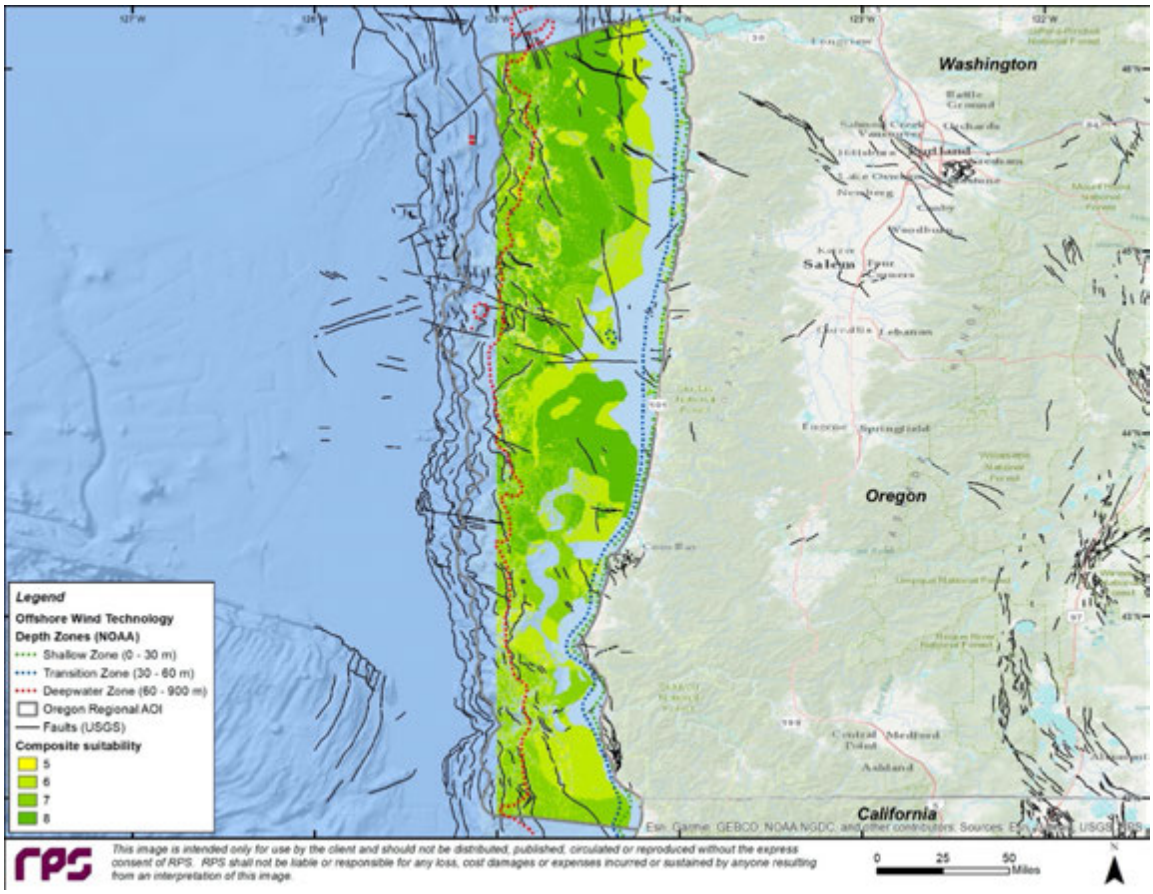

Figure 75. Oregon Regional Composite Suitability Map

8.2.2 California Humboldt

All representative maps of suitability models for the Humboldt AOI (Section 7.2) show the northern part of the study area is more suitable for installation of FOWF in California Humboldt, where the faults are avoided and the muddy soil type is covering the region. It is important to point out that the slope gradient data are poor in this AOI, though it does not appear to be a serious issue and, the bulk seabed soil type is reported to be mud. As earthquake events are very frequent in the AOI, a model that is weighted toward seismicity and to a lesser extent sediment type is likely the most representative to define exclusion area (Figure 58), while the analysis using the soil type as more important factor (Figure 56) clearly identifies the areas which should be avoided.

In the Humboldt Composite Suitability Map (Figure 76) areas of coarse-grained material (sand) and hard ground (Figure 38) and higher slope (Figure 39) are absent. In addition, note that the map is missing the darker shades of green with suitability values of 7 to 8. This is because the entire Humboldt area received a high PGA of 40 or higher (Figure 40); and thus, has reduced suitability values in comparison with other AOIs of this study. Based on these results, the Humboldt area is largely a favorable area for placement of FOWT, though heavily prone to seismicity, and the least suitable block among all 6 regions studied here, in relation to ground acceleration.

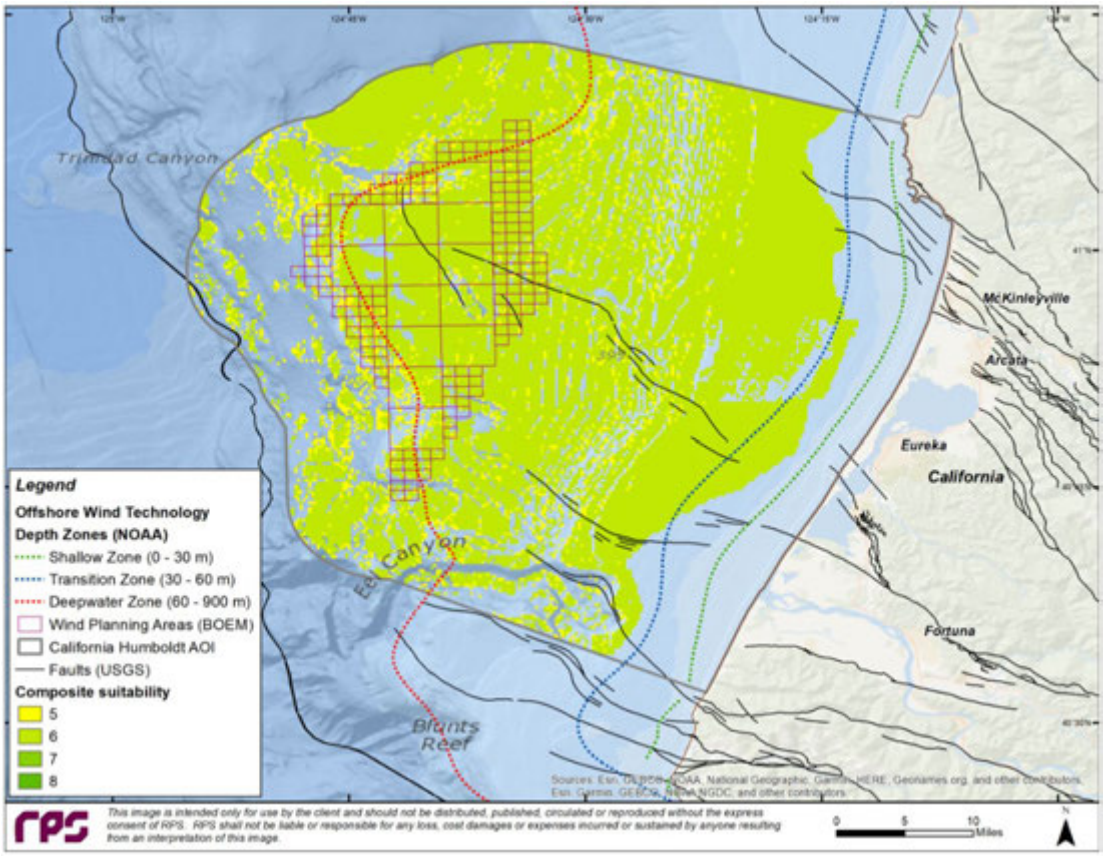

Figure 76. Humboldt California Composite Suitability Map

8.2.3 California Morro Bay and Diablo Canyon

In California Morro Bay and Diablo Canyon (Section 6.4.3 and Section 7.3), slope gradient does not appear to be a serious issue and seismicity appears to be an issue in the shallow waters, away from the proposed study areas. Thus, the suitability analysis with more weights on the soil type (Figure 61) is deemed the most representative of the map models for the Morro Bay/Diablo Canyon AOI. Figure 77 shows Morro Bay is preferable to Diablo Canyon, and the east side of Diablo Canyon is more suitable than the west side. In this area, the bulk of the deep water AOI seabed is likely to be mud except where bedrock outcrops. It is important to note that the slope gradient and soil type data are somewhat poor in this AOI.

In the Morro Bay and Diablo Canyon Composite Suitability Map (Figure 77), areas of exposed bedrock or slump (Figure 41) and higher slope areas (Figure 42) are absent or have reduced suitability. Figure 43 shows lower values of PGA values (i.e., 9, 10, 15, 20, and 25) which have reduced the suitability values only slightly in this map. Based on these results, the Morro Bay and Diablo Canyon AOI are largely a favorable area for placement of FOWT. The nearshore areas of Diablo Canyon AOI close to Morro Bay and San Luis Obispo Bay rate low and are considered to be unfavorable areas. Additionally, due to risk of liquefaction and faults crossing in the center of this AOI, it shows lower suitability than the other parts of the region. More data collection at this AOI for siting of anchorage and mooring and cable burial is recommended.

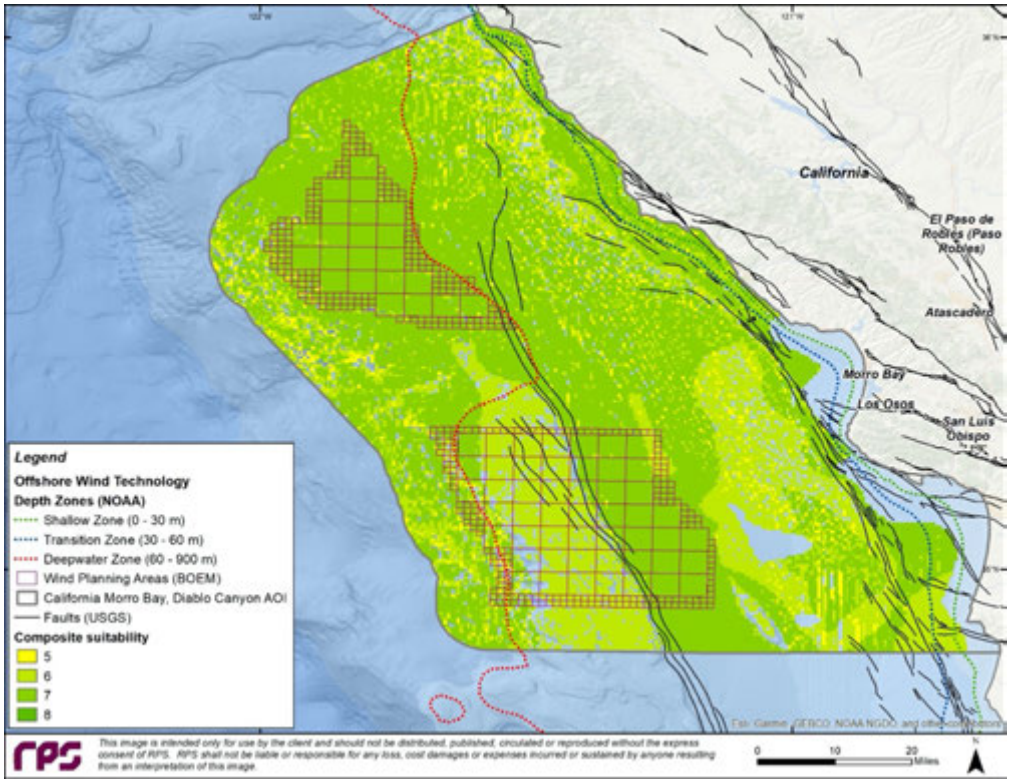

Figure 77. Morro Bay and Diablo Canyon California Composite Suitability Map

8.2.4 Hawaii Oahu North

Hawaii Oahu North Suitability analysis with more weights on the soil type (Figure 66) is deemed the most representative of the map models for the Oahu North AOI (See Section 6.4.4 and Section 7.4). This is because slope gradient does not appear to be a serious issue and seismic activities appear to occur away from the call areas. In this area, the bulk of the deep-water AOI seabed soil type is likely to be limey muds and or sand except where reefs occur. It is important to note that the soil type data are somewhat lacking in this AOI. Thus, the model that is weighted toward sediment type (g50 s30 e20) is likely the most representative.

In the Oahu North Hawaii Composite Suitability Map (Figure 78), slope areas (Figure 44) are absent and slumped areas (Figure 45) that are presented have lesser suitability values of 5 and 6. Figure 46 shows lower values of PGA (values 6-10) which have reduced the suitability values only slightly in this map. There are some blocks without color-coding in Figure 78 which are evident as being unfavorable. Based on these results, the bulk of Oahu North is a moderately favorable area for placement of FOWT, while more field measurements are needed to assess the suitability of siting in this AOI.

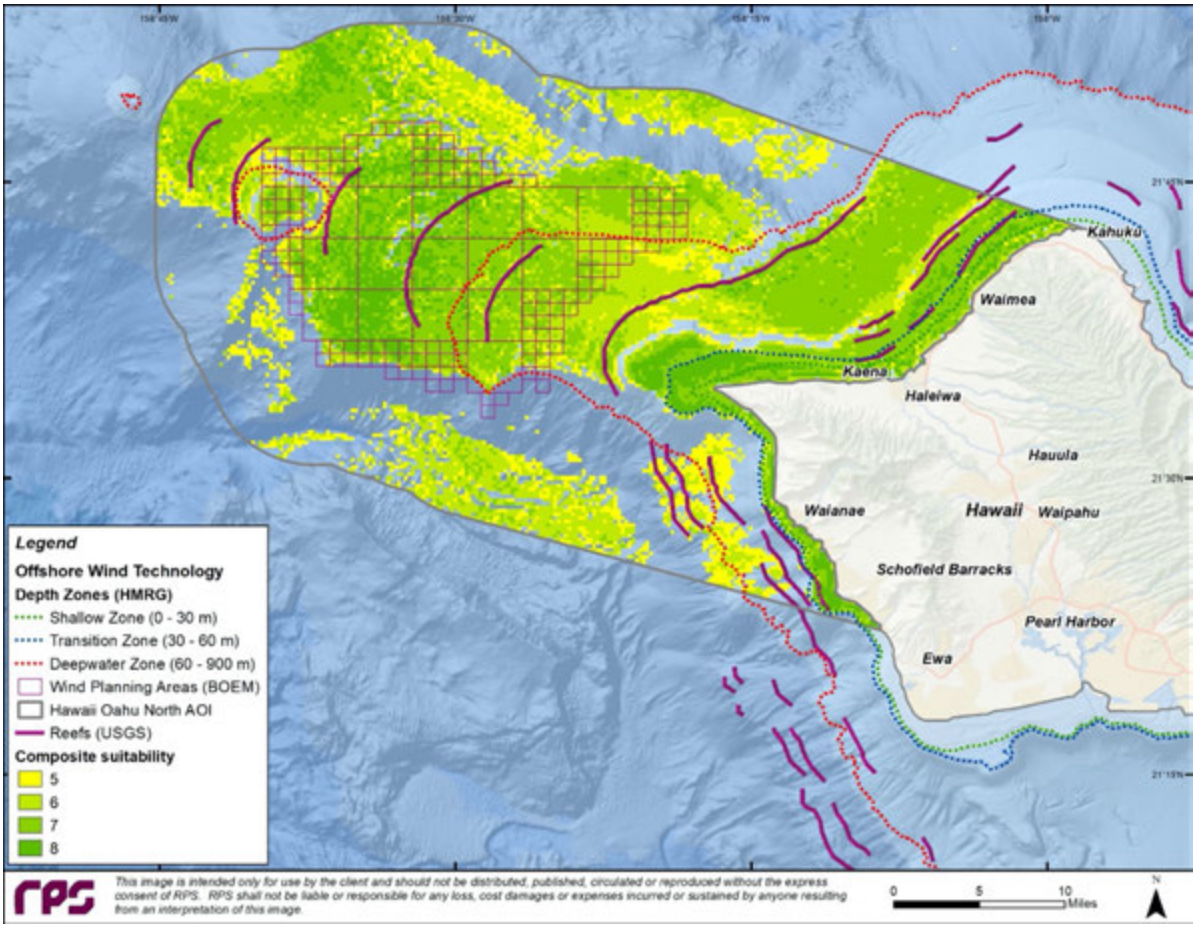

Figure 78. Oahu North Hawaii Composite Suitability Map

8.2.5 Hawaii Oahu South

In Oahu South AOI area (6.4.5 and Section 7.5), the bulk of the deep water AOI seabed soil type is likely to be limey muds and or sand, except where reefs occur and circular and elongate high slope features are evident in the slope gradient data. Therefore, Hawaii Oahu South Suitability analysis equally weighted toward sediment type and slope gradients (g33 s33 e34) is likely the most representative model for this AOI (Figure 70). Suitability values of 7-8 possibly indicating muddy sediments, away from high slope, fault prone and reef prone areas are suggested as acceptable for FOWF infrastructure. It is important to note that the soil type data are somewhat lacking in this AOI.

In the Oahu South Hawaii Composite Suitability Map (Figure 79), the high slope areas (Figure 47) are absent and slumped areas (Figure 48) that remain have lesser suitability values of 5 and 6. Figure 49 shows a low value of 10 for PGA which have reduced the suitability values only slightly in this map. There are some blocks in the western side of the AOI without color-coding in Figure 79 which are evident as being unfavorable. Based on these results, the majority of Oahu South is a favorable area for placement of FOWT, while there are some regions unfavorable for siting.

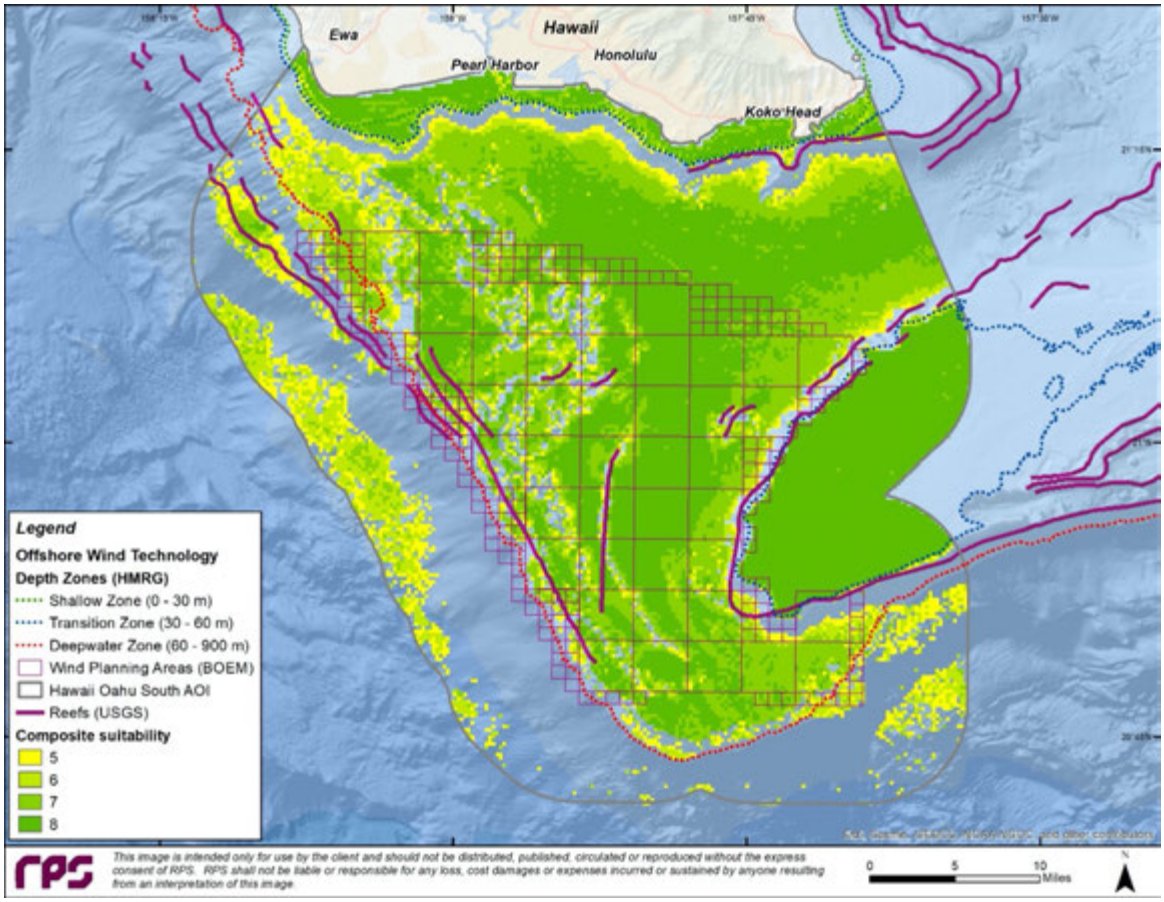

Figure 79. Oahu South Hawaii Composite Suitability Map

9 CONCLUSION AND RECOMMENDATIONS

Composite suitability analysis appears to be a simple and effective methodology of providing a summary map. When performing a comparison, the suitability analysis and composite suitability analysis maps yield similar results. However, it is clear that the composite suitability analysis yields a more comprehensive rendition honoring all of the input criteria, and the elimination of the un-suitable data make them simpler to understand. Also, some considerations should be implemented for different regions, based on the regulations and standards reviewed in Section 3.

9.1 Data Gap Analysis and Limitations

The information on the available datasets and their accuracy was discussed and presented in the Section 6.1 on inputs. In the California AOIs (Humboldt, Morro Bay, and Diablo Canyon), the available public bathymetry data was poor, widely-spaced and resulted in artifacts in the slope maps. Higher resolution bathymetry data with soundings in the 50-meter bin spacing range (or better) worked best for this level of desktop investigation.

In the California Morro Bay and Diablo Canyon AOI and Hawaii Oahu North and South AOIs, very little soil type information was available. A targeted approach to seabed sampling site specific to the proposed AOIs is recommended.

It is important to understand that the data utilized in this desk study were taken from the various sources in the public domain and are limited to the seafloor only. As an overview, the difference in data quality and certainty across the AOIs is described below as a simple summary:

- AOIs Oregon Regional and California Humboldt have the best quality data with most certainty due to a recent BOEM study (2014) by Oregon State University; this study also incorporated subsurface seismic data, and grab samples / box cores in local areas.
- AOIs Hawaii Oahu North and South have moderate data quality and certainty based on age and utility of only regional side-scan sonar mosaics for geological interpretation; no sediment grab sample or core data available specifically within the Oahu AOIs.
- AOI California Morro Bay and Diablo Canyon have the lowest data quality and certainly based on age and quality of regional 2D seismic data for 1982 published USGS report.

9.2 Recommended Follow on Work

In the event that a more in-depth site favorability study follows this initial desk top approach, the following work is recommended in order to increase the accuracy of the input data including slope gradient, the soil type, and the fault locations:

- Collection of High-Resolution Site investigation surveys specific to the AOIs to further determine suitability – multibeam (bathymetry and backscatter), sub-bottom profiler and grab sampling;

- FOWF Feasibility Assessment Reporting – integrate high-resolution survey data and reassess suitability for locating the anchorage and mooring in deep water and offshore, and cable burial, regarding possibilities of landslide and soil strength offshore to shoreline; and
- The additional information can increase the accuracy of the suitability analysis, by decreasing the risk of interpolation from the available datasets while there is a data gap in between.

Also, as there is a growing market of FOWF in U.S., the regulation on establishing FOWF needs further development. Room for improvement in regulation has been identified in the light of potential geohazards in the areas of interest:

- In ABS (2012), importance of wave-induced motion for designing TLP type platform has been discussed. Guidance and regulation that deals with wave-induced hydrodynamic load on the structure which is caused by tsunami or other long waves needs to be developed. Appendix B presents an example review of what is needed to be considered in regard to tsunami-induced currents.
- Specific guidelines should be issued for the selection of anchoring system considering the return period of earthquake for the deployment site of the FOWT.
- Regulations specifying the return period of extreme event need to be developed specifically for the eastern pacific region which has several areas that are prone to geohazards. Selection of this return period for FOWT should not only be based on seismic activity but also should consider the overall design approach.

Finally, the project team recommends case studies with a focus on seismic activity specifically tsunami interaction with the FOWT components and its loads on the floating structure and vortex induced vibration and drags on the mooring and anchorage be conducted. The aim of these studies would be to gain a better understanding of geohazard impacts on FOWT. Additionally, site-specific regulations should be implemented to limit regions with the risk of environmental hazards and geohazards.

10 REFERENCES

30 C.F.R. § 250.201, 2017. What plans and information must I submit before I conduct any activities on my lease or unit? Available at https://www.law.cornell.edu/cfr/text/30/250.201.

46 C.F.R. § 170.185, 2012. Stability test preparations standards. Available at https://www.law.cornell.edu/cfr/text/46/170.185.

ABS, 2012. Floating Wind Turbines, (Contract M11PC00004). American Bureau of Shipping (ABS), 72-210. Available at https://www.bsee.gov/sites/bsee.gov/files/tap-technical-assessment-program//669ab.pdf.

ABS, 2013. Design Guideline for Station keeping Systems of Floating Offshore Wind Turbines (Contract E12PC00027), American Bureau of Shipping (ABS), 179-224. Available at https://www.bsee.gov/sites/bsee.gov/files/tap-technical-assessment-program/tar705finalreport.pdf.

Adam F., Myland T. and Dahlhaus, F. (2015), GICON®-TLP for wind turbines – the path of development. In C. Guedes Soares (Ed.), Renewable Energies Offshore. Taylor & Francis Group, London, 651-656. ISBN: 978-1-138-02871-5.

API RP 2SK (2005). American Petroleum Institute Design and Analysis of Stationkeeping Systems for Floating Structures. American Petroleum Institute (API), 197-199.

API RP 2T (2010). American Petroleum Institute Recommended Practice for Planning, Designing, and Constructing Tension Leg Platforms. American Petroleum Institute (API), 14-51.

ASCE (2010). Minimum Design Loads for Buildings and Other Structures, Standard ASCE/SEI 7-10. American Society of Civil Engineers, 22-71.

Atwater, B.F., Musumi-Rokkaku, S., Satake, K., Tsuji, Y., Ueda, K., and Yamaguchi, D.K., 2015, The orphan tsunami of 1700 — Japanese clues to a parent earthquake in North America, 2nd ed. Seattle, University of Washington Press, US Geological Survey Professional Paper 1707, 135. doi: 10.3133/pp1707

Blue Marble Geographics. 2019. Global Mapper 21. Geographic Calculator. Hallowell, ME: Blue Marble Geographics. Accessed August, 2019 at https://www.bluemarblegeo.com/products/global-mapper.php

Bonilla, M.G., 1960. Landslides in the San Francisco South Quadrangle, California. US Geological Survey, 60-15. doi: 10.3133/ofr6015.

Butterfield, S., Musial, W., Jonkman, J. and Sclavounos, P. (2007). Engineering challenges for floating offshore wind turbines. National Renewable Energy Lab, NREL/CP-500-38776. Retrived from https://www.nrel.gov/docs/fy07osti/38776.pdf.

BV, 2019. Classification and Certification of Floating Offshore Wind Turbines: Guidance Note NI 572. Bureau Veritas (BV), 24. Available at https://marine-offshore.bureauveritas.com/sites/g/files/zypfnx136/files/media/document/572-NI_2019-01.pdf.

Carter L., Burnett D., Drew S., Marle G., Hagadorn L., Bartlett-McNeil D., and Irvine N. (2009). Submarine Cables and the Oceans – Connecting the World. UNEP-WCMC Biodiversity Series, 31, 16.

Chock, G. Y. K. (2015). The ASCE 7 tsunami loads and effects design standard for the United States. In N. Ingraffea and M. Libby (Ed.), Structures Congress 2015. American Society of Civil Engineers, 1446-1456. doi: 10.1061/9780784479117.124.

Clague, D.A. and Dalrymple, G.B., (1987). The Hawaiian-Emperor volcanic chain, Part I: Geologic evolution. Volcanism in Hawaii, 1, 5-54.

Clare, M.A., Talling, P.J., Challenor, P., Malgesini, G. and Hunt, J. (2014). Distal turbidites reveal a common distribution for large (> 0.1 km^3) submarine landslide recurrence. Geology, 42(3), 263-266.

CREW (2005). Cascadia Subduction Zone Earthquakes: A magnitude 9.0 earthquake scenario. Cascadia Region Earthquake Workgroup (CREW).

CREW (2013). Cascadia Subduction Zone Earthquakes: A magnitude 9.0 earthquake scenario, Update 2013. Cascadia Region Earthquake Workgroup (CREW).

Dagher, H., Viselli, A., Goupee, A., Kimball, R. and Allen, C. (2017). The VolturnUS 1: 8 Floating Wind Turbine: Design, Construction, Deployment, Testing, Retrieval, and Inspection of the First Grid-Connected Offshore Wind Turbine in US. DOE-UMaine-3278-2, 8-9. doi: 10.2172/1375022

Devin, M., C. (2019). Optimizing Shared Mooring and Anchoring Strength for Floating Offshore Wind Turbine Arrays (Thesis). Oregon State University, Corvallis, OR, USA.

Diamond, K.E. (2012). Extreme weather impacts on offshore wind turbines: Lessons learned. Natural Resources & Environment, 27(2), 1-5.

Díaz, H., Fonseca, R.B. and Soares, C.G. (2019). Site selection process for floating offshore wind farms in Madeira Islands. In Advances in Renewable Energies Offshore. Taylor & Francis Group, London, 729-737.

Dietrich, F.C., (2014). Evaluation of theoretical capacity models for plate anchors in sand in relation to floating offshore wind turbines (Thesis). University of Rhode Island, Kingston, RI, USA.

Dinh, V.N. and Basu, B. (2015). Passive control of floating offshore wind turbine nacelle and spar vibrations by multiple tuned mass dampers. Structural Control and Health Monitoring, 22(1), 152-176.

DNV-OS-J101 (2004). Offshore Standard for Design of offshore wind turbine structures. Det Norske Veritas- Germanischer Lloyd, 44 – 63.

DNV-OS-J103 (2013). Offshore Standard for Design of floating wind turbine structures. Det Norske Veritas- Germanischer Lloyd, 33.

DNV-GL (2011). Design of Offshore Steel Structures, General (Lrfd Method). OFFSHORE STANDARD DNV-OS-C101. Det Norske Veritas, 73.

DNVGL-ST-0437 (2016). Offshore Standard for Loads and site conditions for wind turbines. Det Norske Veritas- Germanischer Lloyd, 53-60.

DNVGL-ST-0119 (2018). Floating wind turbine structures. Det Norske Veritas- Germanischer Lloyd, 101.

Driscoll, F., Jonkman, J., Robertson, A., Sirnivas, S., Skaare, B. and Nielsen, F.G. (2016). Validation of a FAST model of the statoil-hywind demo floating wind turbine. Energy Procedia, 94, 3-19.

DTL (2016). Environmental Statement: Dounreay Trì Floating Wind Demonstration. Dounreay Trì Limited (DTL), 03363-001010(7).

Esri ArcGIS (2019). An overview of the Reclass toolset. Redlands [CA]: ESRI. Accessed 2019 August at http://desktop.arcgis.com/en/arcmap/latest/tools/spatial-analyst-toolbox/an-overview-of-the-reclass-tools.htm

Esri ArcGIS (2019). How Weighted Overlay works. Redlands [CA]: ESRI. Accessed 2019 August at http://desktop.arcgis.com/en/arcmap/latest/tools/spatial-analyst-toolbox/how-weighted-overlay-works.htm

Etkin, D.S. (2017). Environmental Sensitivity and Associated Risk to Habitats and Species on the Pacific West Coast and Hawaii with Offshore Floating Wind Technologies; Draft Interim Report Task #4 – Incorporation of Accident Spill Impact Probabilities into BOEM Offshore Floating Wind Environmental Sensitivity Analysis (OFWESA) Model. Department of the Interior, Bureau of Ocean Energy Management, Pacific OCS Region, Camarillo, CA. BOEM Task Order: M16PD00038, 71.

Fan, X., Scaringi, G., Korup, O., West, A. J., van Westen, C. J., Tanyas, H., et al. (2019). Earthquake-induced chains of geologic hazards: Patterns, mechanisms, and impacts. Reviews of Geophysics, 57, 421–503. doi: 10.1029/2018RG000626

Field, M.E. and Barber, J.H.J. (1993). A submarine landslide associated with shallow seafloor gas and gas hydrates off Northern California. In Submarine landslides: selected studies in the US exclusive economic zone. Reston, Va, USA: US Geological Survey, 2002, 151-157.

Field, M.E., Clarke Jr, S.H. and White, M.E. (1980). Geology and geologic hazards of offshore Eel River Basin, northern California continental margin. US Geological Survey Professional Paper 80-1080. doi: 10.3133/ofr801080.

Field, M.E., Gardner, J.V., Jennings, A.E., and Edwards, B.D. (1982). Earthquake-induced sediment failures on a 0.25° slope, Klamath River delta: California. Geology, 10, 542-546.

Field, M.E., Schwab, W.C., Lee, H.J. and Twichell, D.C. (1993). Liquefaction of continental shelf sediment: The northern California earthquake of 1980. US Geological Survey Bulletin B, 2002, 143-150.

Fryer, G.J., and Tryon, M.D. (2005), Great earthquakes, gigantic landslides, and the continuing enigma of the April Fool's tsunami of 1946. Eos Transactions AGU86, 52, T11A-0355.

Fuhrman, D. R., Eltard-Larsen, B., Sumer, B. M., Baykal, C., Dogulu, N., Duha Metin, A., et al. (2015). D5.10 - Interaction of the tsunami with the seabed. Implications for wind farms, aquaculture, coastal ecosystems and marine protected areas. Technical University of Denmark, 58.

Goldfinger, C., Henkel, S., Romsos, C., Havron, A., Black, B. (2014). Benthic Habitat Characterization Offshore the Pacific Northwest Volume 1: Evaluation of Continental Shelf Geology. Oregon State University, BOEM 2014-662.

Goldfinger C., Nelson C. H., Morey A. E., Johnson J. E., Patton J. R., Karabanov E., Gutiérrez-Pastor J., Eriksson A. T., Gràcia E., Dunhill G., Enkin R. J., Dallimore A., and T. Vallier (2012). Turbidite Event History-Methods and Implications for Holocene Paleoseismicity of the Cascadia Subduction. US Geological Survey Zone. Professional Paper 1661–F, 171.

Goto, C., (1993). Development of tsunami numerical simulation system for Sanriku coasts in Japan. Rep. Port Harbour Res. Inst., 32(2), 3-44.

Govindji A., James R., and A. Carvallo (2014). Appraisal of the Offshore Wind Industry in Japan. Carbon Trust, 103.

Gutmacher, C.E. and Normark, W.R. (1992). Sur submarine landslide, a deep-water sediment slope failure. Submarine landslides: Selected studies in the US exclusive economic zone, 158.

Hampton, M.A., Lee, H.J. and Locat, J. (1996). Submarine landslides. Reviews of Geophysics, 34(1), 33-59.

Harbitz, C.B., Løvholt, F., Pedersen, G. and Masson, D.G. (2006). Mechanisms of tsunami generation by submarine landslides: a short review. Norwegian Journal of Geology/Norsk Geologisk Forening, 86(3).

Hayes G. P., Myers E. K., Dewey J. W., Briggs R. W., Earle P. S., Benz H. M., Smoczyk G. M., Flamme H. E., Barnhart W. D., Gold R. D., and K. P. Furlong (2017). Tectonic Summaries of Magnitude 7 and Greater Earthquakes from 2000 to 2015. Reston, VA, USA, U.S. Geological Survey, Open-File Report 2016–1192, 158.

Heronemus, W.E., (1972). Pollution-free energy from offshore winds. In 8th Annual Conference and Exposition, Marine Technology Society, Washington, DC, Sep. 11-13, 1972.

Hess, G.R., Normark, W.R., and Gutmacher, C.E., (1979). Sur submarine slide, Monterey Fan, central California: Geological Society of America Abstracts with Programs, 11, 83-84.

Holcomb RT, Robinson JE, (2004). Maps of Hawaiian Islands Exclusive Economic Zone Interpreted from GLORIA Sidescan-Sonar Imagery. Denver, CO, USA: US Geological Survey. Available at https://pubs.usgs.gov/sim/2004/2824/

Hsu, S.K., Kuo, J., Chung-Liang, L., Ching-Hui, T., Doo, W.B., Ku, C.Y. and Sibuet, J.C. (2008). Turbidity currents, submarine landslides and the 2006 Pingtung earthquake off SW Taiwan. TAO: Terrestrial, Atmospheric and Oceanic Sciences, 19(6), 7.

IEC (2005). IEC 61400-1 Ed. 3: Wind turbines - Part 1: Design requirements. International Electrotechnical Commission, Geneva, Switzerland.

IEC (2019). IEC TS 61400-3-2 Ed. 1.0: Wind energy generation systems – Part 3-2: Design requirements for floating offshore wind turbines. International Electrotechnical Commission, Geneva, Switzerland.

IRENA (2016). Floating Foundations: A Game Changer for Offshore Wind Power. International Renewable Energy Agency (IRENA), Abu Dhabi, 5.

ISO (2004). ISO 19901-2:2004: Petroleum and Natural Gas Industries - Specific Requirements for Offshore Structures - Part 2: Seismic design procedures and criteria. International Standards Organisation, Washington, DC, USA.

ISO (2015). ISO 19901-1:2015: Petroleum and natural gas industries – Specific requirements for offshore structures – Part 1: Metocean design and operating conditions. International Standards Organisation, Washington, DC, USA.

James, R. and Ros, M.C. (2015). Floating offshore wind: Market and technology review. Carbon Trust Report, 19-20.

Johnson, H.P., Gomberg, J.S., Hautala, S.L. and Salmi, M.S. (2017). Sediment gravity flows triggered by remotely generated earthquake waves. Journal of Geophysical Research: Solid Earth, 122(6), 4584-4600.

Joseph, D. and Hussong, D.M. (2003). Geospatial management of commercial seafloor data. ESRI User Conference Proceedings.

Kawanishi, T., Katoh, W. and Furuta, H., (1987a). Tension leg platform earthquake motion analysis. In OCEANS'87, Halifax, NS, Canada, 543-547. doi: 10.1109/OCEANS.1987.1160826.

Kawanishi, T., Furuta, H. and Kato, W., (1987b). Earthquake Response of Tension Leg Platform with Gravity Anchor. Journal of the Society of Naval Architects of Japan, 1987(162), pp.517-522.

Kawanishi, T., Takamura, H. and Kobayashi, H. (1991). Earthquake response of the tension leg platform for offset condition. OCEANS 91: Ocean technologies and opportunities in the Pacific for the 90's proceedings, Honolulu HI. Doi: 10.1109/OCEANS.1991.628189.

Keefer, D.K. (1984). Landslides caused by earthquakes. Geological Society of America Bulletin, 95(4), 406-421.

Keefer, D.K. (2002). Investigating landslides caused by earthquakes–a historical review. Surveys in Geophysics, 23(6), 473-510.

Klein, F.W., Frankel, A.D., Mueller, C.S., Wesson, R.L., and Okubo, P.G. (2000). 10% probability of exceedance in 50 years for peak horizontal acceleration and horizontal spectral response acceleration for 0.2, 0.3 and 1.0 second periods (5% of critical damping). Seismic-hazard maps for Hawaii, U.S. Geological Survey Geologic Investigations Series I-2724. Retrieved from https://pubs.usgs.gov/imap/i-2724/i-2724-1.pdf

Klein, F.W. A.D. Frankel, C.S. Mueller, R.L. Wesson, and P.G. Okubo (2001). Seismic hazard in Hawaii: High rate of large earthquakes and probabilistic ground-motion maps. Bulletin of the Seismological Society of America, 91(3): 479-498.

Kokubun. K., Taniguchi, T., and Inoue, S. (2013). Effects of Earthquake and Tsunami on Floating Offshore Wind Turbine. Proceedings of International Symposium on Marine and Offshore Renewable, 5.

Krause, D.C., White, W.C., PIPER, D.J.W. and Heezen, B.C. (1970). Turbidity currents and cable breaks in the western New Britain Trench. Geological Society of America Bulletin, 81(7), 2153-2160.

Kulm, L.D., and Fowler, G.A. (1974). Oregon continental margin structure and stratigraphy: a test of the imbricate thrust model, in Burk, C.A., and Drake, C.L. (Eds.), The geology of continental margins: New York, Springer-Verlag, 261–284.

Kyoki, N. K. (2012). Guidelines for Offshore Floating Wind Turbine Structures. Class NK, 59.

Lander, J.F., Lockridge, P.A. (1989). United States Tsunamis (Including United States Possessions) 1690-1988. National Oceanic and Atmospheric Administration, National Geophysical Data Center, Boulder, Colorado, USA, 41-2, 265.

Lander, J.F., Lockridge, P.A., Kozuch, M.J. (1993). Tsunamis affecting the West Coast of the United States, 1806-1992. National Oceanic and Atmospheric Administration, National Geophysical Data Center, Boulder, Colorado, USA, 29, 242.

Lander (1996). TSUNAMIS AFFECTING ALASKA 1737-1996. National Oceanic and Atmospheric Administration, National Geophysical Data Center, Boulder, Colorado, USA, 31, 205.

Lee, H.J. (2005). Undersea landslides: extent and significance in the Pacific Ocean, an update. Natural Hazards and Earth System Science, 5(6), 877-892.

Lee, H.J., Schwab, W.C. and Booth, J.S. (1993). Submarine landslides: An introduction. Submarine landslides: selected studies in the US exclusive economic zone, 2002, 1-13.

Lee, H.J., Kayen, R.E., Gardner, J.V. and Locat, J. (2003). Characteristics of several tsunamigenic submarine landslides. In Submarine mass movements and their consequences, Springer, Dordrecht, 357-366.

Li, B., and A. Ghosh (2017). Near- continuous tremor and low-frequency earthquake activities in the Alaska- Aleutian subduction zone revealed by a mini seismic array. Geophys. Res. Lett., 44 , 5427 – 5435. doi:10.1002/ 2016GL072088.

Lopéz A. and E. Okal (2006). A seismological reassessment of the source of the 1946 Aleutian 'tsunami' earthquake. Geophys. J. Int., 165, 835–849. doi: 10.1111/j.1365-246X.2006.02899.x

Malhotra, S. (2011). Selection, Design and Construction of Offshore Wind Turbine Foundations. In I. Al-Bahadly (Ed.), Wind Turbines, InTech. ISBN: 978-953-307-221-0, 247-252. Available from: http://www.intechopen.com/books/wind-turbines/selection-design-and-construction-of-offshore-wind-turbinefoundations.

McCulloch DS, Clarke Jr SH, Dolton GL, Field ME, Scott EW, and Utter PA (1982). Geology, Environmental Hazards, and Petroleum Resources for 1982 OCS Lease Sale 73, Offshore Central and Northern California. Denver, CO, USGS. Available at https://pubs.er.usgs.gov/publication/ofr821000

Miller, J.J., von Huene, Roland, and Ryan, H.F. (2014). The 1946 Unimak Tsunami Earthquake Area— Revised tectonic structure in reprocessed seismic images and a suspect near field tsunami source. US Geological Survey, Open-File Report 2014–1024, 19. doi: 10.3133/ofr20141024.

Milliman, J.D. and Meade, R.H. (1983). World-wide delivery of river sediment to the oceans. The Journal of Geology, 91(1), 1-21.

Moore, J.G. and Moore, G.W. (1984). Deposit from a giant wave on the island of Lanai, Hawaii. Science, 226(4680), 1312-1315.

Mori, N., Takahashi, T., Yasuda, T. and Yanagisawa, H. (2011). Survey of 2011 Tohoku earthquake tsunami inundation and run-up. Geophysical Research Letters, 38(7).

Musial, W., Butterfield, S. and Boone, A. (2004). Feasibility of floating platform systems for wind turbines. 42nd AIAA aerospace sciences meeting and exhibit, 1007.

National Oceanic and Atmospheric Administration (NOAA) (2019a). Tsunami events list of runups. Accessed on June 2019 at https://www.ngdc.noaa.gov/nndc/struts/results?EQ_0=4371&t=101650&s=10&d=99,185,186,76,78&nd=display.

National Oceanic and Atmospheric Administration (NOAA) (2019b). NGDC/WDS Global Historical Tsunami Database. National Centers for Environmental Information (NCEI). Accessed on June

2019 at https://www.ngdc.noaa.gov/nndc/struts/results?EQ_0=5413&t=101650&s=9&d=101,91,95,93&nd=display.

National Oceanic and Atmospheric Administration (NOAA) (2019c). NGDC/Natural Hazards Viewer: Tsunamis. Accessed on June 2019 at https://maps.ngdc.noaa.gov/viewers/hazards/?layers=0.

National Oceanic and Atmospheric Administration (NOAA) (2019d). Coastal Relief Digital Elevation Models for bathymetric data analysis. National Centers for Environmental Information (NCEI). Accessed on August 2019 at https://ngdc.noaa.gov/mgg/coastal/crm.html

National Oceanic and Atmospheric Administration (NOAA) (2019e). Bathymetric Data Viewer. National Centers for Environmental Information. Accessed on August 2019 at https://maps.ngdc.noaa.gov/viewers/bathymetry/

Newman, J.N. (1977). Marine Hydrodynamics. The MIT Press, Cambridge Massachusetts, ISBN 0-262-14026-8.

Normark, W.R., Moore, J.G. and Torresan, M.E. (1993). Giant volcano-related landslides and the development of the Hawaiian Islands. Submarine landslides: selected studies in the US Exclusive economic zone. US Geol. Surv. Bull., 2002, 184-196.

Okal, Emile A., and Hébert, Héléne (2007). Far-field simulation of the 1946 Aleutian tsunami. Geophysical Journal International, 169, 1229–1238. doi: 10.1111/j.1365- 246X.2007.03375.x

Petersen, M.D., Moschetti, M.P., Powers, P.M., Mueller, C.S., Haller, K.M., Frankel, A.D., Zeng, Yuehua, Rezaeian, Sanaz, Harmsen, S.C., Boyd, O.S., Field, E.H., Chen, Rui, Luco, Nicolas, Wheeler, R.L., Williams, R.A., Olsen, A.H., and Rukstales, K.S., (2015), Seismic-hazard maps for the conterminous United States, 2014: U.S. Geological Survey Scientific Investigations Map 3325, 6 sheets, scale 1: 7,000,000, https://dx.doi.org/10.3133/sim3325. ISSN 2329-132X (online): https://pubs.usgs.gov/sim/3325/

Price, D., Berger, B., O'Rourke, T.D., Stewart, H.E., Wham, B.P., Pariya-Ekkasut, C. and Hall, H. (2018). Performance Evaluation of iPVC Pipe under Earthquake-Induced Ground Deformation. School of Civil and Environmental Engineering, Cornell University, Ithaca, NY, 1-84.

Prowell, I. and Veers, P. (2009). Assessment of wind turbine seismic risk: Existing literature and simple study of tower moment demand. Sandia National Laboratories: Albuquerque, NM, USA, 13.

Reid, J.A., Reid, J.M., Jenkins, C.J., Zimmermann, M., Williams, S.J., and Field, M.E., (2006), usSEABED: Pacific Coast (California, Oregon, Washington) offshore surficial-sediment data release: U.S. Geological Survey Data Series 182, version 1.0. Online at https://pubs.usgs.gov/ds/2006/182/

Rijken, O. and Leverette, S. (2007). Tension leg platform response to earthquake in Gulf of Mexico. In The Seventeenth International Offshore and Polar Engineering Conference. International Society of Offshore and Polar Engineers.

Roddier, D., Cermelli, C., Aubault, A. and Peiffer, A. (2017). Summary and conclusions of the full life-cycle of the WindFloat FOWT prototype project. In ASME 2017 36th International Conference on Ocean, Offshore and Arctic Engineering. American Society of Mechanical Engineers Digital Collection.

Rodriguez-Pascua, Miguel & Perez-Lopez, Raul & Giner-Robles, J. & Silva, P.G. & Garduño Monroy, Victro & Reicherter, Klaus (2009). A comprehensive classification of Earthquake Archaeological Effects (EAE) for structural strain analysis in Archaeoseismology. 1st INQUA-IGCP-567 International Workshop on Earthquake Archaeology and Palaeoseismology.

Ronold, K.O., Landet, E., Jørgensen, E.R. and Sandberg, J. (2011). Design standards for floating wind turbine structures. Proceedings of the European Wind Energy Conference, 14-17.

Shaji, S. and Jayalekshmi, R. (2016). Earthquake Analysis of Mini Tension Leg Platforms under Random Waves. SSRG International Journal of Civil Engineering, 3(10), 1-5.

Sharples, M. (2011). Offshore Electrical Cable Burial for Wind Farms: State of the Art, Standards and Guidance and Acceptable Burial Depths, Separation Distances and Sand Wave Effect. Washington, DC: Bureau of Safety and Environmental Enforcement, 50-60.

Soloviev, S.L., and Go, C.N. (1975). A catalogue of tsunamis on the eastern shore of the Pacific Ocean [dates include 1513-1968]. Academy of Sciences of the USSR, Nauka Publishing House, Moscow, 204. [Canadian Translation of Fisheries and Aquatic Sciences no. 5078, 1984, translation available from Canada Institute for Scientific and Technical Information, National Research Council, Ottawa, Ontario, Canada K1A OS2, 293].

Statoil (2015). Hywind Scotland Pilot Park, Environmental Statement Non Technical Summary. 22. Available at https://www.equinor.com/content/dam/statoil/documents/impact-assessment/Hywind/Statoil-Non%20Technical%20Summary%20April%202015.pdf

Strand, C. and Masek, J. (2005). Sumatra-Andaman Islands Earthquakes and Tsunami of December 26, 2004 Lifeline Performance: Preliminary. ASCE Technical Council on Lifeline Earthquake Engineering, TCLEE Monograph, (29), 270.

Suzuki, H. (2005). Overview of Megafloat: Concept, design criteria,analysis, and design. Marine Structures,18,111–132.

Suzuki, K., Yamaguchi, H., Akase, M., Imakita, A., Ishihara, T., Fukumoto, Y. and Oyama, T. (2010). Initial design of TLP for offshore wind farm. Proc. of Renewable Energy 2010 International Conference.

Tappin, D.R., Grilli, S.T., Harris, J.C., Geller, R.J., Masterlark, T., Kirby, J.T., Shi, F., Ma, G., Thingbaijam, K.K.S. and Mai, P.M. (2014). Did a submarine landslide contribute to the 2011 Tohoku tsunami? Marine Geology, 357, 344-361.

United States Geological Survey (USGS) (2019a). Severity of an Earthquake. Accessed June, 2019 at https://pubs.usgs.gov/gip/earthq4/severitygip.html.

United States Geological Survey (USGS) (2019b). Map of Ring of Fire. Accessed June, 2019 at https://pubs.usgs.gov/gip/dynamic/fire.html.

United States Geological Survey (USGS) (2019c). Earthquake Lists, Maps, and Statistics. Earthquake Hazards Program. Accessed: June 2019 at https://earthquake.usgs.gov/earthquakes/browse/.

United States Geological Survey (USGS) (2019d). Back to the Future on the San Andreas Fault. Golden, CO, USGS. Accessed June, 2019 at https://earthquake.usgs.gov/learn/topics/safz-paleo/.

United States Geological Survey (USGS) (2019e). Offshore Faults along Central and Northern California. Santa Cruz, CA, USGS. Accessed June, 2019 at https://www.usgs.gov/centers/pcmsc/science/offshore-faults-along-central-and-northern-california?qt-science_center_objects=0#qt-science_center_objects.

United States Geological Survey (USGS) (2019f). USGS Search Earthquake Catalog. Golden, CO, USGS. Accessed August, 2019 at https://earthquake.usgs.gov/earthquakes/search/

University of Hawaii at Manoa (2019). Main Hawaiian Islands Multibeam Bathymetry and Backscatter Synthesis. Manoa, HI: Hawaii Mapping Research Group at the School of Ocean and Earth Science and Technology, University of Hawaii at Manoa. Accessed August, 2019 at https://www.soest.hawaii.edu/HMRG/multibeam/bathymetry.php

Viselli, A.M., Goupee, A.J. and Dagher, H.J. (2015). Model test of a 1: 8-scale floating wind turbine offshore in the gulf of maine. Journal of Offshore Mechanics and Arctic Engineering, 137(4).

Ward, S.N. (2001). Landslide tsunami. Journal of Geophysical Research: Solid Earth, 106(B6), 11201-11215.

Wham, B.P., O'Rourke, T.D., Stewart, H.E., Bond, T.K., Pariya-Ekkasut, C. and Hall, H. (2016). Large-Scale Testing of JFE Steel Pipe Crossing Faults: Testing of SPF Wave Feature to Resist Fault Rupture. Cornell University, Ithaca, NY, 1-83.

Williams E. F., Fernández-Ruiz M. R., Magalhaes R., Vanthillo R., Zhan Z., González-Herráez M. and Martins H. F. (2019). Distributed sensing of microseisms and teleseisms with submarine dark fibers. Nature Communications (10), Article number: 5778

Wilson, R. I., Admire, A.R., Borrero, J.C., Dengler, L.A., Legg, M.R., Lynett, P., McCrink, T.P., Miller, K.M., Ritchie, A., Sterling, K., and Whitmore, P.M. (2012). Observations and Impacts from the 2010 Chilean and 2011 Japanese Tsunamis in California (USA). In Historical and Recent Catastrophic Tsunamis in the World: Volume I. The 2011 Tohoku Tsunami, Pure Appl. Geophys. doi: 10.1007/s00024-012-0527-z

Yoshida, K., Suzuki, H., Hosomi, I. and Nahata, H. (1996). The evaluation on the effect of tsunami and seaquake on the floating structure. Journal of the Society of Naval Architects of Japan (180), 403-409.

APPENDIX A: METADATA

Data type / AOI	Oregon Regional	California Humboldt	California Morro Bay and Diablo Canyon	Hawaii Oahu North	Hawaii Oahu South
Offshore Wind Technology Depth Zones	https://inport.nmfs.noaa.gov/inport/item/56123				
BOEM Planning Areas	Wind_Speed_2017_1100m_EEZ_15mi_NoCables.shp	https://www.boem.gov/Renewable-Energy-GIS-Data/ https://www.boem.gov/BOEM-Renewable-Energy-Shapefiles.zip			
Digital elevation models (DEMs)	https://www.ngdc.noaa.gov/mgg/coastal/crm.html			https://www.soest.hawaii.edu/HMRG/multibeam/bathymetry.php http://www.soest.hawaii.edu/HMRG/multibeam/Version21/mhi_mbsyn_bathyonly_50m_v21.nc	
Bathymetry contours	ftp://ftp.coast.noaa.gov/pub/MSP/ORT/bathymetryContours.zip				
Seabed sediment core samples	https://pubs.usgs.gov/ds/2006/182/data_cata.html			https://maps.ngdc.noaa.gov/viewers/sample_index/#	
Geology (Soil type)	https://tethys.pnnl.gov/publications/benthic-habitat-characterization-offshore-pacific-northwest-volume-1-evaluation http://bhc.coas.oregonstate.edu/boem_data/V4_0_SGH_WA_OR_NCA.zip	https://pubs.er.usgs.gov/publication/ofr821000 https://pubs.usgs.gov/of/1982/1000/report.pdf		https://pubs.usgs.gov/sim/2004/2824/ https://pubs.usgs.gov/sim/2004/2824/SIM2824_data.zip	
Earthquakes	https://earthquake.usgs.gov/earthquakes/search/				
Faults / Reefs	https://earthquake.usgs.gov/static/lfs/nshm/qfaults/Qfaults_GIS.zip			https://pubs.usgs.gov/sim/2004/2824/ https://pubs.usgs.gov/sim/2004/2824/SIM2824_data.zip	
Sidescan sonar	https://coastalmap.marine.usgs.gov/regional/contusa/westcoast/pacificcoast/GLORIA_images.html#Composites https://pubs.usgs.gov/of/2010/1332/htmldocs/pc/pc_overview.html			https://pubs.usgs.gov/of/2010/1332/htmldocs/hw1/hw1_indexmap.html	
Seismic Hazard	https://pubs.usgs.gov/sim/3325/			https://pubs.usgs.gov/imap/i-2724/	

APPENDIX B: PRELIMINARY ANALYSIS OF POTENTIAL FOR VORTEX-INDUCED MOTIONS FROM TSUNAMI CURRENTS ON OFFSHORE WIND INSTALLATIONS

by Dr. Jason Dahl, Associate Professor, Ocean Engineering Department, University of Rhode Island

Background Information:

Proposed floating offshore wind installations utilize similar floating platform designs to floating offshore oil and gas platforms. These types of platforms are known to undergo vortex-induced motions when encountering strong currents as vortex shedding in the wake of these structures can synchronize with the natural frequencies of the structure and mooring system in surge, sway, and yaw. The term vortex-induced motions (VIM) is a general term that can describe self-limiting oscillations of the structure a relatively low non-dimensional flow speeds, often referred to as vortex-induced vibrations (VIV) or it can also refer to an unstable galloping response that can occur for structures at high non-dimensional flow speeds. While VIV is often a concern only in the fatigue life of a structure or in slightly increasing the drag load on the structure due to the self-limiting nature of the vibrations, galloping can cause catastrophic failure of a structure, as in the well-known failure of the Tacoma-Narrows bridge.

In the case of offshore structures encountering a tsunami in deep or shallow water, the resulting large magnitude currents occurring over an extended period of time could induce VIM and the specifics of the design of the structure and resulting currents from a tsunami must be evaluated to assess the effects on the specific design. The following describes an example preliminary evaluation of several example offshore wind floating platform designs to demonstrate whether VIM from tsunami currents would be a problem for the specific structures. Without specific field data and specifics of a tsunami event, it is assumed that the currents generated from the tsunami could range anywhere from 0.5 m/s to 10 m/s. Additionally, without specifics of the mooring system design for each structure, an example depth and mooring specification is used to define a mooring stiffness and natural frequency of the structure according to Faltinsen (1990). This calculation would of course need to be assessed for a specific design but is used for demonstration purposes in this example.

Example Calculations:

The following example platforms will be considered in the evaluation of VIM due to currents: Hywind spar type platform and Volturn semi-submersible. Details of the GICON-TLP platform are also provided, however this concept design appears to be for a smaller scale turbine and without additional details about the design tension in the mooring system, it is not possible to assess this design. However, the same analysis provided for the other platforms could be done on this design, in particular, it will behave similarly to the semi-submersible design with the only difference being that it's natural frequencies will be dependent on the TLP mooring system rather than a catenary mooring system.

Basic design details of the example turbine platforms are given in Table B-1 and pictures of the three design types are shown in Figure B-1 to Figure B-3.

Table B-1. Different types of FOWT along with range/description of parameters.

Type/ Name of Turbine	Status	Draft	Displace-ment	Wind Turbine Generator WTG Unit substructure Dimension			Number of anchor points
				Diameter	Length* Breadth* Height	Length of Each Arm	
Spar-Type/ Hywind	Full-scale and Operational	70 – 82 m	11,500 m^3 – 13,500 m^3	15m (maximum)	-	-	3
Semi-submersible / Volturn US Full Scale	Full-scale but yet to be operational	20 m	15,594 m^3	-	-	52m	3
TLP/GICON	Concept design	10m	2070 m^3	-	32m*32m *28m	-	4

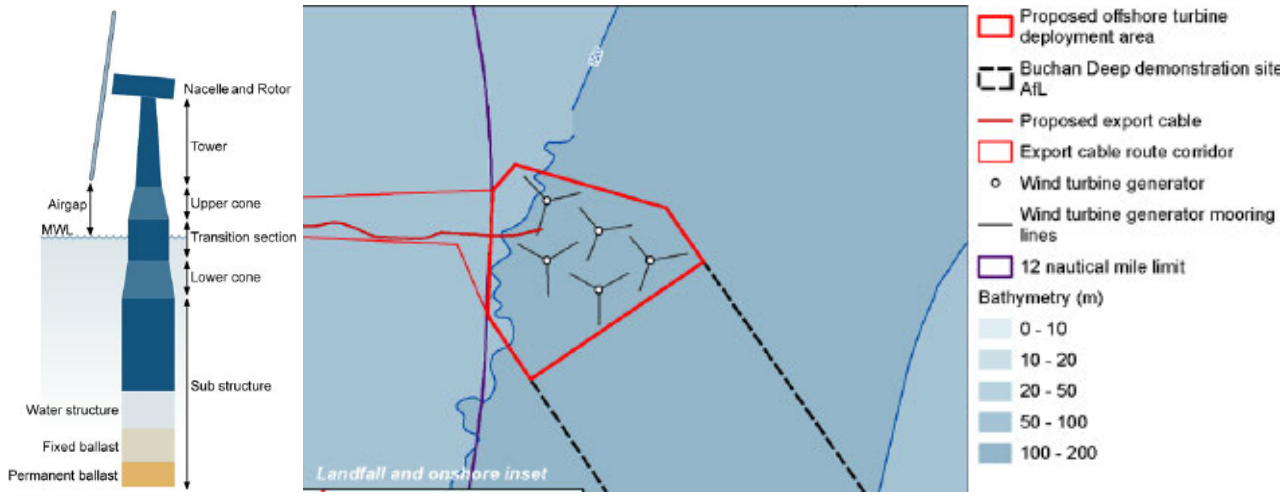

Figure B-1. Spar-type FOWT (Figure from: Statoil, 2015).

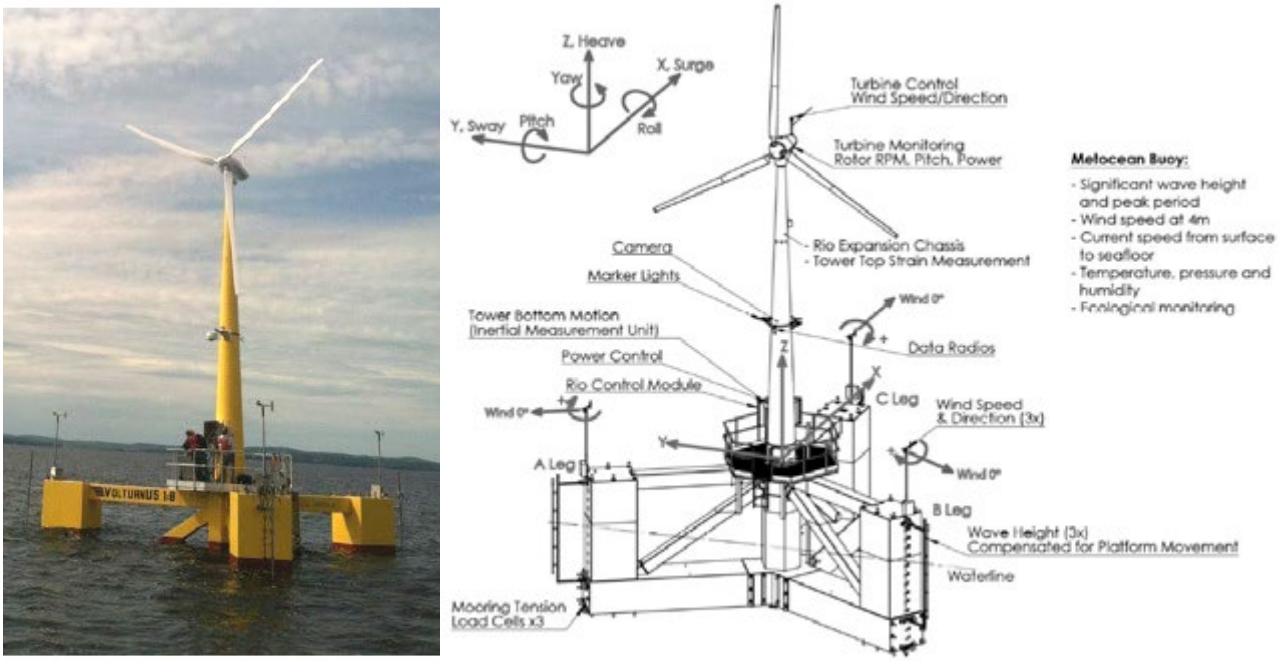

Figure B-2. Semi-submersible FOWT (VolturnUS 1:8-scale) (left panel) and its structural components (right panel) (figure from Viselli, 2015).

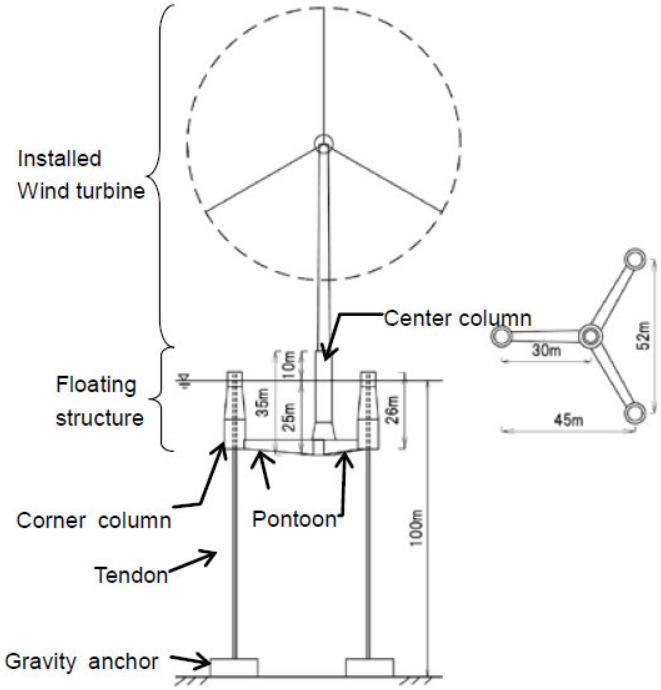

Figure B-3. General arrangement of the TLP (figure from Suzuki et al., 2010).

Based on Figure B-2 for the semi-submersible, assuming that the drawing is to scale, the project team can estimate that the semi-submersible legs have a characteristic length of ¼ the arm length. For the present calculations, the project team can then assume that the characteristic length for the semi-submersible legs is 13 m.

Using a Reynolds number based on the diameter of the spar buoy or using the characteristic length of the semi-submersible hull, the project team would have a minimum Reynolds number associated with the semi-submersible length scale and low current speed of 0.5 m/s. Assuming a kinematic viscosity of $10^6 m^2/s$, the low range of Reynolds number is $6.5*10^6$. Assuming the surfaces of these buoys would not be perfectly smooth (i.e., some roughness exists), this Reynolds number would correspond with a supercritical flow regime and any higher flow speeds would also be supercritical. In this flow regime, there is significant statistical variation in the observed Strouhal number (frequency of vortex shedding * diameter/flow speed = f*D/U) of circular cylinders, where the Strouhal number can vary from 0.1-0.3 in this region, hence one will use a range of Strouhal numbers to assess whether vortex shedding might excite the structure.

First, one must estimate a natural frequency for the structures. For the example, a natural frequency in sway will only be estimated; however, the full dynamics of the structure should be assessed in any true engineering evaluation; hence, the same would normally be done for surge and yaw as these directions could also have excitation. Knowing the displacement of each structure as given in Table B-1, multiple by the fluid density (1025 kg/m^3 for saltwater) to obtain an estimate for the mass of the structure. Additionally, since these structures are operating in a dense fluid, they will have a significant added mass. One can then approximate the added mass as being equal to the displaced mass of fluid for the structure, hence the effective mass of the structure will be equal to twice the dry mass. This gives a mass of $2.77*10^7$ kg for the spar buoy and $3.2*10^7$ kg for the semi-submersible.

To estimate the mooring stiffness, one can use equation 8.22 from Faltinsen (1990), which gives the mooring stiffness in sway for a catenary mooring system as a function of the mean horizontal tension (T_H) in the system, weight of mooring cable in water (w) and depth of water (h):

$$C_{11} = \frac{dT_H}{dX} = w\left[\frac{-2}{(1+2\frac{a}{h})^{1/2}} + cosh^{-1}(1+\frac{h}{a})\right]^{-1}$$

Where

$a = \frac{T_H}{w}$;

X: horizontal position between the anchor point on bottom and the anchor point at surface

And

C_{11}: mooring cable system stiffness in 1 direction due to displacement in 1 direction (effective spring constant of mooring cable)

Assuming a depth of water of 100 m, wetted weight of cable as 828 N/m, and mean horizontal tension in the line as 50,000 N, the resulting stiffness of the individual mooring line will be 2891 N/m. Assuming a 3 mooring point system, using Equation 8.26 from Faltinsen (1990):

$$C_{11} = \sum_{i=1}^{n} k_i cos^2 \psi_i$$

Where:

k_i: stiffness of individual mooring line

ψ_i: angle of individual mooring line in the x-y plane

the mooring system stiffness in sway can be approximated as 4336 N/m. For the spar buoy, this results in a natural frequency in sway of 0.002 Hz and for the semi-submersible, the natural frequency in sway is approximated as 0.0019 Hz.

The vortex shedding frequency or excitation frequency to the structure due to currents will be a function of the Strouhal number. This frequency would be expected to potentially excite vortex-induced vibrations of the structure. The limiting flow frequency case will occur for the lowest possible Strouhal number and lowest flow speed (i.e., St = 0.1, U = 0.5 m/s). Under this condition, the spar buoy would generate vortices with a shedding frequency of 0.003 Hz. This is sufficiently close to the estimated natural frequency of the structure that one would expect some excitation of the structure and a potential for lock-in (i.e., the shedding frequency synchronizes with the natural frequency of the structure). If the flow speed is increased, the shedding frequency will increase and one would then expect the shedding frequency to desynchronize with the natural frequency of the structure, hence motions of the structure would decrease at higher speeds. To properly evaluate the specific motions and loading that a spar buoy structure would encounter, one would need to conduct laboratory experiments or numerical modeling of the fluid structure interaction. An example of laboratory experiments to measure the vortex-induced vibration response of a spar type wind turbine platform is given in Carlson and Modarres-Sadeghi (2017).

A spar buoy with a circular cylindrical shape is not susceptible to galloping instabilities, since its cross-section is symmetric regardless of the direction of the relative flow velocity. Since galloping is triggered due to an asymmetry of an objects cross-sectional shape with respect to the relative flow velocity, the spar buoy will not undergo galloping instabilities unless it has appendages or other subsurface structures that cause an asymmetry to the object shape.

For the semi-submersible, using the characteristic leg dimension of 13 m, the shedding frequency for a Strouhal number of 0.1 and flow speed of 0.5 m/s corresponds with a shedding frequency of 0.004 Hz. Again, this is sufficiently close to the structural natural frequency that one may expect some excitation of the structure due to vortex induced vibrations. The semi-submersible, however, is a much more complex structure since shedding from the individual legs can interact with one another to further enhance or cancel excitation of the structure. There is no formal analytic means to evaluate the response of such a structure without performing a physical mode scale experiment to measure the structural response in a current or perform a fluid-structure interaction simulation. One can, however, look at previous work to evaluate how this structure might be expected to behave.

Goncalves et al. (2012) describes an experimental study of a similar model scale semi-submersible platform exposed to a free stream current. The model is slightly different from the example Volturn semisubmersible in that it has four legs instead of three, however the legs have similar square dimensions and the arm length with respect to the leg characteristic length is similar. Figure B-4 shows

a dye visualization around the semi-submersible model from Goncalves et al. (2012), demonstrating the complex interaction of vortex shedding from each leg.

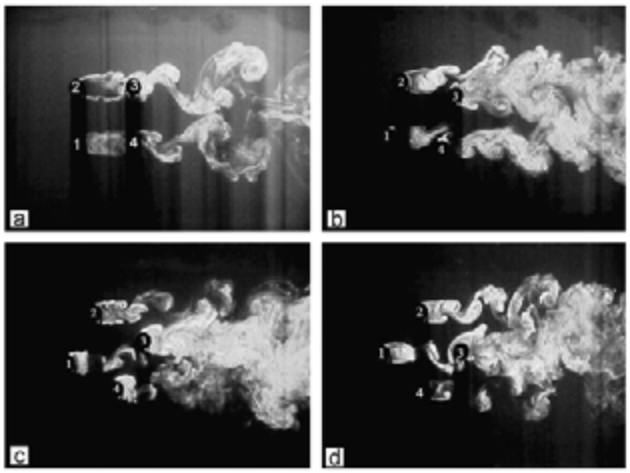

Figure B-4. Figure from Goncalves et al. (2012) showing dye visualization of vortex shedding in the wake of a semi-submersible at various angles relative to the flow velocity.

Figure B-5 shows the transverse (sway) response of the semi-submersible model under various angle configurations of the model with respect to the flow direction. The vertical axis shows the non-dimensional amplitude of sway response, which is the amplitude of motion divided by the characteristic length of the individual semisubmersible float legs (L). So, a value of 0.4 means that the semisubmersible sways with a motion amplitude that is 40% of the float leg dimension. The reduced velocity (which is defined as flow speed/(natural frequency*diameter) = U/(f_n*D)) on the horizontal axis is defined as using the natural frequency in sway, it is a normalized flow speed, so higher reduced velocity corresponds to higher flow speed for a given system (fixed natural frequency and fixed leg dimensions). The response is normalized by the max dimension of the entire platform (dimension L is equivalent to twice the arm length). The peak in the response at reduced velocity of 6 corresponds to the VIV response of the structure, where the shedding frequency of vortices is synchronized with the natural frequency of the structure. Again, this is a self-limiting response. In the example case, one would expect this type of response to occur since the natural frequency of the example system is sufficiently close to the shedding frequency. Of more concern, however, is the system response at higher reduced velocities as seen in Figure B-5.

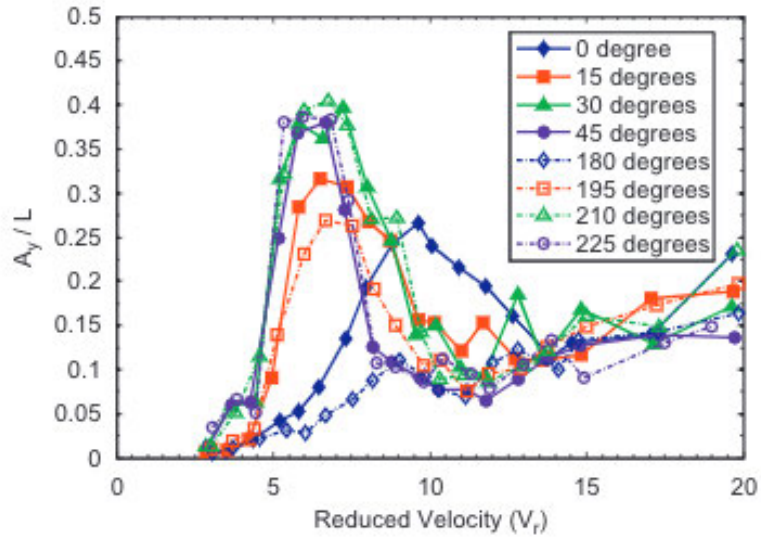

Figure B-5. Transverse (sway) response of the semi-submersible model from Goncalves et al. (2012) under various angle configurations of the model relative to the flow velocity.

At a reduced velocity of 20, the system response appears to be increasing steadily. As described in Goncalves et al. (2012), the response was not measured above this value due to limitations of the experimental apparatus, but the steady growth in response with increasing reduce velocity is typical of a system subject to a galloping response. Figure B-6 shows an example of the galloping response of a triangular prism under different angles relative to the flow direction from the experimental study of Seyed-Aghazadeh, Carlson, and Modarres-Sadeghi (2017). The main feature of a galloping response is the steady increase in response amplitude as a function of the increased reduced velocity.

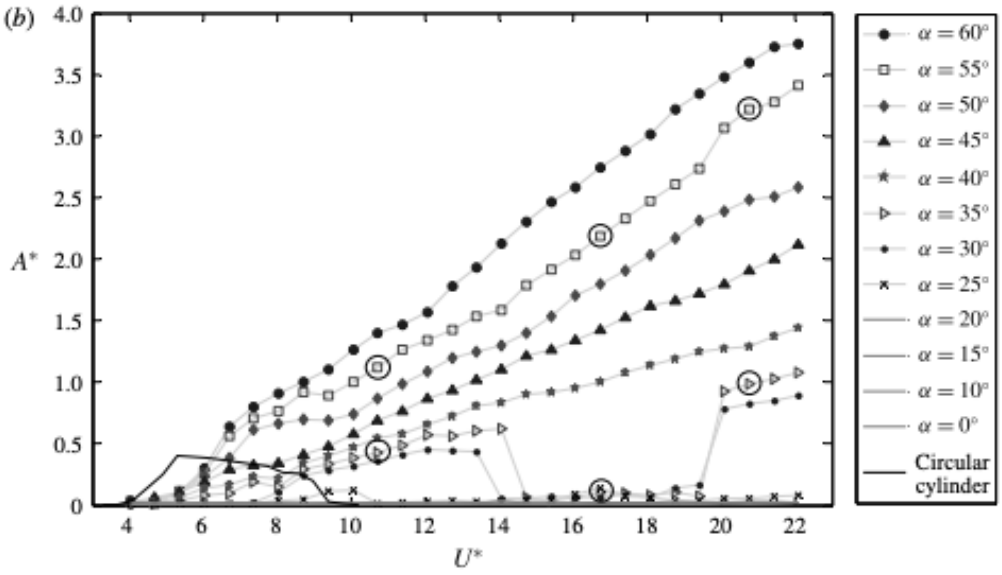

Figure B-6. Galloping response of a triangular prism from Seyed-Aghazadeh et al. (2017).

For the semi-submersible, using the computed natural frequency, the resulting reduced velocity corresponding to 0.5 m/s is Vr = 20, corresponding with the edge of both Figure B-5 and Figure B-6, directly in the galloping region. For larger flow speeds, one would expect the galloping response to grow steadily as shown in Figure B-5 and Figure B-6, hence for currents between 0.5 m/s and 10 m/s, the galloping response would increase in amplitude. If the structure is subjected to a very large amplitude response for only a short period of time, this could lead to structural failure of the mooring system.

Conclusions:

As seen from this example preliminary case study, the magnitude of currents generated by a tsunami could result in vortex-induced motions dependent on the floating structure type. For spar type floating structures, the main concern would be vortex-induced vibrations that could lead to fatigue damage if subjected over long periods of time or increased drag loading on the mooring system. For semi-submersible structures, the lack of an omni-directional shape could lead to galloping instabilities of the floating platform system, which could lead to catastrophic failure of the mooring system. Evaluation of the expected currents associated with the siting of these structures and the impact of these currents on vortex-induced motion of the structure should be evaluated.

References:

Carlson, D. and Modarres-Sadeghi, Y. (2017). Vortex-induced vibration of spar platforms for floating offshore wind turbines. Wind Energy, 21(11):1169-1176.

Faltinsen, O.M. (1990). Sea Loads on Ships and Offshore Structures. Cambridge University Press, Cambridge, U.K.

Goncalves, R.T., Rosetti, G.F., Fujarra, A.L.C., and Oliveira, A.C. (2012). Experimental study on vortex-induced motions of a semi-submersible platform with four square columns, Part I: Effects of current incidence angle and hull appendages. Ocean Engineering, 54: 150-169.

Seyed-Aghazadeh, B., Carlson, D.W., and Modarres-Sadeghi, Y. (2017). Vortex-induced vibration and galloping of prisms with triangular cross-sections. Journal of Fluids Mechanics, 817: 590-618.